UNIVERSITE LIBRE DE BRUXELLES
Faculté des Sciences Appliquées
Services des Milieux Continus & Génie Civil

Finite Element Modeling of Shear in Thin Walled Beams with a Single Warping Function

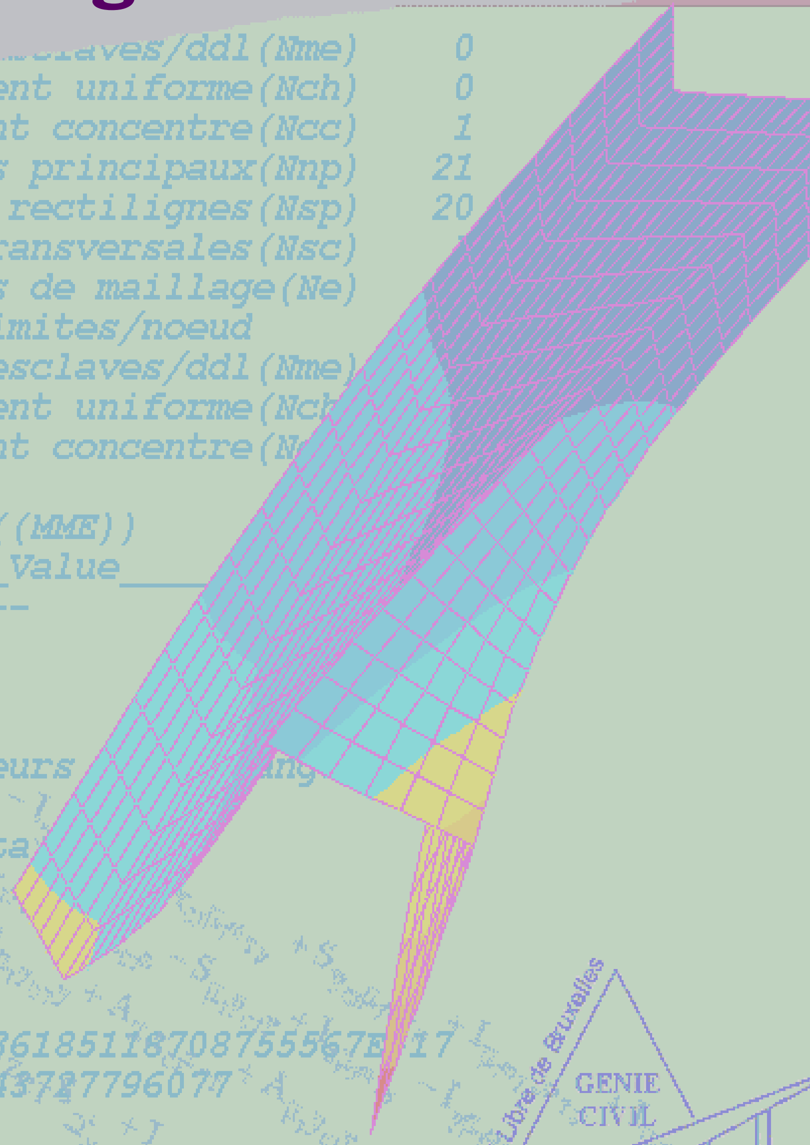

Katy Saadé

Promoteurs:
Bernard Espion & Guy Warzée

Année académique 2004-2005

Dissertation originale présentée en vue de l'obtention du grade de docteur en Sciences Appliquées

ACKNOWLEDGEMENTS

With all the pleasure and pride of a mother after delivery and after several years of pregnancy and several months of labor, here is the thesis. It has been pumping out the best of me for its development and accomplishment. Now that it is almost over, what I had carried around with me for so long is ready for the tough adventure that every newborn and mother have been through. I would like to express my gratitude for all who contributed in a way or another in the accomplishment of this work.

Most importantly, I would like to thank my supervisors Pr. Bernard Espion and Pr. Guy Warzée for their commitment to guiding me through my doctoral research as well as for their patience and supervision. Their helpful comments, advices, suggestions and contributions regarding all the critical aspects of my thesis have been very profitable over the past years. I feel especially indebted to them for the weekends they had spent reading the various drafts of this thesis and overviewing the interminable lists of equations. I imagine now they can say 'Ouuuuuuf'.

I thank Pr. Philippe Bouillard who has also been very helpful in my work. His warm hospitality, enthusiasm, goodwill and energy have played a major role in my integration and well being from the beginning of my stay in Belgium till now.

I would thank all the former and present dear colleagues in Structural and Material Computational mechanics (SMC) and Civil Engineering (SGC) departments for being extremely helpful and for creating a comfortable working environment. Their friendship has provided a real support.

Special thoughts go to my beloved Lebanon in this particular tough period where I was born and where I grew. Many thanks for my sisters, friends and especially for the family of my uncle Boulos and aunt Danielle who made it possible for me to come to Brussels.

I know I would not have been here without those who have been my first and best teachers, the ones who inspired me to learn and to continue learning: my loving father Sayed and mother Damia. Now that I am a mother, I can appreciate and understand all their sacrifices that enabled me to reach my goal.

How can I forget the contribution of my lovely cute Joanne in delaying my project? You decided to be my first child and you managed to choose a critical timing! BIJOU, I thank you for all the joy and the wonderful moments you gave to me and to your daddy.

I would finally give my very special thanks to you Naim. Your patience and comprehensive love enabled me to complete this work. With lot of emotions and gratitude, I thank you Habibi for the inspiration and support you provided throughout my research work. You left everything and you followed me. I know that lately I have been too busy and you have been lonely. You shared, supported and contributed to the entire preparation. I really love you.

CONTENTS

PART II. THEORETICAL DEVELOPMENTS

PART III. DISCRETE MODELS

CHAPTER 0. INTRODUCTION

0.1 Background

Throughout history, thin walled structures have been classified as very common construction elements. Their extensive use originates probably from the trend to reduce the structural weight and to minimize building materials. This very natural optimization strategy constituted an important design principle and guided the evolution process of constructions starting from the ancient 'trial and error' approach. Early developments, aiming at idealizing and predicting structural responses, managed to condense a complex 3D structure to a 'mathematically manageable' beam model and to superpose principal types of mechanical behaviors: tension/compression, bending, torsion and so on… This simple but ingenious formulation is still extensively developed nowadays despite the existing 2D and 3D models and the considerable growth of simulation techniques. Many extensions, such as transverse shear deformation, non uniform warping torsion, cross sectional distortion and further refinements were progressively included over the years. The multitude of efforts recently invested in this research area is probably justified by:

- the complexity of thin walled structure behavior,
- the optimization of profile geometries as much as possible in order to fit esthetics, strength and connectivity requirements,
- the need for brief but accurate and reliable design methods in order to remain time competitive...

0.2 Motivation and purpose of the research

The initial motivation of this thesis was driven by the need for a reliable tool enabling an accurate analysis of thin walled civil engineering beam applications with arbitrary cross sections submitted to torsion (e.g. bridges, towers…). One of the major problems in modeling a real-life structure is the choice of the appropriate model. Which effects are to be taken into consideration and which are to be left apart? Which approximations are useful, what is admissible and what is not? Is it necessary to apply a shell theory and in this case, how many degrees of freedom should be included? Is it crucial to develop a huge amount of numerical results? A multitude of similar questions, coupled with the need for the a scientific background in order to use any existing commercial finite element code, initiated a first interest in advanced torsional kinematical formulations and the resulting numerical properties of thin walled beam finite elements.

Moreover, pure scientific interest motivated other research subjects such as warping effects due to bending shear forces, limitations of a formulation, the influence of shear locking… Later on, the interest in investigating the cross sectional deformation of very thin walled beams in industrial applications (e.g. railroad bridges, stiffeners, diaphragms and bracing in civil, aeronautical and naval constructions…) led to the analysis of distortional behavior. Cold formed and welded members (such as steel framed houses, portal frames, purlins, racking systems…) are in expanding use due to their cost competitiveness, resistance and their 100% recyclable property.

Therefore, this thesis introduces a theoretical background and presents detailed analyses in order to improve the understanding of the linear behavior and stability of thin-walled beam structures, particularly when exhibiting important warping due to non uniform torsion, shear bending and distortion. On the basis of this knowledge, an advanced beam finite element has been developed, implemented into a computer program and used as a general tool for the purpose of analyzing thin walled structures. Despite the wide literature -as it is shown in chapter 1- concerning this general scope and despite the numerous “published” beam finite elements that include warping, this work presents original achievements, namely:

- a detailed understanding and precise comparison of existing theories and finite elements;
- a unified formulation that uses a single warping function for theoretical developments and finite element applications of a general study that covers:
    - uniform and/or non uniform torsion
    - uniform and/or non uniform distortion
    - bending shear effects

  in different cases of:
    - asymmetrical cross sectional shapes where shear centers and centroids do not coincide
    - partial warping transmission in beam assemblies

While developing analytical and numerical formulations, many problems and unclear points had to be solved. Some were related to mechanical model decisions and others were purely due to finite element approximations. Solving these specific problems and inspecting the relation between a mechanical behavior and a mathematical equation inspired lots of research subjects that gave interesting concluding remarks or led to fruitful discussions. Among other problems, here are some examples: the interpretation of mathematical or numerical messages (like non definite symmetrical stiffness matrix), a large error due to a finite element discretization, the influence of the shape function…
Another important motivation throughout all the work was an in-depth examination of existing mechanical models concerned with the present subject. Some unclear conclusions, unjustified links or non-evident remarks led to important investigations about the mechanical content or the importance of some assumptions or remarks (such as a dependency of degrees of freedom, determining distortional rotational ratio in case of asymmetrical profile…).

0.3 Scope and content of the dissertation

The primary aims of this thesis are to provide an understanding of the behavior of thin walled beams in engineering applications (civil, mechanical, naval…) and to produce a reliable tool for accurate prediction of their behavior. In order to fit this objective, a methodology is developed for the beam structural analysis including the identification of a possible instability by following the response of the structure during the deformation process. The analysis focuses on the case of a static beam within the framework of geometrically nonlinear elasticity by considering small deformations and neglecting time dependent effects –i.e. forces whose direction and intensity do not depend on the beam deformation. It is believed that these restrictions respect the above-stated motivation and allow an accurate estimation of the strength and the safety assessment of a structure. The present research could be used for a design analysis or as a guiding tool in an optimization process.

The dissertation is organized as follows. In chapter 1, a general survey summarizes most representative work on the subject and concludes by positioning the thesis within its field and highlighting its contribution to the published material. Chapter 2 presents and compares different existing theories that analyze the behavior of thin-walled members submitted to axial, bending, torsional and distortional loads. Chapter 3 is confined to the kinematics of the present work. The basic assumptions are clearly defined in order to induce the displacement fields that include torsional, distortional and shear bending effects. Chapter 4 introduces the principle of virtual work which is the basis of the present work and offers analytical solutions to some problems. Although the analytical methods shown in this chapter are only valid for simple structures, they constitute a very important part of the developments done in this work. They offer a simple tool that enables focusing on the basic hypotheses, reducing to the principal mechanical behavior and validating mathematical, physical and mechanical approximations. Besides, together with numerical shell analyses, they contribute to the validation of the numerical results presented in chapter 5. General conclusions are drawn in chapter 6 while some useful calculations and non original developments are placed in appendices (such as matrices and calculations too detailed for text presentation, technical notes on methods, common developments…) since they interrupt the guiding line of the report (and the pleasure of reading!).

PART I. OVERVIEW

CHAPTER 1. LITTERATURE REVIEW AND RESEARCH PROBLEM STATEMENT

1.1 Goal of the chapter

Thin-walled structures have gained a growing importance due to their efficiency in strength and cost (see e.g. Nowinski 1959, Davis 2000, Hancock 2003…). While significant advances have been made through experimental testing and theoretical work, new research is still required since many important questions remain partially or controversially answered such as: the importance of shear bending effects, lateral torsional buckling (see Braham 2001) and distortional buckling, the compatibility of connections, the choice of adapted and consistent types of non linear analyses (see Bažant 2000)…
This chapter aims at synthesizing, discussing and criticizing accredited knowledge established from the literature according to the guiding concepts of this thesis. It concludes by highlighting the original contribution of this work to the overviewed research fields.

1.2 Survey of modeling thin walled beam structures

1.2.1 General considerations

Doubtlessly, most analyzed and designed thin walled structures consist of beams and columns with different thin profiles. Recently, a wide variety of cross-sectional shapes have been produced in the market, resulting from an optimization based on strength, stiffness, connectivity and esthetics criteria [Mennink 2003…]. As in other engineering fields, the resulting complexity constitutes a considerable challenge for computational schemes. The accuracy of the structural behavior description depends to a large extent on the assumed approximations.
The following 'state of the art' presents, at several levels of modeling, a multitude of generalizations, simplifications and assumptions in published research. At the geometrical level, the influence of the shape and dimensions of a structure is shown: beam or shell structures, open or closed profiles, prismatic or tapered beams… At the physical or kinematical modeling level, the theoretical assumptions are examined in terms of validity, efficiency and ability to describe the structural behavior: discretizing kinematically a beam structure by its longitudinal axis, including shear deformation due to bending or torsion, relaxing the planar and normality assumptions of a cross section, neglecting warping shear variation through the thickness of a mid-wall, taking into consideration the deformability of a cross section, modeling a partial or total transmission of warping at a connection… At the mathematical level, many questions are raised about the completeness and logical consistency of the chosen formulation and the resulting computations. The description of the deformation and the formulation of the set of equilibrium equations with boundary conditions and constraints are discussed: interpolation functions, shear locking, accuracy of solutions… Among these equations, the constitutive equations are the physical equations associated with the material or mechanical model. The quality and performance of thin walled analyses depend on the convergence of all of these multi-level challenges.

1.2.2 Review at the geometrical level

Several geometrical aspects influence the modelling of thin walled structures. The dimensional aspect ratios (thickness to contour length, contour length to longitudinal dimension) are often used to identify and classify a structure (e.g. Batoz 1990, page 2): solid or thin; shell, plate, membrane or beam. The cross sectional geometry influences to a large extent the behavior of thin walled beams and specifically, whether the section is open or closed. The torsional analysis is generally presented by different methods for open and closed cross sections [Murray 1986; Gjelsvik 1981; Shakourzadeh 1995; …]. Many researchers [De Ville 1989 §3.4; Batoz 1990 & Shakourzadeh 1995; Gjelsvick 1981 pages 10 & 114; Musat 1996 & 1999; …] propose multiple expressions of warping functions for different cross sectional types (open or closed thin profiles). Although often used in order to save weight, non prismatic beams with 'tapered' cross sections are not recovered by most structural analyses. Specific studies have dealt with the linear and non linear behavior of thin-walled beam-column structures with variable cross section along the longitudinal axis [Kitipornchai 1975; Bradford 1988; Chan 1990; Rajasekaran 1994; Dube 1996; Ronagh 2000; Kim 2000…].

1.2.3 Review at the physical modeling level

Beam modeling of a thin-walled structure

There seems to be a general guiding concept [Gjelsvik 1981; Murray 1986; De Ville 1989; Batoz 1990; …] for representing a thin walled structure by its longitudinal beam axis. According to Saint Venant principle, the local perturbation effects of concentrated loads and boundary particularities are neglected [Calgaro 1988 page 1-5; Murray 1986 §1.1 …]. The stresses, and thus the strains, are considered to depend exclusively on beam internal forces caused by the applied loading. The membrane force and bending moments are related to the centroidal axis while the torsional moment and shear forces are related to the shear center axis. One of the most important computational difficulties is the accurate calculation under non uniform torsional loading of the beam response when it exhibits a significant cross sectional warping. Shell or thin plate models offer general and well-adapted solutions to various cases of geometry, loading and boundary conditions of thin walled structures. However, such an approach is not always affordable and requires powerful numerical methods. It generates excessive data so that the post-processing is time and energy consuming. In addition, it does not allow easy physical interpretations. It is unable to isolate membrane, bending, uniform torsion, torsional warping, distortional warping, bending shear warping or local effects (e.g. normal stress computations). Moreover, it does not point out the contribution of individual parts; e.g. the influence of stiffeners on the total resistance of the structure is not obviously highlighted. This explains why various researchers develop and adapt new advanced beam theories to take into consideration the particular behavior of a thin-walled structure and to give satisfactory results that the usual beam theory is unable to provide. They always have limited applications; e.g. beam theories stated hereafter do not take into consideration local effects. Several intermediate theories between beams and shells are based on enriched kinematics, e.g. finite strip method [Cheung 1996; Cheung 1998]. Some researchers propose original ideas in order to minimize the complexity of the problem. Meek (1983) considered that the wall is meshed into rectangular elements. Some degrees of freedom are related to the beam axis and others to rectangular elements or to the nodes connecting them. This technique uses a shell theory for torsion and a beam theory for bending. Musat (1996;1999) introduced the concept of strip-plates to define macro-elements. The wall surface is divided into strip plates with rectangular cross sections connected along longitudinal axes.

Cross-section deformation

When a cross section is assumed to remain planar during deformation, the resulting beam model describes the behavior of a massive and regular cross section outside the application zone of the concentrated loading. However, the behavior of thin-walled beams is essentially different since shear stresses and strains are large. Transversal stiffeners are required in order to minimize these effects but also to prevent the distortion and the local bending.

Most researchers [Reilly 1972; De Ville 1989; Gunnlaugsson 1989; Chen 1989; Batoz 1990; Back 1998; Frey 2000; …] generally agree on the fact that for a beam submitted to tension/compression or bending, the cross section remains planar. Some adopt the normality condition of the cross section, i.e. Bernoulli theory (De Ville 1989, page 2.2), by neglecting the strain energy due to the shear forces [Batoz 1990, page 80]. If the normality assumption is relaxed while the planar assumption is kept, i.e. Timoshenko theory, a constant shear strain is calculated [Reilly 1972; Gunnlaugsson 1982; Chen 1989; Batoz 1990; Back 1998; …] and a shear correction factor is needed [Cowper 1966; Pilkey 1994, page 28; Batoz 1990, page 62; Frey 2000, page 193; …] in order to compensate the fact that the displacement field violates the 'no shear' boundary condition at the edges of open profiles. More detailed theories [Massonnet 1983; Reddy 1997; Wang 2000; Eisenberger 2003…] take into consideration the warping due to shear forces. Batoz refers to Chen (1989) and highlights that shear strain effects may be more important in bending than in torsion.

When submitted to torsion, the profile exhibits a longitudinal out of plane warping. The difficulty of solving exactly the general torsional problem has led many researchers to formulate simplified models. Bredt (1842-1900) gave an approximated model in order to solve the torsional problem of hollow sections. Saint Venant (1855) described the well known primary torsion or uniform torsion where transversal shear stresses result from uniform rotation of two adjacent cross sections. According to Nowinski (1959), the torsional rigidity of composite thin sections was analyzed by Weber in 1924 and important literature work was recast by Foppl in 1928. The case of uniform torsion (uniform moment distribution with unrestrained warping) is not often exhibited in practice. In general cases of loading and boundary conditions, an additional 'secondary torsion' induces normal stresses. Neglecting these normal stresses often leads to important errors. The sum of both primary and secondary torsion, called 'mixed torsion', describes the total behavior due to the applied torque. The terminology 'primary' and 'secondary' [Trahair 1993, page 304] is also used in the literature for the torsional warping in order to distinguish between the contour and the thickness warping [Gjelsvik 1981, page 12] of the thin-walled cross section (known also as global and local respectively [De Ville 1989]).

Many researchers have tackled the problem of non uniform torsion. The most well-known authors are Timoshenko (1905), Weber (1924), Reissner (1926), Wagner (1929), Vlassov (1940), v. Karman (1944), Argyris (1949), Benscoter (1954) [Nowinski, 1959]… Timoshenko studied the problem of non uniform torsion of I beams with constrained torsion by assuming linear normal stress distributions in the flanges. His third order differential equilibrium equation, developed in the particular case of an I beam, is still valid and can be deducted from all subsequent general theories.

Considering or neglecting the strain energy associated with warping generated two principal theories in the non uniform torsional field: respectively Vlassov in 1940 and Benscoter in 1954. The terminology used for these two theories may appear as a controversy in literature. Who is the first to study the general theory of non uniform torsion for closed cross sections? Umanski 1939 [Nowinski 1959; Prokić 1994; Musat 1996; …] or Benscoter 1954 as commonly assumed? Is Vlassov theory suitable for closed cross sections or not? The well known published work by Benscoter is a paper published in the ASME journal in 1954 but Umanski and Vlassov published earlier in Russian important works in 1939 and 1940. The names of these three researchers have been associated with torsional theories till today. In his interesting survey on thin walled beam references, Nowinski (1959) stated that the first investigations of constrained warping of a freely supported box beam is attributed by Ebner to Eggenschwyler in 1920. Reissner (1926) analyzed a particular case of tapered beam box under linearly varying torque.

Vlassov well known hypothesis (1961, Ch I. §2.3) consists of neglecting shear warping at the mid wall of an open cross section. In most literature referring to Vlassov work [Kollbrunner 1970; Reilly 1972; Murray 1986 page 4&115; Mottershead 1988; De Ville 1989; Batoz 1990; Razaqpur 1991; Musat 1999; …], this assumption is used for open profiles and the gradient of torsional angle is taken as warping degree of freedom. Benscoter theory characterizes the warping degree of freedom by an independent function which is different from the gradient of torsional angle. For closed cross sections, this independent warping degree of freedom [Gunnlaugsson 1982; Chen 1989; Back 1998; Shakourzadeh 1995; …] is used instead of the derivative of torsional angle in order to include shear strain in kinematics. However, in other works [De Ville 1989 §3.4.1.3; …], Vlassov theory is stated as applicable for closed cross sections by combining the assumption of neglecting shear warping at mid-walls for the calculation of profile warping function with Benscoter independent warping degree of freedom. Back (1998) used this combination.
Massonnet (1983) generalized Saint Venant theory to the case of a linear distribution of the torsional moment. Without being explicitly stated, a restriction was imposed: the torsional warping must be free. His work is at half way between Saint Venant and Vlassov. The exact stress distribution is found by using Saint Venant theory but the beam equilibrium is ensured by introducing Vlassov bimoment.
Prokić (1990) proposes an original approach using a single warping function in order to analyze both open and closed profiles. The main idea is to discretize a profile into transversal nodes and segments and to develop a new contour warping function based on a linear variation of warping between these transversal nodes. Vlassov hypothesis of no shear strain in mid wall is relaxed for contour warping.
When the hypothesis of cross section non-deformability is relaxed, additional modes called distortional modes are added to the classical ones describing the behavior of a thin-walled beam: tension/compression, bending and torsion. These additional modes are related to the in-plane deformation of a thin-walled cross section. In some early works [Nowinski 1959; Timoshenko 1961 page 211], this phenomenon was identified without being analyzed; Timoshenko presented the bracing in cross sectional planes as a solution to eliminate the distortion. Vlassov (1961, §4) presented an original analysis for the behavior of polygonal thin-walled closed cross sections with deformable contour by representing the displacements in the form of finite series. Later (1977), Trahair illustrated briefly the buckling accentuated by distortion of an I-beam which results in the web bending [Trahair 1995 page 225]. In 1978, Takahashi and Hancock published articles about the distortional behavior. Takahashi (1978, 1980, 1982, 1987, 2003) developed analytical analyses for the distortion of asymmetric open cross sections constituted by the assembly of four or more thin segments without ramifications. He also presented a similar analysis in order to study closed thin walled cross sections (Takahashi 2001, 2003). Other researchers developed different experimental [Hancock 1992; Serrette 1997; Kesti 1999…], analytical [Razapur 1991; Bradford 1992] or numerical methods [Hancock 1997; Ronagh 1996; Bradford 1997, 1998, 1999; Degée 2000…] in order to study the distortion. The 'Generalized beam theory' has been applied extensively during the last years in order to analyze the distortion of prismatic members [e.g. Davies 1998, 2000; Silvestre 2002, 2003, 2004; Gonçalves 2004…]. It is a new approach essentially based on the separation of the behavior of a prismatic member into a series of orthogonal displacement modes.

Connection compatibilities

The carrying capacity and stability of some structures with uniform cross sections are often increased by riveting or welding additional plates in highly stressed parts. The resulting cross section changes abruptly and the stiffness conditions of a connection (flexible, fully or partially rigid) modify the behavior of the structure. Modeling the real connection of cross sections in beam theory is a complicated task since the assembled beams and columns may not have the same centroid and the same torsional center. The non uniform torsional warping (independent, continuous, fully or partially transmitted) is particularly difficult to analyze for beams connected with different orientations. The internal force associated with the warping is auto-equilibrated and cannot be axially projected like other vectors and couples. Different researchers [Gjelsvik 1981; Gunnlaugsson 1982; De Ville 1989; Pedersen 1991; Prokić 1993; Shakourzadeh 1999] consider that warping is partially or totally transmitted by the connection. In general, a transformation matrix links beam degrees of freedom to best ensure the compatibility. Mottershead (1988) proposed to take the most unfavorable conditions. Batoz (1990, page 212) refers to Sharman (1985) for the calculation of transmission coefficients and independent warping coefficients.

1.2.4 Review at the mathematical level

The analytical resolution of all these problems is possible for simple cases but remains inaccessible for most practical applications. The resolution of the differential equations and the calculation of geometrical characteristics for a complete structure require complicated and sometimes impossible calculations. The numerical modeling deals with this complexity by allowing simulations of physical problems. The finite element method is an effective method where the continuum mechanical problem is discretized by a finite number of unknown parameters to be determined by variational formulations. The unknown parameters are the nodal displacements or forces. Some authors [Krajcinovic 1970] used the force method to analyze thin-walled structures but the displacement finite element method is nowadays the most widely used. Complex engineering applications stimulated important developments in this field so that a wide range of different elements have been presented in the literature, depending on several parameters:

-the number of nodes by element and the number of degrees of freedom by node;

-the polynomial or hyperbolic interpolation functions used in order to relate the displacements in any point to the nodal displacement vector.

Usually, polynomial interpolation functions are used in the literature for membrane and bending while the hyperbolic functions are often used for non uniform torsion [Gunnlaugsson 1982; De Ville 1989; Dvorkin 1989; Batoz 1990; Shakourzadeh 1995; …]. A discussion about the use in the literature of the hyperbolic functions is presented in Saadé (2004). Some numerical problems have to be solved, e.g. shear locking that numerically stiffens the structure [Batoz 1990; Wang 2000…].

1.3 Survey of the stability behavior

1.3.1 Increasing need for stability and post-critical behavior analyses

Stability is a fundamental problem in structural mechanics since it must be taken into account in order to ensure the safety against collapse. The collapse must be analyzed for each individual structural member and for the whole structure in order to compute accurately the load-carrying capacity of thin walled structures like beams, columns, frames, trusses, etc… Once the collapse strength is reached, thin-walled members often stop bearing any additional load. A small disturbing force can cause large displacements resulting in a catastrophic collapse. The effects of this elastic instability phenomenon vary from influences on stable equilibrium state up to highly non linear effects as in catastrophic failure processes. The theory of stability or buckling [Gjelsvick 1981; Waszczyszyn 1994;…] deals with critical loads and deformation of structures which are associated with a sudden quantitative change of the structure state at a particular load level by exhibiting previously zero displacement components. An interaction or coupling among bending, twisting and membrane deformations may occur for beam members.

1.3.2 Defining non linear calculations including stability

The difference between linear and non linear analyses lies in the formulation of the equilibrium equations. A linear analysis formulates these equations with respect to the undeformed structure so that strains are evaluated as linear functions of displacement for a linear elastic behavior. In the case of a non linear analysis (including stability), the displacements, rotations and/or deformations are not small and the deformed structure has to be used in order to express the equilibrium equations. The stress, load and deflection cannot be considered to be linear functions of displacements. Thus, with respect to a geometrical non linear behavior, several principal analyses can be distinguished in the literature: first order analysis, bifurcation or eigenvalue buckling analysis, second order analysis, large rotation analysis and large strain analysis. Stability equations, requiring the use of the current configuration of a structure, are nonlinear. Since the complete analysis results in a strongly nonlinear system of equations, the analysis of dominant factors in the geometrical nonlinearities [Hsiao 2000…] justify the selection of one of these different analyses.

First-order and second order terms are used in order to distinguish between analyses that neglect or take into account the actual configuration (influence of deflections upon stresses or P-δ effects). When the non linear equations are linearized, the resulting theory is the so-called linear buckling theory [Murray 1986; Waszczyszyn 1994 §5…]: the structure is assumed to deform linearly till buckling occurs. The terms 'first-order stability analysis' and 'second order stability analysis' are used in the literature in order to distinguish between linearized calculations that lead to the determination of critical loads (i.e. eigenvalue problem) and other non linear computations that compute stresses induced by the generated deflections and reveal the post-buckling response of the structure.

The non linear analysis requires a high level of numerical expertise and experience [Volokh 2001]. In many practical cases [Peng 1998; Chan 1995; Agyris 1978 according to Chen 1991], the assumption of linearity up to the critical load does not give useful results and non linear buckling analysis is necessary. Some researchers [Bakker 2001; Volokh 2001…] propose and discuss how to check the smallness of displacements, rotations and strains in order to choose the related type of geometrical nonlinear analysis. Volokh (2001) presented a numerical criterion which predicts the stage in which the non linear analysis is necessary.

A geometrically non-linear analysis involves complex formulations. Different formulations, theoretically equivalent, have been proposed in the literature: total [Frey 1977; De Ville 1989; Hsiao 2000; …] or updated [Frey 1977; Chen 1991; Yang 1986a,b; Meek 1989; Conci 1990 (see Chen 1991); …] lagrangian formulation and corotational approach [De Ville 1989; Hsiao 2000; …]. Many works in the literature assumed finite rotations such that the strains remain small [Hsiao 2000]. By choosing adapted element sizes, numerical approaches (corotational, natural approaches) validate these assumptions by eliminating and separating rigid body motions from the total displacements. In order to solve the non linear system, several incremental and/or iterative numerical methods are proposed in the literature [Criesfield 1997…].

1.3.3 Historical overview on buckling analyses of thin-walled structures

Early work by Euler (1744) was concerned with flexural buckling of elastic pin ended columns submitted to compression. He used these developments to compute critical loads with various boundary conditions. By the end of the 19th century, many basic elastic problems of structural stability (Kirchhoff 1859; Engesser 1889; …) were solved. According to Nowinski (1959) who gave an interesting survey on most important work on the behavior of thin walled beams, thin-walled open buckling beam theory was influenced by the work of Prandtl and Michell on lateral buckling of narrow beams in 1899. In the 20th century, the stability theory expanded significantly. An important contribution for the analysis of particular buckling problems including the non uniform torsion of open beams was given by Timoshenko [e.g. 1913; 1961 §5…]. Similarly to the major part of his work, his buckling analyses are still consulted today since they offer an important and clear physical way when approaching the subject. Among other researchers, Wagner (1929), Vlassov (1940), Goodier (1942), Koiter (1945) and Nowinski (1947) also contributed to the analytical study of one-member buckling. Wagner investigated in details the torsional buckling of open cross sections. His work is based on a general analysis of non uniform torsion and his creative way is still adopted in present works. In their published and widely used textbooks, Bleich (1952) and Timoshenko (1961) covered analytically a wide range of structural stability problems for columns, continuous beams, trusses and frames in several cases of geometry (changes in cross section), loading and boundary conditions (elastic supports,…). They analyzed the torsional buckling and the lateral buckling of beams and discussed briefly the interaction between bending and torsional buckling. Bleich treated the case of unequal flanges for the elastic and plastic behaviors. Gjelsvik (1981), Murray (1986), Trahair (1993,1995), etc., introduced the basic concepts of the stability theory, detailed the interaction phenomenon and developed the flexural torsional buckling of columns and the lateral torsional buckling of beams. Among nonlinear stability analyses, the problems of strength, general and local stability have been discussed by Bažant (1991) using the classical theory of non uniform torsion of thin-walled beams. During the following years, numerical methods were used for stability analysis [Murray 1986; Trahair 1993; Waszczyszyn 1994]. Intensive research devoted to open thin-walled profiles stability [Ramm 1983; Ronagh 1999; Kwak 2001; Mohri 2003…] were published in both numerical and theoretical procedures taking into account tapered beams [Ronagh 2000; …], joint equilibrium at connections, imperfections [Frey 1977; Bažant 1991; …] and composite cross sections [Bažant 1991, …]. The material and geometrical nonlinear behavior, the dynamic stability, the importance of non conservative systems, etc… were also investigated. Many papers have limited their scope to particular restrictions such as profile with double symmetry [Meek 1998…] or monosymmetry [Kitipornchai 1986; Trahair 1993; Kim 2000; Hsiao 2000; Mohri 2003].

In most early and recent works on general analysis of structural stability, Vlassov hypotheses and kinematics for non uniform torsion have been adopted. The potential energy and the governing equations have been extensively developed in the case of linear elastic stability [Timoshenko 1961; De Ville 1989; Trahair 1993; Mohri 2003;…]. Nevertheless, in the particular case of lateral torsional buckling, current research investigations still aim at elaborating satisfactory practical rules and including them in design codes. Appendix F of the European Code for the Design of Steel Structures (1992) evaluates a critical flexural moment for different cases of profile geometry, loading and boundary conditions. According to Mohri (2000, 2003) and Braham (2001), most of this design rule is inspired from the work of Djalaly (1974). An interesting state of the art related to the formulae of the Eurocode has been given by Braham (2001). It is followed by a comparison between various analytical methods and finite element models for some bisymmetrical and monosymmetrical profiles. By referring to the work of Mohri (2000), Braham emphasizes on the unsafe application of the Eurocode formula for lateral torsional buckling in some cases. This formula and the corresponding data are inappropriate and require adjustments. The carrying capacities resulting from numerical and experimental analyses are shown to be lower than those resulting from Eurocode formula [Mohri 2000, 2003; Braham 2001; Villette 2002; Galéa 2002…]. This problem is probably due to limited availability of numerical techniques at the time of earlier researchers [Djalaly 1974]. Because of the general tendency to increase the slenderness, further research is required for safe and economic calculations and for more accurate design codes.

1.3.4 Analytical and numerical methods used for stability problems

Starting from the total potential energy expression in linear stability, most developments in the literature approximate the buckling loads by elaborating the equilibrium equations corresponding to the buckled state. Different methods are used in the literature: Ritz, Galerkin, finite differences, finite integral (Chan 2001)… The first two methods are extensively used in the literature in order to compute analytically buckling loads. Rayleigh-Ritz method is based on the stationary conditions of the total potential energy while Galerkin method is based on the variational formulation of equilibrium equations. Both methods are based on assumed deflected shapes and therefore are limited to simple problems where the deflected shape can be accurately assumed [Timoshenko 1961; Trahair 1993 §3, Murray 1986; De ville 1989 §4]. The displacement modes in bending and torsion are approximated by analytical functions and the solution depends on this choice. The approximation of a sinusoidal function is suitable for the simple case of uniform moment distribution along a beam with a bisymmetrical cross section. However, for general loading and arbitrary profiles, the displacements must be approximated by sinusoidal series. However, in the EC3 and previous works [Djalaly 1974;…], the analytical analyses based on Vlassov warping function used only one sinusoidal term for the displacement functions. Recent researchers [Mohri 2003; Braham 2001…] emphasize on the inaccurate results obtained by this approach for general asymmetrical cases of loading and geometry.
Since the advent of the computer in the 1950's, research in the numerical stability field has developed extensively: [Frey 1977; De Ville 1989; Trahair 1993 §4 and almost all recent works]. The growth of computer power combined with the use of the discretization concept and the energy method induced intensive recent developments of non linear numerical methods. The finite element method presents many advantages: generality and flexibility for assigning properties, configuration, boundary and load conditions.

1.4 Original contributions of the present work

This paragraph aims at briefly defining the problem statement and at identifying the present work in the previously reviewed research state of the art (§1.2). The main purpose of this thesis is to formulate a unified approach for modeling the behavior of elastic 3D structures consisting of thin walled beams and columns with arbitrary shaped cross sections, including the important influence of warping due to non uniform torsion, to shear forces and to distortion.
The present research work builds itself upon previous and ongoing work on 3D thin walled structure analyses. Particularly, it improves Prokić kinematic formulation (1990, 1993, 1994, 1996) in order to analyze the non uniform torsion of arbitrary thin walled profiles. Rather than using different warping functions for open and closed cross sections (Vlassov or Benscoter theories) as it is extensively done in the literature [Nowinski 1959; Murray 1986; Mohri 2003 …], the present work aims mainly at adapting and validating a single approach to model the behavior of 3D thin walled beam structures. The following first three investigations (1-3) are provided relatively to Prokić work. Resulting from an in-depth examination of Prokić theoretical and practical research limitations, they summarize the original work of the present research in order to implement correctly a thin walled beam model.

1- In a first and global examination of Prokić work, it is surprising to find an unjustified statement that the introduction of the notion of shear center is not necessary. While analyzing the torsional warping of open asymmetrical profiles, no distinction was made between the centroid and the shear center [1990 page 73, 75 & 76; 1993; 1994; 1996]. It is therefore necessary to find out if the proposed kinematic formulation assumes a rotation of the cross section around the centroid which is inadmissible for asymmetrical and even monosymmetrical profiles. The necessity of including the shear center in order to uncouple torsional and bending effects is to be investigated.

2- A more detailed study of Prokić work shows that the presented combination of warping degrees of freedom is not completely associated with the torsional warping of a thin-walled beam structure. Warping degrees of freedom are coupled with membrane and bending degrees of freedom even in linear stiffness matrix (e.g. 1990 page 28). Computations show that the stiffness matrix is not definite positive. In his thesis and published papers, the numerical results have been limited to pure torsional problems. Therefore, it is necessary to investigate the feasibility of an implementation of Prokić formulation in order to study the general behavior of a 3D thin-walled structure, e.g. the flexural-torsional behavior due to a transversal load acting on a asymmetrical cross sections. The possibilities of adding additional kinematic relations in order to restrain the warping degrees of freedom to non uniform torsional behavior (as in Vlassov and Benscoter theories) must be found out. In the case of pure stretching or bending, does Prokić formulation detect undesirable warping (i.e. warping associated with pure tension/compression or flexure)?

3- After finishing the first two investigations and after demonstrating the feasibility of a correct implementation of the previously discussed kinematic formulation, another important unfinished task in Prokić published research is the numerical stability analysis. In his thesis and published papers, Prokić presented the general guideline for non linear analyses using the finite element method without presenting developed details or numerical results. It was noticed in a recent review paper about non linear behavior and design of steel structures [Chan 2001], that, in Prokić work, ‘non linear frame analysis allowing for warping and bimoment has not yet been developed to a stage of practical use, even for relatively simple frames’. Therefore, more investigations are needed in order to analyze the stability of thin-walled structures.

The following investigations (4-9) present general original issues in the study of thin-walled analyses:

4- An interesting task is to investigate the influence of warping induced by shear forces in bending and particularly how it is possible to apply Prokić formulation in order to model this behavior. Is a complete study including warping due to bending shear forces important for the behavior analysis of thin-walled structures? In the case where the modified Timoshenko theory gives satisfying bending results, it is interesting to determine the shear correction factor for arbitrary profiles. Within the same guiding concept defined above, it is interesting to investigate this analysis by keeping the same original unified approach for arbitrary profiles.

5- In the literature, the stability analysis is restricted to the case of beams or columns with open cross sections using Vlassov warping function. This approach is justified by the high torsional and bending stiffness of a closed cross section, so that collapse by local buckling or yielding is more critical than collapse by global instability. However, it is interesting to investigate structural elements with profiles which are neither totally open, nor fully closed. e.g. an open profile with one relatively small cell compared to the profile dimensions.

6- An important contribution to thin walled beam analyses is to adapt Prokić warping function in order to analyze some distortional modes which involve the deformation of the entire profile inducing a non local beam behavior.

7- The physical and pure kinematical separation between different mechanical effects (tension/compression, bending, torsion and distortion) is achieved in this work by imposing restraining conditions on the displacement field. This kinematical step, usually achieved in the literature by imposing restraining conditions on equilibrium equations and stresses, has the advantage of presenting a correct and well-defined kinematical formulation without any restriction on the material law.

CHAPTER 2. BACKGROUND INFORMATION

2.1 Beams with bending shear effects

Beam analyses have been performed by implementing different kinematic formulations for bending shear deformation. The developments given hereafter are limited to the case of elastic behavior, where E and G are respectively Young's and shear modulus. The principal axes are used to uncouple bending effects (xy & xz). For simplicity only, the bending of beams in the (xz) plane is analyzed in this session. Similar developments can be identically made for bending in the (xy) plane.

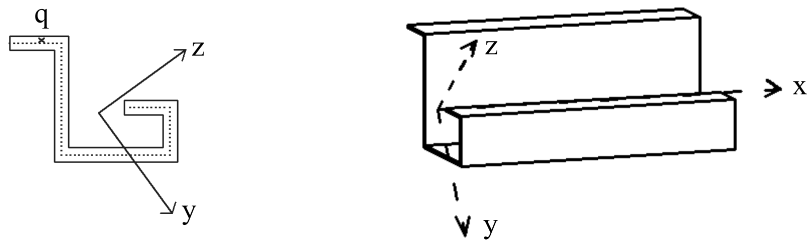

Figure 2.1 Principal axes of a beam profile

2.1.1 Bernoulli

The simplest beam theory is the Euler-Bernoulli theory in which it is assumed that the cross section remains planar and normal to the longitudinal axis after bending deformation. The rotation angle of the cross section is thus equal to the slope ($w_{,x}$). This assumption neglects transverse shear.
This beam theory is based on the displacement field:

$$\begin{Bmatrix} u_q \\ v_q \\ w_q \end{Bmatrix} = \begin{Bmatrix} -zw_{,x} \\ 0 \\ w \end{Bmatrix} \tag{2.1}$$

where q(x,y,z) is an arbitrary point of the beam (figure 2.1).

and the expression of linear part of the strain tensor is reduced to:

$$\begin{Bmatrix} \varepsilon_x \\ 2\varepsilon_{xy} \\ 2\varepsilon_{xz} \end{Bmatrix} = \begin{Bmatrix} u_{q\ ,x} \\ v_{q\ ,x} + u_{q\ ,y} \\ w_{q\ ,x} + u_{q\ ,z} \end{Bmatrix} = \begin{Bmatrix} -zw_{,xx} \\ 0 \\ 0 \end{Bmatrix} \tag{2.2}$$

The strain energy per unit length of the beam is given by:

$$U = \frac{1}{2}\int_A E\varepsilon_{xx}^2 dA \tag{2.3}$$

where A is the cross-sectional area. The strain energy associated with the shearing strain is zero.

The bending moment can be expressed in terms of generalized displacements and the shear force must be found from the equilibrium equation (2.4). The shear stresses, strains and shear internal forces ($\tau_{xz} = G\varepsilon_{xz}$, $T_z = \int_A \tau_{xz} dA$) cannot be found from the kinematic formulation (2.1, 2.2), because if done so, they would be zero.

$$M_y = \int_A z\sigma_x dA = E\int_A z\varepsilon_x dA = -EI_y w_{,xx}$$

$$T_z = M_{y,x} \tag{2.4}$$

where EI_y is the bending stiffness of the beam.

2.1.2 Timoshenko

The Timoshenko beam theory is based on the following displacement field:

$$\begin{Bmatrix} u_q \\ v_q \\ w_q \end{Bmatrix} = \begin{Bmatrix} z\theta_y \\ 0 \\ w \end{Bmatrix} \tag{2.5}$$

where the longitudinal displacement u_q is no more proportional to the gradient $w_{,x}$ of transverse displacement but to a new parameter θ_y that denotes the rotation of the cross section. The normality assumption of Bernoulli theory is thus relaxed and a constant transverse shear strain over the cross section ($w_{,x} + \theta_y$) is assumed.

$$\begin{Bmatrix} \varepsilon_x \\ 2\varepsilon_{xy} \\ 2\varepsilon_{xz} \end{Bmatrix} = \begin{Bmatrix} u_{q\,,x} \\ v_{q\,,x} + u_{q\,,y} \\ w_{q\,,x} + u_{q\,,z} \end{Bmatrix} = \begin{Bmatrix} z\theta_{y,x} \\ 0 \\ w_{,x} + \theta_y \end{Bmatrix} \tag{2.6}$$

The strain energy includes a term associated with the shearing strain:

$$U = \frac{1}{2}\int_A (E\varepsilon_{xx}^2 + 4G\varepsilon_{xz}^2) dA \tag{2.7}$$

The bending moment and the shear force can be expressed in terms of generalized displacements:

$$M_y = \int_A z\sigma_x dA = EI_y\theta_{y,x}$$

$$T_z = \int_A \tau_{xz} dA = k_y GA(\theta_y + w_{,x}) \tag{2.8}$$

where k_y is the shear correction factor.

It is important to note that, from the kinematics (2.5&2.6) and the constitutive equations, shear stresses are found to be uniform over the cross section (2.8, k_y = 1). However, when a cross-section is subject to a shear force T_z, the shear strain $2\varepsilon_{xz} = \tau_{xz}/G$ should vary through the height of the cross section and vanish at free edges. Consequently, the cross section does not remain plane: it warps. The warping is the largest at the neutral axis and vanishes at the extreme fibers. This physical behavior is not compatible with the kinematics (2.5) that assumes a constant transverse shear strain distribution (2.6) and thus constant shear stress distribution. Therefore, the Timoshenko theory requires corrections. To compensate the fact that the displacement field violates the 'no shear' boundary condition at the edges of open profiles, approximate modifications are introduced by a shear correction factor k_y (equation 2.8).

Shear correction factors:

When the above described warping varies along the longitudinal (x) axis, the associated deformation increases the bending transversal displacements. These shear effects on deflection, which are significant for bending of short beams, are described by the shear correction factor k_y. In the case of loading in the xz plane, this factor can be evaluated by an energy approach ([Frey, 2000, page 193]; [Pilkey, 1994, page 28]; [Batoz, 1990, page 62]…):

$$k_y = \frac{A}{I_y^2} \int_A \left(\frac{S_y}{t} \right)^2 dA \tag{2.9}$$

t is the thickness and S_y is the first moment in Jouravski formulation.

The shear correction factor may be viewed as the ratio of total beam cross-sectional area to the effective area resisting shear deformation. Equation (2.9) gives an approximate value [Pilkey, 1994, page 28]. Other determinations of shear correction factors can be made by using the theory of elasticity ([Cowper, 1966]…). The inverse of the shear correction factor, called the shear deflection constant, is often required as an input in general purpose finite element analysis software. It is important to note that the computation of the shear correction factor necessitates the determination of the first moment distribution over the profile contour by choosing appropriate methods usually different for open and closed cross sections ([Calgaro, 1988, Chapter 2]…)

2.1.3 High-order theories

In high-order theories, the planar assumption is not kept. The following Reddy-Bickford displacement field was used by Wang [2000, page 14]:

$$\begin{Bmatrix} u_q \\ v_q \\ w_q \end{Bmatrix} = \begin{Bmatrix} z\theta_y - \alpha z^3(\theta_y + w_{,x}) \\ 0 \\ w \end{Bmatrix} \tag{2.10}$$

where $\alpha = 4/(3h^2)$ for rectangular cross sections.

The strain-displacement relations of Reddy-Bickford beam theory are:

$$\begin{Bmatrix} \varepsilon_x \\ 2\varepsilon_{xy} \\ 2\varepsilon_{xz} \end{Bmatrix} = \begin{Bmatrix} z\theta_{y,x} - \alpha z^3(\theta_{y,x} + w_{,xx}) \\ 0 \\ w_{,x} + \theta_y - \beta z^2(\theta_y + w_{,x}) \end{Bmatrix} \tag{2.11}$$

where $\beta = 4/h^2$ for rectangular cross sections.

Since the transverse shear strain is quadratic through the height of the beam and satisfies the 'no shear' boundary condition (values of α and β depend on the profile geometry), there is no shear correction factor in the Reddy-Bickford beam theory. The boundary conditions and the stress resultants for this theory differ from the others theories. Wang et al. [2000] developed the complicated equilibrium equations, generated solutions for some simple examples of rectangular cross sections, and developed a finite element model free from shear locking phenomenon. The deflections, slopes/rotations, shear forces and bending moments resulting from this theory are compared to those of Bernoulli and Timoshenko (available in most text books on mechanics of materials). Simple cases of simply supported beam with rectangular cross sections are analyzed analytically in the following paragraph and in chapter 4 while the associated numerical computations are done in chapter 5.

2.1.4 Applications

The theories presented in (§2.1.1, §2.1.2 & §2.1.3) are used hereby to evaluate the influence of shear deformation effects on the displacement of simply supported beams: Bernoulli beam theory (BBT), Timoshenko beam theory (TBT) that could be modified by introducing the shear correction factor (TBTM) and high order theories as Reddy-Bickford beam theory (RBT) [Wang, 2000].

Simply supported beam under uniformly distributed load

Consider a simply supported beam under uniformly distributed load q_0. Deriving the equilibrium equations with <u>Bernoulli</u> kinematic formulae (starting from equations 2.1-2.4), the maximal deflection of the Euler-Bernoulli beam (BBT) is:

$$w_{BBT} = \frac{5}{384}\frac{q_0 L^4}{EI} \tag{2.12}$$

By doing the same calculations for <u>Timoshenko</u> beam theory (starting from equations 2.5-2.8), the maximal deflection of the Timoshenko beam (TBT) is modified by introducing (equation 2.8) the shear correction factor k (TBTM):

$$w_{TBTM} = \frac{5}{384}\frac{q_0 L^4}{EI} + \frac{1}{8}\frac{q_0 L^2}{kGA} \tag{2.13}$$

The shear correction factor for a rectangular cross section is 5/6 (equation 2.9, Cowper 1966, Pilkey 1994…).

In case of <u>higher order theories</u> [Wang, 2000, page 33], the expression of the deflection is much more complicated :

$$w_{RBT} = \frac{5}{384}\frac{q_0 L^4}{EI} + \frac{q_0 \mu}{\lambda^4}\frac{\hat{D}_{xx}}{\hat{A}_{xz} D_{xx}}\left[\tanh(\frac{\lambda L}{2})\sinh(\lambda x) + \cosh(\lambda x) + \frac{\lambda^2}{2} x(L-x) - 1\right] \tag{2.14}$$

Where, for a rectangular cross section,

$$\mu = \frac{3h^2}{4}\frac{\hat{A}_{xz}\hat{D}_{xx}}{(F_{xx}\hat{D}_{xx} - \hat{F}_{xx} D_{xx})} \qquad \lambda^2 = \frac{3h^2}{4}\frac{\overline{A}_{xz} D_{xx}}{(F_{xx}\hat{D}_{xx} - \hat{F}_{xx} D_{xx})}$$

$$(A_{xx}, D_{xx}, F_{xx}, H) = E\int(1, z^2, z^4, z^6)dA \qquad (A_{xz}, D_{xz}, F_{xz}) = G\int(1, z^2, z^4)dA$$

$$\hat{D}_{xx} = D_{xx} - \frac{4}{3h^2}F_{xx} \qquad \hat{A}_{xz} = A_{xz} - \frac{4}{h^2}D_{xz}$$

$$\hat{F}_{xx} = F_{xx} - \frac{4}{3h^2}H_{xx} \qquad \hat{D}_{xz} = D_{xz} - \frac{4}{h^2}F_{xz} \qquad \overline{A}_{xz} = \hat{A}_{xz} - \frac{4}{h^2}\hat{D}_{xz} \tag{2.15}$$

For a simply supported beam with a rectangular cross section submitted to uniform loading, the effect of shear deformation beam is thus proportional to the square of the ratio height to length:

$$\frac{w_{TBTM} - w_{BBT}}{w_{BBT}} = 1.92\frac{h^2}{L^2}(1+\upsilon) \tag{2.16}$$

Figure 2.2 shows numerical results from the application of (2.12), (2.13) and (2.14) for different values of length to height ratio of the simply supported beam (L/h). E=210GPa, G= 84GPa. The TBTM is taken as a reference and the difference between its results and those of other theories is plotted in figure 2.2. It should be noted that the curve (RBT) is nearly on the horizontal axis. RBT and TBTM theories give similar results for this simple example. The difference is 0.001% as value for L/h = 8 and 9.10^{-07} % for L/h = 50.

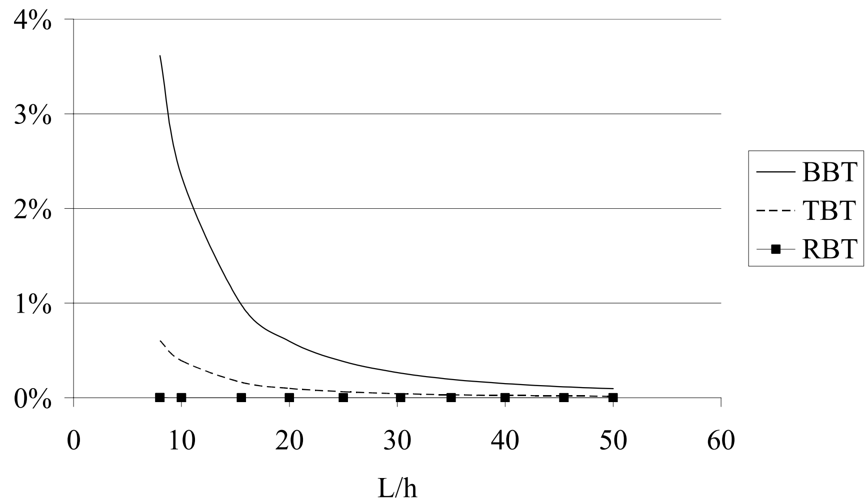

Figure 2.2 Difference between TBTM and (BBT, TBT and RBT) for maximal deflection of rectangular beams submitted to a uniformly distributed load

Simply supported beam with concentrated force P applied at mid span

Similarly, for a concentrated force P applied at mid span of the beam:

$$w_{BBT} = \frac{1}{48}\frac{PL^3}{EI} \tag{2.17}$$

$$w_{TBTM} = \frac{1}{48}\frac{PL^3}{EI} + \frac{1}{4}\frac{PL}{kGA} \tag{2.18}$$

$$\frac{w_{TBTM} - w_{BBT}}{w_{BBT}} = 2.4\frac{h^2}{L^2}(1+\upsilon) \tag{2.19}$$

$$w_{RBT} = -\frac{1}{96}\frac{PL^3}{D_{xx}} + \frac{P\mu}{2\lambda^3}\frac{\hat{D}_{xx}}{\hat{A}_{xz}D_{xx}}(-\cosh(\lambda L)+1)\frac{\tanh(\frac{\lambda L}{2})+1}{\sinh(\lambda L)+\cosh(\lambda L)+1}$$
$$+\frac{1}{32}\frac{Pl}{D_{xx}\hat{A}_{xz}\lambda^2}(\lambda^2 L^2 \hat{A}_{xz} + 8\mu\hat{D}_{xx}) \tag{2.19'}$$

As it is expected from equation (2.19), the difference between (BBT) and (TBTM) depends mostly on the square of the ratio L/h.

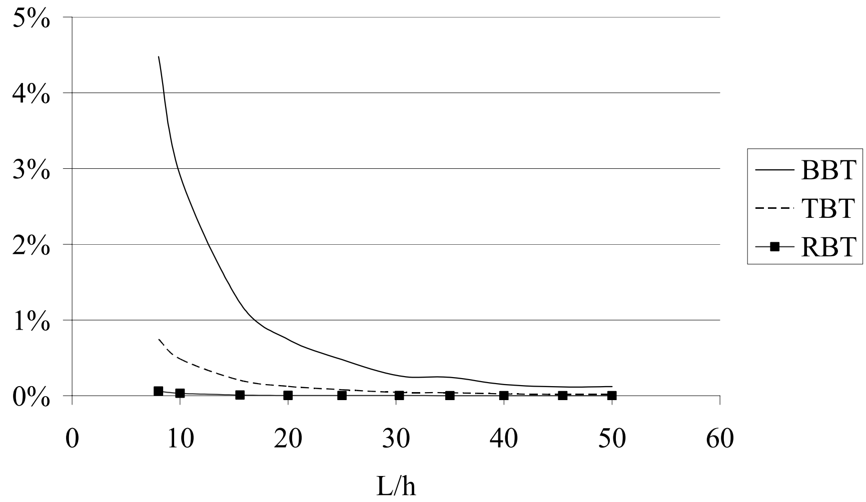

Figure 2.3 Difference between TBTM and (BBT, TBT and RBT) for maximal deflection of rectangular beams submitted to a concentrated force P at mid span

It can be seen in figure 2.3 (where E=210GPa, G= 84GPa) that, for rectangular cross sections, neglecting shear deformation effects will lead to errors superior to 5% for short beams where h/L > 1/8. The curve (RBT) is nearly on the horizontal axis. RBT and TBTM give also similar results for this simple example. The difference between the two theories is 0.061% for L/h = 8 and 0.00026% for L/h = 50.

A numerical application is considered for a simply supported beam (L = 2m) with rectangular cross section 0.002 x 0.25m submitted to a concentrated force P = 10kN. The shear force and bending moment distributions [equations (2.4) and (2.8)] along the span coincide for TBT and BBT. The rotation computed with TBT theory is equal to the slope of BBT ($4.57\ 10^{-03}$ rad). However, for RBT, the rotation ($\theta_y = 4.54\ 10^{-03}$) is different from the slope ($w' = 4.71\ 10^{-03}$). This is due to the higher-order theory where both functions (θ_y and w') along z describe the quadratic nature of the warped cross section (equation 2.11). It is interesting to note that for statically indeterminate structures, different bending moments and shear forces result from (BBT), (RBT) and (TBT) since displacements (and hence stress resultants) are not the same for these theories.

Comparison of shear deformation effects for some thin walled profiles

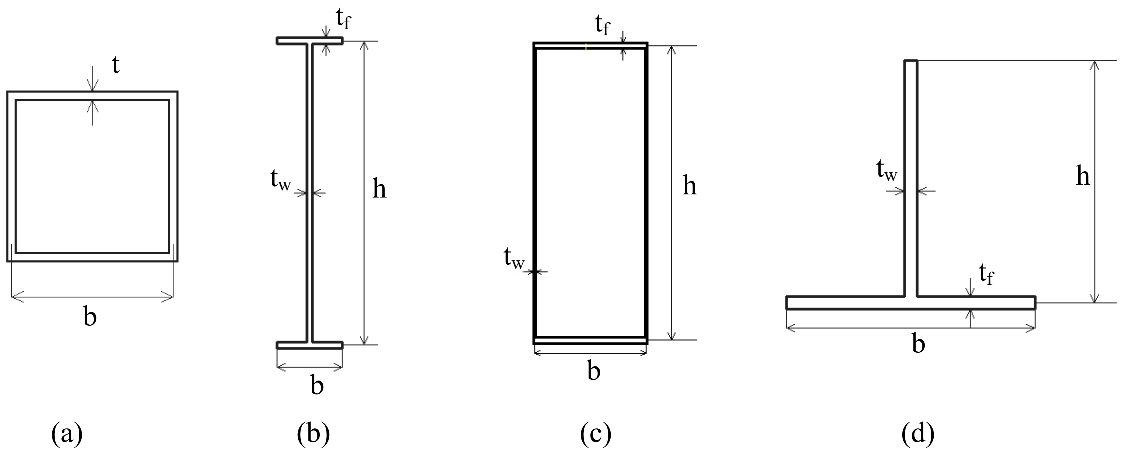

Figure 2.4: (a) Square tubular cross section (b = 0.1m, t = 0.001m), (b) open I cross section (b = 0.08m, t_f = 0.01m, h = 0.38m, t_w = 0.0035m), (c) tubular cross section (b = 0.3m, t_f = 0.008m, h = 0.8m, t_w = 0.001m) and (d) T cross section (b = 0.4m, t_f = 0.01m, h = 0.4m, t_w = 0.01m)

The influence of shear bending effects is analyzed for different cross sections (a), (b), (c) and (d) of a simply supported beam where E=210GPa, G= 84Gpa. Two loading cases are considered: uniformly distributed load (table 2.1 and figure 2.5a) and concentrated load at mid length (table 2.2 and figure 2.5b). Shear correction factors are calculated for the cross profiles in figure 2.4 by using the results of Cowper [Cowper, 1966] who considered the influence of geometrical and material properties of the cross section. The difference between the modified Timoshenko and Bernoulli deflections calculated ((2)/(1)) in tables 2.1 and 2.2 show the influence of shear deformations (2) by comparing it to bending moment effects (1) on the maximal deflection. The difference between simple and modified Timoshenko deflections ((3)/(1)) calculated in the seventh column of tables 2.1 and 2.2 show the influence of the shear correction factor. It could be seen from table 2.2 that short beams are sensitive with respect to shear deformation effects. The influence of shear deformation on deflections reaches 10% for L/h smaller than 10. In general, this percentage is smaller for a uniformly applied loading (table 2.1) than for a concentrated load (table 2.2). In particular, the influence is smaller for the T section than for the I and tubular cross sections in figure 2.4. It could be concluded that the deflection due to shear deformations is small compared to the deflection due to flexure.

Table 2.1 Shear deformation effects on the maximal deflection [m] of beams (Figure 2.4) submitted to a unit uniformly distributed load

Profile	L/h	w_{TBTM} (1)	w_{TBTM}-w_{BBT} (2)	(2)/(1)	w_{TBTM}-w_{TBT} (3)	(3)/(1)
(a)	20	1.57E-06	3.47E-08	*2.2%*	1.97E-08	*1.3%*
(b)		2.76E-06	6.07E-08	*2.2%*	3.23E-08	*1.2%*
(c)		5.25E-06	1.15E-07	*2.2%*	8.60E-08	*1.6%*
(d)		1.90E-06	2.38E-08	*1.2%*	1.19E-08	*0.6%*
(a)	15	5.05E-07	1.95E-08	*3.9%*	1.11E-08	*2.2%*
(b)		9.08E-07	3.41E-08	*3.8%*	1.81E-08	*2.0%*
(c)		1.73E-06	6.44E-08	*3.7%*	4.84E-08	*2.8%*
(d)		6.16E-07	1.34E-08	*2.2%*	6.68E-09	*1.1%*
(a)	10	1.05E-07	8.68E-09	*8.3%*	4.92E-09	*4.7%*
(b)		1.88E-07	1.52E-08	*8.1%*	8.06E-09	*4.3%*
(c)		3.57E-07	2.86E-08	*8.0%*	2.15E-08	*6.0%*
(d)		1.25E-07	5.94E-09	*4.8%*	2.97E-09	*2.4%*
(a)	8	4.48E-08	5.56E-09	*12.4%*	3.15E-09	*7.0%*
(b)		8.04E-08	9.71E-09	*12.1%*	5.16E-09	*6.4%*
(c)		1.53E-07	1.83E-08	*12.0%*	1.38E-08	*9.0%*
(d)		5.26E-08	3.80E-09	*7.2%*	1.90E-09	*3.6%*
(a)	4	3.84E-09	1.39E-09	*36.1%*	7.88E-10	*20.5%*
(b)		6.84E-09	2.43E-09	*35.5%*	1.29E-09	*18.8%*
(c)		1.30E-08	4.58E-09	*35.3%*	3.44E-09	*26.5%*
(d)		4.00E-09	9.51E-10	*23.8%*	4.75E-10	*11.9%*

Table 2.2 Shear deformation effects on the maximal deflection [m] of beams (Figure 2.4) submitted to a unit concentrated load at mid span

Profile	L/h	w_{TBTM} (1)	w_{TBTM}-w_{BBT} (2)	(2)/(1)	w_{TBTM}-w_{TBT} (3)	(3)/(1)
(a)	20	1.26E-06	3.47E-08	*2.8%*	1.97E-08	*1.6%*
(b)		5.97E-07	1.60E-08	*2.7%*	8.49E-09	*1.4%*
(c)		5.40E-07	1.43E-08	*2.7%*	1.08E-08	*2.0%*
(d)		3.87E-07	5.94E-09	*1.5%*	2.97E-09	*0.8%*
(a)	15	5.44E-07	2.60E-08	*4.8%*	1.48E-08	*2.7%*
(b)		2.57E-07	1.20E-08	*4.7%*	6.37E-09	*2.5%*
(c)		2.32E-07	1.07E-08	*4.6%*	8.06E-09	*3.5%*
(d)		1.65E-07	4.46E-09	*2.7%*	2.23E-09	*1.3%*
(a)	10	1.71E-07	1.74E-08	*10.2%*	9.85E-09	*5.8%*
(b)		8.06E-08	7.98E-09	*9.9%*	4.24E-09	*5.3%*
(c)		7.28E-08	7.16E-09	*9.8%*	5.38E-09	*7.4%*
(d)		5.06E-08	2.97E-09	*5.9%*	1.48E-09	*2.9%*
(a)	8	9.24E-08	1.39E-08	*15.0%*	7.88E-09	*8.5%*
(b)		4.36E-08	6.39E-09	*14.7%*	3.40E-09	*7.8%*
(c)		3.94E-08	5.73E-09	*14.5%*	4.30E-09	*10.9%*
(d)		2.68E-08	2.38E-09	*8.9%*	1.19E-09	*4.4%*
(a)	4	1.68E-08	6.94E-09	*41.4%*	3.94E-09	*23.5%*
(b)		7.84E-09	3.19E-09	*40.7%*	1.70E-09	*21.6%*
(c)		7.07E-09	2.86E-09	*40.5%*	2.15E-09	*30.4%*
(d)		4.24E-09	1.19E-09	*28.1%*	5.94E-10	*14.0%*

The same results are illustrated in figure (2.5) where the difference between TBTM and BBT is shown for a uniform distributed load and a mid-length applied concentrated load. It could be seen that the amount of shear effect of the T section (d) is different from the others. The curves corresponding for (a), (b) and (c) nearly coincide. Again, it is noted that the shear effects are important for short beams.

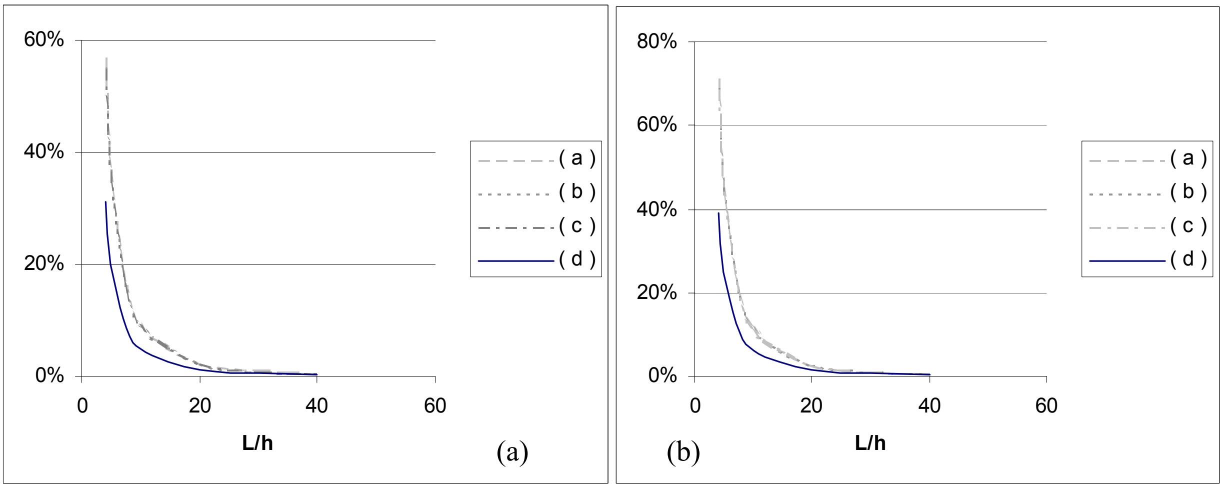

Figure 2.5 Variation [$(w_{TBTM}-w_{BBT})/\ w_{BBT}$] of shear deformation effects on maximal deflection [m] of beams (Figure 2.4) submitted to a uniformly distributed load (a) and to a unit concentrated load at mid length (b)

2.2 Uniform and non uniform torsion (Mixed torsion)

2.2.1 General overview

The torsional behavior of a beam is mainly described by twisting angles (θ_x) of its cross sections with respect to the longitudinal axis (x) passing through the torsional center C (y_c, z_c). The angle of twist per unit length at a particular position is calculated as a function of the torsional moment M_x resulting from the applied load. However, when submitted to a torsional deformation, a cross section does not remain planar: it generally warps. This warping is measured by an axial displacement u.

The total external torque is balanced by the torsional moment M_x that includes:

- a first part (M_x^{st}), well known in the engineering text books of Strength of Materials, characterizes the uniform torsion of Saint Venant and is presented in the paragraph 2.2.2;
- a second part (M_x^{ω}), caused by the prevented warping of the cross section, characterizes the non uniform torsion and is presented in paragraph 2.2.3.

If both M_x^{st} and M_x^{ω} are different from zero, the torsion is known to be mixed:

$$M_x = M_x^{st} + M_x^{\omega} \tag{2.20}$$

2.2.2 de Saint Venant torsion (uniform torsion)

Assumption

The particular case of uniform torsion (Saint Venant) is based on the following assumption:

HYPSV: the warping (u) is constant along the longitudinal axis (x) of the beam.

Kinematics

The axial displacement of any point q of the cross section under Saint Venant torsion is:

$$u = -\ \omega(y,z)\ \theta_{x,x}(x) \tag{2.21}$$

where $\theta_{x,x}$ is the rate of twist and $\omega(y,z)$ is the warping function of the cross section.

The expression of the displacement field is:

$$\begin{Bmatrix} u_q \\ v_q \\ w_q \end{Bmatrix} = \begin{Bmatrix} -\boldsymbol{\omega}\theta_{x,x} \\ -(z - z_C)\theta_x \\ (y - y_C)\theta_x \end{Bmatrix} \tag{2.22}$$

When the assumption HYPSV (uniform warping along x) is adopted, $\omega\theta_{x,x}$ is assumed to be a constant rate with respect to x. Thus, its derivative $\omega\theta_{x,xx}$ vanishes and the linear strain vector deduced from (2.22) is:

$$\begin{Bmatrix} \varepsilon_x \\ 2\varepsilon_{xy} \\ 2\varepsilon_{xz} \end{Bmatrix} = \begin{Bmatrix} 0 \\ -(\boldsymbol{\omega}_{,y} + z - z_c)\theta_{x,x} \\ (-\boldsymbol{\omega}_{,z} + y - y_c)\theta_{x,x} \end{Bmatrix} \tag{2.23}$$

Equilibrium equation

The torsional equation (2.26) is usually deduced from equilibrium considerations. Alternatively, the principle of virtual work can be used with Hooke's law and strain expressions (2.23). The differential equilibrium equation (2.26), relating the rate of twist $\theta_{x,x}$ to the torsional moment M_x (2.24) and to the torsional stiffness GK (2.25), is obtained after integrating and isolating the virtual twisting angle θ_x^*. The torsional resultant is found to be:

$$M_x = \int_A [(y - y_C)\tau_{xz} - (z - z_C)\tau_{xy}]dA \tag{2.24}$$

Let the torsional constant K be given by the expression (2.25):

$$K = \int_A [(-\boldsymbol{\omega}_{,z}(y - y_C) + \boldsymbol{\omega}_{,y}(z - z_C) + (y - y_C)^2 + (z - z_C)^2]dA \tag{2.25}$$

then

$$\theta_{x,x} = \frac{M_x}{GK} \tag{2.26}$$

Equation (2.25) shows that the cross section warping influences the value of K. The warping function (ω) must first be computed in order to determine the torsional stiffness and to solve the Saint-Venant torsional problem. The evaluation of ω is different for each cross section and depends on the boundary conditions of the shear stresses and on the geometrical shape of the profile, especially whether the cross section is open or closed. Batoz et al. [1990, page 170] developed approximate expressions for the warping function (ω) of some thin-walled cross sections so that K can be explicitly evaluated. However, they insisted on the fact that, for open thin walled profiles, approximated values of (ω) lead to an incorrect value of K if directly substituted in (2.25). Deducing the torsional constant from explicit values of $\boldsymbol{\omega}$ is detailed in [Batoz, 1990, page 171].

The Saint Venant theory (with assumption HYPSV) is exact in the case of uniform torsional moment distribution without restrained warping of the cross sections. Similarly, for some particular profiles (◎, +, …) which, due to their radial symmetry, do not warp, the Saint Venant theory of torsion is always exact, even if the torsional moment distribution is not uniform. For other particular geometries (⊥, ∠, …), the contour warping vanishes and, if the thickness warping is neglected, the de Saint Venant theory is used. For all these particular cases, equation (2.26) solves exactly the torsional problem. In other general cases, the Saint Venant torsional theory describes only a part of the problem (equation 2.20) and the term M_x in (2.26) must be substituted by M_x^{st}:

$$\theta_{x,x} = \frac{M_x^{st}}{GK} \tag{2.26'}$$

Stress computations

In this case of pure uniform torsion, the beam is only twisted and each thin walled member resists to this uniform torsion by components of shear stresses τ_{xs}^{st}. s is the coordinate along the contour profile line. There are no longitudinal stresses σ_x directly associated with this torsion. The behavior depends to a large extent on the cross sectional geometry and specifically, whether the section is open or closed. When the cross section is an open profile, shear stresses due to the Saint Venant torsion (τ_{xs}^{st}) vary linearly through the thickness of the walls with zero value on the midline. The maximal value of these stresses, which occurs at upper and inner skins, is proportional to the torsional moment M_x^{st} and to the thickness 'e' and is inversely proportional to the uniform torsional stiffness K.

$$K = \sum \frac{1}{3} l_i e_i^3 \tag{2.27}$$

$$\tau_{xs}^{st} = \frac{M_x^{st}}{K} e \tag{2.28}$$

When the cross section is a closed profile consisting of one or more cells, uniform shear stresses flow through the periphery without changing sign across the thickness of the thin walls. The stiffness is calculated from Bredt formulae ([Kollbrunner, 1970], [Murray, 1986], …). Equations (2.29) are given in case of unicellular cross sections:

$$K = \frac{4A^2}{\oint \frac{ds}{e}} \tag{2.29}$$

$$\tau_{xs}^{st} = \frac{M_x^{st}}{2Ae} \tag{2.30}$$

where A is the area enclosed by the cell. The mean value of these shear stresses at a point of the contour is proportional to the torsional moment M_x^{st} and inversely proportional to the thickness and to the area limited by the contour of the cross section.

Theoretically, a closed profile resists to torsion by a global stiffness (2.29) in case of unicellular profile) related to the circulation of a constant flow along contour (2.30) and by a local stiffness specific to each element of the section (2.27) as if the beam was constituted by the assembly of longitudinal strips. For thin profiles, the local stiffness is negligible when compared to the global one.

The associated stresses whose distribution is linear through the thickness (equation 2.28) are also negligible when compared to those associated to the global stiffness (2.30). At this stage, it is important to emphasize the fact that the behavior of closed profiles (comprising one or more cells) constitutes a problem entirely different from that of open cross sections. Many studies ([Kollbrunner, 1970], [Murray, 1986]…) presented detailed descriptions of the calculation of the torsional stiffness and the stress distribution depending on the type of thin-walled profiles (open or closed). The basic formulae are found in text books on Strength of Materials and are commonly used by engineers in beam analyses regardless of the validity of their application. An interesting analogy between non uniform torsion and shearing flexure has been highlighted by De Ville [1990, page 3.54]), showing the similitude between analyses including shear deformation effects and non uniform torsional warping effects.

Application: uniform torsion of open and closed profiles
Two thin cylindrical tubes (figure 2.6) with identical dimensions (radius = 200mm and thickness = 8mm) differ by a slit so that the cross section of the second tube is an open profile. An exterior torque induces uniform torsion for both closed and open cross sections with the same torsional moment distribution. The strength and stiffness of both open and closed cross sections are compared by using equations (2.27) and (2.29). The tube with open cross section resists to torsion by its local stiffness and behaves as a narrow rectangular section whose dimensions are equal to the length of the developed average line ($2\pi r$) and to the thickness. However, for the close tubular section, an additional stiffness (global stiffness, equation 2.29) is proportional to the square of the entire surface $(\pi r^2)^2$. The stresses resulting from the same torque are 75 times larger in the open than in the closed cross section. The twisting angle is 1875 times larger in the open profile.
For closed cross sections, the global stiffness is much higher than the local one. When the local stiffness is not taken into account the error on the value of twisting angle is 0.05%.
It should however be noted that for this particular geometry, in arbitrary loading or boundary conditions, the closed cross section is always submitted to uniform torsion since it does not warp. However, the open cross section warps and the computations for the open profile should include warping effects.

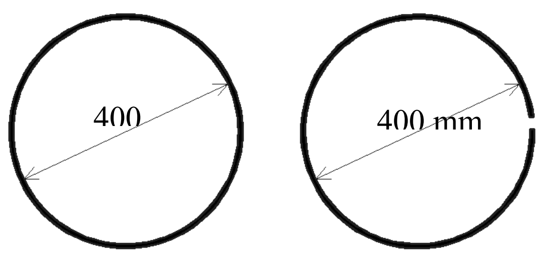

Figure 2.6 Closed and open cross sections

In general, the difference between the behavior of open and closed profiles is more important for Saint Venant torsion (free warping of beams) than for non uniform torsion (prevented warping). Boundary conditions with prevented warping modify considerably the behavior of open profiles which are somehow strongly stiffened. The influence of this phenomenon is much less marked on the closed boxes and the massive sections than on open profiles. Comparisons between the influence of these effects on open and closed cross sections will be shown in paragraph 2.2.3.

2.2.3 Non uniform torsion

For arbitrary profiles, loading cases and boundary conditions, an important non uniform torsional warping occurs so that the Saint Venant torsional theory, strictly restricted to uniform torsion, is no longer sufficient and the equilibrium equation (2.26) no longer valid. A thin walled member resists to non uniform warping by both normal and shear stresses. The stress resultant, i.e. the torsional moment, is divided into two parts (equation 2.20). Shear stresses $\tau_{xs}{}^{st}$, as presented in paragraph 2.2.2 (equation 2.28), derive from the Saint Venant part ($M_x{}^{st}$) and both warping normal stresses $\sigma_x{}^{\omega}$ and warping shear stresses $\tau_{xs}{}^{\omega}$ derive from the non uniform part ($M_x{}^{\omega}$). Usually, the kinematic formula (2.21) is generalized to study the non uniform torsion for a thin walled cross section for arbitrary variation of twisting rate $\theta_{x,x}$. The analysis of torsional behavior of thin walled sections is generally presented by different methods for open and closed cross sections (e.g. [Murray, 1986], [Gjelsvik, 1981], [Shakourzadeh, 1995], …).

2.2.3.1 Vlassov theory for open cross sections

Assumptions

The simplest non uniform torsional theory of a thin walled open cross section is derived from Vlassov theory by neglecting:

-HYPV1: the shear strain ε_{xe}, characterizing the change of angle between longitudinal and thickness coordinate lines; x and e are the coordinates along the longitudinal axis and through the thickness of the mid wall respectively.

-HYPV2: the shear strain ε_{xs} on the mid wall, characterizing the change of angle between longitudinal and contour coordinate lines; x and s are the coordinates along the longitudinal axis and the contour line.

The first assumption results from the equilibrium conditions and the geometry of the profiles. The component τ_{xe} of shear stresses (τ_{xe} would be perpendicular to the contour) vanishes at the external fibers in case of absence of surface loading. Since the walls are very thin, the shear stresses inside a thin-walled member are nearly parallel to the contour; τ_{xe} is neglected and the non zero remaining component is τ_{xs}. The non zero shear strain component is ε_{xs}. An open thin walled beam is thus assimilated to a shell with undeformed section.

The second assumption introduced by Vlassov [1961, Ch I. §2.3.] considers that warping shear strains at the midline are of a secondary nature and are neglected in the kinematic description. Two coordinate lines along x and s (for e = 0), initially perpendicular before loading, are supposed to remain perpendicular after deformation. This is exact for open profiles when the warping is the same along the longitudinal axis x (the torsional moment is constant along the length of the beam with free warping boundary conditions). However, when this is not the case, this assumption is kept to simplify the developments of open profiles.

Kinematics

In Vlassov kinematic formulation, similarly to Saint Venant kinematic formulation (2.21), the displacement field is:

$$\begin{Bmatrix} u_q \\ v_q \\ w_q \end{Bmatrix} = \begin{Bmatrix} -\boldsymbol{\omega}\theta_{x,x} \\ -(z-z_C)\theta_x \\ (y-y_C)\theta_x \end{Bmatrix} \tag{2.31}$$

The axial displacement u is assumed to be proportional to the rate of the twisting angle $\theta_{x,x}$; the warping is then calculated by (2.21) where $\theta_{x,x}$ is no longer constant. The explicit value of Vlassov warping function ω (2.32) is usually deduced [Gjelsvick 1981 §1.1; Murray 1984 page 71; Batoz 1990 page 193; …] from the above assumptions (HYPV1, HYPV2) neglecting shear deformations and is divided into contour warping (or first order warping, ω_1 in 2.33) and thickness warping (second order warping, ω_2 in 2.33). ω_1 (Vlassov 1961 Ch. I §4; Calgaro 1988 page 75…) is called the sectorial area and is generally used in the literature.

$$\boldsymbol{\omega} = \int_0^s h ds + h_n e \tag{2.32}$$

$$\boldsymbol{\omega}_1 = \int_0^s h ds \qquad\qquad \boldsymbol{\omega}_2 = h_n e \tag{2.33}$$

where h is the distance from the shear center C to the tangent to the mid wall at the given point q. h_n is the distance from the normal at the given point to the shear center C (figure 2.7).

De Ville (1989, §3.4.2) deduced a general expression (**ω*)** for an arbitrary open profile from the expression of shear stresses computed with the exact warping function of a thin rectangular profile. He assumed that each open profile behaves similarly to a thin rectangular profile with the same dimensions. His warping function is also divided into a contour warping found to be exactly the sectorial coordinate ω_1 and a second order warping ω_2^*.

The thickness warping function ω_2 was also introduced by Gjelsvik [1981, page 12], Batoz [1990, page 193] and Prokić [1990, 1993, 1994 and 1996] by assuming that the warping varies linearly through the thickness and vanishes along the mid-line. This second order warping derives from HYPV1 (developments are detailed in paragraph 3.2).
The warping function ω can be written in initial Cartesian system (x,y,z):

$$d\boldsymbol{\omega} = (y - y_c)dz - (z - z_c)dy \tag{2.34}$$

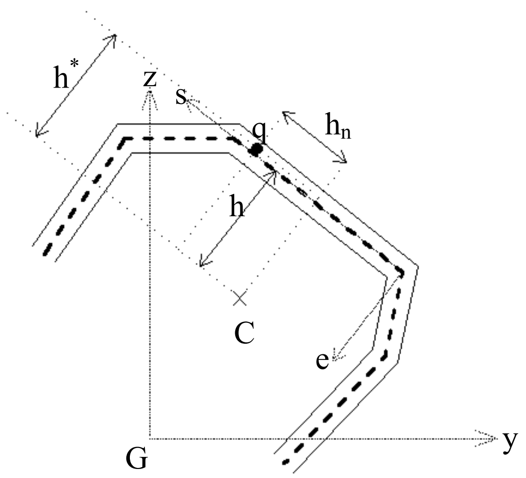

Figure 2.7 Cross sectional geometry

For open profiles, the linear elastic strain expression is deduced from (2.31):

$$\begin{Bmatrix} \varepsilon_x \\ 2\varepsilon_{xy} \\ 2\varepsilon_{xz} \end{Bmatrix} = \begin{Bmatrix} -\boldsymbol{\omega}\theta_{x,xx} \\ -(\boldsymbol{\omega}_{,y} + z - z_c)\theta_{x,x} \\ (-\boldsymbol{\omega}_{,z} + y - y_c)\theta_{x,x} \end{Bmatrix} \tag{2.35}$$

The above listed equations (2.31 - 2.35) are limited to open profiles since:

- The warping function ω is a continuous function with respect to the contour coordinate s of the profile. Equations (2.32), (2.33) and (2.34) allow the computation of an increment $d\omega$ with respect to s starting from an arbitrary origin for which ω is equal to zero. The resulting warping function is therefore discontinuous along the contour of a cell without a slit; and this discontinuity is physically inadmissible.

-These explicit expressions of ω cannot describe at all the behavior of a closed profile since they are developed from hypothesis (HYPV2). This assumption (zero shear strain at the mid wall), acceptable for open profiles, is not admissible at all for closed profiles. It has been seen in paragraph 2.2.2 that even in the case of uniform torsion, shear stresses associated to important shear strains flow through the periphery of a cell.

Equilibrium equations

The torsional equilibrium equation is deduced from the principle of Virtual work by using Hooke's law and expressions (2.35). The following equation is obtained after integration and isolating the virtual twisting angle θ_x^*:

$$-EI_{\boldsymbol{\omega}}\theta_{x,xxxx} + GK\theta_{x,xx} + m_{x\omega,x} + m_x = 0 \tag{2.36}$$

with $m_x = \int_A ((y - y_c)f_{vz} - (z - z_c)f_{vy})dA$ and $m_{x\omega} = \int_A \boldsymbol{\omega}\, f_{vx} dA$

f_{vx}, f_{vy} and f_{vz} are the components of external volume forces.

$$M_x^{st} = GK\theta_{x,x} \tag{2.37}$$

$$B = -EI_\omega \theta_{x,xx} \tag{2.37'}$$

where $EI_{\boldsymbol{\omega}}$ is the non uniform torsional stiffness.

Thus, by using (2.37) and (2.37'), equation (2.36) can be transformed to (2.38):

$$B_{,xx} + M^{st}_{x,x} + m_{x\omega,x} + m_x = 0 \tag{2.38}$$

A first part (M_x^{st}) of the torsional moment arises from the uniform torsion (Saint Venant torsion). A second part (M_x^{ω}) of the total torsional moment arises from the restraint of warping when the bimoment, a new internal equivalent force (B), varies along a beam. B is proportional to the second derivative of the rotation angle (eq. 2.37').

In most analyses using the hypotheses of thin walled beams (assumption HYPTW: thickness << contour length), the thin wall is reduced to a contour line and the second order warping (across the thickness, ω_2) is neglected. The distribution of the warping function is often calculated along the centerline. Kinematics does not include second order warping and the resulting longitudinal

equilibrium equation does not include the part of Saint Venant. The term $M^{st}_{x,x}$ is not present in (2.38) and the Saint Venant term ($GK\theta_{x,xx}$) is eliminated from equation 2.36. The torsional moment is thus assumed to induce entirely non uniform warping stresses while the part of uniform torsion is not included in the equilibrium equation. This is in general theoretically inaccurate since when the element twists, a part of the torque is obtained from the theory of Saint Venant (equation 2.20). The error resulting from this assumption (HYPTW) depends on the cross section profile, the loading and the geometry of the structure. In analyses using the kinematical hypotheses of thin walled beams (HYPTW), the results are often adjusted by introducing the Saint Venant part in the equilibrium equation ($GK\theta_{x,x}$ in 2.36) or in the strain energy ($GK\theta_{x,x}^2$) in order to better describe the phenomenon [Murray, 1986, page 66; Calgaro 1988 page 80; Mohri, 2003, equation (11a); …].
Kolbrunner [1970, page 195] establishes a classification for some profiles and bridge sections. Neglecting Saint Venant term is less important for cold formed steel profiles and orthotropic steel deck bridges than for rolled profiles and concrete bridges.

Stress computations
When a thin-walled beam is submitted to non uniform torsion ($\theta_{x,xx}\neq 0$), normal warping stresses σ_x^{ω} arise from the elongation of longitudinal fibers. These normal stresses, non uniform along the longitudinal axis and inducing τ_{xs}^{ω}, can be found from the associated deformations (by applying Hooke's law to the first row of 2.35). However, it is the equilibrium of an element of a thin-walled beam that enabled Vlassov to find the value of warping shear stresses τ_{xs}^{ω} as they equilibrate the variation of σ_x^{ω}. Their distribution shape over the contour is found to be parabolic along straight segments of a profile. These shear stresses τ_{xs}^{ω} cannot be determined at mid walls directly from the associated shear deformations (by using Hooke's stress-strain relation with the second and third rows of 2.35) because if done so, they would be equal to zero (2.39).

The shear strains ε_{xs} and ε_{xe} , evaluated by using the complete warping function (2.32), are found to vanish at the mid wall so that:

$$2\varepsilon_{xy} = 0$$
$$2\varepsilon_{xz} = 0 \qquad (2.39)$$

The equalities (2.39) are expected since they constitute the hypotheses HYPV2 and HYPV1 respectively. In (2.35), normal strains (ε_x) are due to torsional warping while shear strains are those of Saint Venant uniform torsion kinematics. By using (2.32) as warping function, the Saint Venant strains vanish at the midwall. This is compatible with the second assumption of Vlassov (HYPV2) and shows that the warping function (2.35) is not exact since it does not include the entire warping effects (the resulting shear wrongly vanishes at the midwall).
Once again, the application of the assumption HYPV2 is shown to be restricted for the torsion of open cross sections. It cannot be kept for contours composed of closed cells because both Saint Venant shear stresses (nearly uniformly distributed across the wall of a cell) and warping shear stresses do not vanish through the thickness and their associated shear strains cannot be ignored.
General equilibrium equations are needed to calculate the shear stresses while the normal stresses can be directly derived from Hooke's law. Shear stresses (found equal to zero if computed from 2.35) can be deduced from the equilibrium equation in the longitudinal equation where the longitudinal stresses are calculated from the kinematic formulae.

Analogy between Vlassov non uniform torsion and Bernoulli beam theory

The theories of bending and torsion are often compared in the literature by pointing out an analogy between Bernoulli bending theory and Vlassov torsional theory for open cross sections([Kollbruner 1970 chapter 5]; [De Ville 1989 page 3.54] by referring to the work of Massonet and Cescotto…).. De Ville established an original analogy between Timoshenko and Benscoter theories for closed cross sections. Van Impe (2001) inspected another one between the differential equations for flexural buckling and torsional buckling in order to solve the torsional buckling problem by using the flexural buckling solutions available in the literature.

Hereafter, this interesting similitude is highlighted by showing the analogy between the non uniform torsional part of Vlassov theory and Bernoulli simple beam theory (The comparison between Benscoter and Timoshenko theories is developed in the following paragraph):

Non uniform part of **Vlassov** Torsion theory	←→	**Bernoulli** beam theory
(bimoment) **B**	←→	$\mathbf{M_y}$ (bending moment)
(non uniform torsional moment) $\mathbf{M^{\omega}_x}$	←→	$\mathbf{T_z}$ (shear force)
(twisting angle) $\boldsymbol{\theta_x}$	←→	**w** (bending displacement)
(rate of twist as warping variation along x) $\boldsymbol{\theta_{x,x}}$	←→	$\mathbf{w_{,x}}$ (tangent taken as the slope)
(warping function) $\boldsymbol{\omega}$	←→	**z** (bending distribution over the profile)
$B = -EI_{\omega}\theta_{x,xx}$	←→	$M = -EIw_{,xx}$
$M_x^{\omega} = B_{,x}$	←→	$T = M_{,x}$

Analogy between the non uniform part of Vlassov torsion theory and Bernoulli beam theory

- Bernoulli assumed zero bending shear strains (and thus zero bending shear stresses) since his theory is based on the normality hypothesis: the cross section remains planar and normal to the longitudinal beam axis. Similarly, Vlassov assumption (HYPV2) neglects warping shear strains (and thus warping shear stresses). He described the warping of thin walled structures by a longitudinal elongation (according to x) of the midwall of a thin shell with a rigid undeformable section without allowing any deformation of this midwall in the (xs) plane. Thus, both bending shear stresses and strains are neglected in Bernoulli theory (equation 2.3) and both shear warping stresses and strains (2.35) are not included in Vlassov theory.

- Since Bernoulli theory does not allow for shear calculations, shear stresses must be deduced from equilibrium in the longitudinal direction of the element according to the Jourawsky 'engineering' approach. Hooke's law cannot be used with kinematic formula (2.2) to derive shear stresses due to the shear force because if done so, they would be equal to zero. Similarly, determining torsional warping resultants by using Hooke's law with (2.35) leads to incorrect results. The equilibrium in the longitudinal direction of the element must be considered as in most works based on Vlassov warping function [Batoz, 1990, page 215; De Ville, 1989, page 3.56; …].

- For the same reason, the torsional moment (2.24) cannot be calculated directly from (2.35) as a stress resultant by using shear-strain Hooke's law because if done so, the warping contribution is wrongly considered to vanish at the mid wall and the torsional moment is wrongly reduced to the uniform torsional moment. To solve this problem, equilibrium equations are used to determine shear warping internal forces as in simple Bernoulli beam theory where shear forces T_y and T_z are calculated from the equilibrium equations and not as stress resultants because if so, they would be found to be equal to zero.

The equilibrium of on an element (ds dx) in the longitudinal axis x (figure 2.8) must be considered in order to evaluate the tangential stresses and the corresponding resultants:

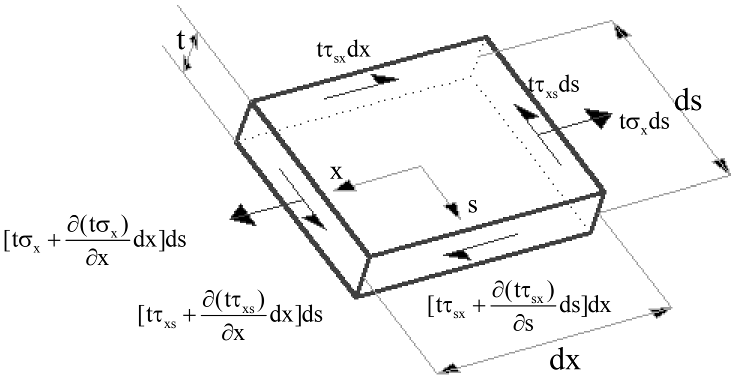

Figure 2.8 Internal stresses acting on the edges of an element (ds dx)

$$\frac{\partial(\tau_{xs}{}^{\omega}t)}{\partial s} = -\frac{\partial(\sigma_x t)}{\partial x} - tf_{vx} \tag{2.40}$$

So that:

$$\int_s \omega \frac{\partial(\tau_{xs}{}^{\omega}t)}{\partial s} ds = -\int_A \omega\sigma_{x,x} dA - m_{x\omega} \tag{2.40'}$$

By integrating by parts (2.40') and taking into account that shear stresses at the extremities of the contour are zero,

$$M_x^{\omega} = \int_s \tau_{xs}^{\omega} h ds = B_{,x} + m_{x\omega} \tag{2.41}$$

or in term of displacements:

$$M_x^{\omega} = -EI_{\omega}\theta_{x,xxx} + m_{x\omega} \tag{2.41'}$$

By inserting (2.41) into (2.36) and then by using equation (2.20), the following equations are found :

$$M_{x,x}^{\omega} + M_{x,x}^{s} + m_x = 0 \text{ so that } M_{x,x} + m_x = 0 \tag{2.42}$$

2.2.3.2 Benscoter theory

Warping function for closed cross sections

The non uniform torsional analysis of closed cross sections is complicated by the fact that torsional shear strains ($2\varepsilon_{xs}$) are not negligible at the mid wall and must be included. As stated before, even in the case of uniform torsion, shear stresses vanish on the mid wall of an open cross section but flow along the mid wall of a cell in a closed cross section (eq 2.30). The assumption of Vlassov theory HYPV2 is no longer acceptable and the calculations presented in the previous paragraph are no longer valid. For Benscoter theory, the warping function is calculated by an approximate theory assuming that only Saint Venant shear strain (uniform torsion) is considered [Murray, 1986, page 72-73]. Similarly to the case of open cross section calculations with Vlassov, non uniform shear stresses (which are considered to be of secondary nature) are neglected and Saint Venant shear stresses are taken into account. However, since the behavior of closed cross sections is different from that of open cross sections, the developments are more complex. The warping function is found to be different for each case. For closed cross sections, after changing and adapting the notations of [Murray, 1986], the warping function is found to vary along the contour as:

$$\boldsymbol{\omega} = \int_0^s (h - \frac{\lambda_i}{e})ds \tag{2.43}$$

λ_i are the unknowns that result from the geometry of the closed cross section and determine the Saint Venant torsion constant of multi-celled profile ([Murray, 1986], [Kollbrunner, 1970],…). The second order warping is neglected in (2.43).

Kinematics of Benscoter theory

Benscoter [1954] presented a theory for contours which are composed of closed cells where the out of plane displacement of the cross section is assumed to be proportional to the warping function $\omega(y,z)$ and to the rate of a deformation parameter $\chi(x)$ that is found to be a function of the angle of rotation θ_x:

$$u = - \omega\,(y,z)\,\chi_{,x}(x) \tag{2.44}$$

The axial displacement is no longer assumed to be proportional to the gradient of the torsional angle as in Vlassov theory, but to $\chi_{,x}$.

The kinematic description of the displacement field can be formulated as follows:

$$\begin{Bmatrix} u_q \\ v_q \\ w_q \end{Bmatrix} = \begin{Bmatrix} -\boldsymbol{\omega}\chi_{,x} \\ -(z - z_C)\theta_x \\ (y - y_C)\theta_x \end{Bmatrix} \tag{2.45}$$

The strain displacement relations (2.46) are deduced from the displacement field (2.45) in case of linear analysis:

$$\begin{Bmatrix} \varepsilon_x \\ 2\varepsilon_{xy} \\ 2\varepsilon_{xz} \end{Bmatrix} = \begin{Bmatrix} -\boldsymbol{\omega}\chi_{,xx} \\ -\boldsymbol{\omega}_{,y}\chi_{,x} - (z - z_c)\theta_{x,x} \\ -\boldsymbol{\omega}_{,z}\chi_{,x} + (y - y_c)\theta_{x,x} \end{Bmatrix} \tag{2.46}$$

This theory is more general than the previous one since it takes into account the effects of non uniform warping in shear strains, contrary to Vlassov formulation. If $\chi_{,x}$ is taken equal to $\theta_{x,x}$, the strain-displacement relations (2.46) are reduced to those of Vlassov or Saint Venant transverse shear strain (2.35). So that for the same cross section (the shape of warping function along the contour $\boldsymbol{\omega}$ is the same), Benscoter degenerates into Vlassov theory. These two theories degenerate into Saint Venant theory if $\chi_{,xx}$ and $\theta_{x,xx}$ are assumed to be equal to zero. Indeed, in (2.46), normal strains (ε_x) and shear strains (ε_{xy} and ε_{xz}) are found to include warping effects. De Ville [1989] transformed (equation 2.46) to (equation 2.47) so that the Saint Venant part can be explicitly found. The additional warping effects can be found from the difference between twisting angle gradient $\theta_{x,x}$ and warping degree of freedom $\chi_{,x}$.

$$\begin{Bmatrix} \varepsilon_x \\ 2\varepsilon_{xy} \\ 2\varepsilon_{xz} \end{Bmatrix} = \begin{Bmatrix} -\boldsymbol{\omega}\chi_{,xx} \\ \boldsymbol{\omega}_{,y}(\theta_{x,x} - \chi_{,x}) - (\omega_{,y} + z - z_c)\theta_{x,x} \\ \boldsymbol{\omega}_{,z}(\theta_{x,x} - \chi_{,x}) + (-\omega_{,z} + y - y_c)\theta_{x,x} \end{Bmatrix} \tag{2.47}$$

Equilibrium equations

The simplest way to solve the torsional problem is to evaluate χ as a function of the twist θ_x. The principle of virtual displacements (χ^*, θ_x^*) is used and the resulting equations can be written in terms of displacements and transformed (as in [Murray, 1986, page 132]) to (2.49) or (2.50).

The equation relating χ to θ_x is found to be:

$$\theta_{x,x} = \chi_{,x} - \frac{1-\eta^2}{\alpha^2}\chi_{,xxx} + \frac{m_{x\omega}}{GI_c\eta^2} \tag{2.48}$$

where $\eta^2 = 1 - \dfrac{K}{I_c}$, $\alpha^2 = \eta^2 \dfrac{GK}{EI_\omega}$.

K is the constant torsion, I_c is the polar constant.

Therefore, one equilibrium equation can be written either with respect to χ (2.49) or to θ_x (2.50).

$$-EI_\omega\chi_{x,xxxx} + GK\frac{I_c - K}{I_c}\chi_{x,xx} + m_{x\omega,x} + m_x\frac{I_c - K}{I_c} = 0 \tag{2.49}$$

or

$$-\frac{EI_\omega I_c}{I_c - K}\theta_{x,xxxx} + GK\theta_{x,xx} + m_{x\omega,x} + m_x - m_{x,xx}\frac{EI_\omega}{G(I_c - K)} = 0 \tag{2.50}$$

The internal forces are also computed as in equations (2.40 and 2.41) :

$$\begin{aligned} M_x^s &= GK\theta_{x,x} \\ M_x^\omega &= m_{x\omega} - EI_\omega\chi_{,xxx} \\ B &= -EI_\omega\chi_{,xx} \end{aligned} \tag{2.51}$$

It is important to note that the torsional moment (2.52), calculated from kinematics (2.43) as a stress resultant (from 2.24), does not include second order warping effects.

$$M_x = GI_c\theta_{x,x} - G(I_c - K)\chi_{,x} \tag{2.52}$$

If second order warping effects are taken into account, the equilibrium equation can be written with respect to θ_x as follows:

$$-\frac{EI_\omega(I_c + K_o)}{I_c - K}\theta_{x,xxxx} + G(K + K_o)\theta_{x,xx} + m_{x\omega,x} + m_x - m_{x,xx}\frac{EI_\omega}{G(I_c - K)} = 0 \tag{2.53}$$

K_o is the local rigidity specific to each element of the section and calculated by (2.27).

Limitations of Benscoter theory and bending – torsion analogy

It is important to note that the formulation (2.45) is not exact since the approximate warping function (ω) (2.43) is calculated by assuming that the shear stresses are those of uniform torsion. The kinematics, more general than in Vlassov analysis, takes into account more non uniform warping effects but they still approximate the real torsional state. As shown below, the associated warping shear strains (2.46) and stresses result from an approximate analysis of a very complex stress state. More developments are required for more accurate theories.

As stated in paragraph 2.3.1, an analogy between Timoshenko bending beam theory and Benscoter torsional theory is highlighted by DeVille (1989, page 3.54) and is developed hereafter:

Non uniform part of **Benscoter** Torsion theory	←→	**Timoshenko** beam theory
(bimoment) **B**	←→	**M** (bending moment)
(non uniform torsional moment) $\mathbf{M^\omega_x}$	←→	**T** (shear force)
(twisting angle) $\boldsymbol{\theta_x}$	←→	**w** (bending displacement)
(warping parameter variation along x) $\chi_{,x}$	←→	$-\theta_y$ (tangent different from the slope)
(warping function) $\boldsymbol{\omega}$	←→	**z** (profile bending distribution)
$B = -EI_\omega\chi_{,xx}$	←→	$M = -EIw_{,xx}$
$M^\omega_x = -G(I_c - K)\chi_{,x}$	←→	$T = GA(\theta_y + w_{,x})$

Analogy between the non uniform part of Benscoter torsion theory and Timoshenko beam theory

- The normality assumption of Bernoulli is relaxed in Timoshenko beam bending theory so that shear effects and a constant state of transverse shear strain is included. Similarly, Vlassov assumption HYPV2 is relaxed in Benscoter formulation. The shear strains ε_{xs} in the mid wall are not neglected.

- In bending, constant shear stresses and strains with respect to the cross section are computed with Timoshenko kinematics. They violate boundary conditions and require shear correction factors to compensate for this inexactitude. In torsion, shear strains and stresses computed from approximate Benscoter kinematics are found to be constant along a prismatic wall. By using Hooke's law and (2.46 or 2.47), an approximate distribution for torsional warping shear stresses is found to be constant along a straight part of a contour (ω is linear with respect to s for prismatic thin walled cross sections). Besides, the kinematics gives non zero constant shear strain ε_{xe} across the thickness:

$$2\varepsilon_{xe} = h_n(\theta_{x,x} - \chi_{x,x}) \tag{2.54}$$

This constant non zero value (2.54) of ε_{xe} across the thickness violates the boundary condition and is not taken into account in the developments that lead to (2.50 – 2.51). Both (τ_{xs} and τ_{xe}) stress states violate the zero boundary condition since, as explained in paragraph 2.2.3.1 (HYPV1), the component of shear stresses which is normal to the outer contours should vanish in case of absence of surface loading.

- For bending, Jourawsky engineering approach is needed to calculate the shear stresses and force by considering an equilibrium equations. Similarly, the exact parabolic shaped distribution of torsional stresses should be deduced from the equilibrium equation (2.55) in the longitudinal direction.

$$\frac{\partial\phi}{\partial s} = -e\frac{\partial\sigma}{\partial x} - p(x,s) \qquad (2.55)$$

where ϕ is the flow of the shear stresses through the thickness and p(x,s) is a distributed surface load acting along the longitudinal axis x.

2.2.3.3 Application: Non uniform torsion of open and closed profiles

In this application, Vlassov and Benscoter theories (developed in paragraphs 2.2.3.1 and 2.2.3.2) are applied to the case of non uniform torsion of asymmetrical closed and open cross sections and the effects of second order warping on Vlassov and Benscoter formulations are computed. In Vlassov formulation, the warping is proportional to the gradient of the twisting angle (equation 2.31) while in Benscoter formulation, the warping is proportional to a new parameter (2.45).

Two cross sections, open (figure 2.9b) and closed (figure 2.9c), are submitted to a non uniform torsional loading (figure 2.9a). The closed cross section is introduced by Kolbrunner [1972, page 195]. A uniform distribution of torque m_x = 500kN/m is applied along the entire length of the beam. L = 20m, t_0 = 0.01m. (E = 206GPa, G = 82.4GPa). The cross sections at both ends are prevented from twisting but are free to warp.

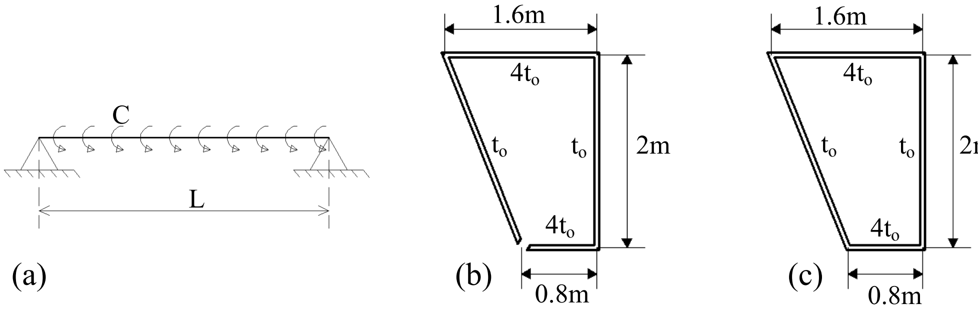

Figure 2.9 Open (b) and closed (c) asymmetrical cross sections submitted to non uniform torsion

Analysis of Open profile

Warping function

The open cross section in figure 2.9b is analyzed by using the kinematics based on Vlassov assumption (eq. 2.31 and 2.32). For the thin-walled open cross section (0.01m << 2m), the warping function is calculated at the contour. As explained in paragraph 2.2.3.1, Vlassov assumption HYPV2 of zero shear strain at mid walls gives the warping function in equation 2.34. The principal warping function that uncouples torsional effects from bending and tension (details are given in equation 3.21) is shown in figure 2.10.

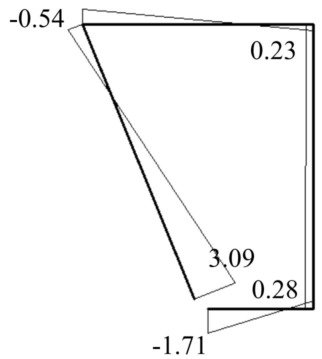

Figure 2.10 Principal warping function [m^2] of open cross section figure 2.9b

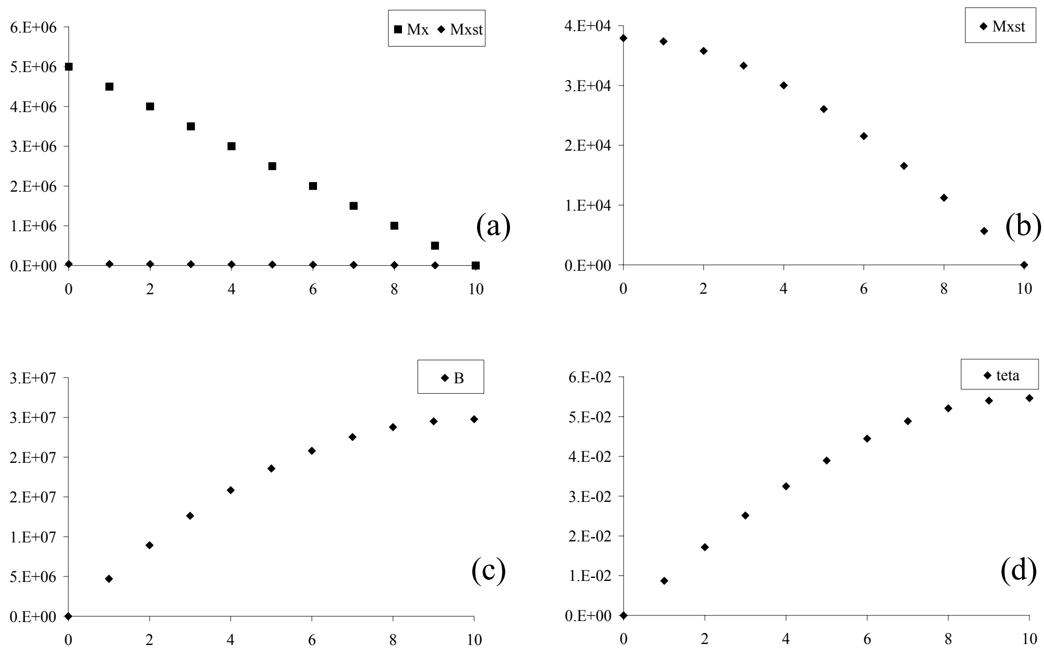

Figure 2.11 Torsional moment $M_x = M_x^{st} + M_x^{\omega}$ [Nm], bimoment B [Nm^2] and twisting angle teta [rad] of an open asymmetrical thin walled beam for x varying from 0 (left support) till 10m (midspan)

Torsional calculations based on Vlassov theory

The torsional computations are governed by equation (2.36) where the influence of second order warping (across the thickness: term $GK\theta_{x,x}$) is included. The twisting moments, bimoments and twisting angle are plotted (figure 2.11) for x varying from zero to L/2 since the loading and the geometry are symmetrical with respect to the mid span. Figures (2.11a) and (2.11b) show the variation of M_x and M_x^{st} with respect to the longitudinal axis part ($M_x = M_x^{st} + M_x^{\omega}$). The non uniform part (M_x^{ω}) of the twisting moment varies between 99.24% for x = 0 (remaining 0.76% is for Saint Venant part M_x^{st}) and 98.86% for x = 9.99m (remaining 1.14% is for Saint Venant part). Figure (2.11d) shows the variation of the twisting angle by solving equation (2.36). If the part of Saint Venant ($GK\theta_{x,x}$) is neglected, the solution gives an error of 0.934% for the maximal twisting angle. Thus, this profile can be analyzed according to the theory of non uniform torsional theory. The Saint Venant part can be neglected. However, applying the Saint Venant theory which is strictly restricted to uniform torsion, as it is done in elementary torsional analysis, is not appropriate in this case.

Comparison between Vlassov and Benscoter theories
It is interesting to see that Benscoter formulation does not give additional accuracy on the previous results for which the thickness is very thin (0.01m << 2m). If a warping parameter $\chi_{,x}$ different from the gradient of the twisting angle $\theta_{x,x}$ is considered with the warping function in figure 2.10, two equilibrium equations are found from the principle of virtual displacements by isolating χ^* and θ_x^*. The resulting equilibrium equations can be written either with respect to $\chi_{,x}$ (2.49) or $\theta_{x,x}$ (2.50). In this particular case of open profile, the ratio of the Saint-Venant torsional constant (K) to the sectorial moment of inertia (I_c) is negligible: 0.0005 in this example. Since K/I_c <<1, both (2.49) and (2.50) are found to converge to equation 2.36 (with Vlassov formulation). Shear stresses at the mid wall, given by 2.56, vanish in this case at the mid wall.

$$\frac{\tau_{xs}}{G} = h\vartheta_{x,x} - h\chi_{,x} \tag{2.56}$$

The difference in the amount of the ratio (K/I_c) usually justifies the well known difference of torsional behavior between closed and open cross sections. Thin open sections have very small torsional rigidity and exhibit large amount of warping effects.

Analysis of Closed profile
Warping function
The closed cross section (figure 2.9c) is now considered. The principal warping function along the contour is deduced from equation 2.43: Vlassov kinematics (2.35) is adopted with strains resulting from Hooke law and shear stresses of uniform torsion (Bredt formulae 2.30). The resulting warping function is represented in figure 2.12.

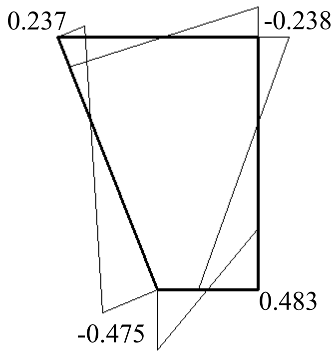

Figure 2.12 Principal warping function [m^2] of closed cross section in figure 2.9c

Torsional calculations based on Benscoter theory
The structure in figure 2.9a is analyzed by using the kinematics of Benscoter (equations 2.49 or 2.50). The diagrams of θ_x, M_x and M_x^{st} are represented in Figure 2.13 by neglecting second order warping. It can now clearly be observed (figure 2.13b) that the largest part of the torsional moment is the Saint Venant part (it varies between 95.89% and 100%). This is a major difference with the previous example that analyzes the same dimensioned cross section with a split.
The bimoment is 158 times larger in the open than in the closed cross section (figure 2.11c and 2.13c). By using Vlassov kinematics (equation 2.36) with the same warping function (figure 2.12), the maximal twisting angle is found to be the same; the maximal bimoment is 0.0004% larger; the maximal warping part of the torsional moment is 36.28% larger and the maximal Saint Venant part of the tosional moment is 1.55% smaller. For this unicellular profile, the Saint Venant part in equation

(2.51) has the major importance. If this part is neglected, the solution gives an error of 13268% while it was 0.934% for the maximal twisting angle of the open cross section!

By using second order warping effects (2.53), the maximal twisting angle is 0.0007% larger; the maximal bimoment is 0.109% smaller; the maximal warping part of the torsional moment is 0.08% smaller and the maximal Saint Venant part of the tosional moment is 0.0034% larger. These small differences were expected since the local rigidity for a closed cross section is very small compared to the global rigidity (0.108% in this case).

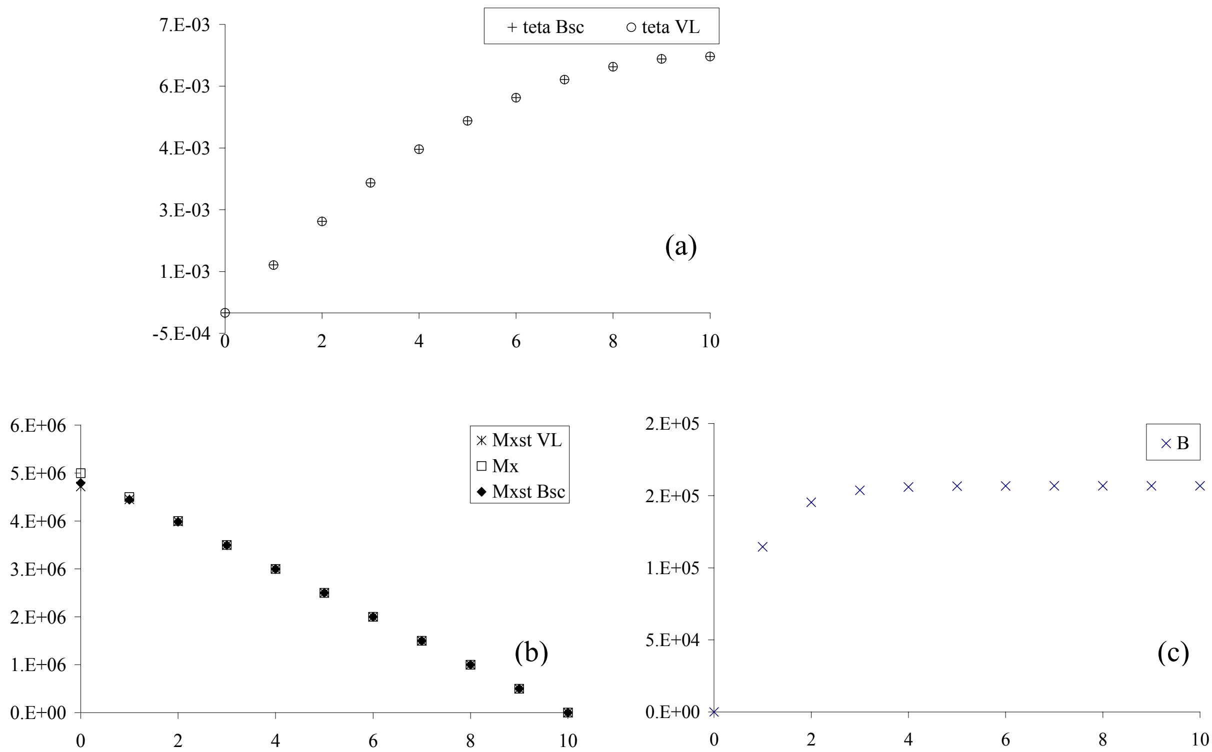

Figure 2.13 Rotating angle teta [rad], torsional moment $M_x = M_x^{st} + M_x^{\omega}$ [Nm], and bimoment B [Nm^2] of closed asymmetrical thin walled beam for x varying from 0 (left support) till 10m (midspan)

2.2.3.4 Prokić warping function

Prokić [1990, 1993, 1994 and 1996] kept the assumption that the thickness warping u_t (second order warping) varies linearly across the thickness and vanishes along the mid-line. In his work, the thickness warping u_t is proportional to the derivative of the torsional rotation angle $\theta_{x,x}$, to the distance to the midline e, and to the perpendicular distance h_n to the normal issued from the centroïd.

$$u_t = -\omega\theta_{x,x} \quad (2.57)$$

The first order warping u_c is also considered in his work as varying linearly along each polygonal segment of the contour. However, he used a different approach than that of Vlassov and Benscoter by taking longitudinal displacements (u_i) at selected points of the contour called hereafter “transversal nodes” as additional parameters. The combination of linear functions Ω^i (varying along the profile contour between adjacent transversal nodes) with these additional parameters describes the contour warping of the cross section. Ω^i is a linear function along walls having a unity value at the transversal node (i).

$$u_c = \sum \Omega^i u_i \qquad (2.58)$$

This warping function $u = u_c + u_t$ has been applied by Prokić to arbitrary shapes of thin-walled cross sections, without any distinction between open and closed profiles. In his thesis [1990] and papers [1990, 1993, 1994 and 1996], Prokić stated that the shear center notion is not necessary even in studying asymmetrical profiles.

However, a deep examination of the work of Prokić shows that the proposed kinematics is very general and not restricted to torsional warping as it was stated in the scope and conclusions of his publications. The warping function represents a longitudinal displacement which is supposed to be piecewise linear along the contour. This general formulation, as presented by Prokić, is not specifically associated with the torsional behavior and produces non zero warping when normal forces, bending moments or shear forces are applied. Besides, the kinematic formulation assumes definitely that the cross section rotates around the centroid. Within these limitations, his theory is limited to pure uncoupled torsional problems for bi-symmetrical cross sections where the centroid and the shear center coincide. His calculations are for instance not valid for beams with asymmetrical cross sections submitted to a transversal load acting along the centroidal axis, since this load induces torsion coupled with bending. In his published articles and thesis, numerical results are indeed limited to uncoupled linear torsional problems.

The purpose of the present work is to contribute to the validation of this new approach of modeling the torsional behavior of thin walled beams by enhancement of Prokić kinematic formulation and by illustration of its application to practical problems not considered by Prokić. In order to define, characterize and uncouple warping effects due to shear forces, torsion and distortion, additional equations are required to adapt this general formulation (2.58) to each specific problem. Detailed analyses and results are given in the following chapters for arbitrary cross sections by discretizing the profile (warping parameters u_i). The second assumption of Vlassov HYPV2 is relaxed so that normal and shear strains include the effects of non uniform warping. They include uniform and non uniform torsional effects. As in Vlassov or Benscoter theories, the exact distribution of normal stresses, which is linear along straight segments of the contour, is found by using Hooke law. In addition, the distribution of shear stresses which is parabolic along straight segments of the contour, is also found by using Hooke law. It is hereby assumed to be constant between two transversal nodes. Therefore, the shape of this distribution is obtained more accurately when the number of transversal nodes increases. This formulation is applied and validated for the complicated behavior of thin walled beams.

2.3 Distortion

2.3.1 General overview

A single thin rectangular plate is very flexible when loaded perpendicularly to its plane and behaves very stiffly if bended in its plane. However, when connected to other thin plates with different orientations (e.g. assembling plates at 90° as shown in figure 2.15), advantageous effects make this assembly an optimal way for carrying transverse loading. An assembly of thin "walls" or plates along their longitudinal axes constitutes a thin walled beam for which local and global deformations can be distinguished as follows:

- A deformation is noted 'global' when the whole member length is involved and when the cross section is assumed to maintain its shape without any distortion (e.g. figure 2.14a). The accuracy of this assumption depends on the stiffness of the transverse frame constituting the shape of the beam profile contour and on the beam loading acting along the longitudinal axis and within the cross sectional plane. A high stiffness resulting from the assembly of all the individual plates is required in order to resist to a loading by tension/compression, bending and/or torsion global beam behaviors.

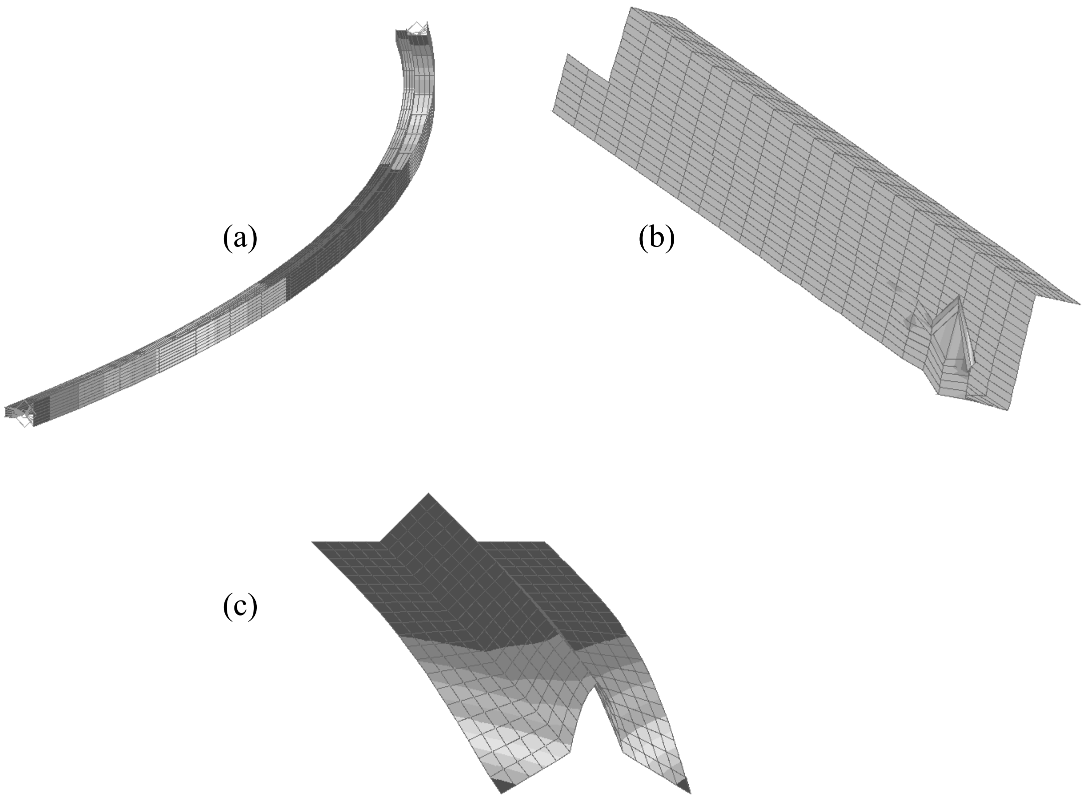

Figure 2.14 (a) A global behavior: bending of an I beam; (b); a local behavior that involves one plate of a Z beam; (c) a distortional behavior

- A 'local' deformation induces 'plate' displacements which are localized on a small area of one thin wall without being extended to other walls or plates (e.g. figure 2.14b). It involves the out-of-plane flexibility of the corresponding plate element and does not include the cross-sectional stiffness.
- A distortional behavior is associated with a change in the shape of the cross section that concerns usually the entire cross section geometry (figure 2.14c). The effects of this deformation vary relatively slowly along the member length. It is classified between the previous deformation types ('global' and

‘local’) considered as two limit cases: the first limit case prevents entirely the distortion and describes the deformation of a rigid cross section that maintains its shape. The second limit case assumes that the beam plates are hinged along their longitudinal edges so that the cross section is no longer forced to maintain its shape and its stiffness is entirely neglected. In the second case, the walls must be loaded in their planes as isolated members.
For instance, a load (figure 2.15a) acting in the cross section plane as shown in figure 2.15 induces not only bending and torsion (2.15b) but also distortion (2.15c). Similarly to the torsional behavior overviewed in section 2.2, the distortion depends to a large extent on the cross sectional geometry and specifically, whether the section is open or closed. A ‘non uniform’ distortion of the cross section, accompanied by an out-of-plane plate bending, induces non uniform shear and axial stresses together with a non uniform warping of the cross section.

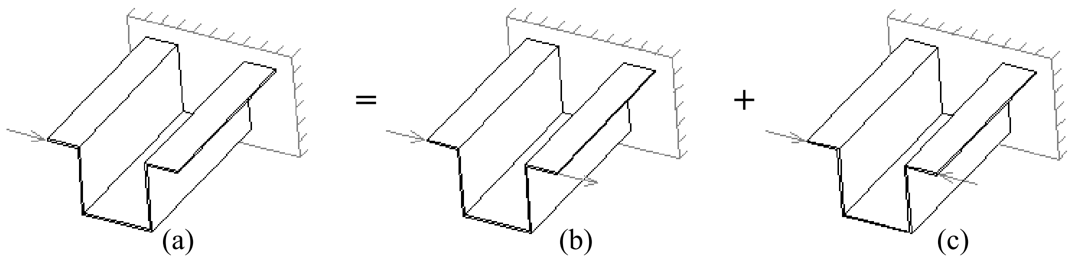

Figure 2.15 A transversal load (a) separated into: flexural & torsional loading (b) and distortional loading (c) (after Takahashi 1978)

The effects of such a distortion, usually significant for very thin walled open sections (and for thin walled closed sections with high distortional loadings), have to be analyzed in order to optimize the design of beams and columns and to determine an economical use of diaphragms and bracing in real life structures. Recent experiments ([Serrette 1997]; [Kesti 1999]…) as well as theoretical investigations ([Takahashi 1978]; [Hancock 1978]; [Bradford 1992]; [Hancock 1998]; [Gonçalves 2004]; [Silvestre 2004]…) have shown the influence of the contour distortion on the behavior of thin walled beams (depending on the wall thickness, profile shape …). Because of the general tendency to increase the slenderness and to optimize the shape, further research is still required for simple, safe and economical calculations.

2.3.2 Problem definition

In this research work, the mechanical type of distortion is mainly derived from the work of Takahashi et al. [1978; 1980; 1982; 1987; 2001; 2003]. Takahashi developed analytical formulations [1978, 1980, 1982, 1987] for open profiles with a warping function based on the well known Vlassov assumptions (HYPV1, HYPV2). Furthermore, he studied the distortion of closed profiles (2001) in a similar approach to that done by Vlassov (1961, chapter IV).
The distortion of a profile induces relative rotations of transversal segments separated by transversal nodes behaving as joints or hinges (figures 2.17, 2.18a…). By taking an arbitrary transversal node as a reference in the cross sectional plane, it is clear that the relative position of the other nodes changes during this type of deformation. In addition, these inner segments, initially straight before loading, bend and become curved (figure 2.17).
A cross sectional distortion results therefore in:
-relative rotations of contour parts in the cross sectional plane,

-local bending of inner transversal segments,
-non uniform warping (beam longitudinal displacement or an out-of-cross-sectional-plane displacement).
In case of pure distortion (neither stretching, nor bending or torsion), the specific point around which each contour part rotates is called the associated distortional center.

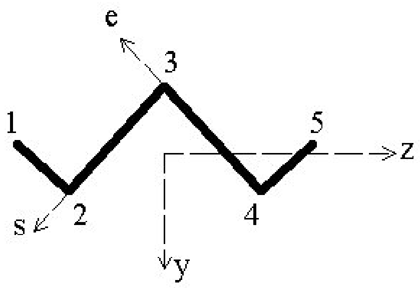

Figure 2.16 ‘yz’ beam axes and ‘se’ local axes

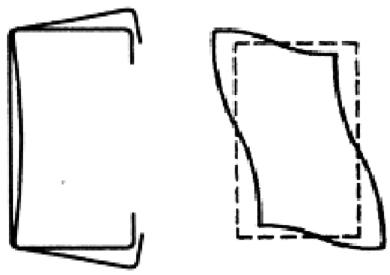

Figure 2.17 Distortional modes

The beam, considered as an assembly of thin plates connected by longitudinal axes, resists to the transverse loading that results from distortion (i.e. loading in figure 2.15) by membrane stiffening at the connecting axes. Each inner plate bends in the se or yz plane (i.e. ❷❸ in figure 2.16) since it is located between two ‘rigidifying’ connections. This plate bending accompanies the relative rotation of inner plates (❷❸ and ❸❹ in figure 2.16) in the (yz) plane around the longitudinal axis (❸) considered to be partially ‘hinged’. However, an outer plate is submitted to the restraining effects at only one connection axis and resists to these effects by rotating ‘freely’ since it has a free edge.

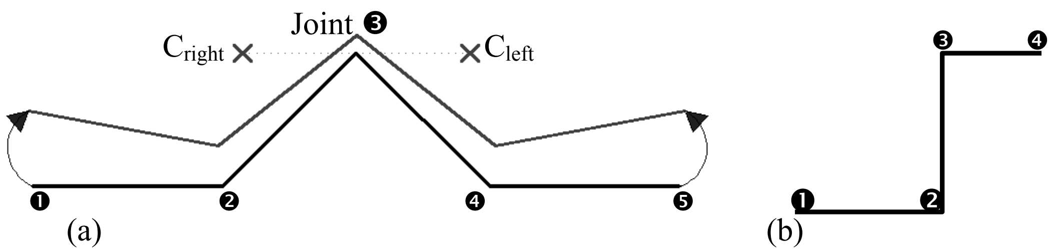

Figure 2.18 (a): Two cross section blocks (1-2-3 & 3-4-5) associated with the distortional joint 3; (b) cross section with no distortional modes

Thus, the bending of transversal edge segments (1/2 & n-1/n of an open profile without ramifications where n is the number of transverse nodes separating straight segments of a profile) is considered to be

a local phenomenon and is not taken into account in the cross sectional distortion studied afterwards. For the same reason, the distortion of particular profiles such as (⊥, ∠, +, z , I…) will not be analyzed within this beam theory since the associated cross sectional deformation is classified to be 'local'. A classified 'local' out-of-plane bending of a single plate (plate ❷❸ in figure 2.18b) occurs without any significant relative plate rotations around an associate transversal node (such as that in 2.18a for example). Consequently, the distortional contour warping function of similar profiles is assumed to be zero in this study.
In order to formulate mathematically the distortional behavior, a superposition of m (m = n-3 for open profiles without ramifications) distortional modes is considered. Each distortional mode "I" is related to a transversal node or joint which divides the cross section into rigid blocks of two or more transversal segments (blocks 1-2-3 & 3-4-5 in figure 2.18a). Each distortional mode is characterized by the relative rotation of these blocks around the corresponding distortional centers (two distortional centers in figure 2.18a). Similarly to torsion, the geometrical location of the distortional centers is determined by ensuring the decoupling of the stretching/bending/torsion/distortion effects. The distortional centers, related to a specific distortional mode "I", are defined by setting that the rotations of the associated rigid parts do not induce any axial, bending, torsional or other distortional (except "I") behaviors. For the clarity of the dissertation, these centers are presumed to be designated. Their determination is developed in §4.4.3 (analytically) and §5.4.3 (numerically).
A transversal node that belongs to an edge transversal segment (1, 2, 4 & 5 in figure 2.18a; 1, 2, 3 & 4 in figure 2.18b) cannot be selected to be a distortional joint. The selection of an edge node (1 & 5 in figure 2.18a; 1 & 4 in figure 2.18b) corresponds to a torsional behavior since there is a one-rigid-cross-sectional rotation. The inner transversal nodes of edge segments are not considered hereby as distortional joints since the associate deformation deals with a classified local phenomenon as explained upwards. A relative rotation of rigid blocks separated by an inner node of edge segments (nodes 2 and 3 in figure 2.18b, 2 and 4 in figure 2.18a) is neglected since it is considered to be insignificant and leading to local out-of-plane bending of individual plates.

2.3.3 Assumptions for Takahashi model

The distortion analyzed by Takahashi [e.g. 1980] is based on the following assumptions:
HYPT1- ε_{xe}. Similarly to Vlassov assumption in the case of torsion (cf. HYPV1 in §2.2.3), the change of angle between longitudinal (x) and thickness (e) coordinate lines is considered to be equal to zero. The no-shear boundary condition implies zero shear stresses at the exterior fibers in case of absence of surface loading. Due to the geometry of very thin profiles, shear stresses (and thus strains) inside a thin-walled member are nearly parallel to the contour.
HYPT2- ε_{xs} at the mid wall of open profiles. Similarly to HYPV2 in §2.2.3, the change of angle between longitudinal (x) and contour (s) coordinate lines is neglected at the midwall of an open profile or branch. Two coordinate lines along x and s on a mid wall, initially perpendicular before loading, are supposed to remain perpendicular after deformation. Similarly to torsional calculations (equation 2.33 in §2.2.3), the warping function used by Takahashi is calculated by an approximate theory considering only uniform distortional shear strain.
In addition, other assumptions are considered below:
HYPT3- The present distortional computations include the local plate bending of the inner plates in the (se) plane. Due to the dimensions of each thin plate constituting the beam ($L_x >> L_s$), the other plate bending (xe plane) is classified as a local phenomenon and is not taken into account in this study.

HYPT4- The Poisson effects are neglected since normal stresses σ_s, associated with a local bending phenomenon vanishing at the mid wall, have small effects compared to those of σ_x. So that for an elastic material:

$$\sigma_x = E\,\varepsilon_x \tag{2.59}$$

$$\sigma_s = E\,\varepsilon_s \tag{2.60}$$

HYPT5- The out-of-plane local bending of thin plates is governed by the normality assumption. A local surface (xe) is assumed to remain planar after deformation and perpendicular to the material points located on the axis (s) before deformation.

2.3.4 Kinematics

Global displacement field

Takahashi [1978, 1980, 1982, 1987] studied the distortion of an open profile without ramifications (e.g. figure 2.19). The 'global' displacement field at any point q(x,y,z) of the cross section associated with the distorsional modes (I = 1…m) is given by:

$$\begin{Bmatrix} u_q \\ v_q \\ w_q \end{Bmatrix} = \begin{Bmatrix} \sum_{I=1}^{m} \bar{\boldsymbol{\omega}}_I \bar{\mu}_I \theta_{xI,x} \\ \sum_{I=1}^{m} -(z - \bar{z}_{CI})\bar{\mu}_I \theta_{xI} \\ \sum_{I=1}^{m} (y - \bar{y}_{CI})\bar{\mu}_I \theta_{xI} \end{Bmatrix} \tag{2.61}$$

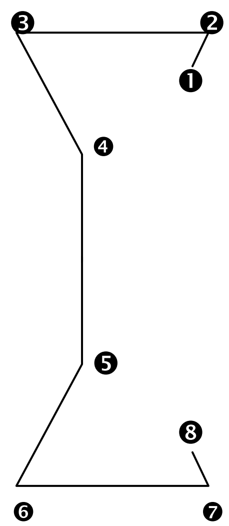

Figure 2.19 Open cross section without ramifications

Each distortional degree of freedom θ_{xI} is associated with a distortional joint I (I = 1…m) and is taken as the rotation of the right part of the contour (I-I+1-…-n) around the right distortional rotation center C_{IR}. The rotation of the left part of the contour (1-2-…I) around the left distortional rotation center C_{IL} is measured by $\mu\theta_{xI}$. μ is the specific rotating ratio between right and left sectional parts. For a monosymmetrical profile (i.e. profile in figures 2.18), μ is equal to -1. $\bar{\boldsymbol{\omega}}_{\mathbf{I}}$, depending on s, is the distortional warping function calculated from (HYPT1 and HYPT2) and found to be:

$$\bar{\boldsymbol{\omega}}_I = \int_0^s \bar{h} ds \tag{2.62}$$

For an arbitrary point q, the function $\bar{h}$ (s) is calculated as the distance from the associated distortional center (right or left part distortional center) to the tangent to the mid wall at q.

For each distortional mode I, $\bar{\mu}_I, \bar{y}_{CI}$ and $\bar{z}_{CI}$ are functions of the contour length (s).

At the right part (I - I+1 - … - n) of the contour of an open profile without ramifications (e.g. figure 2.19), $\bar{\mu}_I$ is equal to 1, $\bar{y}_{CI}$ is equal to the y ordinate of the right distortional rotation center and $\bar{z}_{CI}$ is equal to the z ordinate of the right distortional rotation center. At the left part (1 - 2 - … - I) of the contour, $\bar{\mu}_I$ is equal to the specific rotating ratio μ, $\bar{y}_{CI}$ is equal to the y ordinate of the left distortional rotation center and $\bar{z}_{CI}$ is equal to the z ordinate of the left distortional rotation center.

Additional 'local' displacement field

In addition, for each of the (m = n-3) distortional modes, the relative rotation of the associated cross sectional blocks (mathematically formulated by 2.61) induces a local "out-of-plane" bending of the inner plates. The associated displacement field is localized in the (se) plane. Since the plate bending in the other transversal direction (xe plane) is neglected (HYPT3), it is possible to isolate a unit length strip (figure 2.20a). The local contour system (x,s,e) shown in figure 2.16 is used and the transversal (s,e) displacements associated with a (se) plate bending are:

$$\xi(x,s) = \bar{\Gamma}_I(s)\theta_{xI}(x)e \tag{2.63}$$

$$\eta(x,s) = \bar{\eta}_I(x,s) \tag{2.64}$$

$\bar{\Gamma}_I$, a function of (s), depends in general on the profile geometry and on the material behavior and results from the membrane stiffening of the assembled plates for each distortional mode I associated with block rotations.

The normality assumption through the thickness of the wall is kept (HYPT5) for this local bending, so that the material points, located on a normal to a surface (xe) remain on a line normal to the deformed middle surface. The change in angle between (s) direction and (e) direction is assumed to vanish:

$$\varepsilon_{se} = \bar{\Gamma}_I(s)\theta_{xI}(x) + \bar{\eta}_{I,s}(x,s) = 0 \tag{2.65}$$

so that:

$$-\bar{\eta}_{I,s}(x,s) = \bar{\Gamma}_I(s)\theta_{xI}(x) \tag{2.66}$$

If the material is assumed to be elastic and the Poisson effects are neglected (HYPT4), the strain and stress ε_{ss} and σ_{ss} are thus related by Hooke law:

$$\varepsilon_{ss} = \xi_{,ss} = \Gamma_{I,s}\theta_{xI}e \tag{2.67}$$

$$\sigma_{ss} = E\varepsilon_{ss} = E\bar{\Gamma}_{I,s}\theta_{xI}e \tag{2.68}$$

The corresponding bending moment is calculated by using a variable separation (s and x dependent variables) as a resultant of the above stresses:

$$M^s_{xI}(s)\theta_{xI}(x) = \int e\sigma_{ss} de = E\frac{t^3}{12}\bar{\Gamma}_{I,s}\theta_{xI} \tag{2.69}$$

so that

$$\sigma_{ss} = 12\frac{M^s_{xI}\theta_{xI}}{t^3}e \qquad (2.70)$$

$\theta_{xI}(x)$ measures the amount of twist. Similarly to $\bar{\Gamma}_I$, $M^s_{xI}(s)$ (=$Et^3\bar{\Gamma}_{I,s}/12$) results from the membrane stiffening that rigidifies the internal transversal segments during a relative 'unit' twist of the blocks around the associated joint. This function vanishes at the outer edge segments of an open profile. $M^s_{xI}(s)$ (e.g. figure 2.20c) is calculated by taking the profile shape (figure 2.20b) as a frame with simple supports at inner transversal nodes and free boundary conditions at the edges. A 'unit' relative rotation (1-μ) is applied at the rigid joint I as an imposed relative rotation. The distribution of $M^s_{xI}(s)$ along the profile contour is determined by any standard force or displacement method for determining the bending moment distribution in statically indeterminate frames.

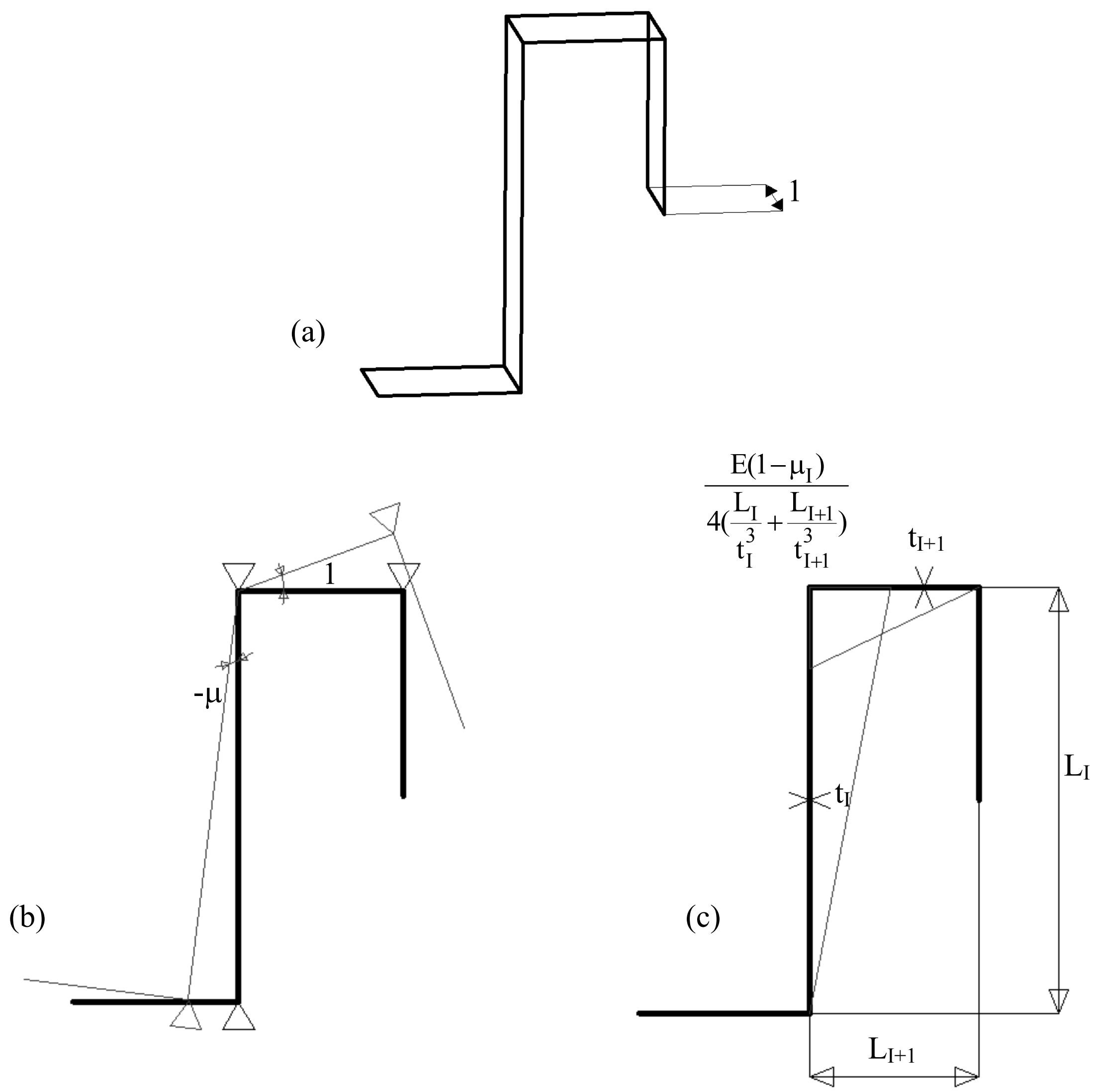

Figure 2.20 (a) An isolated unit length strip; stiffening effects represented by the distribution of M_s^{xI} along the profile contour (c) depending on the profile geometry (b)

Distortional centers and joint dependency:
For each distortional mode, the associated joint and rotation centers are geometrically dependent. A joint I divides the cross section into k_I rigid parts. The joint I is the intersection point that belongs to all of these parts. The rotation of a point q of a specific rigid part (k_I) around its own rotational center (y_{Ck_I}, z_{Ck_I}) is measured by $\mu_{k_I}\theta_{xI}$ so that:

$$v_q = -(z - z_{Ck_I})\mu_{k_I}\theta_{xI} \tag{2.72}$$

$$w_q = (y - y_{Ck_I})\mu_{k_I}\theta_{xI} \tag{2.73}$$

Since the point I belongs to all of these parts, the two following equations are valid for all values of k_I:

$$v_I = -(z_I - z_{Ck_I})\mu_{k_I}\theta_{xI} \tag{2.74}$$

$$w_I = (y_I - y_{Ck_I})\mu_{k_I}\theta_{xI} \tag{2.75}$$

$$z_I - z_{CL_I} = \mu_k(z_I - z_{Ck_I}) \tag{2.76}$$

$$y_I - y_{CL_I} = \mu_k(y_I - y_{Ck_I}) \tag{2.77}$$

From equations (2.76 and 2.77), it is concluded that:
- the distortional centers C_{kI} and joint I are aligned;
- the ratio IC_{kI} /IC_I (distances between distortional joint and distortional centers, one distortional part is taken as reference) is equal to μ_k.

2.4 Buckling of elastic thin walled columns

In a linear analysis (paragraphs 2.1, 2.2 and 2.3), beams and columns deflect according to their applied loading. A beam-column loaded longitudinally through its centroidal axis is supposed to be submitted to pure tension or pure compression without any bending or torsion. However, since thin-walled structures may have low lateral bending and/or torsional stiffnesses, elements may fail in a flexural or flexural-torsional buckling mode. When the load increases, the response of the beam or column remains theoretically linear until the value of the critical load is reached. The element suddenly deflects laterally or/and twists out of the plane of loading. This buckling occurs when the second-order moments caused by the product of the applied axial compression P with the transvesal displacements are equal to the internal bending or torsional resistances (2.78, 2.79 and 2.80). The criterion to determine the buckling state is the singularity of the system of structure equilibrium equations [De Ville 1989 page 4.12; Waszczyszyn 1994 page 45; …].
In this paragraph, the instability analysis of elastic structures originated by the interaction of buckling modes is presented with two different warping functions. Distortion is not considered.

2.4.1 Using Vlassov warping function

For small deflections of arbitrary cross sections, the general governing equations may be obtained in a simple manner by studying the static load-deflection behavior equations (e.g. [Murray, 1986, page 172]):

$$EI_z v_{,xxxx} + P(v_{,xx} + z_C\theta_{x,xx}) = 0 \tag{2.78}$$

$$EI_y w_{,xxxx} + P(w_{,xx} - y_C \theta_{x,xx}) = 0 \tag{2.79}$$

For open cross sections, the third equation (2.80) may be obtained by using Vlassov warping function [Murray, 1986, page 175]:

$$EI_\omega \theta_{x,xxxx} - (GK - Pi_C^2)\theta_{x,xx} + Pz_C v_{,xx} - Py_C w_{,xx} = 0 \tag{2.80}$$

where $i_0^2 = (I_y+I_z)/A$, $i_c^2=i_o^2+y_C^2+z_C^2$, I_z and I_y are the principal moments of inertia of the cross section about the axes of bending, GK is the torsional rigidity, and I_ω is the warping rigidity computed by using Vlassov theory.

It can be easily seen that, for doubly symmetrical cross sections whose centroid and shear center coincide ($y_C = z_C = 0$), equations (2.78, 2.79 and 2.80) are uncoupled. Buckling occurs either in a flexural or in a torsional mode. Only the transversal displacement v (or w) is involved in the flexural buckling of equation 2.78 when $z_C = 0$ (or equation 2.79 when $y_C = 0$). The torsional buckling involves the twisting rotation θ_x of the cross-section in equation 2.80 when $y_C = z_C = 0$. For monosymmetrical cross sections, torsion interacts with bending in the symmetric plane to initiate a flexural-torsional buckling while the other flexure is uncoupled and initiates a pure flexure buckling. In general, for asymmetrical cross sections, the centroid and the shear center do not coincide and the three equilibrium equations are coupled: the column buckles in a flexural-torsional mode. It twists and bends simultaneously and the corresponding buckling mode involves both lateral displacements (v,w) out of the plane of loading and twisting rotation θ_x; buckling is therefore resisted by a combination of bending and torsional resistances.

The system of three equations (2.78), (2.79) and (2.80) represents an eigenvalue problem. The solution of the system is given by solving the previous set of equations and by giving buckling shapes satisfying the boundary conditions. Three sets of discrete values of buckling loads are obtained. Only the lowest critical load is of practical interest.

2.4.2 Using Benscoter warping function

Usually, in the literature, flexural torsional buckling is restricted to the case of beams or columns with open cross sections. Due to its high torsional and bending stiffnesses, a column with a closed cross section will generally not collapse by global instability but rather by local buckling or yielding. Therefore, to study the flexural torsional buckling of a structural element with the kind of cross section represented in figure 2.21 which is neither totally open, nor fully closed, the following governing equations of flexural torsional buckling are developed hereby by using Benscoter torsional theory.

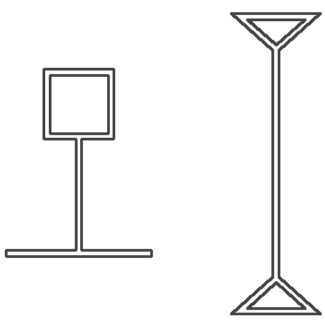

Figure 2.21 Cross sections containing one or more than one cell

The governing equation for torsion of a beam about the x-axis by using Benscoter warping function [Benscoter, 1954] is given by:

$$-EC\theta_{x,xxxx} + GK\theta_{x,xx} + m_x - \frac{EC}{GI_C} m_{x,x} = 0 \tag{2.81}$$

where $C = \frac{I_\omega}{\eta^2}$, $\eta^2 = 1 - \frac{K}{I_c}$, $I_c = \int r^2 eds$

I_c is the polar constant where r is the distance from the shear center to the tangent to the midline of the profile. I_ω is the warping rigidity.

By considering the twisting effect of the elementary loads during the buckling of a cross section and by integrating over the whole cross-section [Murray, 1986, page 175], the second-order torque caused by the applied compression P is expressed as:

$$m_x = P(-v_{,xx} z_C + w_{,xx} y_C - \theta_{,xx} i_C^{\ 2}) \tag{2.82}$$

By substituting (2.82) into (2.81), the governing equation for torsional buckling based on Benscoter theory is found:

$$(EC - P\frac{EC}{GI_c} i_C^{\ 2})\theta_{x,xxxx} - (GK - Pi_C^2)\theta_{x,xx} + Pz_c v_{,xx} + Pz_c v_{,xxxx} - Py_c w_{,xx} - Py_c w_{,xxxx} = 0 \tag{2.83}$$

2.5 Lateral buckling of elastic thin walled beams

When beams are designed to carry very large loads in their main plane (e.g. vertical plane of an I beam), small lateral or twisting disturbances can cause buckling out of the main plane of loading. The lateral torsional buckling mode combines torsion and minor axis bending. The torsion is accompanied by an important warping that influences the overall analysis. In the literature, the governing equations are elaborated by using Vlassov warping function [Murray, 1986, De Ville 1989, Trahair and Bradford 1995…]. In this paragraph, the lateral buckling is analyzed by using Benscoter warping function.
A simply supported beam loaded by equal but opposite end moments M_z is considered; y and z are the principle axes of the profile. In the case of small deformations and arbitrary cross section, M_{x1}, M_{y1} and M_{z1} are the resolved components of the twisting and bending moment acting about the deformed axes x_1, y_1 and z_1 (figure 2.22):

$$M_{z1} = M_z \cos(w_{,x}) \simeq M_z \tag{2.84}$$

$$M_{y1} = -M_z \sin(\theta_x) \simeq -M_z \theta_x \tag{2.85}$$

$$M_{x1} = -M_z w_{,x} + M_z(\frac{I_{yr^2}}{I_z} - 2y_C)\theta_{x,x} \tag{2.86}$$

where $I_{yr^2} = \int_A y(y^2 + z^2)dA$

$$EI_y w_{,xx} = -M_{y1} \tag{2.87}$$

$$EI_z v_{,xx} = -M_{z1} \tag{2.88}$$

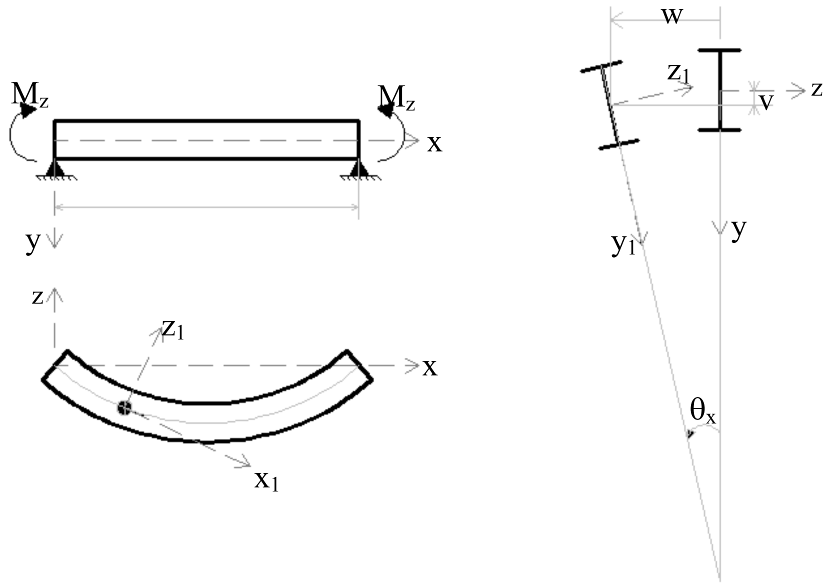

Figure 2.22 Lateral torsional buckling of a beam

The governing equation for twisting is deduced from (2.51) after setting $m_{x\omega}$ equal to zero:

$$-EC\theta_{x,xxx} + GK\theta_{x,x} = M_{x1} - \frac{EC}{GI_c} M_{x1,xx} \tag{2.89}$$

where $C = \frac{I_\omega}{\eta^2}$, $\eta^2 = 1 - \frac{K}{I_c}$. K is the torsional constant, $I_c = \int r^2 eds$ is the polar constant.

By substituting (2.84), (2.85) and (2.86) in (2.87), (2.88) and (2.89), the following equations are obtained:

$$EI_z v_{,xx} = -M_z$$
$$EI_y w_{,xx} = M_z \theta_x$$
$$(-EC + M_z(\frac{I_{yr^2}}{I_z} - 2y_C))\theta_{x,xxx} + (GK - M_z(\frac{I_{yr^2}}{I_z} - 2y_C))\theta_{x,x} + M_z w_{,x} - M_z \frac{EC}{GI_C} w_{,xxx} = 0 \tag{2.90}$$

The critical elastic moment is given by the solution of (2.91) deduced from the set of equation (2.90):

$$(-EC + M_z(\frac{I_{yr^2}}{I_z} - 2y_C))\theta_{x,xxxx} + (GK - \frac{EC}{GI_C}\frac{M_z^2}{EI_y} - M_z(\frac{I_{yr^2}}{I_z} - 2y_C))\theta_{x,xx} + \frac{M_z^2}{EI_y}\theta_x = 0 \tag{2.91}$$

Equation (2.91) has a general form similar to that obtained classically for open cross sections [Murray 1986, page 184] and its solution is thus given by:

$$\theta_x = A_1 \sin(mx) + A_2 \cos(mx) + A_3 e^{nx} + A_4 e^{-nx} \tag{2.92}$$

where $m = \sqrt{-a + \sqrt{a^2 + b}}$ and $n = \sqrt{a + \sqrt{a^2 + b}}$

with $a = \dfrac{1}{2(EC - M_z(\frac{I_{yr^2}}{I_z} - 2y_C))}(GK - \dfrac{EC}{GI_C}\dfrac{M_z^2}{EI_y} - M_z(\dfrac{I_{yr^2}}{I_z} - 2y_C))$

$$b = \frac{M_z^2}{(EC - M_z(\frac{I_{yr^2}}{I_z} - 2y_C))EI_y}$$

The constants $A_1 \dots A_4$ are determined by setting that (2.92) must satisfy the boundary conditions. For a simply supported beam, each end is free to warp (θ_x = 0, $\theta_{x,xx}$ = 0) and the following equations are obtained:

$$\begin{aligned} &A_2 = 0 \\ &A_3 = -A_4 \\ &A_1 \sin(mL) - 2A_4 \sinh(nL) = 0 \\ &-A_1 m^2 \sin(mL) + 2A_4 n^2 \sinh(nL) = 0 \end{aligned} \tag{2.93}$$

In order to obtain a non trivial solution, the determinant of the system of equations (2.93) should be zero and the solution is:

$$\theta_x = A_1 \sin(mx) \tag{2.94}$$

The lowest buckling mode occurs for:

$$m = \frac{\pi}{L} \tag{2.95}$$

and the lowest buckling moment is then solution of:

$$(EC - M_z(\frac{I_{yr^2}}{I_z} - 2y_C))(\frac{\pi}{L})^4 + (GK - \frac{EC}{GI_C}\frac{M_z^2}{EI_y} - M_z(\frac{I_{yr^2}}{I_z} - 2y_C))(\frac{\pi}{L})^2 = \frac{M_z^2}{EI_y} \tag{2.96}$$

PART II. THEORETICAL DEVELOPMENTS

CHAPTER 3. KINEMATICS OF THE PRESENT ANALYSIS OF THIN WALLED BEAMS

3.1 Geometric description and assumptions

A fixed right-handed cartesian coordinate system (X,Y,Z) is used for the analysis of three dimensional structures with beam elements composed of thin plates. The thickness is smaller than the other dimensions. Each beam element is prismatic and has a local x axis parallel to its longitudinal direction. The intersection of a plane normal to the x axis with the middle surface is a polygonal line called "contour" of the cross section. The vertices of the polygonal contour are called hereafter "transversal nodes". Let G be the centroid, C the shear center and y and z the principal axes of the cross section. A right handed local curvilinear coordinate system (e,s,x) is placed in the middle surface with (e) normal to and (s) following the contour (figure 3.1).

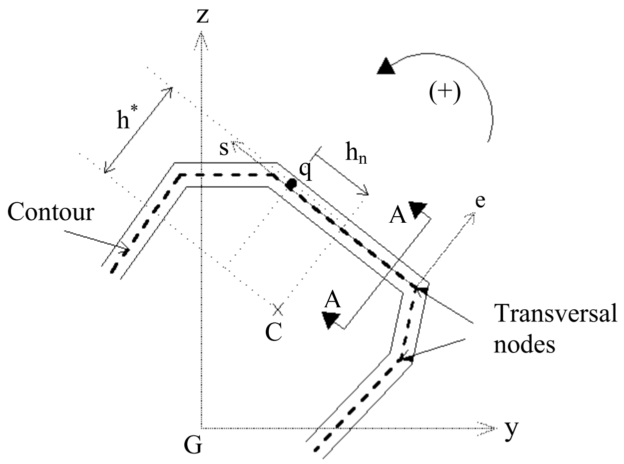

Figure 3.1 General form of a cross section

The theory of torsion and flexure of thin walled beams is based on the following kinematic assumptions:

HYP1. In the analysis of torsion and bending of thin walled beams and columns, the contour of a cross section is considered as undeformed in its own plane. The local distortion, flexure or plate buckling are not taken into account. This assumption, which is critical in the case of very thin cross sections, requires in practice rigid diaphragms placed at short distances along the length of the beam. This assumption is relaxed when the distortion is studied (paragraph 3.4).

HYP2. The cross section remains plane when subjected to pure tension/compression or pure bending; warping due to torsion is analyzed in paragraph 3.2, warping due to shear bending is analyzed in §3.3 and warping due to distortion is analyzed in paragraph 3.4.

HYP3. The warping is assumed to vary linearly along each branch of the contour between two transversal nodes (contour warping).

HYP4. The material points, located before deformation on a normal to the surface (xs), are assumed to remain on a line normal to the deformed middle surface. This normality assumption allows the determination of the second order warping (through the thickness of the thin wall) of the thin 'plates'.

3.2 Torsional warping of the cross section

As introduced at the end of §2.2.3, Prokić warping function is modified in this chapter in order to study the behavior of arbitrary thin walled cross sections. The torsional warping of an arbitrary point q of the cross section (figure 3.1) is equal to the sum of a contour warping u_c and a thickness warping u_t.

$$u_q^T = u_c + u_t \tag{3.1}$$

3.2.1 Contour warping function

If the cross section is composed of polygonal segments, the contour torsional warping u_c is linear along each branch. At mid wall, this axial displacement (u_c) due to torsional warping is computed as a sum of combinations of linear contour functions and displacement parameters (u_i) at transversal nodes (figure 3.2).

$$u_c = \sum \Omega^i u_i \tag{3.2}$$

The unknowns u_i are the longitudinal displacements of the transversal nodes (i=1,…n) due to the torsional warping. The functions Ω^i (i=1,…n) represent the shape of the distribution of the contour warping along the branches of the contour between transversal nodes (i=1,…n). Since the contour warping is assumed to be linear between two longitudinal nodes (HYP3), a function Ω^i describes a linear variation between node (i) and its adjacent transversal nodes. Ω^i varies linearly along the branches between the transversal node i where $\Omega^i = 1$ and the adjacent nodes where $\Omega^i = 0$ and vanishes along the other segments (figure 3.2 b & c).

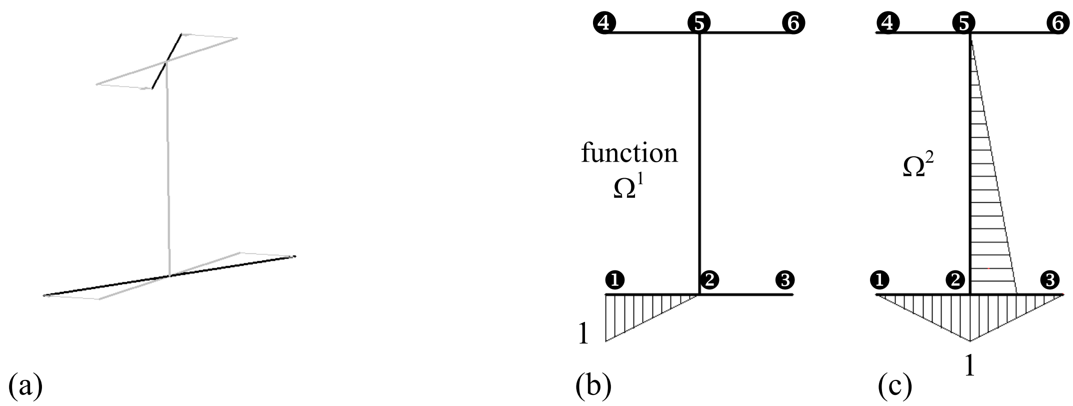

Figure 3.2 (a): Warping along the contour of the profile; (b) & (c): functions Ω^1 and Ω^2

3.2.2 Thickness warping function

The thickness torsional warping u_t varies linearly through the thickness and vanishes along the mid wall (figure 3.3). It is proportional to the derivative of the torsional rotation angle $\theta_{x,x}$, to the distance to the midline e, and to the perpendicular distance h_n to the normal issued from the shear center.

$$u_t = -\omega\theta_{x,x} \tag{3.3}$$

where $\omega(y,z) = h_n(s).e$, figure 3.1. h_n is positive when the normal to the midline rotates counterclockwise around the shear center (h_n is negative in the case of figure 3.1).

It is shown hereafter that equation (3.3) results directly from hypothesis HYP4. The local contour system (e, s, x) shown in figure (3.1) is used. The torsional displacements of a point q are described with respect to this contour coordinate system by ($u_q^T(x,s,e)$, $\xi_q^T(x,s,e)$, $\eta_q^T(x,s,e)$).

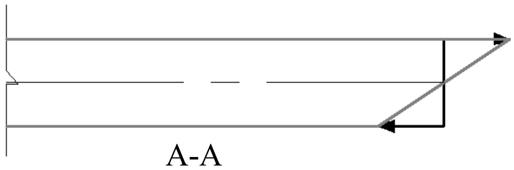

Figure 3.3 Thickness warping function, cut A-A of figure 3.1

When the cross section is submitted to torsion, it twists with respect to the shear center axis. For small values of torsional rotation θ_x, the transversal displacements are found by simple geometrical descriptions as being proportional to the distance to the shear center. In the principal axes system (y,z), the expressions of v_q^T and w_q^T are given in equation (2.22). By using the local system axis (e,s), the transversal displacements η_q^T and ξ_q^T are found to be:

$$\eta_q^T(x,s) = h_n\theta_x$$

$$\xi_q^T(x,s) = h^*\theta_x \tag{3.4}$$

According to the normality assumption (HYP4) through the thickness of the wall, the normal to the surface (xs) remains normal during deformation. The shear deformation ε_{xe} (3.5) is neglected. A straight line through the thickness (e) normal to the surface (xs) is assumed to remain straight and normal so that the rotation is equal to the slope (3.6).

$$2\varepsilon_{xe}^T = \eta_{q,x}^T + u_{q,e}^T \tag{3.5}$$

$$2\varepsilon_{xe}^T = 0 \Rightarrow u_{q,e}^T = -\eta_{q,x}^T \tag{3.6}$$

By substituting the transversal component of displacement η_q^T by its expression (3.4) in equation (3.6), the derivative of the longitudinal displacement with respect to the thickness coordinate is given in (3.7).

$$u_{q,e}^T = -h_n\theta_{x,x} \tag{3.7}$$

The displacement u^T of any point q is thus given by:

$$u_q^T(x,s,e) = u^T(x,s) + e\frac{\partial\eta_q^T(x,s)}{\partial x} = u^T(x,s) - eh_n\theta_{x,x} \tag{3.8}$$

The first term $u^T(x,s)$ in (3.8) describes the variation of the longitudinal displacement along the mid wall. By comparing (3.8) to (3.1), this term represents the contour warping (u_c) given in equation (3.2). The second term is the thickness warping (u_t) in equation (3.3).

Once again, an analogy between Bernoulli bending beam kinematics or Kirchhoff bending plate kinematics and torsional kinematics is highlighted through the normality assumption HYP4. The theory of Kirchhoff for thin plates is based on the assumption that straight lines normal to the mid plane before deformation remain normal after deformation. This implies that shear transversal deformations are negligible; the slope and the tangent coincide.

3.2.3 Torsional warping function and decoupling equations:

Complete kinematic formulation

As stated before, Prokić warping function is very general but must be restrained adequately in order to study a specific problem. In this paragraph, the theory is developed in order to study the torsional behavior of a 3D beam structure. In a general loading with tension-compression, biaxial bending and torsion, equation (3.9) gives the displacement of any point q(x,y,z) of the cross section for each of these loading effects:

$$\begin{Bmatrix} u_q \\ v_q \\ w_q \end{Bmatrix} = \begin{Bmatrix} u_0 \\ 0 \\ 0 \end{Bmatrix} + \begin{Bmatrix} z\theta_y \\ 0 \\ w \end{Bmatrix} + \begin{Bmatrix} -y\theta_z \\ v \\ 0 \end{Bmatrix} + \begin{Bmatrix} -\omega\theta_{x,x} + \sum_{i=1}^{n}\Omega^i(y,z)u_i(x) \\ -(z-z_C)\theta_x \\ (y-y_C)\theta_x \end{Bmatrix} \qquad (3.9)$$

Total = axial

+ bending(xz)

+ bending(xy)

+ torsion.

On the right hand side of equation (3.9), the first bracket $\{u_0,0,0\}$ denotes the in-plane compression or tension, the second bracket $\{z\theta_y,0,w\}$ refers to in-plane (xz) bending by using Timoshenko beam theory for shear effects, and the third bracket $\{-y\theta_z,v,0\}$ refers to (xy) bending. The fourth bracket of (3.9) gives the warping $u^T = -\omega\theta_{x,x} + \sum\Omega^i u_i$ and the transverse displacements $\{-(z-z_C)\theta_x\ ,\ (y-y_C)\theta_x\}$ related to the torsion. $\theta_{x,x}$ is the rate of twisting angle and $u_1 \dots u_n$ are n unknowns, where n is the number of transversal nodes. These parameters are additional axial displacements that introduce for each transversal node the quantity of the warping displacement (u_i) to that induced by tension/compression (u_0) and bending ($z\theta_y$-$y\theta_z$) and represented by the centroidal degrees of freedom. As presented in (3.9), the kinematic expression of u^T is more general than the usual torsional warping theory of thin walled beams: it is not limited to the torsional warping and can describe any general displacement of the cross section constituted by linear combination of u_i. Thus, to satisfy HYP2 (paragraph 3.1), it is necessary to prescribe additional constraints in order to restrain the parameters u_i to the modeling of torsional warping. This separates warping from tension-compression and bending effects and ensures the uncoupled axial/bending/torsional warping: when subject to pure tension/compression or flexure, the cross section does not warp (HYP 2).

Uncoupling of tension/compression and bending effects

The dissociation of the axial displacement into three parts (a constant mean value u_0 and linear values $z\theta_y$ et $y\theta_z$) corresponds to the separation of tension/compression and (xy & xz) bending effects. It is well known that these three effects are uncoupled if the centroid (G) of the cross section is used as origin and if the principal axes are used as reference axes.

Uncoupling of pure torsion and bending

It is also well known that pure torsion and pure bending are defined by introducing the shear center and the torsional center as particular points of a profile. A transversal load P passing through the shear center does not induce a torsional torque. However, if this transversal load P acts within a non zero distance r_C from C, a torsional torque $C_x = P\ r_C$ is induced. Alternatively, if a torque twists the cross section with respect to the torsional center axis, a pure torsion occurs about this "natural" axis of rotation without involving bending displacements. The torsional center is found ([Kollbrunner, 1970, page 112],…) to be identical to the shear center.

Uncoupling of torsional warping and tension/compression

The average axial displacement of the cross section must be reduced to the term (u_0): a tension or compression of the whole cross section must only derive from the centroidal degree of freedom (u_0). Within the present beam theory, a cross section resists to stretching (figure 3.4a) by a "rigid" extension (figure 3.4b) and remains planar and perpendicular to the longitudinal axis. The configuration represented in figure 3.4c with non zero values of u_i (relative longitudinal displacement with respect to the displacement of the centroid u_0) is undesirable since warping degrees of freedom (u_i) are related to torsion.

$$u_{average} = \frac{\int_A u_q dA}{A} = u_0 \tag{3.10}$$

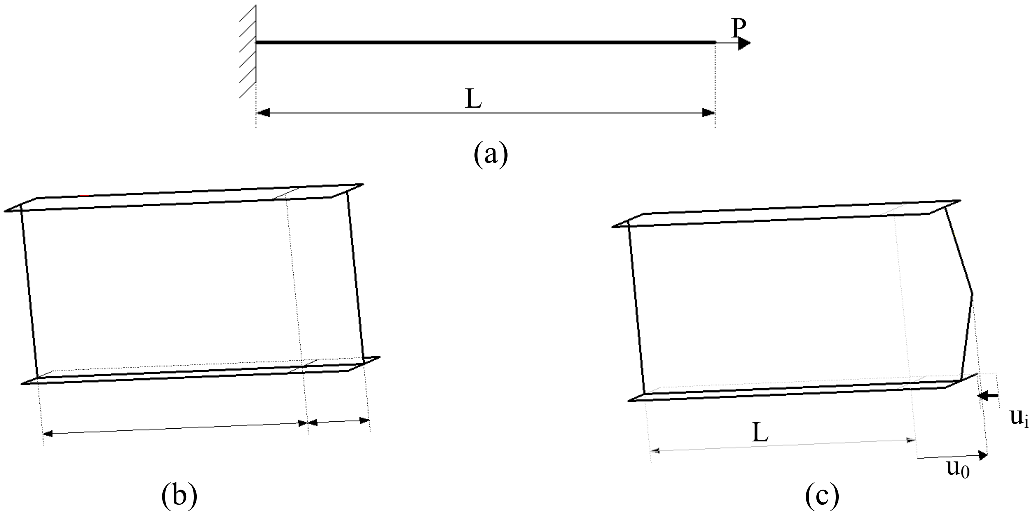

Figure 3.4 (a) Tension of an I beam; (b) extension u_0 of the beam with u_i vanishing; (c): possible configuration when uncoupling is not satisfied: warping ($-u_i$) related to tension.

The numerator of (3.10) is found to be:

$$\int_A u_q dA = u_0 A + \sum_{i=1}^{n} S_{\Omega^i} u_i \tag{3.11}$$

The first equation that ensures the uncoupled tension-compression and torsional warping effects is thus deduced from (3.10):

$$\int_A u_{warping}^T dA = 0 \tag{3.12}$$

or

$$\sum_{i=1}^{n} S_{\Omega^i} u_i = 0 \tag{3.13}$$

Uncoupling of torsional warping and pure bending

The average bending displacement must also be reduced to the flexural terms ($z\theta_y$) and ($-y\theta_z$). The rotation along the axis Oz (or Oy) must be limited to θ_z (or θ_y) and the displacements associated with this rotation are only represented by the term $-y\theta_z$ or ($z\theta_y$) (figure 3.5).

In the case of (xy) plane flexure, Timoshenko bending equilibrium equation includes a term θ_z which is the mean angle of rotation of each cross section about the neutral axis. As in equation (2.5), Timoshenko kinematics gives the expression of the longitudinal displacement:

$$u_q^F = -y\theta_z \tag{3.14}$$

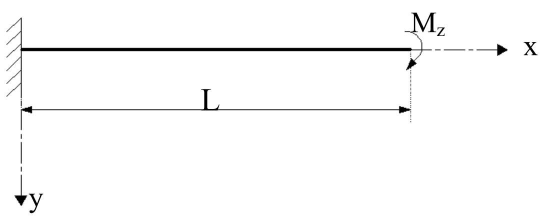

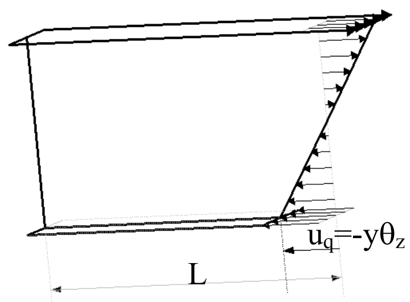

Figure 3.5 Pure bending of an I beam

θ_z has been given various definitions and interpretations (after [Cowper, 1966]). If the cross section remains planar as the beam bends, θ_z is exactly equal to the angle of rotation of the whole cross section. However, if a cross section warps in addition to rotating, θ_z is then the angle of inclination of the plane that most nearly coincides with the position of the warped cross section. Cowper [1966] defined the quantity θ_z by the following relation:

$$\theta_z = -\frac{1}{I_z}\int_A y u_q \, dA \tag{3.14'}$$

Equation (3.14') is found by mutliplying Timoshenko kinematics (3.14) by y and by integrating over the cross section.

To uncouple the torsional warping from bending effects, the first line of the fourth bracket of (3.9), related in this paragraph to torsional warping effects, must be separated from bending warping which is not taken into account hereby. The flexural mean rotation θ_z must be related to the flexural degrees of freedom and not to the warping degrees of freedom u_i.

$$\int_A y u_q^T \, dA = 0 \tag{3.15}$$

(3.15) gives the second transformation equation to satisfy:

$$-I_{y\omega}\theta_{x,x} + \sum_{i=1}^{n} I_{y\Omega^i} u_i = 0 \qquad (3.16)$$

In the case of plane flexure (xz), a similar transformation equation is found by the same method by setting that the warping resulting from bending (xz) is not taken into account.

$$\int_A z u_q^T dA = 0$$

$$-I_{z\omega}\theta_{x,x} + \sum_{i=1}^{n} I_{z\Omega^i} u_i = 0 \qquad (3.17)$$

Illustration of torsional warping uncoupling

Equations (3.12, 3.15 and 3.17) represent respectively the separation of warping effects from tension/compression, (xy) bending and (xz) bending. This separation is alternatively illustrated by plotting the axial displacement over the cross section. When a plot shows a strong relationship between two variables (y,f), the regression line is a line drawn through a plot so that it comes as close to the points (y,f) as possible. The regression line (f' in figure 3.6a) is the best fitting straight line for a given set of points in a plot and is defined by a f-intercept ($f_{(y=0)}$) and a slope. More technically, the regression line is obtained by minimizing, for a function f(y), the sum of the squared differences between (f') and (f). The slope and the f-intercept may be thus determined by setting that the sum of these squared differences $\sum|f-f'|^2$ is smaller than it would be for any other straight line through the data.

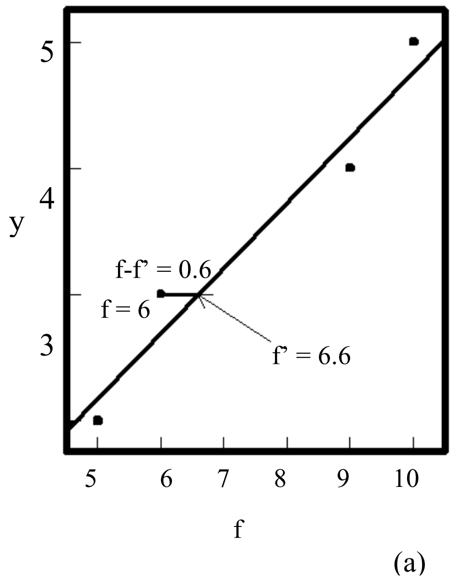

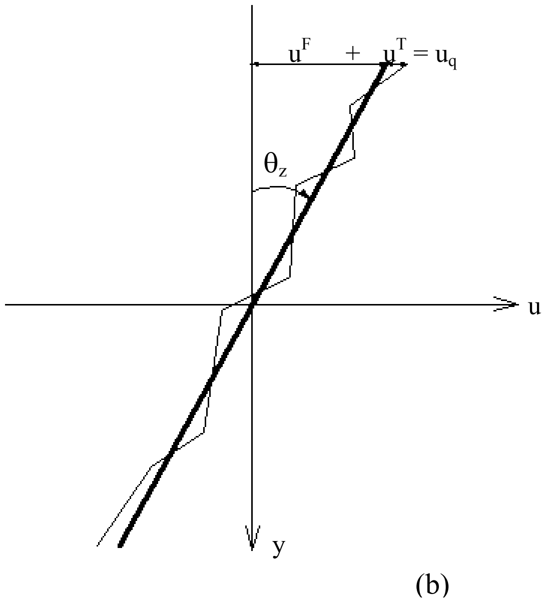

Figure 3.6 Regression lines of plots (a): (y,f) and (b): (y,u)

In the case of bending (xy), the axial displacement of a point q ($u_q = u^T + u^F$) varies with (y) and is plotted against this cross section co-ordinate. The plane $u^F = y\theta_z$ is a straight plane (a line in figure 3.6b) associated with the rotation of the whole cross section around the z axis (θ_z) that most nearly coincides with the position of the warped cross section (u_q). The additional displacement function u^T represents the torsional warping and is not related to the flexural bending of the cross section. Even if the statistical notion of regression line does not give an exact demonstration as it was done in the previous paragraph (equations 3.14-3.16), it is presented hereby to illustrate physically the nature and the importance of the uncoupling phenomenon. The axial displacement of the points q of the cross section ($u_q = -y\theta_z + u^T$) is separated into an arbitrary straight distribution line ($y\theta$) and a function u. The regression line minimizes the function $g(\theta)$ constituted of squared differences, when the slope θ varies.

$$g(\theta) = \int (u_q - \theta y)^2 dA \tag{3.18}$$

Mathematically, to limit the average rotation of the cross section to θ_z, $g(\theta)$ must be a minimum when θ equals $-\theta_z$:

$$\begin{aligned}
g(\theta) &= \int (u_q - \theta y)^2 dA \\
g(\theta) &= \int (u_q^T - (\theta + \theta_z) y)^2 dA \\
g(\theta) &= \int (u_q^T)^2 dA + (\theta + \theta_z)^2 \int y^2 dA - 2(\theta + \theta_z) \int y u_q^T dA \\
\frac{dg(\theta)}{d\theta} &= 2(\theta + \theta_z) \int y^2 dA - 2 \int y u_q^T dA
\end{aligned} \tag{3.19}$$

By setting $g'(\theta)$ zero for $\theta = -\theta_z$, the second expression to ensure the uncoupled bending (xy) and warping effects is found to be (3.15). Equation (3.17) can be obtained similarly by considering the case of bending (xz).

The transformation equation (3.12) can be illustrated by the same method by setting that, since the warping resulting from axial effects is neglected and not included hereby, the x-intercept (y=0, z=0) of the regression plane ($u_q = u_0 + z\theta_y - y\theta_z - \omega\theta_{x,x} + \sum\Omega^i u_i$) must be prescribed to u_0 (centroid axial displacement).

Torsional transformation equations

Thus, as the additional parameters (u_i) should only describe the torsional warping of the cross section associated with torsion and should not induce global elongation or bending of the whole cross section, these n degrees of freedoms (u_i) must therefore satisfy the three equations (3.20).

$$\int_A u^T dA = 0, \qquad \int_A y u^T dA = 0, \qquad \int_A z u^T dA = 0 \tag{3.20}$$

where A denotes the area of a cross section.

If n is the number of transversal nodes of a cross section, from the 6+n degrees of freedom, only 3+n degrees of freedom are thus independent: three translations (u,v,w), three rotations ($\theta_x,\theta_y,\theta_z$) and n-3 relative longitudinal displacements.

This step (equations 3.20), that supplements the use of centroïd, shear center and principal axes, transforms arbitrary coordinate system (1, x, y, $\sum\Omega_i u_i/\theta_{x,x}$,…) to a particular one that ensures the uncoupling between $\sum\Omega_i u_i/\theta_{x,x}$ and the others. It is similar to the well-known selection of the principal sectorial warping function (**ω, ψ**) when using the models of Vlassov and Benscoter respectively to study the non uniform torsion. The principal sectorial pole is found to be the shear center and the sectorial origin is a particular point obtained by satisfying the following equations ([Gjelsvik,1981, page 49], [Murray, 1986, page 86-87]…):

$$\int_A \omega dA = 0, \int_A y\omega dA = 0, \int_A z\omega dA = 0 \text{ for open profiles, Vlassov theory} \quad (3.21)$$

$$\int_A \psi dA = 0, \int_A y\psi dA = 0, \int_A z\psi dA = 0 \text{ for closed profiles, Benscoter theory} \quad (3.22)$$

Note that the equations listed above (3.21-3.22) are needed to determine the location of the tortional or shear center according to Vlassov and Benscoter theory. Equations (3.21-3.22) are found in the literature by setting that Vlassov and Benscoter torsional kinematics must not produce any axial force or bending moment.

3.3 Warping associated with bending shear effects

3.3.1 Problem presentation

When a beam is submitted to bending, a varying bending moment is necessarily accompanied by a shear force resulting from the equilibrium of rotation. An accurate study of the influence of the shear force is very complicated. Similarly to the case of shear effects induced by a torsional loading, the cross section does not remain plane when submitted to a shear force. Shear stresses resulting from a shear force acting along a principal axis (eg. z) of the beam cannot be uniformly distributed over the cross section. It is not possible to find a simple kinematic description allowing their calculation (see also Frey 2000).
The configuration (a b' c' d) assuming uniform sliding of the profile is impossible (the change in angles (ab,ab') and (dc,dc') must vanish in figure 3.7) since the equilibrium condition of a solid requires the vanishing of transverse shear stress (and hence shear strain) on the free edges of the beam (ab and cd in figure 3.7).

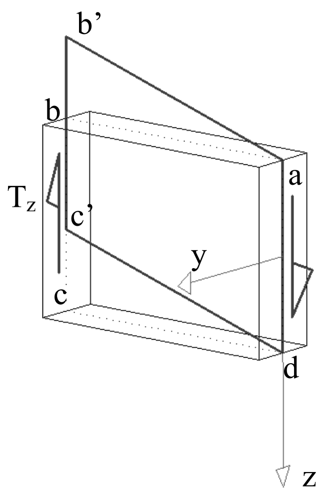

Figure 3.7 A beam submitted to a shear force

The variation of the angle ($2\varepsilon_{xz}$) (figure 3.8c) is thus not uniform across the cross section. The cross section does not remain plane but warps. In figure 3.8, $2\varepsilon_{xz}$ is maximal at the neutral axis of the rectangular profile and vanishes at the extreme fibers.
When the distribution of the shear force is uniform along the x axis and without restraining conditions, the shear warping is also uniform along the longitudinal axis (fig. 3.8c). In a general case, warping is

not free or uniform and the mean sliding angle (θ_y) is the angle of inclination of the plane that best coincides with the warped cross section.

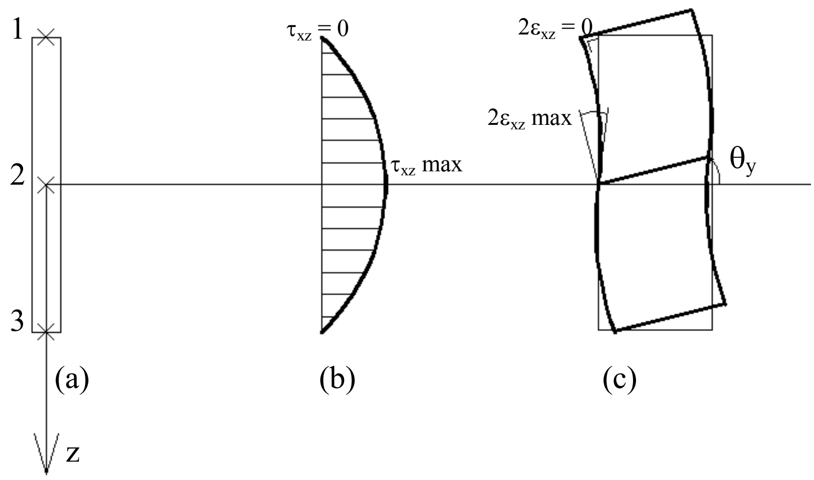

Figure 3.8 (a): Beam cross section; (b): shear stresses; (c): warping of the cross section with a constant shear force (after Frey 2000)

3.3.2 Warping function with shear bending effects

Advanced kinematics is presented in this paragraph in order to adequately describe shear deformations and to improve the results obtained from approximate Timoshenko kinematics violates the 'no shear' boundary conditions at the edges of open profiles by assuming a constant state of transverse shear strain through the cross section. The planar assumption of Bernoulli and Timoshenko theories is removed and the formulation is based on an enriched description of the shear bending warping by discretizing the contour of the thin walled profile. The bending warping is presented hereby in the case of (xz) flexure and is based on the following displacement field:

$$\begin{Bmatrix} u_q \\ v_q \\ w_q \end{Bmatrix} = \begin{Bmatrix} z\theta_y + \sum \Omega^i u_i \\ 0 \\ w \end{Bmatrix} \tag{3.23}$$

Similarly to the case of torsional warping, the parameters u_i at transversal nodes are the longitudinal displacements at selected transversal nodes (i=1,2,…n). The functions Ω_i (i=1,…n) represent the shape of the distribution of the contour warping along the branches of the contour between transversal nodes (i=1,…n).

By using the additional term $\sum\Omega_i\, u_i$, the warping induced by shear deformation is included and the cross section does not remain plane after deformation. θ_y does not represent any longer the rotation of a plane cross section but rather the slope at particular points of the cross section where the warping vanishes (for a rectangular cross section, θ_y is the slope at z=0). θ_y and u_i (i=1,n) capture together the non planarity nature of the deformed cross section.

The expression of strains is written as follows:

$$\begin{Bmatrix} \varepsilon_x \\ 2\varepsilon_{xy} \\ 2\varepsilon_{xz} \end{Bmatrix} = \begin{Bmatrix} z\theta_{y,x} + \sum \Omega^i u_{i,x} \\ \sum \Omega^i{}_{,y} u_i \\ w_{,x} + \theta_y + \sum \Omega^i{}_{,z} u_i \end{Bmatrix} \tag{3.24}$$

$w_{,x}+\theta_y$ is considered to be an approximate average deformation of the cross section as in Timoshenko beam theory and the additional terms $\sum\Omega_{i,y}\, u_i$ and $\sum\Omega_{i,z}\, u_i$ are given to improve this approximation by including local deformation due to the warping.

3.3.3 Additional equations

In order to achieve the kinematic description of the displacement field and to adapt the general formula $u_{warping} = \sum\Omega^i\, u_i$ in (3.23) to describe bending shear effects of a thin walled-cross section, additional equations are required to satisfy the boundary conditions setting that the transverse shear stresses (and therefore strains) must vanish at free edges of open profiles and to restrain the additional degrees of freedom to the above described phenomenon.

Similarly to developments of the kinematics of torsional warping (§3.2.3), additional kinematic conditions must be satisfied in order to uncouple the (xz) warping bending effects from axial, (xy) bending and torsional effects. The condition (3.17) is relaxed in order to relate the n degrees of freedom (u_i) to the (xz) warping bending effects. Regarding axial and (xy) bending effects, the following kinematical equations must be satisfied:

$$\int_A u_{warping}\, dA = 0 \qquad \Rightarrow \qquad \sum_{i=1}^{n} S_{\Omega^i} u_i = 0 \tag{3.25}$$

$$\int_A y u_{warping}\, dA = 0 \qquad \Rightarrow \qquad \sum_{i=1}^{n} I_{y\Omega^i} u_i = 0 \tag{3.26}$$

For closed profiles, no boundary conditions are required. For an open profile, the zero shear boundary conditions give additional constraints on the parameters u_i by prescribing that at the edge, ε_{xs} vanishes and thus:

$$\varepsilon_{xs} = 0 \tag{3.27}$$

Since the variation of transverse shear strain is not linear but quadratic, non linear functions Ω^i are necessary to accommodate exactly a quadratic variation of the transverse shear strain with a minimum profile discretization. However, for simplicity, the functions Ω^i are hereby considered as linear and the discretization of the profile is refined.

(3.27) is developed by using (3.24) and is reduced to the following condition:

$$-u_e+u_d=0 \tag{3.28}$$

where e is the edge transversal node (it represents all nodes related to only one segment of the profile; e.g. nodes 1 and 3 in figure 3.8) and d is the adjacent node (node 2 in figure 3.8). u_e and u_d are the corresponding degrees of freedom.

Furthermore, to uncouple the (xz) warping effects considered in this paragraph from the (xy) bending, an additional equilibrium condition is required setting that u_i do not represent a warping resulting from shear forces along the perpendicular direction (y). For an elastic behavior and a homogeneous profile:

$$G\int_A \varepsilon_{xy} dA = 0 \qquad => \qquad \sum_{i=1}^{n} S_{\Omega^i{}_{,y}} u_i = 0 \tag{3.29}$$

3.4 Distortional warping

3.4.1. Introduction

The warping function presented in §3.2 is adapted in order to adequately describe the distortional behavior introduced in §2.3. Depending on the beam geometry, m distortional modes are associated with m joints separating the cross section into two or more parts. Each distortional mode is characterized by the rotation of each part around its own specific center and by an out of plane bending of the inner plates constituting the beam. Each part is assumed to remain rigid and undeformable regarding the associated distortional mode.

3.4.2 Warping function and displacement field

Similarly to the developments presented in §3.2, the distortional warping function is divided into two terms: the contour warping function u_c and the thickness warping function u_t. The general Prokić warping function, for which the warping is assumed to vary linearly along straight branches of the contour, is adapted in order to determine u_c. The thickness distortional warping (or second order distortional warping) u_t is considered to vary linearly through the thickness and to vanish along the midwall. For each distortional mode I (I = 1…m), u_t is proportional to $\theta_{xI,x}$ the derivative of the distortional rotation angle, to the distance to the midline e, and to the perpendicular distance h_{nI} to the normal issued from the associated distortional center.
A distortional degree of freedom θ_{xI} is associated with a distortional joint I (I = 1…m) and is taken as the rotation of a specific part of the contour (I-I+1-…-n) around the associated distortional rotation center. For open profiles without ramifications, the rotation of the left part of the contour (1-2-…j) around the left distortional rotation center C_{Ig} is measured by $\mu_I\theta_{xI}$. μ_I is the specific rotating ratio between the right and the left sectional parts. For a monosymmetrical profile with one distortional mode, μ is found to be equal to -1. For arbitrary profiles, $\overline{\mu}_I$, $\overline{y}_{CI}$ and $\overline{z}_{CI}$ are functions of the contour length (s) for a distortional mode I. $\overline{y}_{CI}$ (s) and $\overline{z}_{CI}$ (s) represent, for each value of s, the coordinates of the distortional rotation center of the associated part. At the reference part, θ_{xI} is the distortional rotational angle and $\overline{\mu}_I$ is equal to 1. For the other parts of the contour, $\overline{\mu}_I$ represents the rotating ratio.

$$u_{tI} = -\,\overline{\omega}_I\ \overline{\mu}_I\,\theta_{xI,x} \tag{3.30}$$

where $\omega_I(y,z) = h_{nI}(s).e$. h_{nI} is positive when the normal to the mid line rotates counterclockwise around the distortional center.

The displacement of any point q(x,y,z) of the cross section associated with the distortional mode I (I = 1…m) is given by:

$$\begin{Bmatrix} u_q^D \\ v_q^D \\ w_q^D \end{Bmatrix} = \begin{Bmatrix} -\overline{\omega}_I \overline{\mu}_I \theta_{xI,x} + \sum_{i=1}^{n} \Omega^i u_i \\ -(z - \overline{z}_{CI}) \overline{\mu}_I \theta_{xI} \\ (y - \overline{y}_{CI}) \overline{\mu}_I \theta_{xI} \end{Bmatrix} \tag{3.31}$$

3.4.3 Kinematics decoupling

In this section, similarly to the work developed in §3.3 and §3.4.3, the distortion is separated from axial, bending and tortional effects. The general function (equation 3.2) must be adapted in order to associate the additional longitudinal displacements u_i (i = 1,n) of the transversal nodes with the distortional behavior. Kinematic conditions that must be satisfied in order to uncouple the distortional warping ($u^D = u_c + u_t$) from axial, bending, torsional effects (u^T computed in §3.2) are:

$$\int_A u^D dA = 0 \tag{3.32}$$

$$\int_A y u^D dA = 0 \tag{3.33}$$

$$\int_A z u^D dA = 0 \tag{3.34}$$

$$\int_A u^T u^D dA = 0 \tag{3.35}$$

This step (equations 3.32-3.35), that ensures the uncoupling between the distortional degrees of freedom and the others, is similar to the selection of the principal distortional sectorial warping function ω_I when using the models of Takahashi [1978, 1980…]. The principal sectorial poles are found to be the distortional centers and the sectorial origin is a particular point obtained by satisfying the following equations:

$$\int_A \boldsymbol{\omega}_I dA = 0 \tag{3.36}$$

$$\int_A y \boldsymbol{\omega}_I dA = 0 \tag{3.37}$$

$$\int_A z \boldsymbol{\omega}_I dA = 0 \tag{3.38}$$

$$\int_A \omega_0 \boldsymbol{\omega}_I dA = 0 \tag{3.39}$$

where ω_0 is the torsional warping function.

Note that the four equations listed above (3.36-3.39) contribute to the determination of the distortional centers and the rotating ratio according to Takahashi theory. These equations were found by Takahashi by setting that the distortional degree of freedom θ_{xI} must not be associated to any axial force, bending moment or torsional bimoment [Takahashi 1978].

CHAPTER 4. ANALYTICAL DEVELOPMENTS

4.1 Introduction

The analysis of engineering structures requires the formulation of theoretical models. Due to the complexity of the physical problem, many assumptions are elaborated and the mathematical model has to be formulated carefully in order to provide an acceptable description of the structural behavior during the loading process. A structural analysis problem consists of solving a set of equations with boundary conditions and prescribed constraints. When available, analytical solutions are the most convenient for modeling a structure. They enable clear analyses, physical interpretations and illustrated applications of an intricate theory on a simple structure. However, it is obvious that they do not respond to all complex requirements of a designer: simply supported beams are seldom found in practice.

In structural mechanics problems, it is thus usually preferred to formulate an approximate approach: instead of analyzing the whole structure as a continuous model, a corresponding discrete system with a finite number of parameters is used. This transition is required when the complexity of the structure necessitates the use of computer techniques.

Analytical developments for a linear elastic behavior of a structure are presented in paragraphs 4.2, 4.3 and 4.4 in order to take into account separately the warping due to torsion, bending and distortion respectively. In paragraph 4.5, a structural stability analysis is developed with torsional warping effects. These analytical analyses introduce and contribute to validate the numerical methods that will be presented in Chapter 5.

4.2 Linear elastic analysis with torsional warping effects

4.2.1 Deformations

The expression of linear strains can be written in a matrix notation as:

$$\begin{Bmatrix} \varepsilon_x \\ 2\varepsilon_{xy} \\ 2\varepsilon_{xz} \end{Bmatrix} = \begin{Bmatrix} u_{q,x} \\ u_{q,y} + v_{q,x} \\ u_{q,z} + w_{q,x} \end{Bmatrix} \tag{4.1}$$

In order to study the torsional warping problem, equations (3.9) developing u_q, v_q and w_q are substituted in (4.1).

$$\begin{Bmatrix} \varepsilon_x \\ 2\varepsilon_{xy} \\ 2\varepsilon_{xz} \end{Bmatrix} = \begin{Bmatrix} u_{0,x} \\ 0 \\ 0 \end{Bmatrix} + \begin{Bmatrix} z\theta_{y,x} \\ 0 \\ w_{,x} + \theta_y \end{Bmatrix} + \begin{Bmatrix} -y\theta_{z,x} \\ v_{,x} - \theta_z \\ 0 \end{Bmatrix} + \begin{Bmatrix} -\omega\theta_{x,xx} + \sum_{i=1}^{n} \Omega^i u_{i,x} \\ -(\omega_{,y} + z - z_c)\theta_{x,x} + \sum_{i=1}^{n} \Omega^i{}_{,y} u_i \\ (-\omega_{,z} + y - y_c)\theta_{x,x} + \sum_{i=1}^{n} \Omega^i{}_{,z} u_i \end{Bmatrix} \tag{4.2}$$

total = axial + bending (xz) + bending (xy) + torsion & warping

4.2.2 Hooke law

If a linear elastic behavior is assumed, the strains are related to the stresses by:

$$\sigma_x(x,y,z) = E\varepsilon_x(x,y,z)$$
$$\tau_{xy}(x,y,z) = G2\varepsilon_{xy}(x,y,z)$$
$$\tau_{xz}(x,y,z) = G2\varepsilon_{xz}(x,y,z) \tag{4.3}$$

4.2.3 Principle of virtual work

The equilibrium is considered for a thin-walled member with volume V. Virtual functions are denoted by the superscript *.
The principle of virtual work expression is:

$$W = W_{int} - W_{ext} = 0 \;\forall\; u_0^*, v^*, w^*, \theta_x^*, \theta_y^*, \theta_z^*, \theta_{x,x}^*, u_i^* \text{ (i=1,..n).} \tag{4.4}$$

The internal virtual work is:

$$W_{int} = \int_V (\varepsilon_x^* \sigma_x + 2\varepsilon_{xy}^* \tau_{xy} + 2\varepsilon_{xz}^* \tau_{xz}) dV \tag{4.5}$$

By considering virtual kinematics that has the same form of (3.9) and by substituting the corresponding strain-displacement relations (4.2) into (4.5), the virtual internal work becomes:

$$W_{int} = \int_V [\sigma_x (u_{0,x}^* + z\theta_{y,x}^* - y\theta_{z,x}^* - \omega\theta_{x,xx}^* + \sum_{i=1}^{n} \Omega^i u_{i,x}^*) + \tau_{xy}(\gamma_{xy}^{F*} - (\omega_{,y} + z - z_c)\theta_{x,x}^* + \sum_{i=1}^{n} \Omega^i{}_{,y} u_i^*)$$
$$+ \tau_{xz}(\gamma_{xz}^{F*} + (-\omega_{,z} + y - y_c)\theta_{x,x}^* + \sum_{i=1}^{n} \Omega^i{}_{,z} u_i^*)] dV \tag{4.6}$$

The external virtual work is:

$$W_{ext} = \int_V (u_q^* f_{vx} + v_q^* f_{vy} + w_q^* f_{vz}) dV \tag{4.7}$$

where f_{vx}, f_{vy} and f_{vz} are the components of applied volume forces.

$$W_{ext} = \int_V \{f_{vx}[u_0^* + z\theta_y^* - y\theta_z^* - \omega\theta_{x,x}^* + \sum_{i=1}^{n} \Omega^i u_i^*] + f_{vy}[v^* - (z - z_C)\theta_x^*] + f_{vz}[w^* + (y - y_C)\theta_x^*]\} dV \tag{4.8}$$

Let A be the cross section area and L the length of the thin walled member. By substituting (4.6) and (4.8) into (4.4) and after integrating by parts and isolating coefficients of virtual displacements, the principle of virtual work can be expressed as:

$$\int_L u_0^* [\int_A \sigma_{x,x} dA + f_x] dx - [u_0^* \int_A \sigma_x dA]\Big|_0^L + \int_L v^* [\int_A \tau_{xy,x} dA + f_y] dx - [v^* \int_A \tau_{xy,x} dA]\Big|_0^L$$
$$+ \int_L w^* [\int_A \tau_{xz,x} dA + f_z] dx - [w^* \int_A \tau_{xz} dA]\Big|_0^L$$
$$+ \int_L \theta_x^* [\int_A (-(\omega_{,y} + z - z_c)\tau_{xy,x} + (-\omega_{,z} + y - y_c)\tau_{xz,x} + \omega\sigma_{x,xx}) dA + m_x + m_{x\omega,x}] dx$$

$$
\begin{aligned}
&+[\theta^*_x \int_A \left((\omega_{,y}+z-z_c)\tau_{xy}+(\omega_{,z}-y+y_c)\tau_{xz}\right)dA]\Big|_0^L+[\theta^*_{x,x}\int_A \omega\sigma_x dA]\Big|_0^L-[\theta^*_x\int_A \omega f_{vx}dA]\Big|_0^L \\
&-[\theta^*_x\int_A \omega\sigma_{x,x}dA]\Big|_0^L+\int_L \theta^*_y[\int_A\left(z\sigma_{x,x}-\tau_{xz}\right)dA+m_y]dx-[\theta^*_y\int_A\left(z\sigma_x\right)dA]\Big|_0^L \\
&+\int_L \theta^*_z[\int_A(-y\sigma_{x,x}+\tau_{xy})dA+m_z]dx+[\theta^*_z\int_A\left(y\sigma_x\right)dA]\Big|_0^L \\
&+\sum_{i=1}^{n}\{\int_L u^*_i[\int_A\left(\Omega^i\sigma_{x,x}-\Omega^i{}_{,y}\tau_{xy}-\Omega^i{}_{,z}\tau_{xz}\right)dA+f_{\Omega^i}]dx-[u^*_i\int_A\left(\Omega^i\sigma_x\right)dA]\Big|_0^L\}=0 \qquad (4.9)
\end{aligned}
$$

The expressions of applied body loads by unit length of the beam are given by (4.10):

$$
\begin{aligned}
f_x &= \int_A f_{vx}dA \\
f_y &= \int_A f_{vy}dA \\
f_z &= \int_A f_{vz}dA \\
m_x &= \int_A ((y-y_c)f_{vz}-(z-z_c)f_{vy})dA \\
m_y &= \int_A (zf_{vx})dA \\
m_z &= -\int_A (yf_{vx})dA \\
f_{\Omega^i} &= \int_A (\Omega^i f_{vx})dA \\
m_{x\omega} &= \int_A \omega f_{vx}dA \qquad (4.10)
\end{aligned}
$$

4.2.4 Stress resultants

To continue the developments of the beam theory, the following stress resultants acting on the complete cross section are introduced:

Axial force:

$$N = \int_A \sigma_x dA$$

Shear forces:

$$
\begin{aligned}
T_y &= \int_A \tau_{xy}dA \\
T_z &= \int_A \tau_{xz}dA
\end{aligned}
$$

Torsional stress resultants:

$$M_\omega = \int_A \omega\sigma_x dA \qquad \text{(second order bimoment)}$$

$$M_x^1 = \int_A \left(-(\omega_{,y} + z - z_c)\tau_{xy} + (-\omega_{,z} + y - y_c)\tau_{xz}\right)dA \qquad \text{(moment)}$$

$$B_i = \int_A \Omega^i \sigma_x dA \qquad (i=1,2,\ldots n) \qquad \text{(biforces)}$$

$$\varphi_i = \int_A (\Omega_{,y}{}^i \tau_{xy} + \Omega_{,z}{}^i \tau_{xz})dA \qquad (i=1,2,\ldots n) \qquad \text{(biflows)}$$

Bending moments:

$$M_y = \int_A z\sigma_x dA$$

$$M_z = -\int_A y\sigma_x dA \qquad (4.11)$$

It is important to note that the definition of the biforces is related in this case to the usual definition of the bimoment in Vlassov or Benscoter theory (moment multiplied by a distance). Hereby, the biforces are internal forces applied on transversal nodes and associated with the u_i. The usual bimoment –as defined in Vlassov or Benscoter theories– can be computed as a resultant of these warping forces.

By substituting (4.2) into (4.3) and by integrating the stresses over the whole cross section, the stress resultants (4.11) are expressed as function of the kinematics:

$$N = EAu_{0,x} + \sum_{i=1}^{n} S_{\Omega^i} u_{i,x}$$

$$T_y = G(Av_{,x} - A\theta_z - (S_{\omega_{,y}} - z_C A)\theta_{x,x} + \sum_{i=1}^{n} S_{\Omega^i_{,y}} u_i)$$

$$T_z = G(Aw_{,x} + A\theta_y - (S_{\omega_{,z}} + y_C A)\theta_{x,x} + \sum_{i=1}^{n} S_{\Omega^i_{,z}} u_i)$$

$$M_y = E(I_y\theta_{y,x} - I_{z\omega}\theta_{x,xx} + \sum_{i=1}^{n} I_{z\Omega^i} u_{i,x})$$

$$M_z = E(I_z\theta_{z,x} + I_{y\omega}\theta_{x,xx} - \sum_{i=1}^{n} I_{y\Omega^i} u_{i,x})$$

$$\begin{aligned} M_x^1 = G[&(-S_{\omega_{,z}} - y_C A)(w_{,x} + \theta_y) + (-S_{\omega_{,y}} + z_C A)(v_{,x} - \theta_z) + \sum_{i=1}^{n}(-I_{\Omega^i} + z_C S_{\Omega^i_{,y}} - y_C S_{\Omega^i_{,z}})u_i \\ &+ (I_z + I_y + 2I_\omega + I_{\omega_{,y}\omega_{,y}} + I_{\omega_{,z}\omega_{,z}} + 2y_C S_{\omega_{,z}} - 2z_C S_{\omega_{,y}} + y_C{}^2 A + z_C{}^2 A)\theta_{x,x}] \end{aligned}$$

$$M_\omega = E(I_{z\omega}\theta_{y,x} - I_{y\omega}\theta_{z,x} - I_{\omega\omega}\theta_{x,xx}) \qquad i=1,2,3,\ldots\ldots n$$

$$B_i = E(I_{z\Omega^i}\theta_{y,x} - I_{y\Omega^i}\theta_{z,x} + \sum_{j=1}^{n} I_{\Omega^i\Omega^j} u_{j,x})$$

$$\varphi_i = G[(S_{\Omega^i_{,y}}(v_{,x}-\theta_z)+S_{\Omega^i_{,z}}(w_{,x}+\theta_y)+(-I_{z\Omega^i_{,y}}+I_{y\Omega^i_{,z}}+z_C S_{\Omega^i_{,y}}-y_C S_{\Omega^i_{,z}})\theta_{x,x}+\sum_k (I_{\Omega^i_{,y}\Omega^k_{,y}}+I_{\Omega^i_{,z}\Omega^k_{,z}})u_k)]$$

$$i=1,2,3,\ldots\ldots n \qquad (4.12)$$

Since the additional equations (3.20) are not yet considered, the resultant forces in (4.12) are not written in their uncoupled form. In order to restrain the warping degrees of freedom to the description of the torsional behavior and to reduce (4.12) to its most useful form, each resultant forces (axial and shear forces, bending moments, torque and biforces) have to be only associated with the corresponding degrees of freedom. The axial force N must depend on the axial strain $u_{0,x}$. M_y and T_z must depend on the curvature $\theta_{y,x}$, on the rotation angle θ_y and on the derivative of w. Similarly, M_z and T_y must depend on the curvature $\theta_{z,x}$, on the rotation angle θ_z and on the derivative of v. Torsional internal forces M_x^1, M_ω, B_i and ϕ_i must derive from θ_x and u_i.
It could be easily demonstrated that, if the kinematic equations (3.13, 3.16 and 3.17) are satisfied, the axial force and bending moments are therefore written in their uncoupled form (4.13). Indeed, if a function (equations 3.13, 3.16, 3.17) vanishes for any value of x, its derivative is also equal to zero. As expected, N, M_y and M_z are reduced therefore to their usual form:

$$\begin{aligned} N &= EAu_{0,x} \\ M_y &= EI_y\theta_{y,x} \\ M_z &= EI_z\theta_{z,x} \end{aligned} \qquad (4.13)$$

Besides, the expressions of T_y and T_z in (4.12) are transformed to (4.16) by introducing additional constraints:

$$-(S_{\omega,y}-z_C A)\theta_{x,x}+\sum_{i=1}^{n} S_{\Omega^i_{,y}}u_i = 0 \qquad (4.14)$$

$$-(S_{\omega,z}+y_C A)\theta_{x,x}+\sum_{i=1}^{n} S_{\Omega^i_{,z}}u_i = 0 \qquad (4.15)$$

Equations (4.14) and (4.15) are used to calculate the co-ordinates (y_C,z_C) of the shear center. The usual uncoupled form of T_y and T_z is then given by (4.16):

$$\begin{aligned} T_y &= G(Av_{,x}-A\theta_z) \\ T_z &= G(Aw_{,x}+A\theta_y) \end{aligned} \qquad (4.16)$$

Equations (3.13, 3.16, 3.17, 4.14 and 4.15) are also prescribed for the virtual displacements introduced in (4.4) so that the principle of virtual work (4.9) can be developed in an uncoupled form. If done so, M_x^1, M_ω, B_i and ϕ_i are written in their uncoupled form (4.17). The torsional biforces, biflows and moments are thus associated only with the torsional degrees of freedom.

$$M_x^1 = G[(I_z+I_y+2I_\omega+I_{\omega_{,y}\omega_{,y}}+I_{\omega,z\omega,z}+y_C S_{\omega_{,z}}-z_C S_{\omega_{,y}})\theta_{x,x}+\sum_{i=1}^{n}(-I_{\Omega^i})u_i]$$

$$M_\omega = -EI_{\omega\omega}\theta_{x,xx}$$

$$B_i = E\sum_{j=1}^{n} I_{\Omega^i\Omega^j}u_{j,x} \qquad i=1,2,3,\ldots\ldots n$$

$$\varphi_i = G[(-I_{z\Omega^i_{,y}} + I_{y\Omega^i_{,z}} + z_C S_{\Omega^i_{,y}} - y_C S_{\Omega^i_{,z}})\theta_{x,x} + \sum_k (I_{\Omega^i_{,y}\Omega^k_{,y}} + I_{\Omega^i_{,z}\Omega^k_{,z}})u_k] \qquad i=1,2,3,\ldots\ldots n \qquad (4.17)$$

4.2.5 Equilibrium equations

Since (4.9) must be satisfied for any admissible set of virtual displacements u_0^*, v^*, w^*, θ_x^*, θ_y^*, θ_z^*, $\theta_{x,x}^*$ and u_i^* (i=1,..n) per unit length (L = 1), the expressions into brackets ([…]) associated with each of these arbitrary variables should be set to zero. The following equilibrium equations are then obtained:

$$N_{,x} + f_x = 0$$

$$T_{y,x} + f_y = 0$$

$$T_{z,x} + f_z = 0$$

$$M^1_{x,x} + M_{\omega,xx} + m_x + m_{x\omega,x} = 0$$

$$M_{y,x} - T_z + m_y = 0$$

$$M_{z,x} + T_y + m_z = 0$$

$$B_{i,x} - \varphi_i + f_{\Omega^i} = 0 \qquad (4.18)$$

In term of displacements, (4.18) can be written as:

$$EAu_{0,xx} + f_x = 0$$

$$G(Av_{,xx} - A\theta_{z,x}) + f_y = 0$$

$$G(Aw_{,xx} + A\theta_{y,x}) + f_z = 0$$

$$-EI_{\omega\omega}\theta_{x,xxxx} + G[(I_z + I_y + 2I_\omega + I_{\omega_{,y}\omega_{,y}} + I_{\omega_{,z}\omega_{,z}} + y_C S_{\omega_{,z}} - z_C S_{\omega_{,y}})\theta_{x,xx} + \sum_{i=1}^{n}(-I_{\Omega^i})u_{i,x}] + m_x + m_{x\omega} = 0$$

$$EI_y\theta_{y,xx} - G(Aw_{,x} + A\theta_y) + m_y = 0$$

$$EI_z\theta_{z,xx} + G(Av_{,x} - A\theta_z) + m_z = 0$$

$$E\sum_{j=1}^{n} I_{\Omega^i\Omega^j}u_{j,xx} - G[(-I_{z\Omega^i_{,y}} + I_{y\Omega^i_{,z}} + z_C S_{\Omega^i_{,y}} - y_C S_{\Omega^i_{,z}})\theta_{x,x} - \sum_k (I_{\Omega^i_{,y}\Omega^k_{,y}} + I_{\Omega^i_{,z}\Omega^k_{,z}})u_k] + f_{\Omega^i} = 0$$

$$i=1,2,3,\ldots\ldots n \qquad (4.18')$$

The form of the boundary conditions for x=0 and x=L is:

$$
\begin{array}{lll}
N = \overline{F}_x & \text{or} & u_0 = \overline{u}_0 \\
T_y = \overline{F}_y & \text{or} & v_0 = \overline{v}_0 \\
T_z = \overline{F}_z & \text{or} & w_0 = \overline{w}_0 \\
M_x^1 + M_{\omega,x} + m_{x\omega} = \overline{m}_x & \text{or} & \theta_x = \overline{\theta}_x \\
M_\omega = \overline{m}_{x\omega} & \text{or} & \theta_{x,x} = \overline{\theta}_{x,x} \\
M_y = \overline{m}_y & \text{or} & \theta_y = \overline{\theta}_y \\
M_z = \overline{m}_z & \text{or} & \theta_z = \overline{\theta}_z \\
B_i = \overline{f}_{\Omega^i} & \text{or} & u_i = \overline{u}_i \qquad i=1,2,\ldots n
\end{array}
\tag{4.19}
$$

The prescribed displacements ($\overline{u}_o$, $\overline{v}$…) are the kinematic or geometric boundary conditions and the prescribed forces ($\overline{F}_x$, $\overline{F}_y$,…) are the statical or force boundary conditions.

4.3 Linear elastic analyses with bending shear effects

4.3.1 Displacement field and strains

The advanced shear deformation theory, introduced in paragraph 3.3, is developed hereby to adequately describe adequately the (xz) shear bending beam deformation. The developments for (xy) shear bending effects are not reproduced hereby since they are exactly identical to these (xz) calculations. Besides, since the complete effects including non uniform torsion have been analyzed in the previous paragraph and since the uncoupling of the different effects has been described in paragraph (3.2.3), the displacement field considered hereby does only take into account (xz) shear bending effects.

$$
\begin{Bmatrix} u_q \\ v_q \\ w_q \end{Bmatrix} = \begin{Bmatrix} z\theta_y + \sum_{i=1}^{n} \Omega^i u_i \\ 0 \\ w \end{Bmatrix} \tag{4.20}
$$

The strain-displacements relations are derived by using the expression of the displacement field (4.20):

$$
\begin{Bmatrix} \varepsilon_x \\ 2\varepsilon_{xy} \\ 2\varepsilon_{xz} \end{Bmatrix} = \begin{Bmatrix} z\theta_{y,x} + \sum_{i=1}^{n} \Omega^i u_{i,x} \\ \sum_{i=1}^{n} \Omega^i{}_{,y} u_i \\ w_{0,x} + \theta_y + \sum_{i=1}^{n} \Omega^i{}_{,z} u_i \end{Bmatrix} \tag{4.21}
$$

As explained in detail in paragraph (3.2) for torsional warping effects and in (3.3) for beam shear effects, additional equations must be satisfied in order to solve the problem. These equations can be written as:

$$\sum_{i=1}^{n} S_{\Omega^i} u_i = 0$$

$$\sum_{i=1}^{n} S_{\Omega^i_{,y}} u_i = 0$$

$$\sum_{i=1}^{n} I_{y\Omega^i} u_i = 0$$

$$u_e - u_d = 0 \tag{4.22}$$

The fourth series of equations (4.22) is related to the free edges of a profile with open branches. e is an edge node and d is the adjacent one.

4.3.2 Principle of virtual work

The governing equations are derived from the principle of virtual work of the beam (4.23). Similarly to paragraph 4.2.3, a thin-walled beam is considered with V as volume. Virtual parameters are denoted by the superscript *.

$$W = W_{int} - W_{ext} = 0 \qquad \forall\, w^*, \theta_y^* \text{ and } u_i^* (i=1,..n). \tag{4.23}$$

The internal virtual work is:

$$W_{int} = \int_V (\varepsilon_x^* \sigma_x + 2\varepsilon_{xy}^* \tau_{xy} + 2\varepsilon_{xz}^* \tau_{xz}) dV \tag{4.24}$$

By considering virtual kinematics that has the same form of (4.20) and by substituting the corresponding strain-displacement relations (4.21) into (4.24), the virtual internal work becomes:

$$W_{int} = \int_V [\sigma_x (z\theta_{y,x}^* + \sum_{i=1}^{n} \Omega^i u_{i,x}^*) + \tau_{xy} (\sum_{i=1}^{n} \Omega^i{}_{,y} u_i^*) + \tau_{xz} (w_{,x}^* + \theta_y^* + \sum_{i=1}^{n} \Omega^i{}_{,z} u_i^*)] dV \tag{4.25}$$

By assuming that there is only a transverse load on the beam, the external virtual work of the element is:

$$W_{ext} = \int_V (u_q^* f_{vx} + w_q^* f_{vz}) dV \tag{4.26}$$

where f_{vx} and f_{vz} are the components of external volume forces.

$$W_{ext} = \int_V \{f_{vx} [z\theta_y^* + \sum_{i=1}^{n} \Omega^i u_i^*] + f_{vz} [w^*]\} dV \tag{4.27}$$

Let A and L be the cross section area and the length of the thin walled member. By substituting (4.25) and (4.27) into (4.23) and after integrating, the principle of virtual work can be expressed as:

$$\int_L w^*\{\int_A \tau_{xz,x}dA + f_z\}dx - [w^*\int_A \tau_{xz}dA]\Big|_0^L + \int_L \theta_y^*\{\int_A \left(z\sigma_{x,x} - \tau_{xz}\right)dA + m_y\}dx - [\theta_y^*\int_A \left(z\sigma_x\right)dA]\Big|_0^L$$
$$+\sum_{i=1}^{n}\{\int_L u_i^*\{\int_A \left(\Omega^i\sigma_{x,x} - \Omega^i{}_{,y}\tau_{xy} - \Omega^i{}_{,z}\tau_{xz}\right)dA + f_{\Omega^i}\}dx - [u_i^*\int_A \left(\Omega^i\sigma_x\right)dA]\Big|_0^L\} = 0 \qquad (4.28)$$

with

$$f_z = \int_A f_{vz}dA$$
$$m_y = \int_A (zf_{vx})dA$$
$$f_{\Omega^i} = \int_A (\Omega^i f_{vx})dA \qquad (4.29)$$

4.3.3 Stress resultants

The required stress resultants are defined hereafter:

$$T_z = \int_A \tau_{xz}dA$$
$$M_y = \int_A z\sigma_x dA$$
$$B_i = \int_A \Omega^i\sigma_x dA, \qquad i=1,2,\ldots n$$
$$\varphi_i = \int_A (\Omega_{,y}{}^i\tau_{xy} + \Omega_{,z}{}^i\tau_{xz})dA, \qquad i=1,2,\ldots n \qquad (4.30)$$

The displacement-dependant internal forces are given by:

$$T_z = G(Aw_{,x} + A\theta_y + \sum_{i=1}^{n} S_{\Omega^i_{,z}} u_i)$$
$$M_y = E(I_y\theta_{y,x} + \sum_{i=1}^{n} I_{z\Omega^i} u_{i,x})$$
$$B_i = E(I_{z\Omega^i}\theta_{y,x} + \sum_{j=1}^{n} I_{\Omega^i\Omega^j} u_{j,x}), \qquad i=1,2,3,\ldots\ldots n$$
$$\varphi_i = GS_{\Omega^i_{,z}}(w_{,x} + \theta_y) + G\sum_k (I_{\Omega^i_{,y}\Omega^k_{,y}} + I_{\Omega^i_{,z}\Omega^k_{,z}})u_k \qquad i=1,2,3,\ldots\ldots n \qquad (4.31)$$

(4.25 and 4.26) can then be written with the following form:

$$W_{int} = \int_0^L [M_y\theta^*_{y,x} + T_z w^*_{,x} + T_z\theta_y^* + \sum_{i=1}^{n}(B_i u^*_{i,x} + \varphi_i u_i^*)]dx \qquad (4.32)$$

$$W_{ext}=\int_0^L \{m_y\theta_y^* + \sum_{i=1}^{n} f_{\Omega^i}u_i^* + f_z w^*\}dx \tag{4.33}$$

4.3.4 Equilibrium equations

Since (4.32) must be equal to (4.33) for any value of w^*, θ_y^*, u_i^* (i=1,..n), the expressions per unit length L = 1, associated with each of these arbitrary variables is set to zero. The following equilibrium equations are obtained:

$$T_{z,x} + f_z = 0$$

$$M_{y,x} - T_z = 0$$

$$B_{i,x} - \varphi_i + F_{\Omega^i} = 0 \tag{4.34}$$

The form of the boundary conditions for x=0 and x=L is:

$$\begin{array}{llll} T_z = \bar{F}_z & \text{or} & w_0 = \bar{w}_0 & \\ M_y = \bar{m}_y & \text{or} & \theta_y = \bar{\theta}_y & \\ B_i = \bar{f}_{\Omega^i} & \text{or} & u_i = \bar{u}_i & i=1,2,\ldots n \end{array} \tag{4.35}$$

The prescribed displacements ($\bar{u}_i$, $\bar{w}$…) are the kinematic or geometric boundary conditions and the prescribed forces ($\bar{F}_z$, $\bar{m}_y$,…) are the statical or force boundary conditions.

Case of a simply supported beam

For a beam under a distributed load (q_0), the equilibrium equations (4.34) are expressed in terms of displacements as:

$$G(Aw_{,xx} + A\theta_{y,x} + \sum_{k=1}^{n} S_{\Omega^k_{,z}} u_{k,x}) + q_0 = 0$$

$$-GAw_{,x} - GA\theta_y + EI_y\theta_{y,xx} + E\sum_{i=1}^{n} I_{z\Omega^i} u_{i,xx} - G\sum_{k=1}^{n} S_{\Omega^k_{,z}} u_k = 0$$

$$GS_{\Omega^i_{,z}}(w_{,x} + \theta_y) - EI_{z\Omega^i}\theta_{y,xx} + G\sum_k (I_{\Omega^i_{,y}\Omega^k_{,y}} + I_{\Omega^i_{,z}\Omega^k_{,z}})u_k - E\sum_{j=1}^{n} I_{\Omega^i\Omega^j} u_{j,xx} = 0 \tag{4.36}$$

The solution of (4.36), which must also satisfy (4.22), depends on the boundary conditions (4.35) that can be written for a simply supported beam for example as:

- 2 kinematic conditions :

$$w(x=0) = 0 \qquad\qquad w(x=L) = 0$$

- 2+2n statical conditions:

$$\begin{array}{lll} M_y(x=0) = 0 & M_y(x=L) = 0 & \\ B_i(x=0) = 0 & B_i(x=L) = 0 & i=1,2,\ldots n \end{array} \tag{4.37}$$

or, in terms of displacements:

$$w(0) = 0 \qquad\qquad w(L) = 0$$

$$(I_y \theta_{y,x} + \sum_{i=1}^{n} I_{z\Omega^i} u_{i,x})|_{x=0} = 0 \qquad\qquad (I_y \theta_{y,x} + \sum_{i=1}^{n} I_{z\Omega^i} u_{i,x})|_{x=L} = 0$$

$$(I_{z\Omega^i} \theta_{y,x} + \sum_{j=1}^{n} I_{\Omega^i\Omega^j} u_{j,x})|_{x=0} = 0 \qquad\qquad (I_{z\Omega^i} \theta_{y,x} + \sum_{j=1}^{n} I_{\Omega^i\Omega^j} u_{j,x})|_{x=L} = 0 \tag{4.38}$$

4.3.5 An application: simply supported beam with uniformly distributed load

In this paragraph, the present linear elastic analysis is used with bending shear warping effects (PBT). The results are compared to other beam theories introduced in paragraph 2.1: Bernoulli beam theory (BBT), Timoshenko beam theory (TBT), modified Timoshenko beam theories (TBTM), high order theories as Reddy-Bickford beam theory (RBT) [Wang, 2000, page 14].

A simply supported beam is considered under uniformly distributed load of intensity q_0=10kN/m. The cross section is a thin rectangle (b = 0.02m) x (h = 0.2m). E = 210 MPa, G=84MPa.

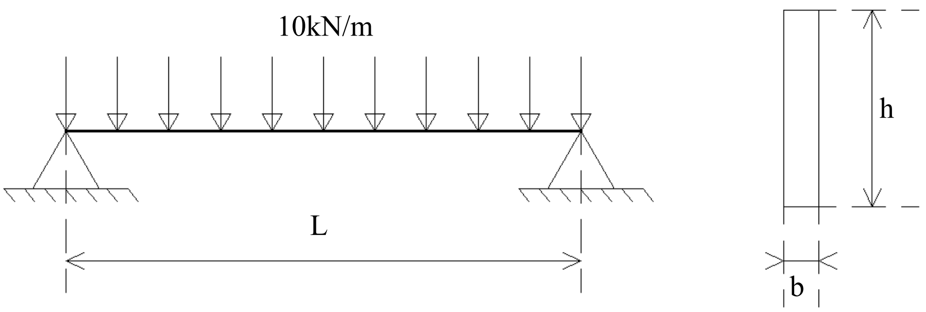

Figure 4.1 Simply supported beam with rectangular cross section (bxh) under uniformly distributed load

The equilibrium equations (4.36) and boundary conditions in (4.38) are implemented in Maple® code and solved. For the numerical application given above (L=10m), the deflection of the beam is found to be :

$$w := x \to .5363657967\ 10^{-152}\ e^{(33.12314686\,x)} + .3814697266\ 10^{-8}\ e^{(-33.12314686\,x)} + .0001488095238\,x^4 - .002976190476\,x^3 - .00001697358631\,x^2 + .1489792597\,x - .3814697266\ 10^{-8} \tag{4.39}$$

The values of maximal deflection are given for (BBT) by (2.12), for (TBTM) with k = 5/6 by (2.13), and for (RBT) by (2.14).

From table 4.1, it is clear that, for rectangular cross-sections, (RBT) and (PBT) are not justified since the gain in accuracy with respect to (TBT) is not significant. For L/h = 50, Bernoulli beam theory gives a deflection with a difference of 0.1%. The (RBT) (same for (PBT)) solution is very close in that case (0.02%) to the Timoshenko theory solution (TBT). The results coincide with those of Timoshenko modified theory (TBTM) with k=5/6. For L/h = 10, the differences between the theories are larger than above (BBT - TBTM : 2.34%, RBT - TBTM : 0.4%).

Table 4.1 Analytical values of maximal deflection [m] of beam (Figure 4.1)

	L/h=50	L/h=10
Bernoulli beam theory (BBT)	4.65030E-01	7.44048E-04
Timoshenko beam theory (TBT)	4.65402E-01	7.58929E-04
Modified TBT with k (TBTM)	4.65476E-01	7.61905E-04
Reddy beam theory (RBT)	4.65476E-01	7.61901E-04
Present beam theory (PBT) with nn=5	4.65454E-01	7.61017E-04

The correction factor of (TBTM) (eq. 2.9) is usually deduced from the geometry of the cross section by approximating the complex phenomenon. However, in real applications, it depends not only on the material (Poisson ratio) and geometric parameters, but also on the loading and boundary conditions.
A close examination shows that although the RBT does not include explicit correction factors, the kinematic relation (2.11) are characterized by two coefficients α and β that must be evaluated according to the cross section geometry. The influence of the loading and boundary conditions is included in the formulation. The solution given in (2.14 and 2.15) is only valid for rectangular cross sections. For other shapes, similar developments should be accomplished with different values of α and β deduced from the geometry and the no shear boundary conditions for open profiles. The (PBT) has the advantage of being applicable to arbitrary profiles without any restrictions or additional formulations. The automatic discretization of the profile does not require coefficient calculations.
The validation and the performance of (PBT) is shown in Chapter 5 by comparing numerical results using the proposed theory with those of other theories. The effect of shear deformation is evaluated for different types of cross sections with the length of the beam as varying parameter.

4.4 Linear elastic analysis with distortional warping effects

As introduced in paragraph 3.4, an advanced theory is presented hereby to describe the distortional behavior. The uncoupling of the different effects (tension-compression / bending / torsion / distortion) has been described previously and the displacement field considered hereby is associated to one distortional mode I (the sum on m distortional modes is omitted for presentation simplification).

4.4.1 Deformations

The expression of linear strains is deduced from the displacement field (3.31) and from (2.63):

$$\begin{Bmatrix} \varepsilon_{xx} \\ \varepsilon_{ss} \\ 2\varepsilon_{xy} \\ 2\varepsilon_{xz} \end{Bmatrix} = \begin{Bmatrix} -\omega_I \bar{\mu}_I \theta_{xI,xx} + \sum_{i=1}^{n} \Omega^i u_{i,x} \\ \bar{\Gamma}_{I,s} \theta_{xI} e \\ -(z-\bar{z}_{CI}+\omega_{I,y})\bar{\mu}_I \theta_{xI,x} + \sum_{i=1}^{n} \Omega^i_{,y} u_i \\ (y-\bar{y}_{CI}-\omega_{I,z})\bar{\mu}_I \theta_{xI,x} + \sum_{i=1}^{n} \Omega^i_{,z} u_i \end{Bmatrix} \tag{4.40}$$

4.4.2 Principle of virtual work

The equilibrium is studied for a thin-walled member with volume V. Virtual functions are denoted by the superscript *.

The principle of virtual work expression is:

$$W=W_{int}-W_{ext}=0\ \forall\ \theta^*_{xI},\theta^*_{xI,x},u^*_i\ (i=1,..n). \tag{4.41}$$

By considering virtual kinematics that has the same form of (3.31 and 2.63) and by substituting the corresponding strain-displacement relations (4.40) into (4.5), the virtual internal work becomes:

$$W_{int}=\int_V [\sigma_x(-\omega_I\bar{\mu}_I\theta^*_{xI,xx}+\sum_{i=1}^{n}\Omega^i u^*_{i,x})+\sigma_s\bar{\Gamma}_{I,s}\theta^*_{xI}e+\tau_{xy}(-(z-\bar{z}_{CI}+\omega_{I,y})\bar{\mu}_I\theta^*_{xI,x}+\sum_{i=1}^{n}\Omega^i_{,y}u^*_i)$$
$$+\tau_{xz}((y-\bar{y}_{CI}-\omega_{I,z})\bar{\mu}_I\theta^*_{xI,x}+\sum_{i=1}^{n}\Omega^i_{,z}u^*_i)]dV \tag{4.42}$$

The external virtual work is the product of forces and displacements (equation 4.7):

$$W_{ext}=\int_V f_{vx}[-\omega_I\bar{\mu}_I\theta^*_{xI}+\sum_{i=1}^{n}\Omega^i u^*_i]+f_{vy}[-(z-\bar{z}_{CI})\bar{\mu}_I\theta^*_{xI}]+f_{vz}[(y-\bar{y}_{CI})\bar{\mu}_I\theta^*_{xI}]\}dV \tag{4.43}$$

Let A and L be the cross section area and the length of the thin walled member. By substituting (4.42) and (4.43) into (4.41) and after integrating by parts and isolating coefficients of virtual displacements, the principle of virtual work can be expressed by (4.44).

$$\int_L \theta^*_{xI}[\int_A(-\sigma_s\bar{\Gamma}_{I,s}e-(\omega_{I,y}+z-\bar{z}_{CI})\bar{\mu}_I\tau_{xy,x}+(-\omega_{I,z}+y-\bar{y}_{CI})\bar{\mu}_I\tau_{xz,x}+\omega_I\bar{\mu}_I\sigma_{x,xx})dA$$
$$+m_{xI}+m_{x\omega I,x}]dx+\theta^*_{xI}\int_A\left((\omega_{I,y}+z-\bar{z}_{cI})\bar{\mu}_I\tau_{xy}+(\omega_{I,z}-y+\bar{y}_{cI})\bar{\mu}_I\tau_{xz}\right)dA\Big|_0^L-[\theta^*_{xI}m_{x\omega I}]\Big|_0^L$$
$$+[\theta^*_{xI,x}\int_A\omega_I\bar{\mu}_I\sigma_x dA]\Big|_0^L-[\theta^*_{xI}\int_A\omega_I\bar{\mu}_I\sigma_{x,x}dA]\Big|_0^L$$
$$+\sum_{i=1}^{n}\{\int_L u^*_i[\int_A\left(\Omega^i\sigma_{x,x}-\Omega^i_{,y}\tau_{xy}-\Omega^i_{,z}\tau_{xz}\right)dA+f_{\Omega^i}]dx-[u^*_i\int_A\left(\Omega^i\sigma_x\right)dA]\Big|_0^L\}=0 \tag{4.44}$$

The expressions of applied body loads by unit of length of the beam are:

$$m_{xI}=\int_A((y-\bar{y}_{CI})\bar{\mu}_I f_{vz}-(z-\bar{z}_{CI})\bar{\mu}_I f_{vy})dA$$
$$f_{\Omega^i}=\int_A(\Omega^i f_{vx})dA$$
$$m_{x\omega I}=\int_A\omega_I\bar{\mu}_I f_{vx}dA \tag{4.45}$$

4.4.3 Stress resultants

The distortional stress resultants acting on the complete cross section are:

$$M_{\omega I}=\int_A\omega_I\bar{\mu}_I\sigma_x dA \qquad \text{(second order bimoment)}$$

$$M_{xI}^1 = \int_A \left(-(\omega_{I,y} + z - \overline{z}_{CI})\overline{\mu}_I \tau_{xy} + (-\omega_{I,z} + y - \overline{y}_{CI})\overline{\mu}_I \tau_{xz} \right) dA \qquad \text{(moment)}$$

$$B_i = \int_A \Omega^i \sigma_x dA \qquad (i=1,2,\ldots n) \qquad \text{(biforces)}$$

$$\varphi_i = \int_A (\Omega_{,y}{}^i \tau_{xy} + \Omega_{,z}{}^i \tau_{xz}) dA \qquad (i=1,2,\ldots n) \qquad \text{(biflows)}$$

$$M_{sI} = \int_A \sigma_s \overline{\Gamma}_{I,s} e dA \tag{4.46}$$

It is important to note that the biforces are applied on transversal nodes and are associated to the degrees of freedom u_i. The usual distortional bimoment can be computed as a resultant of these warping forces.

By substituting (4.40) into (4.3) and by integrating the stresses over the whole cross section, the stress resultants (4.46) are found to be:

$$\begin{aligned}
M_{xI}^1 = G\sum_{J=1}^{m} & (I_{z\overline{\mu}_I\overline{\mu}_J\omega_{I,y}} - I_{y\overline{\mu}_I\overline{\mu}_J\omega_{I,z}} - S_{\overline{z}_{CJ}\overline{\mu}_I\overline{\mu}_J\omega_{I,y}} + S_{\overline{y}_{CJ}\overline{\mu}_I\overline{\mu}_J\omega_{I,z}} + I_{\overline{\mu}_I\overline{\mu}_J\omega_{I,y}\omega_{J,y}} + I_{\overline{\mu}_I\overline{\mu}_J\omega_{I,z}\omega_{J,z}} \\
& + I_{\overline{\mu}_I\overline{\mu}_J zz} + I_{\overline{\mu}_I\overline{\mu}_J yy} - S_{\overline{\mu}_I\overline{\mu}_J\overline{z}_{CJ}z} - S_{\overline{\mu}_I\overline{\mu}_J\overline{y}_{CJ}y} + I_{z\overline{\mu}_I\overline{\mu}_J\omega_{J,y}} - I_{y\overline{\mu}_I\overline{\mu}_J\omega_{J,z}} \\
& - S_{\overline{\mu}_I\overline{\mu}_J\overline{z}_{CI}z} - S_{\overline{\mu}_I\overline{\mu}_J\overline{y}_{CI}y} + A_{\overline{\mu}_I\overline{\mu}_J\overline{z}_{CI}\overline{z}_{CJ}} + A_{\overline{\mu}_I\overline{\mu}_J\overline{y}_{CI}\overline{y}_{CJ}} - S_{\overline{\mu}_I\overline{\mu}_J\overline{z}_{CI}\omega_{J,y}} + S_{\overline{\mu}_I\overline{\mu}_J\overline{y}_{CI}\omega_{J,z}})\theta_{xJ,x} \\
& + \sum_{i=1}^{n} G(-I_{z\overline{\mu}_I\Omega^i_{,y}} + S_{\overline{\mu}_I\overline{z}_{CI}\Omega^i_{,y}} + I_{y\overline{\mu}_I\Omega^i_{,z}} - S_{\overline{\mu}_I\overline{y}_{CJ}\Omega^i_{,z}})u_i
\end{aligned}$$

$$M_{\omega I} = -E\sum_{J=1}^{m} I_{\overline{\mu}_J\overline{\mu}_I\omega_J\omega_I}\theta_{xJ,xx}$$

$$M_{sI} = E\theta_{xI}\int_A \overline{\Gamma}^2_{I,s} e^2 dA$$

$$B_i = E\sum_{j=1}^{n} I_{\Omega^i\Omega^j} u_{j,x} \qquad i=1,2,3,\ldots\ldots n$$

$$\varphi_i = G[\sum_{I=1}^{m}((-I_{z\overline{\mu}_I\Omega^i_{,y}} + I_{y\overline{\mu}_I\Omega^i_{,z}} + S_{\overline{\mu}_I z_{CI}\Omega^i_{,y}} - S_{\overline{\mu}_I y_{CI}\Omega^i_{,z}})\theta_{xI,x} + \sum_k (I_{\Omega^i_{,y}\Omega^k_{,y}} + I_{\Omega^i_{,z}\Omega^k_{,z}})u_k)] \quad i=1,2,3,\ldots\ldots n \tag{4.47}$$

In order to uncouple the distortional modes from torsion, stretching and bending, the distortional degrees of freedom θ_{xI} and u_i must induce zero axial resultant, zero shear forces, zero bending moments and zero torsional resultants.

$$\begin{aligned}
& (I_{z\overline{\mu}_J\omega_{T,y}} - I_{y\overline{\mu}_J\omega_{T,z}} - S_{\overline{z}_{CJ}\overline{\mu}_J\omega_{T,y}} + S_{\overline{y}_{CJ}\overline{\mu}_J\omega_{T,z}} + I_{\overline{\mu}_J\omega_{J,y}\omega_{T,y}} + I_{\overline{\mu}_J\omega_{J,z}\omega_{T,z}} \\
& + I_{\overline{\mu}_J zz} + I_{\overline{\mu}_J yy} - S_{\overline{\mu}_J\overline{z}_{CJ}z} - S_{\overline{\mu}_J\overline{y}_{CJ}y} + I_{z\overline{\mu}_J\omega_{J,y}} - I_{y\overline{\mu}_J\omega_{J,z}} \\
& - S_{\overline{\mu}_J z_{CT}z} - S_{\overline{\mu}_J y_{CT}y} + A_{\overline{\mu}_J\overline{z}_{CJ}z_{CT}} + A_{\overline{\mu}_J\overline{y}_{CJ}y_{CT}} - S_{\overline{\mu}_J z_{CT}\omega_{J,y}} + S_{\overline{\mu}_J y_{CT}\omega_{J,z}})\theta_{xJ,x} \\
& + \sum_{i=1}^{n} G(-I_{z\Omega^i_{,y}} + z_{CT}S_{\Omega^i_{,y}} + I_{y\Omega^i_{,z}} - y_{CT}S_{\Omega^i_{,z}})u_i = 0
\end{aligned} \tag{4.48}$$

$$-(S_{\bar{\mu}_J z} - A_{\bar{\mu}_J \bar{z}_{CJ}} + S_{\bar{\mu}_J \omega_{J,y}})\theta_{xJ,x} + \sum_{i=1}^{n} S_{\Omega^i_{,y}} u_i = 0 \tag{4.49}$$

$$(S_{\bar{\mu}_J y} - A_{\bar{\mu}_J \bar{y}_{CJ}} - S_{\bar{\mu}_J \omega_{J,z}})\theta_{xJ,x} + \sum_{i=1}^{n} S_{\Omega^i_{,z}} u_i = 0 \tag{4.50}$$

In addition, it could be easily seen that, if the kinematic equations (3.32, 3.33, 3.34 and 3.35) are satisfied, no axial force, bending moments or torsional bimoment derive from (4.40). However, for each distortional mode I, additional equations (4.48), (4.49) and (4.50) are required in order to uncouple torsional moment resultant M^1_x and bending shear resultants T_y and T_z respectively from distortion.

Equations (4.48), (4.49) and (4.50) are used to calculate or condensate μ_I, y_{CI} and z_{CI}. For an open profile without ramifications, the unknowns are:

- m unknowns: μ_I; I =1,…m
- 4m unknowns: m x (y_{CI} , z_{CI}); I =1,…m

The equations corresponding to the resolution of the 5m unknowns are:

- 2m equations: dependency of distortional centers and corresponding joint (equations 2.76 and 2.77)
- 3m equations: (4.48), (4.49) and (4.50).

Note that torsion can be considered as a particular distortional mode I by taking:

I = T (torsion) with $\mu_T=1$, $y_{CI} = y_{CT}$, $z_{CI} = z_{CT}$ (4.51)

y_{CT} and z_{CT} denote the coordinates of the torsional or shear center.

For instance, equation (4.48) can be obtained from (4.47) by setting that the torsional moment M^1_{xT} (equation 4.47 where I = T) must not derive from degrees of freedom related to a distortional mode J.

4.4.4 Equilibrium equations

Since (4.44) must be satisfied for any admissible set of virtual displacements θ^*_{xI} (I = 1,..m) and u^*_i (i = 1,..n) per unit length, the expressions into brackets ([…]) associated with each of these arbitrary variables is set to zero. The following equilibrium equations are obtained in case of one 'I' distortional mode:

$$M^1_{xI,x} + M_{\omega I,xx} - M_{sI} + m_{xI} + m_{x\omega I,x} = 0 \tag{4.52}$$

$$B_{i,x} - \varphi_i + f_{\Omega^i} = 0 \tag{4.53}$$

The form of the boundary conditions for x=0 and x=L is:

$M^1_{xI} + M_{\omega I,x} + m_{x\omega I} = \bar{m}_{xI}$	or	$\theta_{xI} = \bar{\theta}_{xI}$	I=1,2,…m
$M_{\omega I} = \bar{m}_{x\omega I}$	or	$\theta_{x,xI} = \bar{\theta}_{x,xI}$	I=1,2,…m
$B_i = \bar{f}_{\Omega^i}$	or	$u_i = \bar{u}_i$	i=1,2,…n (4.54)

The prescribed displacements ($\bar{\theta}_{xI}$ …) are the kinematic or geometric boundary conditions and the prescribed forces ($\bar{m}_{xI}$ …) are the statical or force boundary conditions.

4.5 Basic equations for linearized structural stability analysis

4.5.1 Introduction

In this paragraph, analytical developments (similar to those presented in paragraphs 4.2, 4.3 and 4.4) deal with bifurcation and linear stability in order to determine the buckling loads at which a structure becomes unstable. The characteristic shapes associated with the response of a buckled structure are the buckled mode shapes. When an equilibrium position is critical, the second variation of the total potential energy vanishes [Trahair 1993 page 30; Waszczyszyn 1994 page 35…]. Critical loads are calculated by taking into consideration that a structure reaches instability if there is more than one equilibrium position for the same load level [De Ville 1989 page 4.12…]. Mathematically, instability occurs when the determinant of the equilibrium equations is zero [Waszczyszyn 1994 page 45 …].

4.5.2 Displacement field and stresses

The displacement vector at any point has three coordinates $\{u_q, v_q, w_q\}$. In case of large displacements, the Green strain vector has components related to the gradients of displacement by means of a non-linear kinematic relation detailed in appendix A8 (equation A8.8).

To simplify the presentation of analytical calculations in this paragraph, Bernoulli bending model is adopted and strains are assumed to be small enough to neglect $u_{q,x}$ when compared with unity [De Ville 1989, page 4.3; Shakourzadeh 1996].

$$\begin{aligned} &u_{q,x} \ll 1 \\ &u^2_{q,x} \ll u_{q,x} \end{aligned} \tag{4.55}$$

The two approximations described above are relaxed in the finite element analysis (§5.6).

The Green strain vector can thus be expressed as follows:

$$\begin{Bmatrix} E_x \\ 2E_{xy} \\ 2E_{xz} \end{Bmatrix} = \begin{Bmatrix} u_{q,x} \\ (u_{q,y} + v_{q,x}) \\ (u_{q,z} + w_{q,x}) \end{Bmatrix} + \begin{Bmatrix} \frac{1}{2}(v^2_{q,x} + w^2_{q,x}) \\ (v_{q,y} v_{q,x} + w_{q,y} w_{q,x}) \\ (v_{q,x} v_{q,z} + w_{q,x} w_{q,z}) \end{Bmatrix} \tag{4.56}$$

By assuming that the cross section is transversally rigid (no distortion deformation), the transverse displacements are continuous and differentiable functions of x, y and z:

$$\begin{Bmatrix} v_q \\ w_q \end{Bmatrix} = \begin{Bmatrix} 0 \\ w(x) \end{Bmatrix} + \begin{Bmatrix} v(x) \\ 0 \end{Bmatrix} + \begin{Bmatrix} -(y - y_C)(1 - \cos\theta(x)) - (z - z_C)\sin\theta(x) \\ (y - y_C)\sin\theta(x) - (z - z_C)(1 - \cos\theta(x)) \end{Bmatrix} \tag{4.57}$$

θ is the twisting angle.

The transverse strains are:

$$\begin{Bmatrix} 2E_{xy} \\ 2E_{xz} \end{Bmatrix} = \begin{Bmatrix} u_{q,y} \\ u_{q,z} \end{Bmatrix} + \begin{Bmatrix} v'\cos\theta + w'\sin\theta - (z - z_C)\theta' \\ -v'\sin\theta + w'\cos\theta + (y - y_C)\theta' \end{Bmatrix} \tag{4.58}$$

The longitudinal displacement is divided into three parts ($u_q = u_0 + u_F + u_T$). u_0 is a constant tension/compression term, u_F is the flexural term that derives from Bernoulli hypothesis neglecting shear deformation in the mean surface of the section and u_T is the torsional warping.

$$2E_{xy} = 2E_{xy}|_F + 2E_{xy}|_T$$
$$2E_{xy}|_F = 2E_{xz}|_F = 0 \qquad \text{or} \qquad 2E_{xy} - 2E_{xy}|_T = 2E_{xz} - 2E_{xz}|_T = 0 \tag{4.59}$$

By substituting (4.58) into (4.59), (4.60) is obtained:

$$u_{F,y} + v'\cos\theta + w'\sin\theta = 0$$
$$u_{F,z} - v'\sin\theta + w'\cos\theta = 0 \tag{4.60}$$

and the expression of u_F is deduced:

$$u_F = - y\,\{v'\cos\theta + w'\sin\theta\} - z\{w'\cos\theta - v'\sin\theta\} \tag{4.61}$$

u_T is the torsional warping term:

$$u_T = -\omega\theta' + \sum\Omega^i u_i \tag{4.62}$$

by using (4.62) and (4.61) the longitudinal displacement is thus found to be equal to:

$$u_q = u_0 - y\,\{v'\cos\theta + w'\sin\theta\} - z\{w'\cos\theta - v'\sin\theta\} - \omega\theta' + \sum\Omega^i u_i \tag{4.63}$$

and the complete strain vector is then:

$$\begin{Bmatrix} E_{xx} \\ 2E_{xy} \\ 2E_{xz} \end{Bmatrix} = \begin{Bmatrix} u_0' - y(v''\cos\theta + w''\sin\theta) - z(w''\cos\theta - v''\sin\theta) - \omega\theta'' + \sum\Omega^i u_i' \\ +\frac{1}{2}(v'^2 + w'^2 + r_C^2\theta'^2) + \theta' v'(y_C\sin\theta + z_C\cos\theta) + \theta' w'(z_C\sin\theta - y_C\cos\theta) \\ -(z - z_C + \omega_{,y})\theta' + \sum\Omega^i_{,y}u_i \\ (y - y_C - \omega_{,z})\theta' + \sum\Omega^i_{,z}u_i \end{Bmatrix} \tag{4.64}$$

where

$$r_C^2 = (y - y_C)^2 + (z - z_C)^2$$

Assuming that rotations and displacements are moderate, the higher order terms can be neglected ($v'\theta'\theta$ and $w'\theta\theta'$) and the rotational angle can be considered to be small:

$$\sin\theta \approx \theta \qquad \cos\theta \approx 1 \tag{4.65}$$

Thus (4.57), (4.63) and (4.64) can be expressed as:

$$\begin{Bmatrix} u_q \\ v_q \\ w_q \end{Bmatrix} = \begin{Bmatrix} u_0 - y(v'+w'\theta) - z(w'-v'\theta) - \omega\theta' + \sum \Omega^i u_i \\ v - (z - z_C)\theta \\ w + (y - y_C)\theta \end{Bmatrix} \tag{4.66}$$

$$\begin{Bmatrix} E_{xx} \\ 2E_{xy} \\ 2E_{xz} \end{Bmatrix} = \begin{Bmatrix} u_0' - y(v''+w''\theta) - z(w''-v''\theta) - \omega\theta'' + \sum \Omega^i u_i' \\ +\frac{1}{2}(v'^2 + w'^2 + r_C^2\theta'^2) + z_C\theta' v' - y_C\theta' w' \\ -(z - z_C + \omega_{,y})\theta' + \sum \Omega^i_{,y} u_i \\ (y - y_C - \omega_{,z})\theta' + \sum \Omega^i_{,z} u_i \end{Bmatrix} \tag{4.67}$$

4.5.3 Principle of virtual work

The principle of virtual work can be written as:

$$W = W_{int} - W_{ext} = 0 \ \forall \ u_0^*, v^*, w^*, \theta^*, \theta^{*\prime}, u_i^* \ (i=1,..n). \tag{4.68}$$

$$\text{or} \int_V (S_{ij}\delta E_{ij})dV = \int_V \delta u_i df_i dV \tag{4.69}$$

where V is the volume in the reference configuration. E_{ij} is the Green-Lagrange strain tensor; S_{ij} is the Piola Kirchhoff stress tensor; f_i is the external force vector. The material is assumed to be homogeneous, isotropic, linear and elastic so that the relationship between stresses and strains is given by Hooke's law.

$$\begin{aligned} W_{int} = \int_V [& S_x \{u_0^{*\prime} - y(v^{*\prime\prime} + \theta w^{*\prime\prime} + w''\theta^*) - z(w^{*\prime\prime} - \theta v^{*\prime\prime} - w''\theta^*) - \omega\theta^{*\prime\prime} + \sum_{i=1}^{n} \Omega^i u_i^{*\prime} \\ & + v' v^{*\prime} + w' w^{*\prime} + r_C^2 \theta' \theta^{*\prime} + z_C(v'\theta^{*\prime} + v^{*\prime}\theta') - y_C(w'\theta^{*\prime} + w^{*\prime}\theta')\} \\ & + S_{xy}\{-(\omega_{,y} + z - z_c)\theta^{*\prime} + \sum_{i=1}^{n} \Omega^i_{,y} u_i^*\} + S_{xz}\{(-\omega_{,z} + y - y_c)\theta^{*\prime} + \sum_{i=1}^{n} \Omega^i_{,z} u_i^*\}]dV \end{aligned} \tag{4.70}$$

$$\begin{aligned} W_{ext} = \int_V \{ & f_{vx}[u_0^* - y(v^{*\prime} + w'\theta^* + \theta w^{*\prime}) - z(w^{*\prime} - v'\theta^* - \theta v^{*\prime}) - \omega\theta^{*\prime} + \sum_{i=1}^{n} \Omega^i u_i^*(x)] \\ & + f_{vy}[v^* - (z - z_C)\theta_x^*] + f_{vz}[w^* + (y - y_C)\theta_x^*]\}dV + f_{sy}[v^* - (z - z_C)\theta_x^*] \end{aligned} \tag{4.71}$$

4.5.4 Governing equations

(4.70) and (4.71) are substituted into (4.68) and the result is integrated in order to obtain expressions associated with arbitrary values for $u_0^*, v^*, w^*, \theta^*, \theta^{*\prime}, u_i^*$ (i=1,..n). These expressions must be set to zero.

The following equilibrium equations are obtained:

$N' + f_x = 0$

$M_y'' - (M_z\,\theta)'' + (w'N)' - y_C(\theta'N)' - (m_z\theta)' + f_z + m_y' = 0$

$$M_z'' + (M_y\,\theta)'' - (v'N)' - z_C(\theta'N)' + (m_y\theta)' - f_y + m_z' = 0$$
$$M_\omega'' + M^1_x{}' - M_z w'' - M_y v'' + (M_{tr}\,\theta')' + z_C(Nv')' - y_C(Nw')' + m_x + m_{x\omega,x} + m_z w' + m_y v' = 0$$
$$B_{i,x} - \varphi_i + f_{\Omega^i} = 0 \tag{4.72}$$

with

$$N = \int_A S_x dA$$

$$M_y = \int_A z S_x dA \qquad M_z = -\int_A y S_x dA \qquad M_\omega = \int_A \omega S_x dA$$

$$M_x^1 = \left[\int_A \left(-(\omega_{,y} + z - z_c)S_{xy} + (-\omega_{,z} + y - y_c)S_{xz}\right)dA\right]$$

$$M_{tr} = \int_A r_C^2 S_x dA$$

$$B_i = \int_A \Omega^i S_x dA\,, \qquad i=1,2,\ldots n$$

$$F_x = \int_A f_x dA$$

$$m_x = \int_A (y - y_c)f_z - (z - z_c)f_y)dA$$

$$m_y = \int_A (z f_x)dA \qquad m_z = -\int_A (y f_{vx})dA$$

$$f_{\Omega^i} = \int_A (\Omega^i f_{vx})dA \qquad m_{x\omega} = \int_A \omega f_{vx} dA$$

The internal forces are calculated in terms of displacements. By limiting the following developments to a linearized stability, the first order terms are considered:

$$N = EAu_0{}'$$
$$M_y = -EI_y w''$$
$$M_z = EI_z v''$$
$$M_\omega = -EI_{\omega\omega}\theta_{x,xx}$$
$$B_i = E\sum_{j=1}^{n} I_{\Omega^i\Omega^j} u_{j,x}$$
$$M_{tr} = E\{(I_y + I_z + y_C{}^2A + z_C{}^2A)u_0{}' - (I_{yr^2} - 2y_C I_z)v'' - (I_{zr^2} - 2z_C I_y)w''$$
$$-(I_{r^2\omega} - 2y_C I_{y\omega} - 2z_C I_{z\omega})\theta'' + \sum\ (I_{y^2\Omega^i} + I_{z^2\Omega^i} - 2y_C I_{y\Omega^i} - 2z_C I_{z\Omega^i} + y_C{}^2 S_{\Omega^i} + z_C{}^2 S_{\Omega^i})u_i{}'$$
$$M_x^1 = G[(I_z + I_y + I_{\omega,y\omega,y} + I_{\omega,z\omega,z} + 2y_C S_{\omega_{,z}} - 2z_C S_{\omega_{,y}} + y_C{}^2A + z_C{}^2A - 2I_{y\omega_{,z}} + 2I_{z\omega_{,y}})\theta_{x,x}$$
$$+\sum_{i=1}^{n}(-I_{\Omega^i} + z_C S_{\Omega^i_{,y}} - y_C S_{\Omega^i_{,z}})u_i]$$

$$\varphi_i = G\{(-I_{z\Omega^i_{,y}} + I_{y\Omega^i_{,z}} + z_C S_{\Omega^i_{,y}} - y_C S_{\Omega^i_{,z}})\theta_{x,x} + \sum_k (I_{\Omega^i_{,y}\Omega^k_{,y}} + I_{\Omega^i_{,z}\Omega^k_{,z}})u_k)\} \tag{4.73}$$

The analytical analysis of instability of elastic structures originated by the interaction of buckling modes is deduced from these equations. The criterion to determine the buckling state is the singularity of the system of the structure equilibrium equations. When the critical load is reached, the structure has at least two equilibrium positions. So, equations (4.72) and (4.73) are combined, differentiated by keeping in mind that the external loads are not incremented.

$$EAdu'' = 0$$

$$-EI_y dw'''' - M_z d\theta'' + Ndw'' - y_C Nd\theta'' - m_z d\theta' = 0$$

$$EI_z dv'''' + M_y d\theta'' - Ndv'' - z_C Nd\theta'' + m_y d\theta' = 0$$

$$\begin{aligned}
&-EI_{\omega\omega} d\theta'''' - M_z dw'' - M_y dv'' + z_C Ndv'' - y_C Ndw'' + m_z dw + m_y dv \\
&\quad + (I_y + I_z + y_C^2 A + z_C^2 A)\frac{N}{A} d\theta'' - (I_{yr^2} - 2y_C I_z)\frac{M_z}{I_z} d\theta'' + (I_{zr^2} - 2z_C I_y)\frac{M_y}{I_y} d\theta'' \\
&\quad - (I_{r^2\omega} - 2y_C I_{y\omega} - 2z_C I_{z\omega})\theta'' d\theta'' \\
&\quad + \sum (I_{y^2\Omega^i} + I_{z^2\Omega^i} - 2y_C I_{y\Omega^i} - 2z_C I_{z\Omega^i} + y_C^2 S_{\Omega^i} + z_C^2 S_{\Omega^i})u_i' d\theta'' \\
&\quad + G(I_z + I_y + 2I_\omega + I_{\omega,y\omega,y} + I_{\omega,z\omega,z} + 2y_C S_{\omega_{,z}} - 2z_C S_{\omega_{,y}} + y_C^2 A + z_C^2 A - 2I_{y\omega_{,z}} + 2I_{z\omega_{,y}})d\theta'' \\
&\quad + G\sum_{i=1}^{n} (-I_{\Omega^i} + z_C S_{\Omega^i_{,y}} - y_C S_{\Omega^i_{,z}})du_i' = 0
\end{aligned}$$

$$E\sum_{j=1}^{n} I_{\Omega^i\Omega^j} du_j'' - G(-I_{z\Omega^i_{,y}} + I_{y\Omega^i_{,z}} + z_C S_{\Omega^i_{,y}} - y_C S_{\Omega^i_{,z}})d\theta' - G\sum_k (I_{\Omega^i_{,y}\Omega^k_{,y}} + I_{\Omega^i_{,z}\Omega^k_{,z}})du_k = 0 \tag{4.74}$$

4.5.5 Buckling of simply supported columns

General equations (4.72) using the adapted Prokić warping function are applied in the case of thin walled structure buckling analysis. The resulting governing equations, including torsional effects, are valid for any type of thin walled cross sections. If a simply supported column is submitted to an axial force P passing through any point p of the cross section, the internal forces are found to be:

$$N = -P; \quad M_y = -Pz_p; \quad M_z = Py_p; \quad M_x^1 = 0; \quad M_\omega = 0; \quad B_i = 0; \tag{4.75}$$

The secondary warping effects are completely taken into consideration within these calculations and the last 3 + n equations that are deduced from (4.72) can be written as follows:

a)1 torsional buckling equation with respect to derivatives of θ_x and u_i (i=1,2,… n):

$$EI_{\omega\omega}\frac{d^4\theta_x}{dx^4}-G(I_y+I_z+I_{\omega,y\omega,y}+I_{\omega,z\omega,z}-2I_{y\omega,z}+2I_{z\omega,y}+y_CS_{\omega,y}-z_CS_{\omega,z})\frac{d^2\theta_x}{dx^2}$$
$$+\sum_{i=1}^{n}G(-I_{y\Omega^i_{,z}}+I_{z\Omega^i_{,y}})\frac{du_i}{dx}+Pi_C^2\frac{d^2\theta_x}{dx^2}-P(y_C-y_p)\frac{d^2w}{dx^2}+P(z_C-z_p)\frac{d^2v}{dx^2}$$
$$+Py_p(\frac{I_{yr^2}}{I_z}-2y_C)\frac{d^2\theta_x}{dx^2}+Pz_p(\frac{I_{zr^2}}{I_y}-2z_C)\frac{d^2\theta_x}{dx^2}=0 \qquad (4.76)$$

b) 2 flexural buckling equations with respect to derivatives of v, w and θ_x:

$$EI_z v''''+Pv''+P(z_C-z_p)\theta_x''=0 \qquad (4.77)$$
$$EI_y w''''+Pw''-P(y_C-y_p)\theta_x''=0 \qquad (4.78)$$

c) n equations (i=1,2,….n) which relate u_k (k=1,2,….n) to θ_x:

$$-EI_{\Omega^i\Omega^k}\frac{d^2u_k}{dx^2}+G(I_{\Omega^i_{,y}\Omega^k_{,y}}+I_{\Omega^i_{,z}\Omega^k_{,z}})\frac{du_k}{dx}+G(I_{y\Omega^i_{,z}}-I_{z\Omega^i_{,y}}+z_CS_{\Omega^i_{,y}}-y_CS_{\Omega^i_{,z}})\frac{d\theta_x}{dx}=0 \qquad (4.79)$$

4.5.6 Buckling of simply supported beams with equal end moments

The lateral buckling is analytically calculated hereby by using the equilibrium equations obtained from equation (4.72). The second torsional warping effects are taken into account and the internal forces are found as:

$$N=0,\qquad M_y\neq 0,\qquad M_z=0,\qquad M_x^1=0,\qquad M_\omega=0,\qquad B_i=0 \qquad (4.80)$$

In this case, the set of equations (4.74) is reduced to:

$$-EI_y dw''''=0$$

$$EI_z dv''''+M_y d\theta''=0$$

$$-EI_{\omega\omega}d\theta''''-M_y dv''+(I_{zr^2}-2z_CI_y)\frac{M_y}{I_y}d\theta''+G\sum_{i=1}^{n}(-I_{\Omega^i}+z_CS_{\Omega^i_{,y}}-y_CS_{\Omega^i_{,z}})du_i'$$
$$+G(I_z+I_y+2I_\omega+I_{\omega,y\omega,y}+I_{\omega,z\omega,z}+2y_CS_{\omega_{,z}}-2z_CS_{\omega_{,y}}+y_C^2A+z_C^2A-2I_{y\omega_{,z}}+2I_{z\omega_{,y}})d\theta''=\mathbf{0}$$

$$E\sum_{j=1}^{n}I_{\Omega^i\Omega^j}du_j''-G(-I_{z\Omega^i_{,y}}+I_{y\Omega^i_{,z}}+z_CS_{\Omega^i_{,y}}-y_CS_{\Omega^i_{,z}})d\theta'-G\sum_k(I_{\Omega^i_{,y}\Omega^k_{,y}}+I_{\Omega^i_{,z}\Omega^k_{,z}})du_k=0 \qquad (4.81)$$

Different methods are used in the literature to solve analytically similar problems (Galerkin, Ritz,…) [Galéa 2002; Villette 2002; Mohri 2003…]. Appropriate displacement modes must be chosen in order to solve the system of (n+3) equations (4.81). One sinuzoidal function for dv, dw and dθ and one cosine function for each du_i (eq. 4.82) are usually suitable for beams with bisymmetrical profiles submitted to equal end moments. In this case, (4.81) is developed into (4.83).

$$dv = A_1 \sin\left(\frac{\pi x}{L}\right),\ \ dw = A_2 \sin\left(\frac{\pi x}{L}\right), d\theta = A_3 \sin\left(\frac{\pi x}{L}\right),\ \ du_i = a_i \cos\left(\frac{\pi x}{L}\right) \tag{4.82}$$

$$A_2 = 0$$

$$EI_z A_1\left(\frac{\pi}{L}\right)^4 - M_y A_3\left(\frac{\pi}{L}\right)^2 = 0$$

$$- EI_{\omega\omega} A_3\left(\frac{\pi}{L}\right)^4 + M_y A_1\left(\frac{\pi}{L}\right)^2 - (I_{zr^2} - 2z_C I_y)\frac{M_y}{I_y} A_3\left(\frac{\pi}{L}\right)^2$$

$$- G(I_z + I_y + 2I_\omega + I_{\omega,y\omega,y} + I_{\omega,z\omega,z} + 2y_C S_{\omega_{,z}} - 2z_C S_{\omega_{,y}} + {y_C}^2 A + {z_C}^2 A - 2I_{y\omega_{,z}} + 2I_{z\omega_{,y}})A_3\left(\frac{\pi}{L}\right)^2$$

$$- G\sum_{i=1}^{n}(-I_{\Omega^i} + z_C S_{\Omega^i_{,y}} - y_C S_{\Omega^i_{,z}})a_i\left(\frac{\pi}{L}\right) = 0$$

$$- E\sum_{k=1}^{n} I_{\Omega^i\Omega^k} a_k\left(\frac{\pi}{L}\right)^2 - G(-I_{z\Omega^i_{,y}} + I_{y\Omega^i_{,z}} + z_C S_{\Omega^i_{,y}} - y_C S_{\Omega^i_{,z}})\left(\frac{\pi}{L}\right)A_3 - G\sum_k (I_{\Omega^i_{,y}\Omega^k_{,y}} + I_{\Omega^i_{,z}\Omega^k_{,z}})a_k = 0$$

$$\tag{4.83}$$

The critical moment is calculated by taking the determinant of the system of equilibrium equations (4.83) equal to zero. Practically the last n equations in (4.83) are resolved to evaluate each constant a_k in function of A_3. The resulting expressions are then inserted in the two previous equations in order to evaluate the determinant which must be equal to zero. The value of M_y is thus found to be the solution of (4.83').

$$-EI_{\omega\omega}\left(\frac{\pi}{L}\right)^4 - G\sum_{i=1}^{n}(-I_{\Omega^i} + z_C S_{\Omega^i_{,y}} - y_C S_{\Omega^i_{,z}})f_i\left(\frac{\pi}{L}\right) + \frac{{M_y}^2}{EI_z} - (I_{zr^2} - 2z_C I_y)\frac{M_y}{I_y}\left(\frac{\pi}{L}\right)^2$$

$$- G(I_z + I_y + 2I_{z\omega_{,y}} - 2I_{y\omega_{,z}} + I_{\omega,y\omega,y} + I_{\omega,z\omega,z} - 2I_{y\omega_{,z}} + 2I_{z\omega_{,y}})\left(\frac{\pi}{L}\right)^2 = 0 \tag{4.83'}$$

By solving equations (4.74) for a uniform moment distribution M_z on a simply supported beam ($N = 0$, $M_y = 0$, $M_z \neq 0$, $M_x^1 = 0$, $M_\omega = 0$, $B_i = 0$), the lowest buckling moments, based on Prokić warping function leads to the equation (4.84). One sinusoidal function is used for transversal displacements and rotations while one cosine function approximates the warping displacement modes.

$$-EI_{\omega\omega}\left(\frac{\pi}{L}\right)^4 - G\sum_{i=1}^{n}(-I_{\Omega^i} + z_C S_{\Omega^i_{,y}} - y_C S_{\Omega^i_{,z}})f_i\left(\frac{\pi}{L}\right) + \frac{{M_z}^2}{EI_y} + (I_{yr^2} - 2y_C I_z)\frac{M_z}{I_z}\left(\frac{\pi}{L}\right)^2$$

$$- G(I_z + I_y + 2I_{z\omega_{,y}} - 2I_{y\omega_{,z}} + I_{\omega,y\omega,y} + I_{\omega,z\omega,z} - 2I_{y\omega_{,z}} + 2I_{z\omega_{,y}})\left(\frac{\pi}{L}\right)^2 = 0 \tag{4.84}$$

where $I_{\omega\omega} = \int \omega\omega dA$, $I_{\omega_{,y}\omega_{,y}} = \int_A \omega_{,y}\omega_{,y} dA$, $I_{\omega_{,z}\omega_{,z}} = \int_A \omega_{,z}\omega_{,z} dA$, $I_{y\omega_{,z}} = \int y\omega_{,z} dA$, $I_{z\omega_{,y}} = \int z\omega_{,y} dA$,

$I_{\Omega^i} = \int_A (-y\Omega^i_{,z} + z\Omega^i_{,y})dA$, $S_{\Omega^i_{,y}} = \int_A \Omega^i_{,y} dA$, $S_{\Omega^i_{,z}} = \int_A \Omega^i_{,z} dA$

The f_i terms are found by solving the set of equations associated with the n warping degrees of freedom. They relate the warping variables u_i to the twisting angle θ_x.

4.5.7 Analytical analyses of thin walled structure buckling

The present calculations, based on one single warping function, are shown hereby to give excellent results for arbitrary asymmetrical (closed or/and open) profiles. They are compared to other analytical computations with different warping functions for flexural-torsional and lateral torsional buckling of columns and beams.

- In the first example, the influence of second order torsional warping is evaluated while computing the torsional, flexural, flexural torsional and lateral torsional buckling of rectangular, cruciform, I shaped, U shaped and L shaped columns.
- In the second example, the flexural torsional and lateral torsional buckling are analyzed for asymmetric profiles comprising one closed cell.
- In the third example, the lateral torsional buckling of a monosymmetrical I beam is analyzed while varying the linear bending moment distribution along a simply supported beam.
- The fourth example compares the lateral torsional buckling behavior of five profiles for a simply supported beam submitted to a uniform load.

The application of several analytical methods is illustrated in the third and fourth examples. The Maple® software is used in order to solve the differential equations by using Galerkin method with series of sine and cosine functions. “EC3” denotes the analytical calculations deduced from the European Code for the Design of Steel Structures. “VL1” represents another analytical solution adopting either a Vlassov or a Benscoter warping function depending on the profile (open or closed respectively). Galerkin method is used with one sinuzoidal function as displacement mode. For “VL5”, the displacement modes are described by a series of sinusoidal functions with five terms. A similar analytical method “PR1” with a single sinuzoidal function as displacement mode is developed with Prokić warping function instead of Vlassov warping function.

Example 1: Secondary warping effects

In this example, a column with a cruciform cross section is submitted to an axial load passing through the centroid (Fig. 4.2.). The thickness of the walls is t = 8mm. G = 80GPa, E = 200GPa.

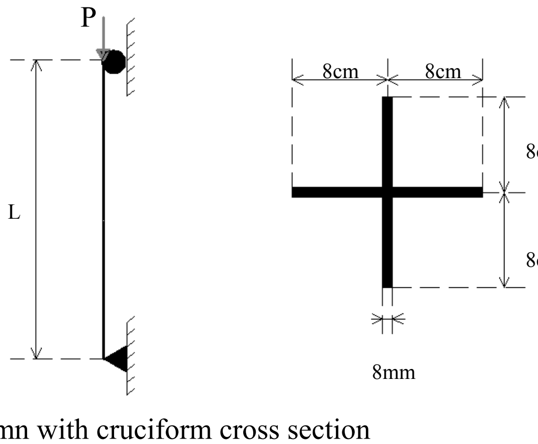

Figure 4.2 Column with cruciform cross section

The first-order theory gives three homogeneous equations and represents an eigenvalue problem. The cross section is symmetric, the shear center (C) and the centroid (G) coincide and the second moment of area is the same with respect to any axis in the plane of the cross section and passing through the centroid. Thus, the equations are uncoupled and the solutions of (2.78, 2.79 and 2.80) give two discrete sets of buckling modes: one associated with the flexural mode and the other associated with the torsional mode. For the flexural buckling set, the critical loads are inversely proportional to the square of the length of the column; and for each flexural mode, the critical load is proportional to the square of the number of waves n.

The torsional warping of this kind of cross section reduces to second order warping. The particular geometry of the profile allows a warping along the thickness of each wall while the entire midline remains in the same plane.

According to standard buckling analyses with Vlassov theory, the torsional critical load does not depend on the length L of the column since it depends only on the Saint Venant constant. Equation (2.80) is reduced to (4.85) and the torsional critical load is in this case equal to 1.363MN.

$$(GK - Pi_G^2)\frac{d^2\theta_x}{dx^2} = 0 \qquad (4.85)$$

The torsional critical load and the first critical load of the flexural buckling set are represented in figure 4.3 with varying values for the length L of the column.

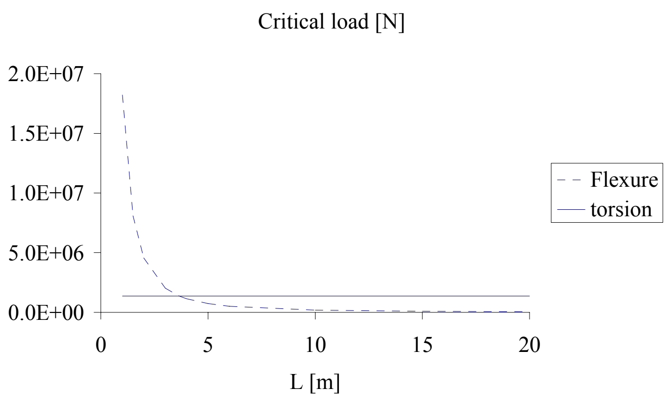

Figure 4.3 Critical loads for flexural and torsional buckling of a column

By using the adapted Prokić warping function, the set of equations (4.76 and 4.79) is reduced in this particular case to a single equation:

$$EI_{\omega\omega}\frac{d^4\theta_x}{dx^4} - G(I_y + I_z + I_{\omega_{,y}\omega_{,y}} + I_{\omega_{,z}\omega_{,z}} - 2I_{y\omega_{,z}} + 2I_{z\omega_{,y}})\frac{d^2\theta_x}{dx^2} + Pi_G^2\frac{d^2\theta_x}{dx^2} = 0 \qquad (4.86)$$

Unlike the developments done by using equation (4.85), the torsional critical loads are found to be a function of the length L. This is due to the fact that, within this kinematic formulation, the effects of second order torsional warping are taken into account as defined in paragraph 3.2. The difference between the first value of this set and Vlassov critical torsional load is given in figure 4.4. As expected, the influence of the second order torsion is negligible for slender beams but is not negligible for small values of length L (3% for L=1m). If second order warping effects are neglected, equation (4.86) degenerates into (4.85) and the difference between analytical calculations based on Prokić and Vlassov formulations vanishes.

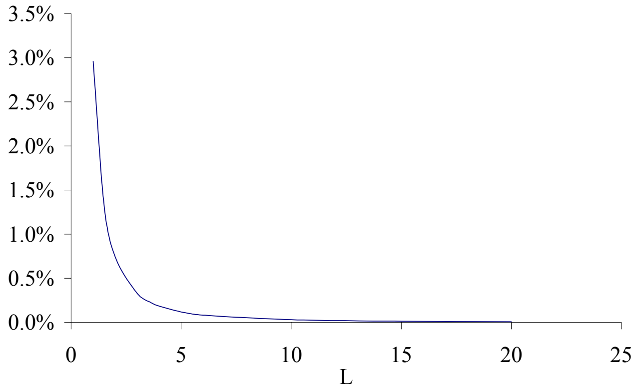

Figure 4.4 Difference between analytical calculations of torsional critical loads by using Vlassov and adapted Prokić kinematic formulations

The same phenomenon is shown for other types of cross sections (table 4.2) and the difference between the analytical calculations of critical loads based on the adapted Prokić formulation and those based on Vlassov theory is shown to be important for small values of L.

Table 4.2: Data for profile geometries

Profile I	Rectangular profile	Profile L
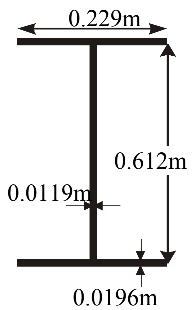	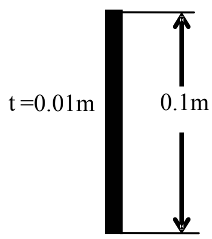	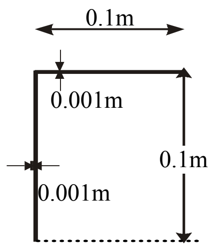

Profile U	Cruciform profile
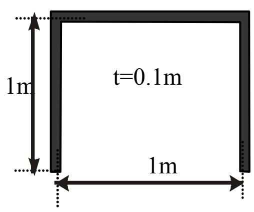	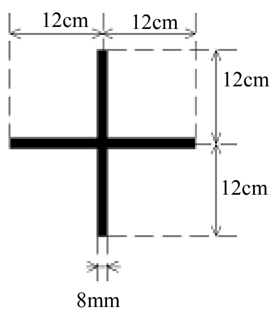

Figures 4.5 and 4.6 show this phenomenon for columns submitted to axial force and for beams submitted to uniform bending respectively. Second order warping is more important for the L, cruciform and rectangular cross sections than for the I and U shaped profiles. Indeed, in the first three cases, the torsional axial deformations are linear functions with respect to the thickness coordinate

since the first order warping vanishes along the entire midline. This remark is also stated in [Batoz and Dhatt, 1990, page 195] by making reference to previously published work.

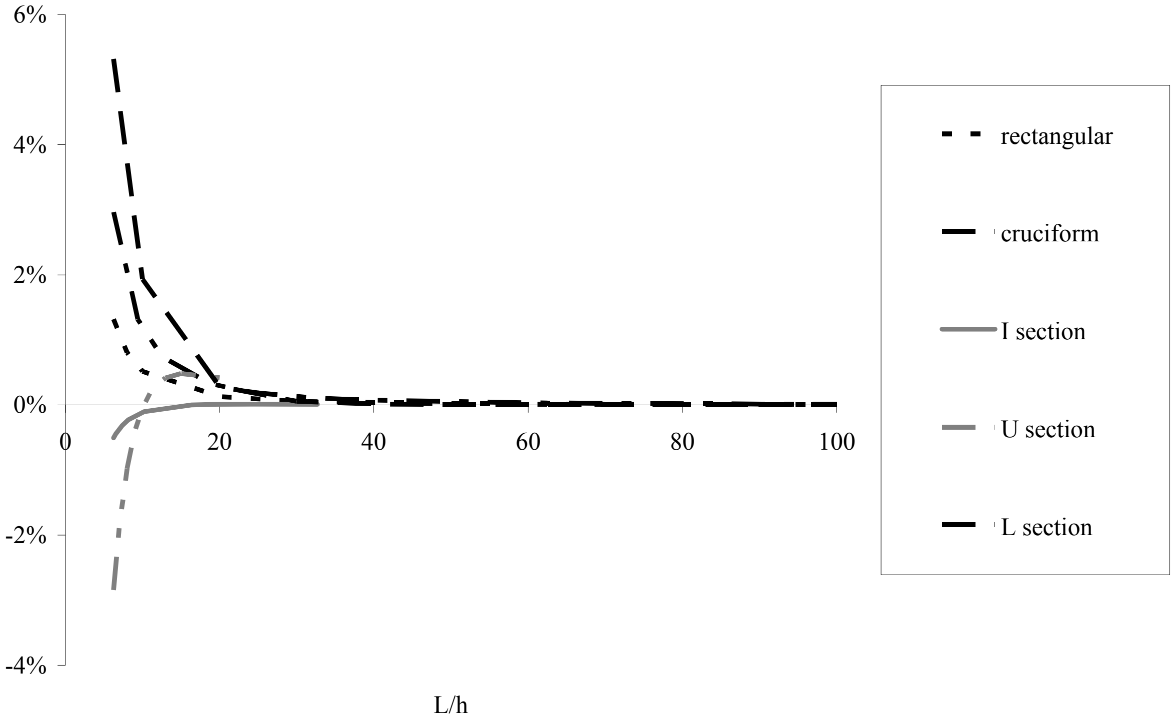

Figure 4.5 Difference between analytical calculations (Vlassov and adapted Prokić kinematic formulations) of torsional critical loads for columns with rectangular, cruciform and I sections and of coupled flexural torsional loads for columns with channel (U) and angle (L) cross sections

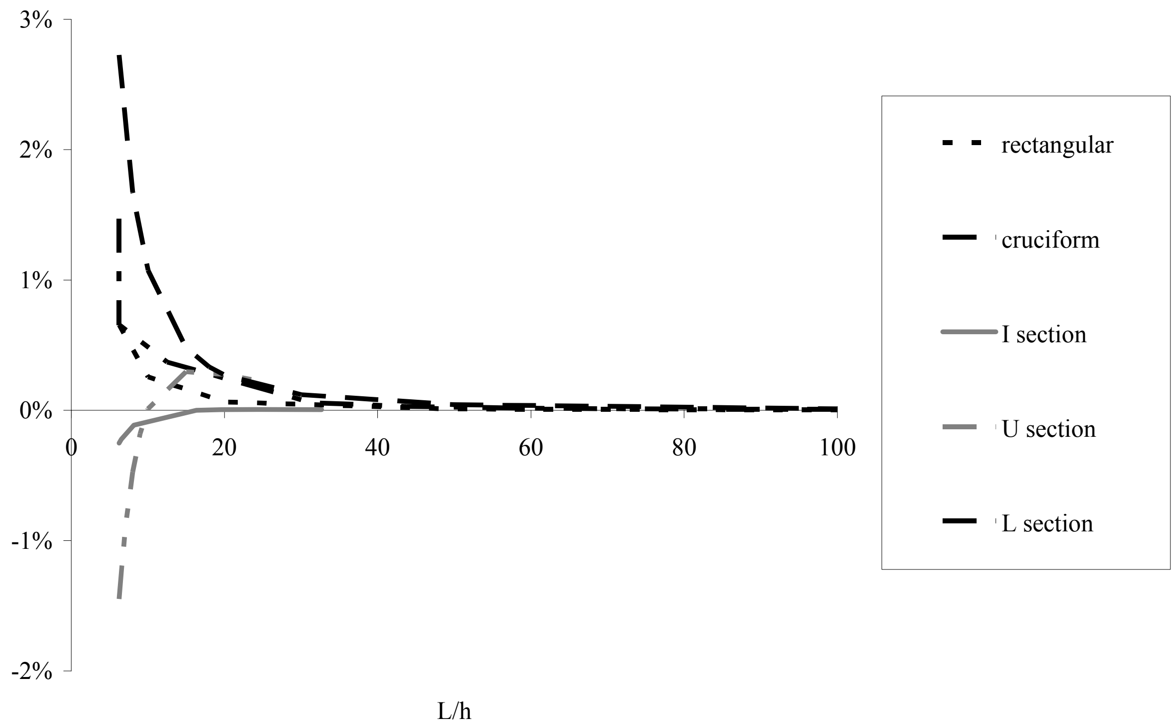

Figure 4.6 Difference between analytical calculations (Vlassov and Prokić kinematic formulations) of lateral torsional critical moments for beams with rectangular, cruciform, I, U and L cross sections

Example 2: Buckling of celled-profile beams

A column (a) is submitted to an axial load and a beam (b) is submitted to uniform bending (figure 4.7). Two cross-sections are considered (① consists of one cell and two walls, and ② is a closed cross-section). Note that this close profile was introduced by Kollbrunner [1972, page 195]. L= 20m, E=206GPa, G=82.4GPa.

Firstly, the column (a) is submitted to an axial load. In case (①-a), a mono-symmetrical cross-section is considered. The lowest critical load (161kN) corresponds to a coupling between flexural and torsional buckling. The other critical load (111 MN) associated with the coupling of flexural and torsional buckling is very large. The intermediate critical load (923kN) is associated with a pure bending mode and is given exactly by the two theories (Benscoter and the proposed theory) since it depends on the flexural characteristics of the beam and not on the warping shape and characteristics.

The same column (a) is studied with the closed cross-section (case ②-a). In practice, a column with this kind of closed cross-section ② will not collapse by global instability because of its high torsional and bending stiffnesses but rather by local buckling or yielding. This may be the reason why torsional buckling analysis of columns with closed cross-section is not found in the literature. However, this cross-section is analyzed here for testing the model and the critical loads obtained are indeed very large. These computations are rather important for the buckling analysis of beams or columns with cross sections such as ① that are neither totally open, nor fully closed.

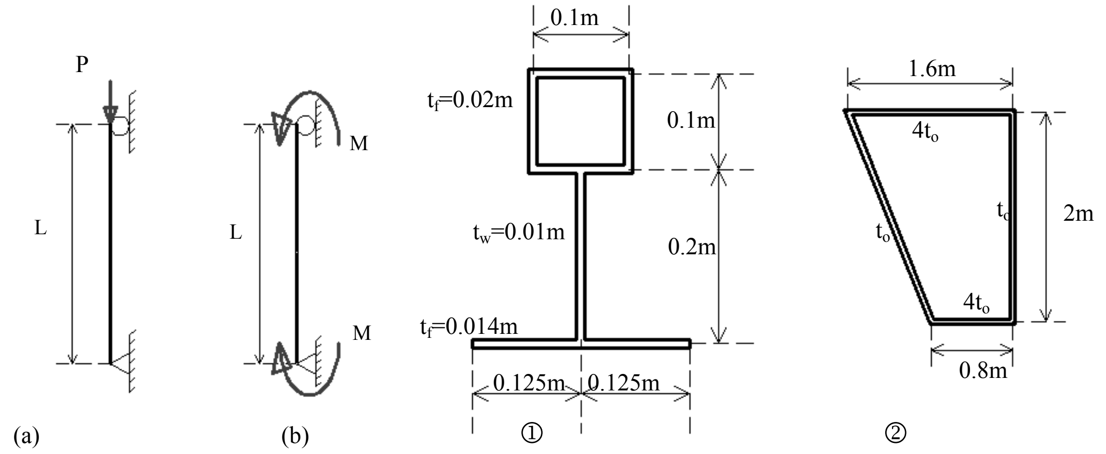

Figure 4.7 Flexural, flexural-torsional and lateral-torsional buckling of beams and columns

Table 4.3: Difference between critical loads or bending moments calculated by using Benscoter and adapted Prokić warping functions

		First critical load	second critical load	Third critical load
case 1-a	(Pcr [MN])	(0.161) 0.001%	(0.923) 0.001%	(111) 0.530%
case 1-b	(Mcr MNm])	(+0.528) 0.006%	(-0.538) 0.006%	
case 2-a	(Pcr [MN])	(148.4) 0.005%	(549) 0.002%	(4044) 0.250%
case 2-b	(Mcr MNm])	(–831) 0.052%	(721) 0.055%	

Secondly, the beam (b) is subjected to uniform plane bending by applying at its ends two couples acting along the main principal axis. The critical bending moments (+528 /-538 kN.m) of the first cross-section correspond to the lateral-torsional buckling. The sign of the bending moment is very important. In the second case (②-b for the mono-cellular cross-section), the first critical moment calculated by using Benscoter warping function is –831MN.m for one orientation and 721MN.m for the other. The analytical values of critical loads and bending moments are calculated by using Benscoter warping function and the above described warping function. The difference is given is table 4.3.

Example 3: A monosymmetrical I beam with linear bending moment distribution

A simply supported beam with an open monosymmetric cross section (Figure 4.8b) is submitted to unequal end moments as shown in Figure 4.8a. Five loading cases are considered: “C1”, “C5”, “C0”, “C-5”, “C-1”, for different values of end moment ratio k = 1 (uniform moment distribution), 0.5, 0, -0.5 and −1 respectively. Six different values of beam length are considered: L = 3, 5, 8, 10, 15 and 20 meters. E = 210GPa, G = 80 GPa.

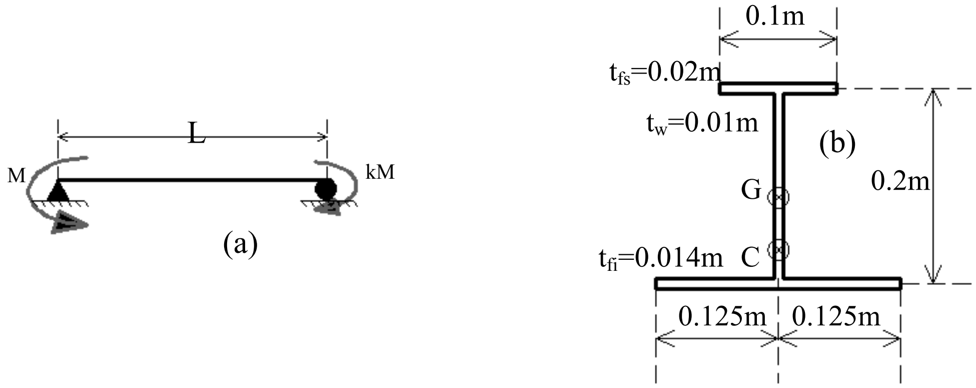

Figure 4.8 A monosymmetrical I beam

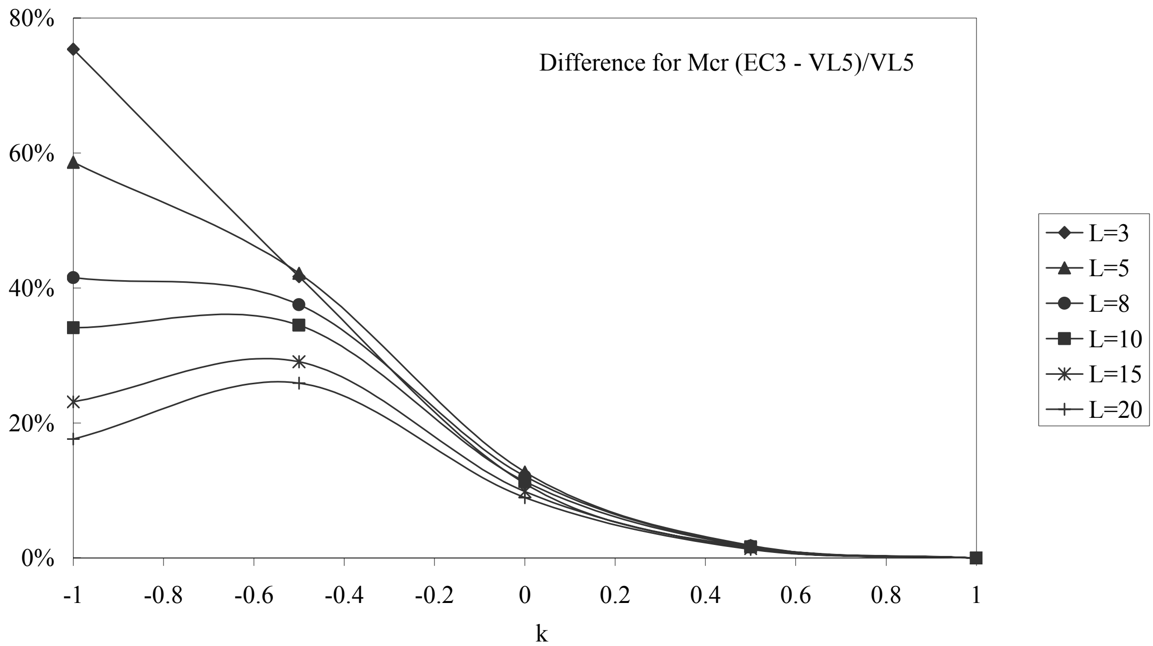

Figure 4.9 Lateral torsional buckling of monosymmetrical I beam

The following comparisons are made:

-firstly, the European Code for the design of Steel Structures EC3 is compared with the present analytical calculations VL1. The difference for M_{cr} between EC3 and VL1 (0.00%, 0.04%, 0.07%, 0.25% and 0.51% for C1, C5, C0, C-5 and C-1 respectively) is small and does not vary with the length of the beam.

-secondly, the present warping function is compared to that of Vlassov. The difference for M_{cr} between PR1 and VL1 is found to be similar for the five loading cases. However it varies with the length of the beam: 0.088%, 0.049%, 0.021%, 0.013%, 0.006% and 0.003% for L = 3, 5, 8, 10, 15 and 20 meters respectively (case C1). As expected, the influence of the thickness warping is negligible in the case of very thin walled structures and decreases with increasing values of the length L.

-thirdly, the influence of the choice of displacement functions in analytical calculations is analyzed. VL5 is used with five terms of sinusoidal functions in order to refine the modelling of the displacement modes. The difference for M_{cr} between EC3 and VL5 is shown in Figure 4.9. The difference is very large for the case C-1 (75% for L = 3m) where each flange of the I beam changes from compression to tension along the length of the beam. EC3 critical moments are found to be very high compared to VL5. This result coincides with the conclusions of previous works [Mohri (2000), Braham (2001)…]. However, it should be noted that the risk of buckling is relatively reduced in this case (C-1) since the critical moment is larger than that of the other loading cases.

The non coincidence of the centroid (G) with the shear center (C) of the monosymetrical cross section (Figure 4.8b) leads to two different buckling moments (M^+ and M^-) depending on which side (upper or lower) of the profile is submitted to compression. The difference between the two buckling moments (M^+ and M^-) reaches 67.3% for C1 where a whole flange is under compression along the entire length of the beam (uniform moment distribution).

Example 4: A simply supported beam with uniformly distributed load

Table 4.4: Data for profile geometries under uniformly distributed load

Profile I	Profile II	Profile III
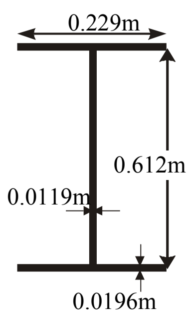	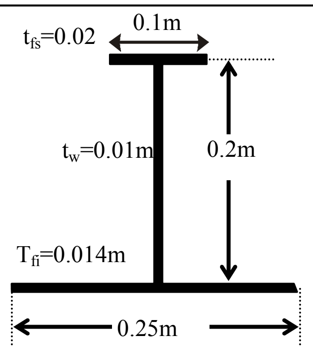	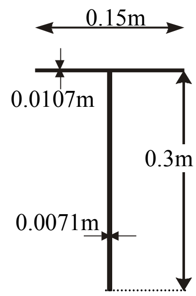

Profile IV	Profile V
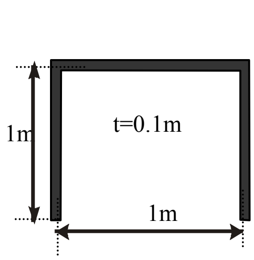	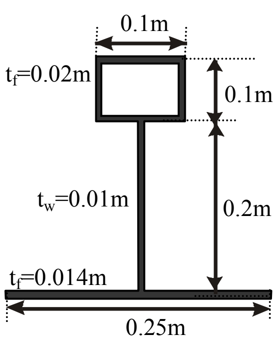

A simply supported beam (with length L) is submitted to a uniformly distributed load q. Five cross sections are considered (Table 4.4). E = 210GPa, G = 80 GPa.

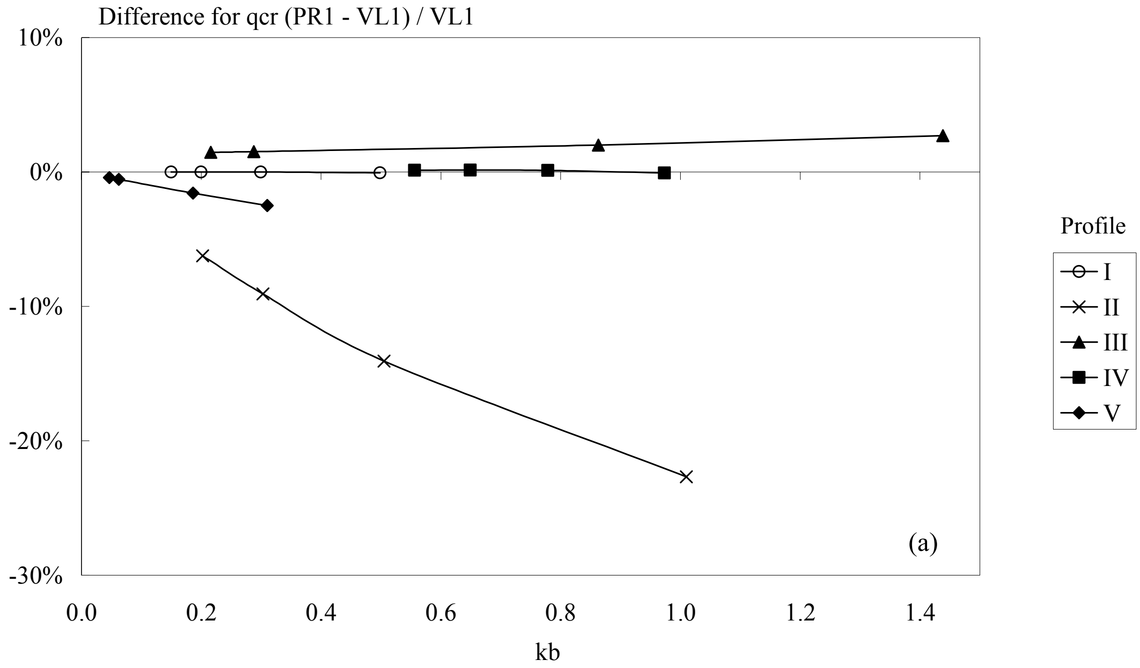

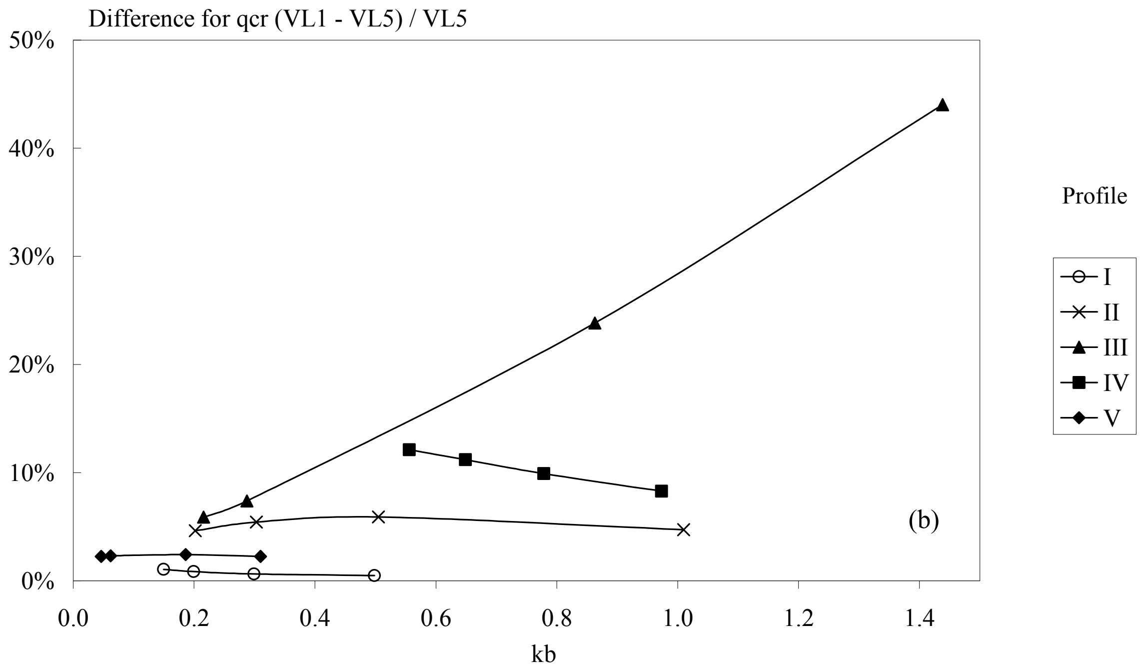

Figure 4.10: Lateral torsional buckling of simply supported beam with different profiles (Table 4.4) under uniformly distributed load

Figure 4.10a shows the influence of the choice of the warping functions for the five profiles and for a varying beam length on the critical value of the load q. Vlassov warping function is used for all profiles except for the single celled profile V for which Vlassov warping function is not applicable.

Benscoter warping function is thus used for this profile with a single sinusoidal function as displacement mode for VL1 and with a series of five sinusoidal functions for VL5. The critical load for this profile cannot be computed by using the formulae of the Eurocode (EC3). Figure 4.10b shows the difference for the critical load q_{cr} between VL1 (a single sinusoidal function for displacement modes) and VL5 (a series of five terms). The data variation is represented on the horizontal axis of Figure 4.10a and 4.10b by the beam parameter k_b used by Conci (1992) and defined by (4.87).

$$k_b = \sqrt{\frac{\pi E I h^2}{4L^2 G K}} \tag{4.87}$$

h is the total depth of the beam and I is the second moment of area about the vertical bending axis.

The following conclusions can be drawn from the parametric study:

- the results of the European Steel code EC3 are found to closely match those of present analytical calculations VL1 (0.043%, 0.027%, 0.044% and 0.017% for profiles I, II, III and IV).
- the difference between the present warping function (PR1) and Vlassov or Benscoter warping function (VL1) increases in general with small values of beam length (Figure 4.10a). This is due to the influence of the thickness warping (second warping function $-\omega\theta_{x,x}$ in equation 3.9) which is important for short thin walled beams. The second order torsional warping is not included in Vlassov and Benscoter warping function in the present VL analytical calculations and in the European Code EC3. The profile II exhibits the largest deviation.
- the importance of the choice of displacement mode functions depends on the profile asymmetry. For the bisymmetrical I profile (Profile I), the difference between VL5 and VL1 is 1% ($k_b = 0.15$). For the other monosymmetrical cross sections (Profile II, III, IV and V), the difference is larger (Figure 4.10b). The T cross section (profile III) exhibits the largest deviation.

PART III. DISCRETE MODELS

CHAPTER 5. FINITE ELEMENT DISCRETIZATION

5.1 Introduction

The analysis of complex behavior of solid mechanics as a continuous problem cannot be always solved analytically since the available techniques limit the possibilities to simplified situations. Engineers use adequate numerical models with a finite number of well-defined components and approximations in order to converge to the exact continuum solution when the number of discrete variables increases. Among these discretization procedures, the finite element method offers a very well-known methodology for the analysis of the structural behavior. The continuum is divided into a finite number of parts called elements with a finite number of parameters. For each element of the structure, a force-displacement relationship is established. The elements of the entire structure are then assembled and the resolution of the equilibrium equations yields the unknown displacements. In this chapter, different elements are developed to illustrate the application of the kinematics presented in paragraphs 2.1.1, 2.1.2 and in Chapter 3.

5.2 Finite elements with torsional warping

5.2.1 A 2-node beam model "FEM1"

Displacement field

The finite element 'FEM1' described hereafter is based on the flexural and torsional kinematics previously described in §2.1.1 and §3.2. The simplest bending beam kinematics is the Bernoulli beam theory based on the hypothesis that a plane cross section normal to the beam axis remains plane and normal during bending. This assumption is based on neglecting transverse shear strains. The displacements are small and the rotation angle of the cross section is assimilated to the slope of the deflected line shape. The torsional theory includes a thickness and a contour warping. The first is assumed to be proportional to the gradient of the torsional angle and the second is evaluated as a linear combination of warping displacements of transversal nodes selected from a geometrical discretization of the profile.

In a general loading with tension-compression, biaxial bending and torsion, the displacement vector at any point q is:

$$\begin{Bmatrix} u_q \\ v_q \\ w_q \end{Bmatrix} = \begin{Bmatrix} u_0 \\ 0 \\ 0 \end{Bmatrix} + \begin{Bmatrix} -zw_{,x} \\ 0 \\ w \end{Bmatrix} + \begin{Bmatrix} -yv_{,x} \\ v \\ 0 \end{Bmatrix} + \begin{Bmatrix} -\omega\theta_{x,x} + \sum_{i=1}^{n} \Omega^i u_i \\ -(z-z_c)\theta_x \\ (y-y_c)\theta_x \end{Bmatrix} \tag{5.1}$$

As developed in §3.2.3, the torsional warping problem requires additional kinematical equations (equations 3.12, 3.15 and 3.17).

Finite element definition

The finite element is defined by two end nodes; each one is characterized by 6+n degrees of freedom (u_0, v, w, $v_{,x}$, $w_{,x}$, θ_x, u_i,…) (figure 5.1). The beam displacements at any point within the element is approximated by expressions (5.2) in which the components of N are chosen functions of position.

Linear shape functions are used for tension / compression and torsion and cubic shape functions give exact bending solutions at nodes.
The degrees of freedom (u_0, v, w, θ_x, u_i,…) are related to the finite element nodal displacements (5.2) by using the interpolation functions (5.3).

$$u_0 = \langle N_u \rangle \{q_{u0}\}$$
$$v = \langle N_v \rangle \{q_v\} \qquad w = \langle N_w \rangle \{q_w\}$$
$$\theta_x = \langle N_u \rangle \{q_{\theta x}\} \qquad u_i = \langle N_u \rangle \{q_{ui}\};\ i=1,2,\ldots n \tag{5.2}$$

with
$$\{q_{u0}\}^t = \langle u_{01}, u_{02} \rangle$$
$$\{q_v\}^t = \langle v_1, v_{1,x}, v_2, v_{2,x} \rangle \qquad \{q_w\}^t = \langle w_1, w_{1,x}, w_2, w_{2,x} \rangle$$
$$\{q_{ui}\}^t = \langle u_{i1}, u_{i2} \rangle \qquad \{q_{\theta x}\}^t = \langle \theta_{x1}, \theta_{x2} \rangle$$

The components of N_u, N_v and N_w are given by:

$$N_{u1} = 1 - (\frac{x}{L}) \qquad N_{u2} = (\frac{x}{L})$$
$$N_{v1} = N_{w1} = 1 - 3(\frac{x}{L})^2 + 2(\frac{x}{L})^3 \qquad N_{v2} = -N_{w2} = [(\frac{x}{L}) - 2(\frac{x}{L})^2 + (\frac{x}{L})^3]L$$
$$N_{v3} = N_{w3} = 3(\frac{x}{L})^2 - 2(\frac{x}{L})^3 \qquad N_{v4} = -N_{w4} = 4[-(\frac{x}{L})^2 + (\frac{x}{L})^3]L \tag{5.3}$$

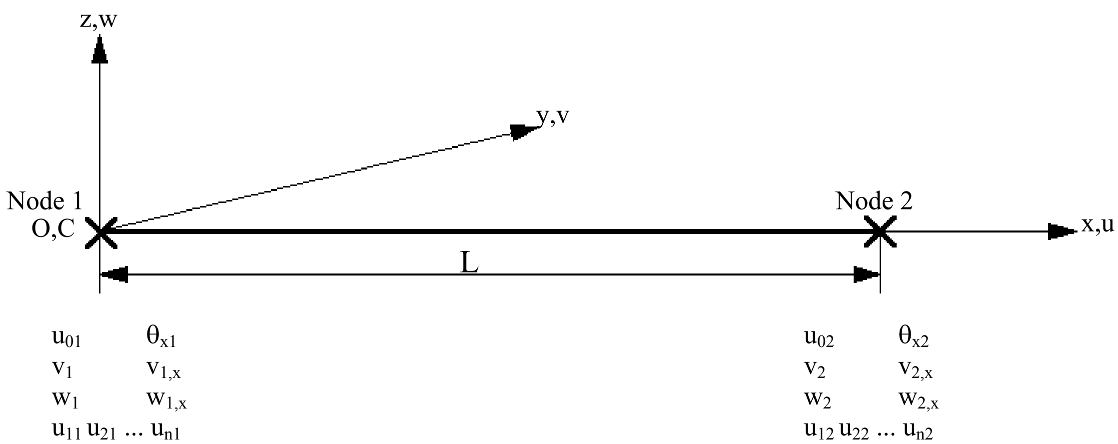

Figure 5.1 Beam finite element without shear effects

Stiffness matrix
The displacements at any point q within an element are deduced from (5.1), (5.2) and (5.3), in a matrix expression :

$$\begin{Bmatrix} u_q \\ v_q \\ w_q \end{Bmatrix} = [\eta]\{q\} \tag{5.4}$$

where $\{q\}$ is the (12+2n) nodal displacement vector (5.5) and $[\eta]$ the (12+2n x 12+2n) matrix given below in (5.6):

$$\{q\}^t = \langle q \rangle = \Big\langle \langle q_{u0} \rangle \ \langle q_v \rangle \ \langle q_w \rangle \ \langle q_{\theta_x} \rangle \ \langle q_{u^1} \rangle \ \dots \ \langle q_{u^i} \rangle \ \dots \ \langle q_{u^n} \rangle \Big\rangle \tag{5.5}$$

$$[\eta] = \begin{bmatrix} \langle N_u \rangle & -y\langle N'_v \rangle & -z\langle N'_w \rangle & -\omega\langle N'_u \rangle & \Omega^1\langle N_u \rangle \ \dots \ \Omega^i\langle N_u \rangle \ \dots \ \Omega^n\langle N_u \rangle \\ & \langle N_v \rangle & & -(z-z_c)\langle N_u \rangle & \\ & & \langle N_w \rangle & y-y_c)\langle N_u \rangle & \\ & & & & \end{bmatrix} \tag{5.6}$$

The generalized strain vector is also presented in a matrix formulation:

$$\begin{Bmatrix} \varepsilon_x \\ 2\varepsilon_{xy} \\ 2\varepsilon_{xz} \end{Bmatrix} = [B_L]\{q\} \tag{5.7}$$

where

$$[B_L] = \begin{bmatrix} \frac{\partial}{\partial x} & & \\ \frac{\partial}{\partial y} & \frac{\partial}{\partial x} & \\ \frac{\partial}{\partial z} & & \frac{\partial}{\partial x} \end{bmatrix} [\eta]$$

$$[B_L] = \begin{bmatrix} \langle N'_u \rangle & -y\langle N''_v \rangle & -z\langle N''_w \rangle & & \Omega^i\langle N'_u \rangle \\ & & & -(z-z_c+\omega_{,y})\langle N'_u \rangle & \Omega^i{}_{,y}\langle N_u \rangle \\ & & & (y-y_c-\omega_{,z})\langle N'_u \rangle & \Omega^i{}_{,z}\langle N_u \rangle \end{bmatrix} \tag{5.8}$$

By using the principle of minimum potential energy, the governing equilibrium equations are presented for an element as:

$$[k_{el}]\ \{q\} = \{F\} \tag{5.9}$$

The element stiffness matrix is:

$$[k]_{el} = \int_0^L \int_A \ [B_L]^t [H][B_L] dA dx \tag{5.10}$$

where [H] is the Hooke matrix.

$$[H] = \begin{bmatrix} E & & \\ & G & \\ & & G \end{bmatrix}$$

5.2.2 A 3-node beam model "FEM2"

Displacement field

The finite element described hereafter 'FEM2' is based on the flexural and torsional kinematics that was previously described in §2.1.2 and §3.2. The normality assumption of the Bernoulli beam theory is relaxed and transverse shear strain is supposed to be constant in each cross section. The shear stresses computed from the constitutive equations are also assumed to be constant and a shear correction factor is thus applied (§2.1.2).

In a general loading with tension-compression, biaxial bending and torsion, the displacement vector at any point q is expressed as:

$$\begin{Bmatrix} u_q \\ v_q \\ w_q \end{Bmatrix} = \begin{Bmatrix} u_0 \\ 0 \\ 0 \end{Bmatrix} + \begin{Bmatrix} z\theta_y \\ 0 \\ w \end{Bmatrix} + \begin{Bmatrix} -y\theta_z \\ v \\ 0 \end{Bmatrix} + \begin{Bmatrix} -\omega\theta_{x,x} + \sum_{i=1}^{n}\Omega^i u_i \\ -(z-z_c)\theta_x \\ (y-y_c)\theta_x \end{Bmatrix} \tag{5.11}$$

In addition, kinematical equations (equations 3.12, 3.15 and 3.17) must be satisfied.

Finite element definition

The beam finite element is defined by three longitudinal nodes. For each end node, there are 6+n degrees of freedom (u_0,v,w,θ_x,θ_y,θ_z,u_i,…). The central node is characterized by 5 degrees of freedom (v,w,θ_x,θ_y,θ_z). The beam displacements at any point within the element are approximated in terms of nodal displacements by using two prescribed functions. The transverse displacements (v,w) and the rotations (θ_x, θ_y, θ_z) are interpolated by a quadratic shape function N. For the longitudinal displacements, a linear interpolation function N_u is used.

$$\langle N\rangle^T = \begin{Bmatrix} 1-3\xi \ +2\xi^2 \\ 4\xi(1-\xi) \\ -\xi(1-2\xi) \end{Bmatrix} \qquad \langle N_u\rangle^T = \begin{Bmatrix} 1-\xi \\ \xi \end{Bmatrix} \quad \text{with } \xi = \frac{x}{L} \tag{5.12}$$

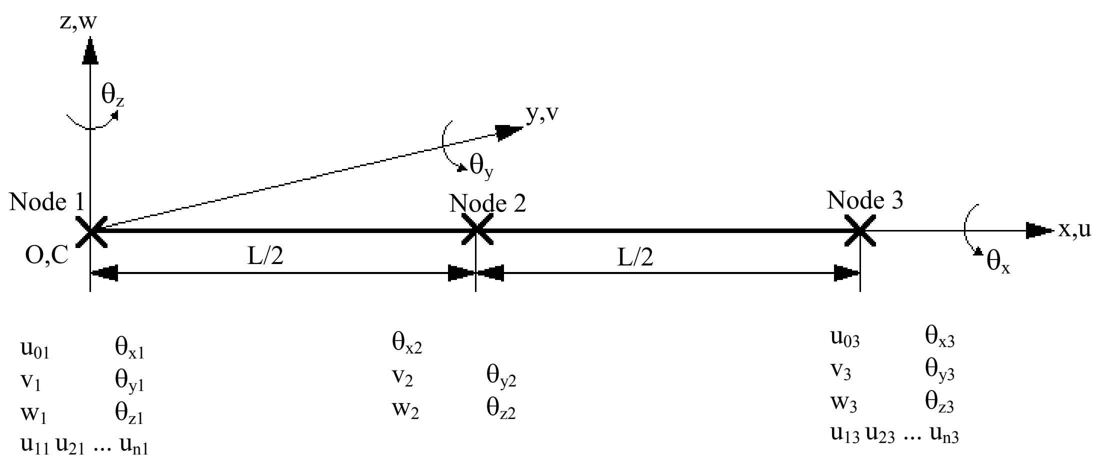

Figure 5.2 Beam finite element with shear effects

The displacements (u_0,v,w,θ_x,θ_y,θ_z,u_i,…) are related to the finite nodal displacements by using the interpolation functions as follows:

$u_0=\langle N_u\rangle\{q_{u0}\}$
$v=\langle N\rangle\{q_v\}$
$w= \langle N\rangle\{q_w\}$
$\theta_x = \langle N\rangle\{q_{\theta x}\}$
$\theta_y = \langle N\rangle\{q_{\theta y}\}$
$\theta_z =\langle N\rangle\{q_{\theta z}\}$
$u_i = \langle N_u\rangle\{q_{ui}\}$; i=1,2,…n (5.13)

with
$\{q_{u0}\}^t = \langle u_{01} , u_{02} \rangle$
$\{q_v\}^t = \langle v_1 , v_2 , v_3 \rangle$
$\{q_w\}^t = \langle w_1 , w_2 , w_3 \rangle$
$\{q_{ui}\}^t = \langle u_{i1} , u_{i2} \rangle$
$\{q_{\theta x}\}^t = \langle \theta_{x1} , \theta_{x2}, \theta_{x3} \rangle$
$\{q_{\theta y}\}^t = \langle \theta_{y1} , \theta_{y2}, \theta_{y3} \rangle$
$\{q_{\theta z}\}^t = \langle \theta_{z1} , \theta_{z2}, \theta_{z3} \rangle$

Stiffness matrix
The displacements at any point q within an element are deduced from (5.11), (5.12) and (5.13) by using the following matrix notation :

$$\begin{Bmatrix} u_q \\ v_q \\ w_q \end{Bmatrix} = [\eta]\{q\} \tag{5.14}$$

where

$$[\eta] = \begin{bmatrix} \langle N_u\rangle & & & -\omega\langle N'\rangle & z\langle N\rangle & -y\langle N\rangle & \dots & \Omega^i\langle N_u\rangle & \dots \\ & \langle N\rangle & & -(z-z_c)\langle N\rangle & & & & & \\ & & \langle N\rangle & (y-y_c)\langle N\rangle & & & & & \end{bmatrix} \tag{5.15}$$

and

$$\{q\}^t = \left\langle \langle q_u\rangle \; \langle q_v\rangle \; \langle q_w\rangle \; \langle q_{\theta_x}\rangle \; \langle q_{\theta_y}\rangle \; \langle q_{\theta_z}\rangle \; \langle q_{u_1}\rangle \; \dots \; \langle q_{u_i}\rangle \; \dots \; \langle q_{u_n}\rangle \right\rangle \tag{5.16}$$

The generalized strain vector is also presented in a matrix formulation:

$$\begin{Bmatrix} \varepsilon_x \\ 2\varepsilon_{xy} \\ 2\varepsilon_{xz} \end{Bmatrix} = [B_L]\{q\} \tag{5.17}$$

where

$$[B_L]=\begin{bmatrix} \frac{\partial}{\partial x} & & \\ \frac{\partial}{\partial y} & \frac{\partial}{\partial x} & \\ \frac{\partial}{\partial z} & & \frac{\partial}{\partial x} \end{bmatrix}[\eta] \tag{5.18}$$

$$[B_L]=\begin{bmatrix} \langle N'_u \rangle & & & -\omega\langle N'' \rangle & z\langle N' \rangle & -y\langle N' \rangle & \Omega^i\langle N'_u \rangle \\ & \langle N' \rangle & & -(z-z_c+\omega_{,y})\langle N' \rangle & & -\langle N \rangle & \Omega^i{}_{,y}\langle N_u \rangle \\ & & \langle N' \rangle & (y-y_c-\omega_{,z})\langle N' \rangle & \langle N \rangle & & \Omega^i{}_{,z}\langle N_u \rangle \end{bmatrix} \tag{5.19}$$

And the element stiffness matrix is:

$$[k]_{el}=\int_0^L\int_A [B_L]^t[H][B_L]dAdx \tag{5.20}$$

The above quadratic Timoshenko element is modified in order to take into account a reduced selective integration. For the element stiffness matrix (Appendix A3), this affects only the matrix [K_1]. For the resulting finite element, called hereafter 'FEM2', the shear locking problem is eliminated and the finite element solution is ameliorated. Jirousek 1984 shows that the quadratic isoparametric beam element integrated with two Gauss points solves exactly a beam segment with a parabolic distribution of bending moment.

Properties of the Timoshenko beam finite element

In the literature, various choices of interpolation functions for bending degrees of freedom have resulted in different Timoshenko beam finite elements. Some elements present numerical problems like shear locking since they are unable to represent bending deformations for which transverse shear must vanish. For deformations in which the normal to the midline remains straight and normal, these elements exhibit a spurious penalizing stiffness that leads to the appearance of erroneous transversal shear. This penalty term becomes in some cases more important than the stiffness of the correct deformation and the inappropriate transversal shear absorbs a large part of the energy due to the external forces leading to inaccurate deflections and strains. In particular, when identical linear interpolations of transversal displacements and section rotations are used with exact integrations to calculate the stiffness matrix [Batoz 1990 page 83; Belytschko 2000 page 556; …], an inconsistency of the formulation results in its inability to capture a zero state of transverse shear strain. The locking phenomenon appears by displaying a strong over-stiffening and inducing significant errors. The convergence deteriorates as the thickness (or ratio height/length) of the Timoshenko beam model tends to zero. A large number of references [Batoz 1990 page 86, Reddy 1997, Yunhua 1998, Binkevich 1998, Wang 2000, Mukherjee 2001…] have elaborated and developed diverse beam finite element models and have shown many techniques to avoid the problem of shear locking so that the application to thin walled structures becomes feasible.

In this work, the quadratic Timoshenko element ('FEM2') is used with a reduced selective integration since this technique was found to suppress, for beam elements, the locking without requiring additional computing costs.

For the proposed quadratic element, the shear strain ($\gamma_{xz} = w_{0,x}+\theta_y$) and the curvature ($\chi = \theta_{y,x}$) can be expressed as functions of the bending nodal displacements (transverse displacements w and cross sectional rotations θ_y) by using (5.12) and (5.13):

$$\gamma_{xz}^{F} = \left\{-\frac{3}{L}w_1 + \frac{4}{L}w_2 - \frac{1}{L}w_3 + \theta_{y1}\right\} + \frac{x}{L}\left\{-3\theta_{y1} + 4\theta_{y2} - \theta_{y3} + \frac{4}{L}w_1 - \frac{8}{L}w_2 + \frac{4}{L}w_3\right\}$$
$$+\frac{x^2}{L^2}\left\{2\theta_{y1} - 4\theta y_2 + 2\theta_{y3}\right\} \quad (5.21)$$

$$\chi = \left\{-\frac{3}{L}\theta_{y1} + \frac{4}{L}\theta_{y2} - \frac{1}{L}\theta_{y3}\right\} + \frac{x}{L}\left\{\frac{4}{L}\theta_{y1} - \frac{8}{L}\theta_{y2} + \frac{4}{L}\theta_{y3}\right\} \quad (5.22)$$

An absence of shear strains ($\gamma_{xz} = 0$) along the beam element induces three equations (5.23):

$$\left\{-\frac{3}{L}w_1 + \frac{4}{L}w_2 - \frac{1}{L}w_3 + \theta_{y1}\right\} = 0$$
$$\left\{-3\theta_{y1} + 4\theta_{y2} - \theta_{y3} + \frac{4}{L}w_1 - \frac{8}{L}w_2 + \frac{4}{L}w_3\right\} = 0$$
$$\left\{2\theta_{y1} - 4\theta y_2 + 2\theta_{y3}\right\} = 0 \quad (5.23)$$

It could be shown that if the third equation of (5.23) is satisfied, the curvature (5.24) is found to be constant along the element:

$$\chi = \left\{-\frac{3}{L}\theta_{y1} + \frac{4}{L}\theta_{y2} - \frac{1}{L}\theta_{y3}\right\} \quad (5.24)$$

Thus, by using a three-node beam element with quadratic interpolations, the shear locking is not present as in simple linear Timoshenko element (Appendix A3) since the curvature does not vanish. The following bending cases and the numerical examples in §5.3.4 show detailed results.

Pure bending case

If a state of pure bending is considered,

$$w_1 = w_3 = 0,\ w_2 = \alpha L/4, \qquad -\theta_{y1} = \theta_{y3} = \alpha,\ \theta_{y2} = 0 \quad (5.25)$$

Substituting (5.25) into (5.21) shows that the transverse shear vanishes through the element. Thus, shear locking is not expected in this case.

Second bending case with zero shear

However, it is not the case if another state corresponding to a situation where normals remain normal is considered. For instance, the variation of the displacement along the length of the beam is considered to be cubic:

$$w = \alpha(-1+2\xi)^3,\ \ \theta_y = -w_{,x} = -6\alpha\,(-1+2\xi)^2\,/L$$

so that

$$-w_1 = w_3 = \alpha,\ w_2 = 0, \qquad \theta_{y1} = \theta_{y3} = -6\alpha/L,\ \theta_{y2} = 0 \tag{5.26}$$

By substituting (5.26) into (5.21), the transverse shear is given by:

$$\gamma_{xz}^{F} = 8[-\frac{1}{2}\frac{\alpha}{L} + 3\frac{\alpha}{L^2}x - 3\frac{\alpha}{L^3}x^2] \tag{5.27}$$

(5.27) represents a parasitic shear strain since, by using the kinematic hypothesis of Timoshenko, this shear strain should be zero for (5.26). The transverse shear given by (5.27) gives nonzero shear everywhere except at:

$$x = \frac{1}{2}(1 \pm \frac{\sqrt{3}}{3}) \tag{5.28}$$

These two points are precisely the locations for the two Gauss point integration rule. It is already shown in the literature that, for the quadratic element, the points for which the transverse shear deformation tends to zero coincide with the nodes of the Gauss integration of second order [Jirousek 1984; Binkevich 1998; Belytschko 2000].
Thus, to avoid shear locking phenomenon and to ameliorate the finite element solution [Jirousek 1984], a selective reduced integration is used with two point (5.28) integration rule for the stiffness matrix terms associated with the transverse shear strain and an exact integration is used for the other terms (matrix [K_1] in appendix A3).

5.2.3 Adapting 'FEM1' and 'FEM2' to the torsional theory of thin-walled beams

Neglecting second order warping effects

For thin-walled structures, the thickness warping (or so-called second order warping) is usually neglected [Batoz (1990) page 195, Murray (1986), Benscoter (1954), De Ville (1989), …] in linear analysis since it induces small effects in comparison with those of the contour warping. The second order warping has indeed a small influence and is neglected in most analyses. In this work, when the thickness is considered to be small compared to the mid-wall length, terms such as $I_{z\omega}$, $I_{y\omega}$ and $I_{\omega\omega}$ are neglected when integrating (5.20) since it can be postulated that:

$$\left(\frac{e}{L}\right)^2 << 1\,; \tag{5.29}$$

Thus:

- $I_{\omega\omega}$ can be neglected when compared to I_h in the (4^{th},4^{th}) matrix term of k_{el} since:

$$\int\left(\frac{e}{L}\right)^2 h_n^{\,2}dA << \int h_n^{\,2}dA$$

- the terms $I_{z\omega}$ and $I_{y\omega}$ can be neglected when compared to $S_{\omega,z}$ and $S_{\omega,y}$ in the (4^{th},5^{th}) and (4^{th},6^{th}) matrix term of k_{el} since

$$\int \left(\frac{e}{L}\right)^2 h_n \cos\alpha \; dA << \int h_n \cos\alpha \;\; dA$$
$$\int \left(\frac{e}{L}\right)^2 h_n \sin\alpha \; dA << \int h_n \sin\alpha \;\; dA \qquad (5.30)$$

These approximations are adopted in this work if not otherwise mentioned.

Finite element developments of the additional equations

It is important to note that the warping function must be related to torsion by satisfying additional equations and that the simplest form for the equilibrium equations is the uncoupled one. It was previously shown in §3.2.3 that, for equations (5.1) & (5.11), principal axes are used and the orthogonality equations (3.13, 3.16, 3.17) have to be satisfied. The stiffness matrixes of the preceding beam finite elements result from developing equations (5.10 & 5.20) and from combining the orthogonality relationships (3.13, 3.16, 3.17, 4.14 & 4.15). The latter equations are developed by using 'FEM2' finite element discretization (similar equations are developed in the case of using 'FEM1' finite element).

$$(3.13) \quad => \quad \sum_{i=1}^{n} S_{\Omega^i} \langle N_u \rangle \{q_{u_i}\} = 0 \qquad (5.31)$$

$$(3.16) \quad => \quad -I_{z\omega} \langle N' \rangle \{q_{\theta_x}\} + \sum_{i=1}^{n} I_{z\Omega^i} \langle N_u \rangle \{q_{u_i}\} = 0 \qquad (5.32)$$

$$(3.17) \quad => \quad -I_{y\omega} \langle N' \rangle \{q_{\theta_x}\} + \sum_{i=1}^{n} I_{y\Omega^i} \langle N_u \rangle \{q_{u_i}\} = 0 \qquad (5.33)$$

$$(4.14) \quad => \quad -G(S_{\omega_{,y}} - z_c A) \langle N' \rangle \{q_{\theta_x}\} + \sum_{i=1}^{n} G S_{\Omega^i_{,y}} \langle N_u \rangle \{q_{u_i}\} = 0 \qquad (5.34)$$

$$(4.15) \quad => \quad -G(S_{\omega_{,z}} + y_c A) \langle N' \rangle \{q_{\theta_x}\} + \sum_{i=1}^{n} G S_{\Omega^i_{,z}} \langle N_u \rangle \{q_{u_i}\} = 0 \qquad (5.35)$$

Expressions (5.31) to (5.35) must be verified for any value of x, which implies that:

$$(5.31) \quad => \quad \sum_{i=1}^{n} S_{\Omega^i} (u_{i1}) = 0 \qquad (5.36)$$

$$(5.31) \quad => \quad \sum_{i=1}^{n} S_{\Omega^i} (u_{i3}) = 0 \qquad (5.36')$$

$$(5.32) \quad => \quad I_{z\omega} \frac{1}{l} \{3\theta_{x1} - 4\theta_{x2} + \theta_{x3}\} + \sum_{i=1}^{n} I_{z\Omega^i} \{u_{i1}\} = 0 \qquad (5.37)$$

$$(5.32) \quad => \quad I_{z\omega} \frac{1}{l} \{-\theta_{x1} + 4\theta_{x2} - 3\theta_{x3}\} + \sum_{i=1}^{n} I_{z\Omega^i} \{u_{i3}\} = 0 \qquad (5.37')$$

$$(5.33) \quad => \quad I_{y\omega} \frac{1}{l} \{3\theta_{x1} - 4\theta_{x2} + \theta_{x3}\} + \sum_{i=1}^{n} I_{y\Omega^i} \{u_{i1}\} = 0 \qquad (5.38)$$

(5.33) => $I_{y\omega}\frac{1}{l}\{-\theta_{x1}+4\theta_{x2}-3\theta_{x3}\}+\sum_{i=1}^{n} I_{y\Omega^i}\{u_{i3}\}=0$ (5.38')

(5.34) => $(S_{\omega_{,y}}-z_c A)\frac{1}{l}\{3\theta_{x1}-4\theta_{x2}+\theta_{x3}\}+\sum_{i=1}^{n} S_{\Omega^i{}_{,y}}\{u_{i1}\}=0$ (5.39)

(5.34) => $(S_{\omega_{,y}}-z_c A)\frac{1}{l}\{-\theta_{x1}+4\theta_{x2}-3\theta_{x3}\}+\sum_{i=1}^{n} S_{\Omega^i{}_{,y}}\{u_{i3}\}=0$ (5.39')

(5.35) => $(S_{\omega_{,z}}+y_c A)\frac{1}{l}\{3\theta_{x1}-4\theta_{x2}+\theta_{x3}\}+\sum_{i=1}^{n} S_{\Omega^i{}_{,z}}\{u_{i1}\}=0$ (5.40)

(5.35) => $(S_{\omega_{,z}}+y_c A)\frac{1}{l}\{-\theta_{x1}+4\theta_{x2}-3\theta_{x3}\}+\sum_{i=1}^{n} S_{\Omega^i{}_{,z}}\{u_{i3}\}=0$ (5.40')

Elimination of the coupled terms in the stiffness matrix

It is found that equations (5.36 and 5.36') eliminate the warping/tension-compression coupled terms, that (5.38, 5.38', 5.39 & 5.39') eliminate the warping/bending (xy) coupled terms and that equations (5.37, 5.37', 5.40 & 5.40') eliminate the warping/bending (xz) coupled terms in the stiffness matrix. This numerical approach is equivalent to the analytical work done in paragraph 4.2.4 setting that the warping degrees of freedom should not induce normal forces, shear forces or bending moments. And inversely, the tension-compression and bending generalized forces should not be related to the torsional warping terms u_i. This eliminates the symmetrical coupled terms in the stiffness matrix. The non zero terms of k^{el} (computed from equations 5.10 & 5.20) obtained after eliminating the coupled terms (5.36-5.40' for FEM2) and after neglecting the second warping effects (taking into account 5.30) are given in Appendices 2 & 3 respectively.

Relating u_i to torsional warping

The orthogonality equations (5.36 to 5.40') that simplify the system of equilibrium equations (previous paragraph) must again be used to relate the degrees of freedom. Therefore, there are (n-3) independent degrees of freedom among the (6+n) of each longitudinal end node of the finite element. For one finite element, six dependent axial displacements u_i must be separated from the other independent ones. The displacement vector {q} is thus divided into two parts: dependent degrees of freedom $\{q_d\}$ and independent ones $\{q_i\}$. Kinematic equations obtained by neglecting second torsional warping (as stated in equation 5.30) into (3.13, 3.16, 3.17) give the relationships that can be written in the following forms :

$[C]\{q\}=0$

or

$\{q_d\}=[D]\ \{q_i\}$ (5.41)

The entire set of equilibrium equations can be solved by using the Lagrange multipliers (5.42) or by condensing the stiffness matrix.

$$\begin{bmatrix}[K] & [C]^t\\ [C] & 0\end{bmatrix}\begin{Bmatrix}\{q\}\\ \{\lambda\}\end{Bmatrix}=\begin{Bmatrix}\{F\}\\ \{b\}\end{Bmatrix} \quad (5.42)$$

For the condensation method, the set of equilibrium equations is transformed into:

$$\begin{bmatrix} [K_{ii}] & [K_{id}] \\ [K_{di}] & [K_{dd}] \end{bmatrix} \begin{Bmatrix} \{q_i\} \\ \{q_d\} \end{Bmatrix} = \begin{Bmatrix} \{F_i\} \\ \{F_d\} \end{Bmatrix} \tag{5.43}$$

By combining (5.41) and (5.43), the final system to be solved is then reduced to:

$$[[K_{ii}]+[K_{id}][D]+[D]^t[K_{id}] +[D]^t[K_{dd}]\,[D]]\ \{q_i\}=\{F_i\}+[D]^t\{F_d\} \tag{5.44}$$

The (6,2n) C matrix is constituted by two sets of three equations. Each set is related to a longitudinal end node and is deduced from equations (5.36-5.38) by neglecting second order torsional warping (taking into account 5.30).

$$\sum_{i=1}^{n} S_{\Omega^i} u_{ij} = 0 \qquad\qquad j=1,2$$

$$\sum_{i=1}^{n} I_{y\Omega^i} u_{ij} = 0$$

$$\sum_{i=1}^{n} I_{z\Omega^i} u_{ij} = 0$$

$$[C] = \begin{bmatrix} \dots & S_{\Omega^k} & \dots & 0 & 0 & 0 \\ \dots & I_{y\Omega^k} & \dots & 0 & 0 & 0 \\ \dots & I_{z\Omega^k} & \dots & 0 & 0 & 0 \\ 0 & 0 & 0 & \dots & S_{\Omega^m} & \dots \\ 0 & 0 & 0 & \dots & I_{y\Omega^m} & \dots \\ 0 & 0 & 0 & \dots & I_{z\Omega^m} & \dots \end{bmatrix} \tag{5.45}$$

Equations (5.34 & 5.35) are used to calculate the coordinates of the shear center y_C and z_C: the full system of equations is solved after a static condensation that uses (5.39 - 5.40') in order to eliminate y_C and z_C.

Static condensation of mid node degrees of freedom

This final step is not mandatory but is done in order to reduce the total number of degrees of freedom of a structure. The local unknowns of the central node 2 of each element are statically condensed before assembling the entire structure so that the total number of degrees of freedom is reduced. The columns and lines of the stiffness matrix associated with the degrees of freedom of the central node are eliminated: the terms associated with i^{th} (varies from 7+n till 11+n) degree of freedom are eliminated by modifying all the terms (m, j varying from 1 till 17+2n) of the stiffness matrix as follows:

$$k'_{mj} = k_{mj} - \frac{k_{mi}}{k_{ii}} k_{ij} \tag{5.46}$$

The condensed matrix is computed numerically and is not developed hereafter analytically.

5.2.4 Nodal forces equivalent to distributed loads

In the finite element method, distributed forces (5.47) along the element in the direction of the (x,y,z) axes are transformed into nodal forces.

$$f = ax + b \tag{5.47}$$

The resulting nodal forces {F}, statically equivalent to the forces distributed along the element, are calculated for any (virtual) nodal displacements {q} (17+2n) by equating the external and the internal work done by the various forces.

$$\{q\}^t \{F\} = \int_0^L \left\{u^h\right\}^T \{f\} dx \tag{5.48}$$

$\{u^h\}$ is the (6+n) displacement vector (u_0, v, w, θ_x, θ_y, θ_z, u_i) of any point within the element. $\{u^h\}$ is computed by multiplying a matrix [M] (6+n,12+2n for FEM1; 6+n,17+2n for FEM2) constituted from the interpolation functions by the nodal displacement vector {q}.
Since (5.48) is valid for any value of virtual displacements {q}, the contribution of the distributed forces to those of each node is calculated by:

$$\{F\} = \int_0^L [M]^T \{f\} dx \tag{5.49}$$

For an axial distributed force f_x:

$f_x = ax+b$

$$\begin{Bmatrix} F_{x1} \\ F_{x2} \end{Bmatrix} = \int_0^1 \langle N_u \rangle^T f_x L d\xi = \begin{bmatrix} \frac{1}{6} al^2 + \frac{bL}{2} \\ \frac{al^2}{3} + \frac{bL}{2} \end{bmatrix} \tag{5.50}$$

For a lateral distributed force f_y (and identically for f_z) and in the case of FEM2:

$f_y = ax+b$

$$\begin{Bmatrix} F_{y1} \\ F_{y2} \\ F_{y3} \end{Bmatrix} = \int_0^1 \langle N \rangle^T f_y L d\xi = \begin{Bmatrix} \frac{bL}{6} \\ \frac{1}{3}(aL + 2b) \\ \frac{1}{6}(aL + 2b) \end{Bmatrix} \tag{5.51}$$

For a torsional distributed torque m_x and in the case of FEM2 (and identically for m_y and m_z):

m_x=ax+b

$$\begin{Bmatrix} m_{x1} \\ m_{x2} \\ m_{x3} \end{Bmatrix} = \int_0^1 \langle N \rangle^T m_x L d\xi = \begin{Bmatrix} \frac{aL}{6} \\ \frac{1}{3}(aL + 2b) \\ \frac{1}{6}(aL + b) \end{Bmatrix} \tag{5.52}$$

The condensation of F_{y2}, F_{z2}, m_{x2}, m_{y2} or m_{x2} gives the equivalent nodal vector with components associated with the end nodes of each element. If i is associated with the term to be eliminated (one of the 5 degrees of freedom of the central node), a j term (one of the remaining 12+2n degrees of freedom) is affected as follows:

$$f_j^{'} = f_j - \frac{f_i}{k_{ii}} k_{ij} \tag{5.53}$$

The condensed (12+2n) vector {F} is developed numerically.
It is interesting to note that, for a uniformly distributed lateral force $f_y = q$, the corresponding condensed vector {F} (using 'FEM2') is found to be the same as that of the Hermitian cubic element based on the Euler-Bernoulli beam theory ('FEM1'). By using (5.53) to condensate (5.51) (with a = 0 and b = q), the nodal vector is found to be $\{qL/2, -qL^2/12, qL/2, -qL^2/12\}$.

5.2.5 Assembly of beam elements

The behavior of a general three dimensional structure composed of thin walled beams with different profile geometries is significantly influenced by assembly details. In practice, the carrying capacity and the stability of beams with uniform cross sections may be increased by bolting or welding additional plates in highly stressed parts so that the cross section changes abruptly.
The influence of a connection and the assembly of different beam structures are not easily taken into account in beam analyses. Beam forces and displacements are transferred from one finite element to another through nodal components on particular points of each element. This can be done routinely if all the components refer to the same physical point. However, assembled beams and columns may not have their centroid G or torsional center C (Fig. 5.3) situated on the same axis. This kind of assembly necessitates a particular treatment. The handling of the torsional axial displacement is particularly complex since the assembled cross sections do not necessarily fit together after deformation, but may have some parts of the contour in common. Modeling the real compatibility of the connected cross sections is a complicated task.
The influence of an assembly is hereby analyzed for each uncoupled loading effect: tension-compression, flexure, torsion and warping. Regarding tension-compression, bending or uniform torsion, the transmission is considered to be either ensured (rigid connection) or not. The assembly of general three dimensional thin walled beams and columns is limited to the usual beam study as done by Gunnlaugsson (1982), Pedersen (1991) or Shakourzadeh (1999). The displacements (u, v, w, θ_x, θ_y, θ_z) of the connected nodes refer to a common assembling point A. This assembling point A, defined as the point where the continuity is ensured, is assumed to be defined somewhere within the common contour of the connected cross sections: for example, in Figure 5.3, point A is taken anywhere along the common line 123.
The influence of the assembly details on the torsional warping of each assembled cross section is accurately described in the present work. The longitudinal displacements (u_i) of selected transversal

nodes (i=1,…n), chosen as additional degrees of freedom to model the torsional warping of thin walled structures, enable the description of compatibility equations for arbitrary joints. The warping of each cross section may be described as totally independent, partially or fully dependent from the other connected cross sections. When warping is continuous, one finite element node is used to model the connection. When it is not the case, two or more longitudinal nodes are taken at the same geometrical connection point; each node belongs to a connected element. One is the master node, and the other slave nodes are related to it by compatibility equations.

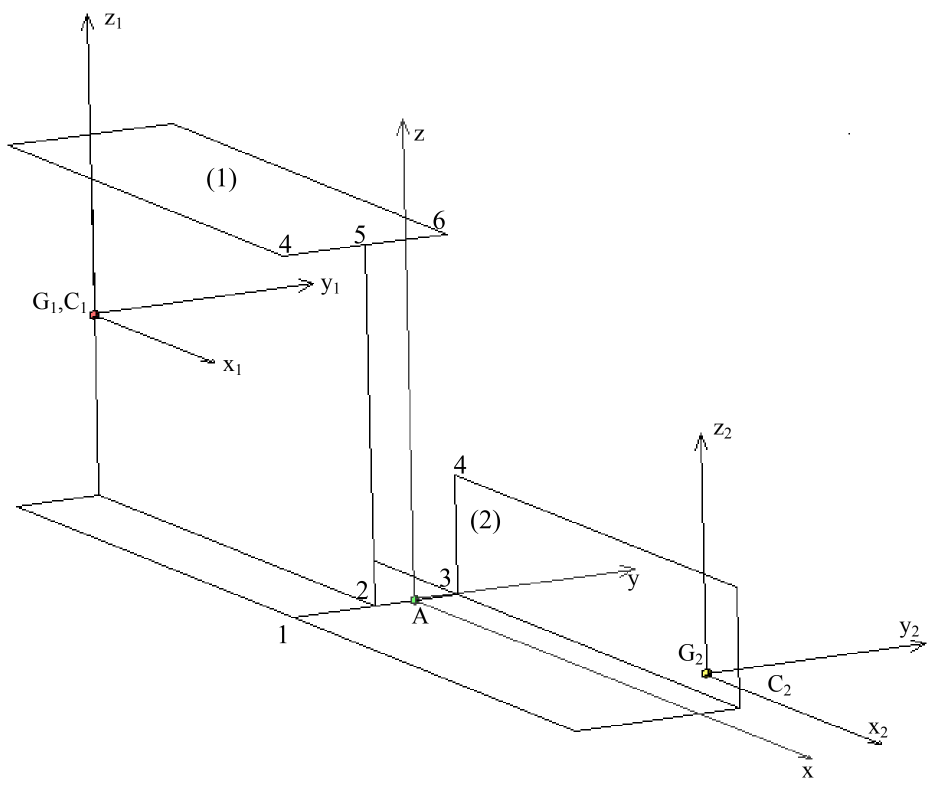

Figure 5.3 A straight connection

- The axial displacement due to in-plane tension or compression, usually considered at the centroid, is a mean value of the longitudinal displacement of the cross section. In particular, it could be taken at the common reference A.

$$u_{0A}^{a} = u_{0G}^{a} = u_{0C}^{a} \tag{5.54}$$

- The constant mean value of transversal translation due to plane flexure can be taken for the same reason at the common reference A.

$$\begin{aligned} v_A^F &= v_G^F = v_C^F \\ w_A^F &= w_G^F = w_C^F \end{aligned} \tag{5.55}$$

However the axial displacement, varying linearly along the plane of bending is proportional to the flexural rotation of the cross section. At an assembling point, centroids may not coincide and the adjacent cross sections are assumed to rotate around a common point A depending on the connection.

$$u_A^F = u_{0G}^F - y_A\,\theta_z + z_A\,\theta_y \tag{5.56}$$

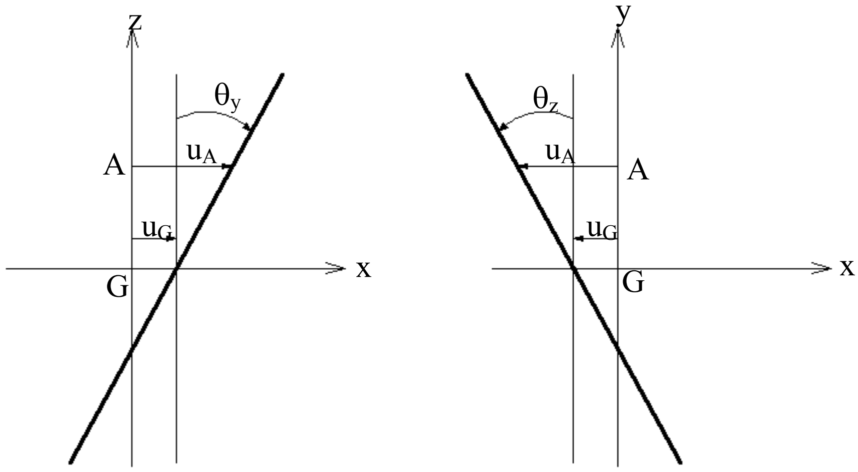

Figure 5.4 Plane flexure

- When submitted to torsional effects, a cross section rotates around the shear center. If shear centers of adjacent cross sections do not coincide, the corresponding eccentricity should be taken into account.

$$v_A^T = v_C^T - (z_A - z_C)\,\theta_x$$
$$w_A^T = w_C^T + (y_A - y_C)\,\theta_x \tag{5.57}$$

- Compatibility equations are required to model the transmission of the first order torsional warping. They describe exactly how the warping is free on some parts of the contours or partially or totally restrained on others. For instance, for the straight connection represented in Figure 5.3, the compatibility conditions between the two beams (1) and (2) are:

$$u_1^{(1)} = u_1^{(2)},\ u_2^{(1)} = u_2^{(2)},\ u_3^{(1)} = u_3^{(2)},\ u_4^{(1)} \neq u_4^{(2)},\ u_5^{(1)} \neq 0,\ u_6^{(1)} \neq 0 \tag{5.58}$$

Some other examples are given in Figures 5.5a, 5.5b and 5.5c. f_i are the internal forces associated with the degrees of freedom u_i.

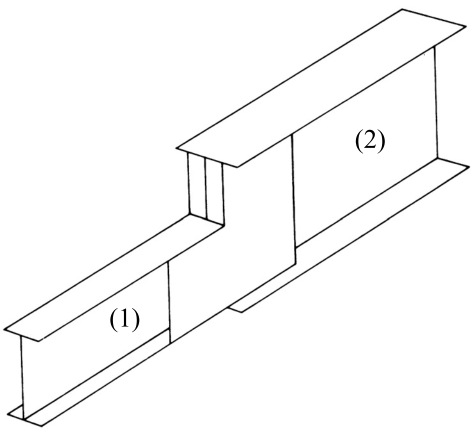

Figure 5.5a Rigid connection, warping restrained (after Gjelsvik 1981) ($u_i^{(1)} = 0$, $u_i^{(2)} = 0$)

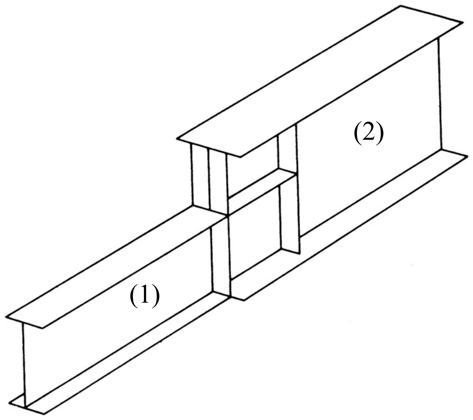

Figure 5.5b Semi rigid connection, warping transmitted (after Gjelsvik 1981) ($u_i^{(1)} = u_i^{(2)}$)

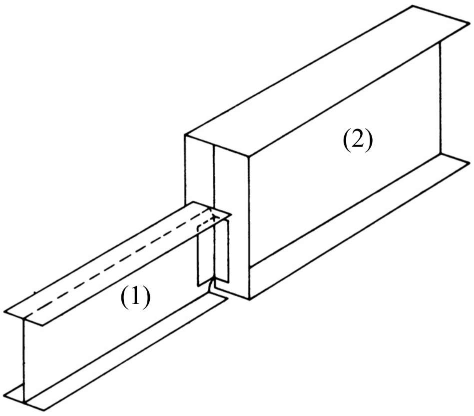

Figure 5.5c Hinged connection, independent warping (after Gjelsvik 1981) ($u_i^{(1)} \neq u_i^{(2)}$, $f_i^{(1)} = f_i^{(2)} = 0$)

The contour warping formulation does not depend directly on the assembling point since functions Ω_i describe a linear variation between the transversal nodes that relate the nodal displacements u_i of the cross section. However, the thickness warping is proportional to the perpendicular distance to the normal issued from the shear center. When the cross section is rotating around an arbitrary point A, the continuity must be insured.

$$\omega_A = \omega_C + h_{nAC}\, e \qquad (5.59)$$

where h_{nCA} is the distance between the normal issued from the shear center C to the midline and that issued from the assembling point A. Thus,

$$u_A^T = u_C^T - h_{nAC} e\, \theta_{x,x} \qquad (5.60)$$

The transformation matrix (eq. 5.61) applied to the displacements and the forces of each connected node allows the assembly process (5.54, 5.55, 5.56 and 5.57) by unifying the point of application of the nodal unknowns and neglecting second order warping continuity (neglecting 5.60).

$$\begin{Bmatrix} u \\ v \\ w \\ \theta_x \\ \theta_y \\ \theta_z \\ u_i \end{Bmatrix}_{\%G,C} = \begin{bmatrix} 1 & & & & -z_A & y_A & \\ & 1 & & (z_A - z_C) & & & \\ & & 1 & -(y_A - y_C) & & & \\ & & & 1 & & & \\ & & & & 1 & & \\ & & & & & 1 & \\ & & & & & & 1 \end{bmatrix} \begin{Bmatrix} u \\ v \\ w \\ \theta_x \\ \theta_y \\ \theta_z \\ u_i \end{Bmatrix}_{\%A} \tag{5.61}$$

or

$$\{q_n\}_{\%G}=[A]\{q_n\}_{\%A} \tag{5.62}$$

Hereafter, the force vector is considered. If external forces $\{f_n\}_{\%G}$ are applied on the centroid, the nodal force vector at the assembly point $\{f_n\}_{\%A}$ can be deduced from simple equilibrium equivalence equations.
The three translation equilibrium equations can be expressed as follows:

$$\begin{aligned} f_{x\,\%G} &= f_{x\,\%A} \\ f_{y\,\%G} &= f_{y\,\%A} \\ f_{z\,\%G} &= f_{z\,\%A} \end{aligned} \tag{5.63}$$

The three rotating equilibrium equations can be expressed as follows:

$$\begin{aligned} M_{x\,\%A} &= M_{x\,\%G} - f_{z\,\%G}\,(y_A - y_C) + f_{y\,\%G}\,(z_A - z_C) \\ M_{y\,\%A} &= M_{y\,\%G} - f_{x\,\%G}\,(z_A) \\ M_{z\,\%A} &= M_{z\,\%G} + f_{x\,\%G}\,(y_A) \end{aligned} \tag{5.64}$$

Thus the force vector and the stiffness matrix are transformed as follows:

$$\{f_n\}_{\%G} = [A]^T\{f_n\}_{\%A}$$

$$[k]_{\%A}=[A]^T\,[k]_{\%G}[A] \tag{5.65}$$

5.2.6 Applications: a thin walled beam behavior including torsional warping

Elastic finite elements 'FEM1 and FEM2' analyze the thin-walled beam behavior including the torsional warping of open, closed and multi-celled profiles with or without branches and without any restriction of symmetry. Their performance and convergence are shown for the following examples submitted primarily to torsion. Arbitrary open (examples 1, 4, 5, 7 and 9) and closed (examples 2, 3 and 6) cross sections are analyzed by using the same warping function and the same finite element model. If not mentioned otherwise, the calculations are done with a minimal kinematical profile discretization (minimum number of nodes that describe the geometry of the profile).

The numerical results are compared with analytical computations using various kinematical models depending on the profile geometry, the loading case and the boundary conditions. The reference theory is selected to be the de Saint Venant theory when the warping is uniform along the beam length. This is the case when the warping vanishes (e.g. example 2) due to the radial symmetry of the profile (circular, square tubular, particular rectangular tubular profiles..). For other particular shapes (L section, example 1…), the contour warping vanishes and the de Saint Venant theory is taken to be the reference if the second warping (thickness warping) is neglected. For other general forms of profiles, the uniform torsion is restricted to the case of a uniform distribution of torsional moment and free warping along the longitudinal axis of the beam (example 3a). In all these particular cases, the analytical and numerical results degenerate exactly into Saint Venant theory. In other general cases, the finite element results converge for refined meshes to:

- the solution obtained with Vlassov theory for open cross sections (examples 4,5,7,8 and 9)
- the solution obtained with Benscoter theory for closed cross sections (examples 3b, 6)

The following examples, summarized in table 5.1, show the difference between the theories in case of absence or strong non uniformity of warping.

Table 5.1 Description of examples

# Example	Profile type	Profile symmetry	Torsion	Applied torque	Warping	Reference theory
1	Open	bisymmetry	Uniform	Concentrated	Free	de St Venant
2a	Closed	radial symmetry	Uniform	Uniformly distributed	Free	de St Venant
2b	Closed	radial symmetry	Uniform	Uniformly distributed	Constrained	de St Venant
3a	Closed	bisymmetry	Uniform	Concentrated	Free	de St Venant
3b	Closed	bisymmetry	Non Uniform	Concentrated	Constrained	Benscoter
4a	Open	bisymmetry	Non Uniform	Uniformly distributed	Free	Vlassov
4b	Open	bisymmetry	Non Uniform	Uniformly distributed	Constrained	Vlassov
5	Open	monosymmetry	Non Uniform	Uniformly distributed	Free	Vlassov
6	Closed	asymmetry	Non Uniform	Uniformly distributed	Free	Benscoter
7	Open	bisymmetry	Non Uniform	Uniformly distributed	Transmitted	Vlassov
8	Open	bisymmetry	Non Uniform	None	Free	Vlassov
9	Open	monosymmetry	Non Uniform	Concentrated	Different cases	Vlassov

Example 1: Saint Venant torsion of a thin rectangular cross section

A thin rectangular cross section (figure 5.6b) is considered in order to show that, when the solution of Saint Venant is exact, the finite element solution degenerates into that one. The beam is simply supported at its two ends in such a way that the torsional rotation is prevented at the ends and that the sections are free to warp. A concentrated torque is applied at mid span (Figure 5.6a). G=80GPa; E=210GPa.

The torsional moment distribution is not uniform along the entire length of the beam but the first order warping (contour warping ω_1 in equation 2.33) is equal to zero. According to the theory of Vlassov, $I_\omega = 0$ and the solution degenerates into that of Saint Venant: this is the case of pure uniform torsion.

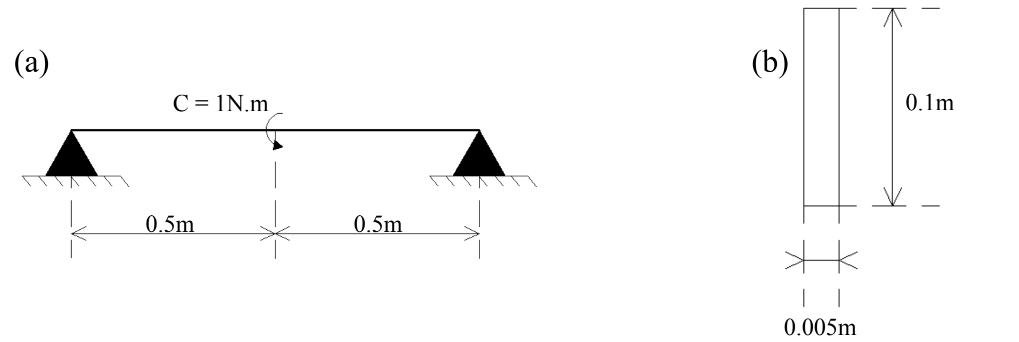

Figure 5.6 Simply supported beam submitted to a concentrated torque

The distribution of the torsional angle along the beam length is linear and thus, for both finite elements 'FEM1' and 'FEM2' (neglecting second order effects; equations 5.30) with linear and quadratic interpolation of the torsional angle, the exact solution is obtained with minimum discretization required for the geometry and the definition of the problem. The maximal torsional angle is found to be 7.5 10^{-4}rad and the maximal tangential stresses are found numerically and analytically equal to 0.6MPa.

Example 2 : Saint Venant torsion of a square tubular cross section

For the same purpose of the previous example, a square tubular cross section (figure 5.7c) beam is submitted to a uniformly distributed torque leading to a linear distribution of torsional moment. E = 206GPa and G = 82.4GPa.

Two boundary conditions are considered:

-simply supported beam with free warping (figure 5.7a),

-bi-fixed beam with constrained warping at the supports (figure 5.7b).

In both cases, the finite element solution reaches, with minimum discretization (two elements), the Saint Venant value for the mid span torsional rotation (θ_x=7.58 10^{-7}rad). Indeed, the monocellular cross section has a particular shape (tubular section with specific dimensions so called Neuber) that does not warp (ω_1 in equation 2.43 is equal to zero). Benscoter theory degenerates into Saint Venant theory. In this example as in the previous one, there are no effects of restrained warping and the uniform torsional theory is the exact solution.

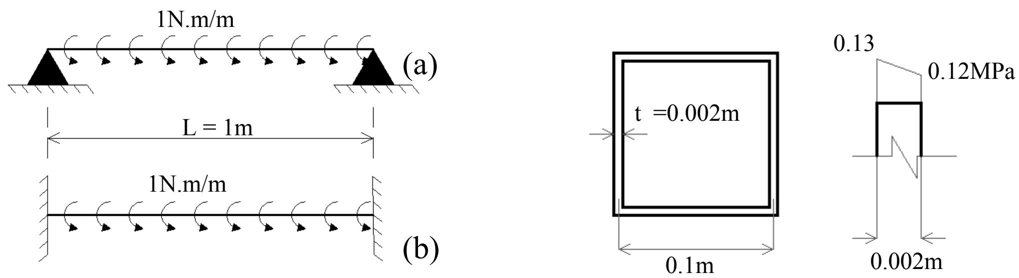

Figure 5.7 Square tubular beam with uniform density of torque

Since the cross section does not warp, there are no warping shear stresses (τ_{xs}^{ω}). The shear flow of Saint Venant stresses is uniform along the periphery of the cross-section. The same value is found for the mean shear stress by numerical and analytical results (τ_{xs}^{s} = 0.125MPa at the left support). Besides, additional shear stresses vary linearly through the thickness variation, vanish along the centerline and reach a maximum value on the outer skin ($\Delta\tau_{xs}$ = 5kPa at the left support). The total variation of the shear stresses ($\tau_{xs}^{s} + \Delta\tau_{xs}$) along the thickness (0.002m) is given in Figure 5.7d.

Example 3: torsion of a rectangular tubular cross section

In this example, the influence of warping constraint is discussed for a beam with a closed cross section (figure 5.8c) subjected to a uniform distribution of torsional moment. G=82,4GPa; E=206GPa.

Two boundary conditions are considered:

-simply supported beam: fixed rotation at left support; but with free warping at both supports (figure 5.8a),

-free fixed beam: fixed rotation and warping prevented at the left end (figure 5.8b).

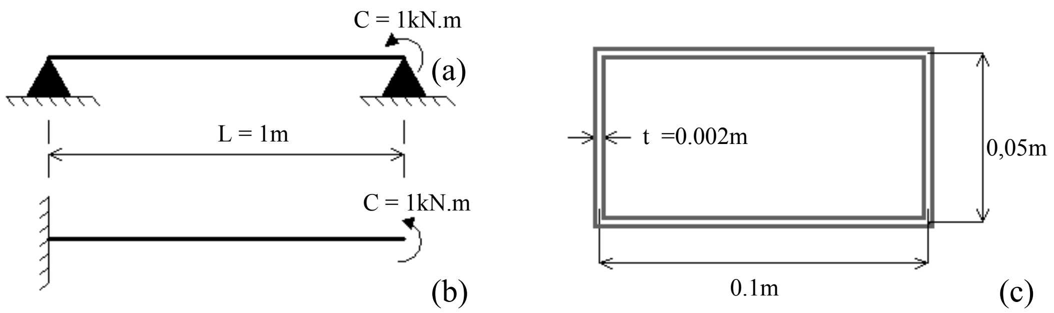

Figure 5.8 Torsion of a tubular cross section

When all cross sections are free to warp, the numerical results match those of Saint Venant (θ_x=1,82 10^{-2} rad) which are exact in this theoretical case. If one section is prevented from warping, the warping is no longer uniform and the solution of Saint Venant is no longer exact. The numerical solutions approach that of Benscoter (θ_x=1,813 10^{-2} rad) (figure 5.9).

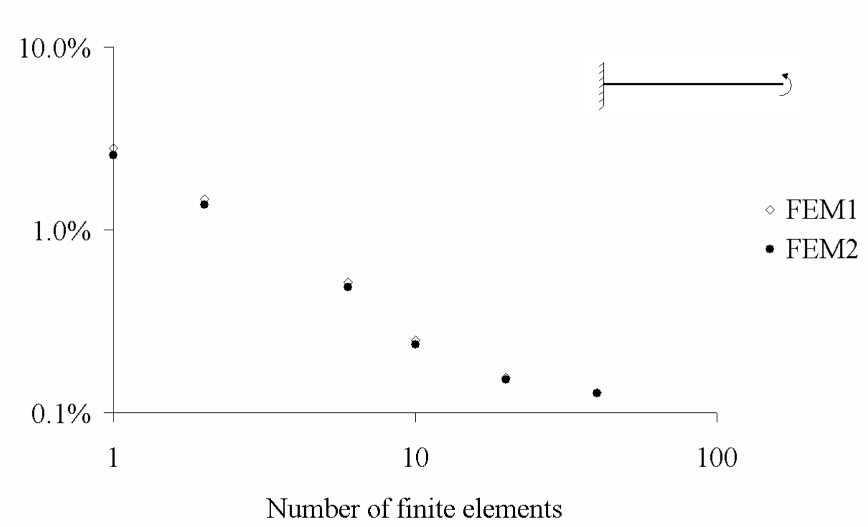

Figure 5.9 Relative difference between values of maximal torsional angle of the beam in 5.8b obtained by the theory of Benscoter and the finite elements FEM1 and FEM2

In paragraph 2.2, the difference between the torsional behavior of closed and that of open cross sections has been discussed. The non uniform warping effects have been shown to be much more important for open cross sections than for closed ones. The approximation that results from solving a

torsional problem with the de Saint Venant theory is in general more acceptable for closed (0.25% in this example) than for open cross sections.
The torsional problem of this example is found to be mostly governed by the de St Venant torsion (for which M_x^{st} is proportional to the first derivative of the torsional angle θ_x) rather than by the non uniform torsional term (for which M_x^{ω} is proportional to the third derivative of the torsional angle θ_x). The distribution of the torsional angle along the beam longitudinal axis is quasi linear and the finite element discretization of FEM1 (linear interpolation functions) is sufficient (figure 5.9: FEM1 and FEM2 results nearly coincide).

Example 4: non uniform torsion of an open cross section
A non uniform warping is considered in this example along a beam with an open cross section in order to show the convergence of the finite element solution towards that of Vlassov. The theory of Saint Venant is not exact in this case. A simply supported I beam (figure 5.10a), is sollicited by a uniform density of torque C = 100Nm/m which leads to a linear distribution of torsional moment along the length of the beam. The torsional angle is prevented at the ends and the sections are free to warp. G=82.4GPa; E=206GPa.

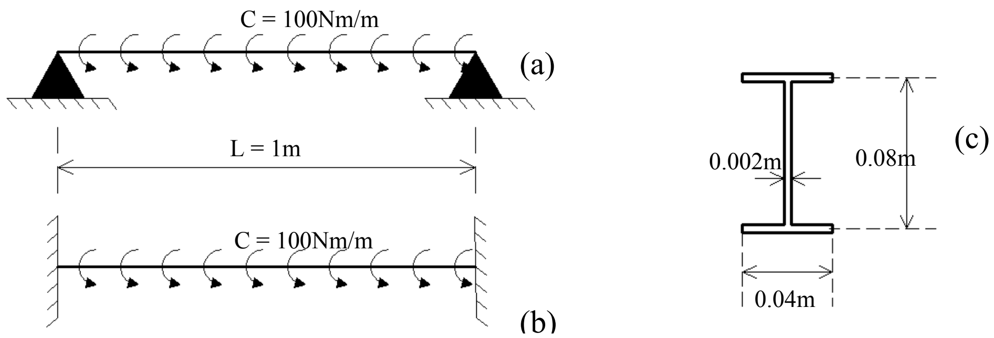

Figure 5.10 Simply supported beam submitted to a uniform density of torque

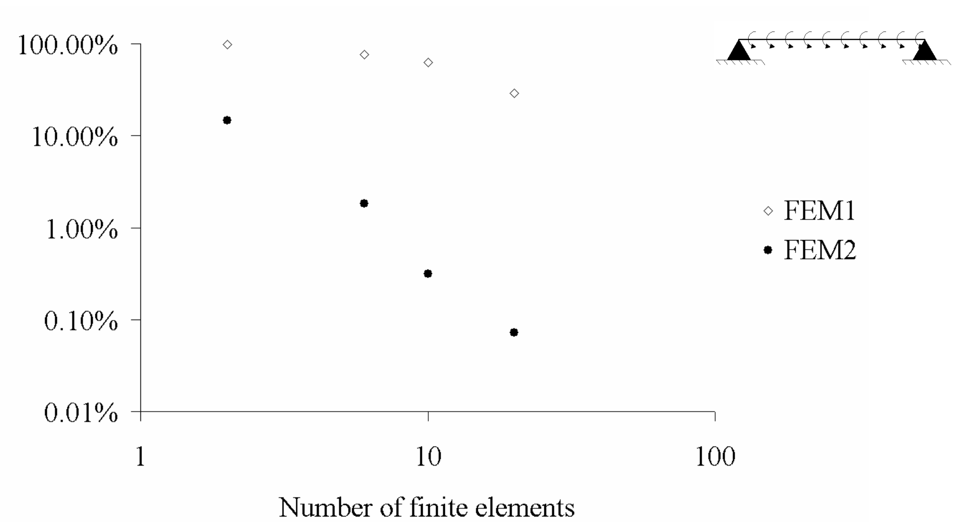

Figure 5.11 Relative difference between the values of mid span torsional rotation obtained by the theory of Vlassov and the finite elements FEM1 and FEM2

This is the case of mixed torsion (uniform + non uniform torsion) whose results must converge to those obtained with Vlassov theory. Figure 5.11 shows how the numerical solution converges to that of Vlassov when varying the number of finite elements. As expected, the result obtained by the theory

of Saint-Venant (θ_x=3,56 10^{-1} rad) is different from the solutions of Vlassov theory (θ_x=1,227 10^{-1} rad) and of finite element FEM2. In this example, the non uniform torsion governs a large part of the torsional problem and the distribution of the torsional angle along the beam longitudinal axis is exponential and not linear. The finite element 'FEM2' (quadratic interpolation functions) is shown (figure 5.11) to behave far better than 'FEM1' (linear interpolation function). Since 'FEM1' is not suitable for important non uniform torsional effects, 'FEM2' is used hereafter when analyzing the torsional behavior.
Now, the same beam is considered with warping restrained at the supports (5.10b) in order to show the influence of constrained warping. The results obtained with the finite element model 'FEM2' converge to the solution of Vlassov (figure 5.12). The difference between the finite element FEM2 and Vlassov is 3% for 10 beam elements. The variation with the solution of Saint Venant is even larger than in the previous case. This is quite logical since the theory of Saint Venant does not take into account the effects of non uniform warping, and these effects are stronger when the ends of the beam itself are prevented from warping. The value of maximal torsional angle with Saint Venant theory is the same as in the previous case (3.56 10^{-1} rad) and is almost ten times larger than Vlassov one (3.29 10^{-2} rad). The effects of non uniform warping on open cross sections (981% in this example) are really large compared with those of closed cross sections (0.25% in example 3).

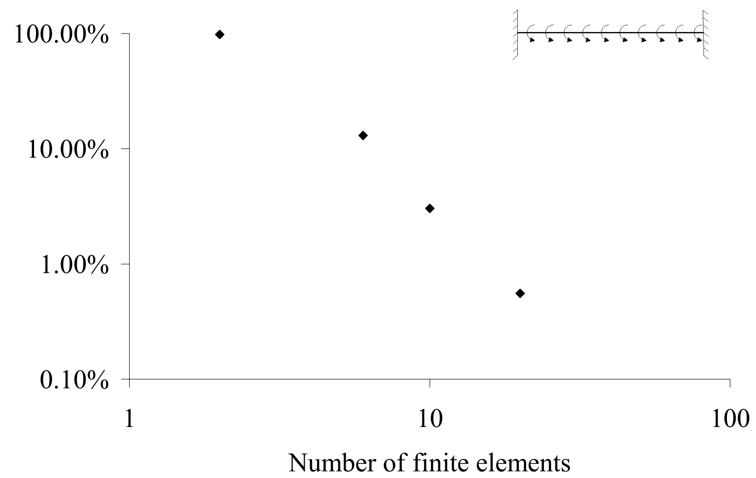

Figure 5.12 Relative difference between values of mid span rotating angle obtained by the theory of Vlassov and the finite element FEM2

Example 5: a channel cross section beam submitted to uniform transversal load
A beam with a channel cross section is submitted to a uniform transversal load (Fig. 5.13a). The torsional angle is prevented at the ends and the sections are free to warp. E = 210GPa, G = 80GPa.
Flexural analyses
Firstly, the uniform transversal load induces a bending in the plane of the load. The numerical solutions of both finite elements 'FEM1 and FEM2' developed in §5.2.1 and §5.2.2 respectively give the exact value of bending rotation at the supports (θ_z = 2.115 10^{-3}rad) regardless of the number of elements. The maximum deflection occurs at the middle of the beam. The analytical value of this deflection are obtained by using Bernoulli (without taking into account the shear effects) and modified Timoshenko (by taking into account a constant shear strain over the cross section) theories. The difference (5.175%) between these two theories measures the error induced by neglecting shear deformation effects on beam deflections. The finite element 'FEM1' that neglects shear bending effects gives with minimum discretization (two elements) the Bernoulli analytical value of maximal

deflection ($v = 2.64\ 10^{-3}$m). FEM2, based on Timoshenko theory with a selective numerical reduced integration with two Gauss points gives exactly [Jirousek 1983] Timoshenko value ($v = 2.78\ 10^{-3}$m). FEM1 and FEM2 give exact results for bending displacements regardless the number of finite elements.

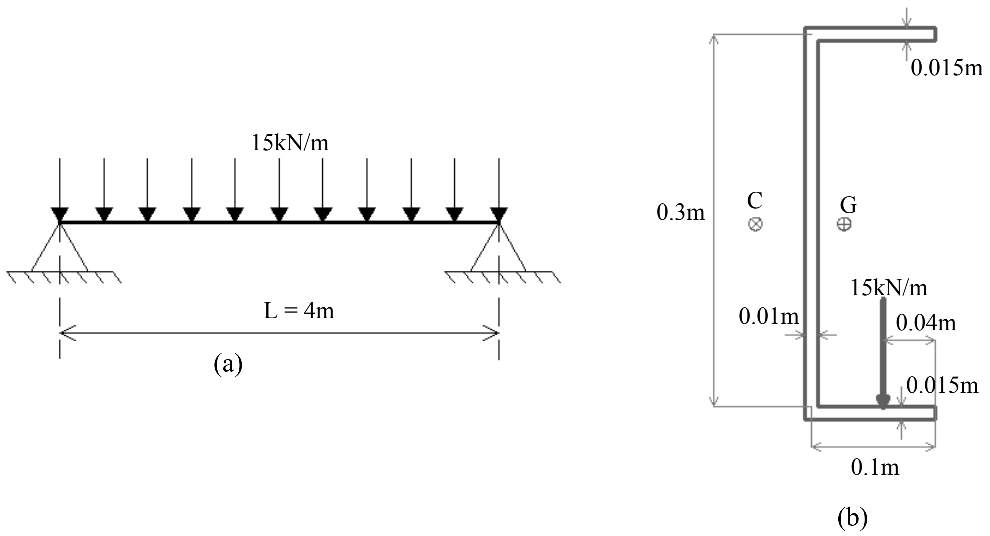

Figure 5.13 Channel beam submitted to non-uniform torsion

<u>Prescribing the location of the shear center for the torsional analyses</u>

Secondly, since the load is not applied at the shear center C (Fig. 5.13b), the beam is also submitted to torsion. For Vlassov theory, taken as the reference solution for this open profile, the distance between the centroid and the shear center is equal to 0.0625m. This value, computed from equations (3.21), is found to depend exclusively on the profile geometry. This is a consequence of Vlassov approximation (HYPV2, §2.2.3.1) stating that warping shear strains are assumed to vanish in the middle surface of a thin walled beam. With the finite element 'FEM2', this distance is found to be exactly the same in the case of uniform torsion (uniform torsional moment and free warping); this particular case satisfies the absence of warping shear stresses (as assumed by Vlassov).

If this location is prescribed within the present finite element analyses, the difference for the maximal torsional angle between FEM2 results (with 20 elements) and Vlassov analytical solution ($\theta_x = 7.7165\ 10^{-2}$rad) is 0.023%. It is interesting to note that computing analytically the maximal angle of torsion with Saint Venant theory and neglecting the non uniform torsion lead to a difference of 45.8%! The theory of Saint Venant is indeed not applicable here because the torsional moment is not constant and the warping is not uniform.

The distributions of normal stresses σ_x and contour warping shear stresses τ_{xs}^{ω} caused by the non uniform distribution of torsional moments are shown in figures 5.14b and 5.14c. Since Vlassov theory assumes zero warping shear stresses at the mid wall, the analytical calculation of warping shear stresses τ_{xs}^{ω} are computed from the equilibrium equations (equation 2.40') and yield a parabolic shaped distribution (Figure 5.14c). The numerical study (between parentheses) gives values of shear stresses for each small segment of the thin wall; the number of these transversal segments result from discretizing the contour by a finite number of nodes and segments (for results in figure 5.14c, 14 transversal segments are used). The variation of shear stresses along the thickness is linear and is given by Saint Venant shear stresses τ_{xs}^{s}. They are uniform along the contour (coordinate s), for a wall with constant thickness and vanish at the centerline. The variation of $\tau_{xs}{}^{s}$ through the thickness is given in Figure 5.14a.

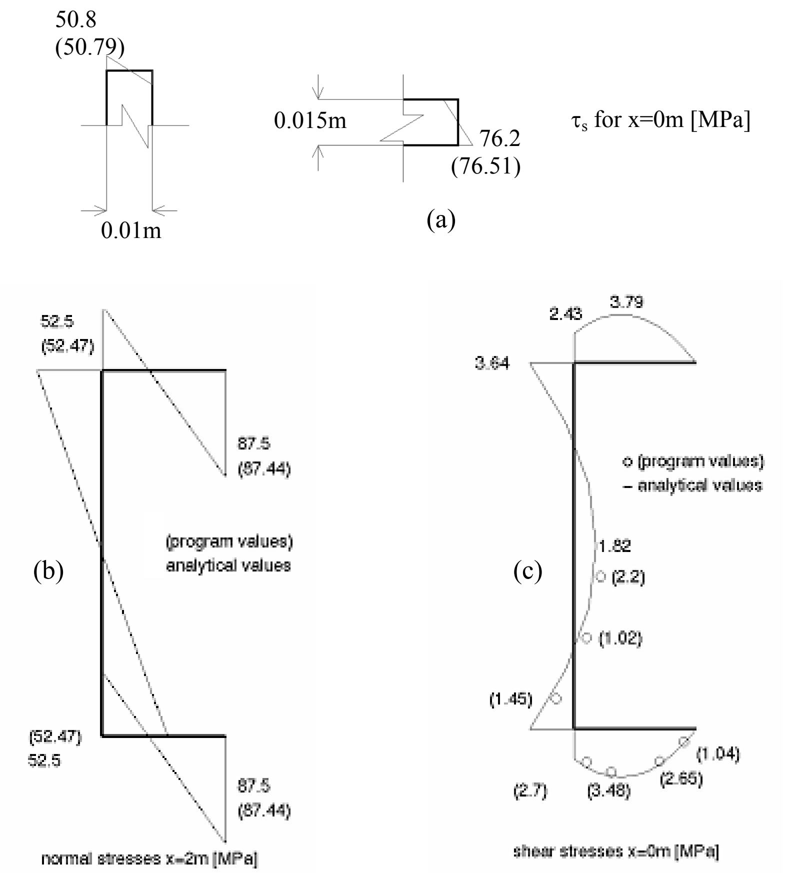

Figure 5.14 Normal and shear stresses due to non-uniform torsion for a channel beam

It is important to note that refining the kinematical discretization (increasing the number of the transversal nodes that describe the geometry of the profile) has a very small incidence on the torsional angle and normal stresses distributions. In this example, the difference between Vlassov solution for the maximal torsional angle and FEM2_18 (FEM2 computations with eighteen transversal segments) is 0.003% while the difference computed with minimum kinematical discretisation (FEM2_3; three transversal segments for the entire profile) is 0.023%.

Condensing the location of the shear center for the torsional analyses

If the coordinates of the torsional center are not prescribed but condensed according to equations (4.14) & (4.15), the values of the torsional angle and the distribution of the normal stresses do not change significantly. The difference between the two finite elements (prescribing and condensing the coordinates of the torsional center) is found to be 0.032% for the maximal rotating angle and 0.532% for the normal stresses at mid span. The location of the torsional center may be then computed as a function of the finite element solution (equations 4.14 and 4.15). The difference between Vlassov and FEM2 computations for the distance between the torsional center and centroid (e.g. curve FEM2_3 in figure 5.15a) is maximal at the ends of the beam since the ratio between the non uniform effects and the uniform torsional effects is largest for x = 0m. Indeed, the torsional moment may be considered as being the sum of two parts (equation 2.20): the uniform torsional part M_x^{st} and the non uniform torsional part M_x^{ω}. For this example, the ratio M_x^{ω} / M_x^{st} (0.77 at the beam ends and 0.35 for x = 1m) decreases when moving from one end to the midspan of the beam.

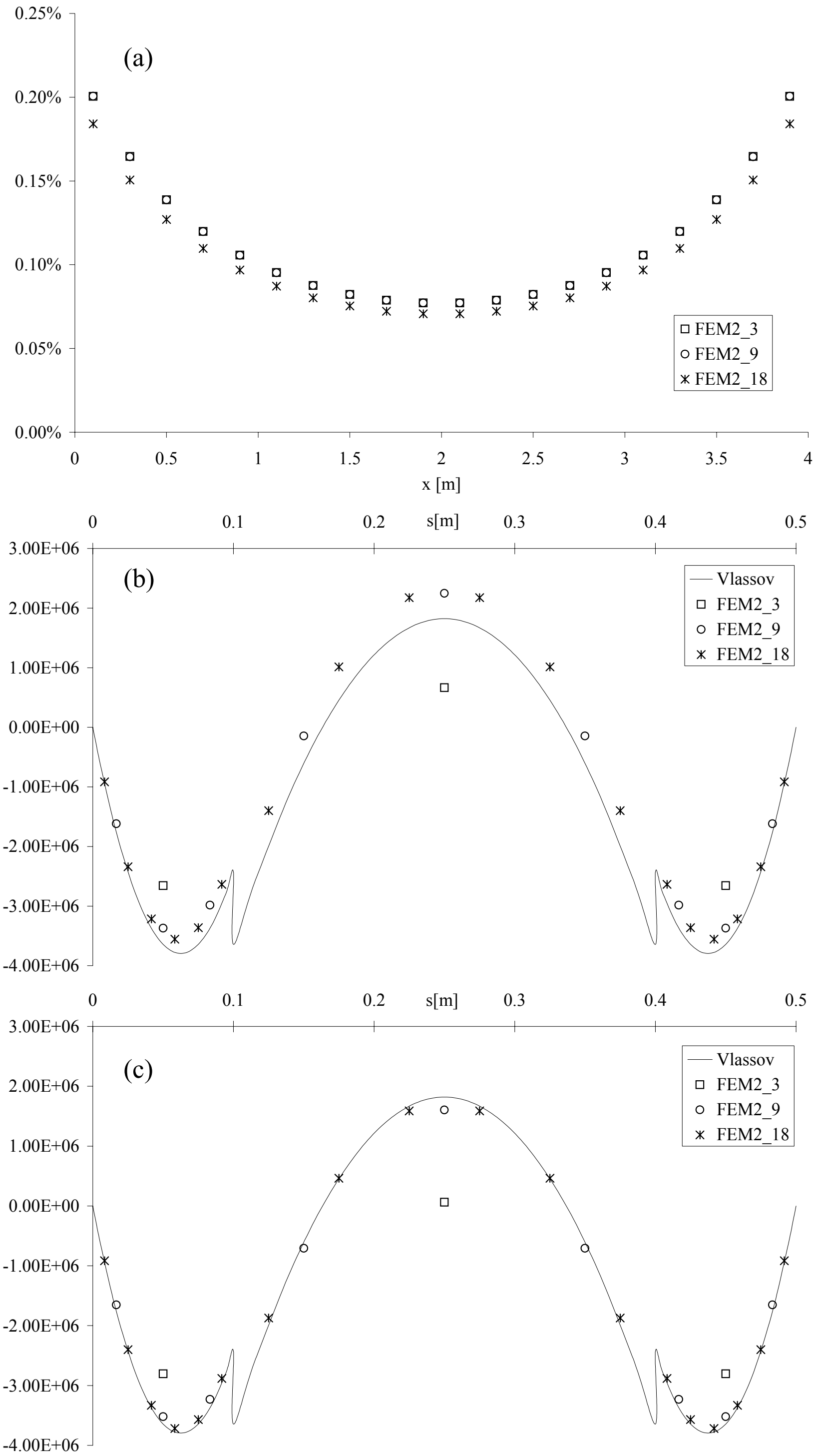

Figure 5.15 (a) Difference between Vlassov and FEM2 calculations for the distance between the centroid and the shear center, (b) warping shear stresses (x = 0m) at the mid wall when prescribing shear center coordinates, (c) warping shear stresses (x = 0m) at the mid wall when condensing the shear center coordinates

In figures 5.15b and 5.15c, the distributions of warping shear stresses at the left support of the beam are plotted against the contour coordinate (s) in both above cases: prescribing the location of the shear center as being that of Vlassov (or that of uniform torsion) and condensing the location of the shear center. These distributions are computed by using Hooke's law and the present kinematics. In the first case (figure 5.15b), shear warping stresses (3 transversal nodes and 4 nodes describe the geometry of the monosymmetrical profile for FEM2_3; 9 transversal nodes for FEM2_9 and 18 transversal nodes for FEM2_18) do not match exactly the analytical solution. The prescribed location of the shear center is not exact and gives, for these warping shear stresses, a vertical bending shear force. Figure 5.15c presents accurate computations of torsional warping shear stresses computed with the adequate location of shear center. This difference between the two cases is more marked in the case of an open asymmetrical profile where both coordinates of the shear center differ from those of the centroid. Hereafter, the location of the shear center is taken as being that of uniform torsion in order to compare the torsional rotation and longitudinal stresses to those computed with Vlassov theory. However, warping shear stresses will be computed by using the condensation technique.

Example 6: non uniform torsion for a beam with a closed cross section

A beam with a non-symmetric closed cross section (figure 5.16b) is submitted to a uniform distribution of torque (figure 5.16a). E = 206GPa, G = 82.4GPa, t_0 = 0.01m. The torsional angle is prevented at the ends and the sections are free to warp. As in the previous example, the beam is submitted to non uniform torsion.

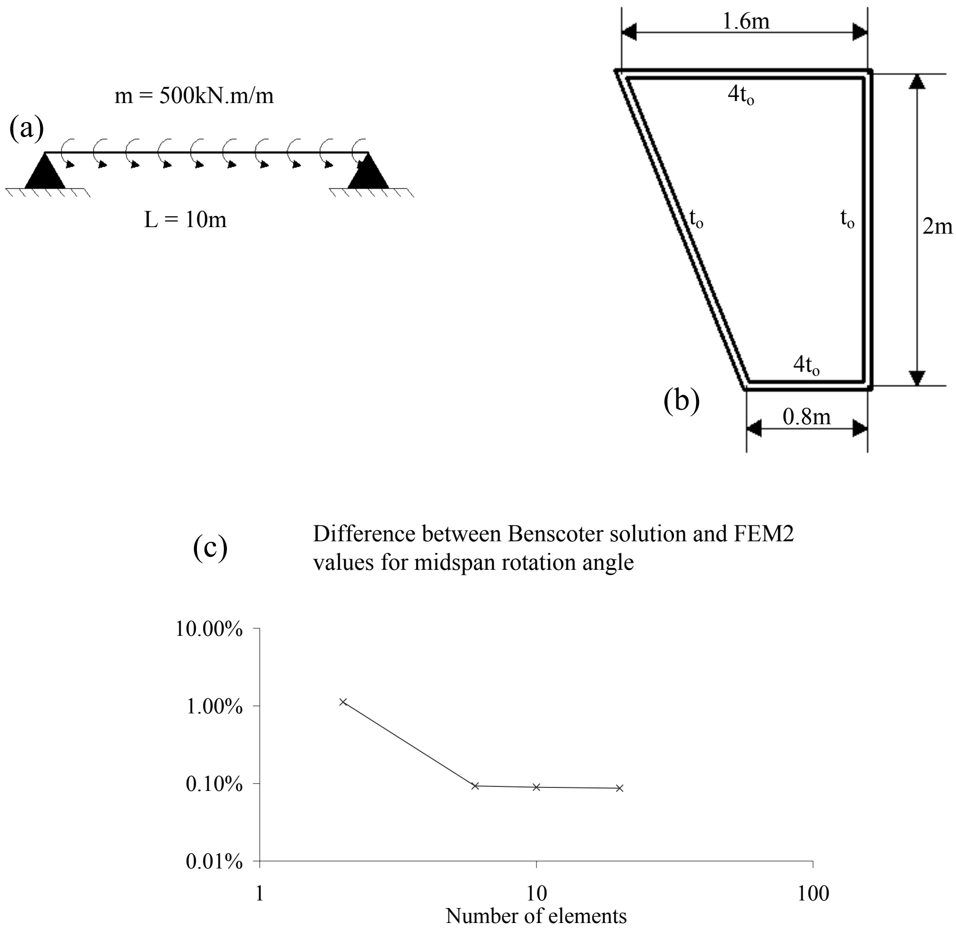

Figure 5.16 Maximum torsional rotation angle in case of non uniform torsion for a closed cross section

The difference for the maximum torsional rotation angle between the finite element analysis 'FEM2' and the analytical solution based on Benscoter theory (θ_x = 0.153 10^{-2}rad) is shown in Figure 5.16c for various descritizations. The error obtained by using Saint Venant theory for the torsional angle is

2.6%. As expected (discussed in paragraph 2.2), the effects of non uniform torsion are more important for an open (47.79%, example 5) than for a closed cross section.
Figure 5.17 shows normal and shear stresses caused by non uniform torsion. Shear stresses flow through the periphery of the cross section. The analytical study gives a parabolic shaped distribution of these contour shear stresses by considering an equilibrium equation (equation 2.55) in Benscoter theory. The numerical study gives constant values for shear stresses at transversal segments, obtained directly from the kinematics by using Hooke's law by discretizing the contour by a finite number of nodes and segments (for results in figure 5.17c, 13 transversal segment are used). All the previous computations are ensured by prescribing the location of the shear center as being that of uniform torsion (as in Benscoter theory).

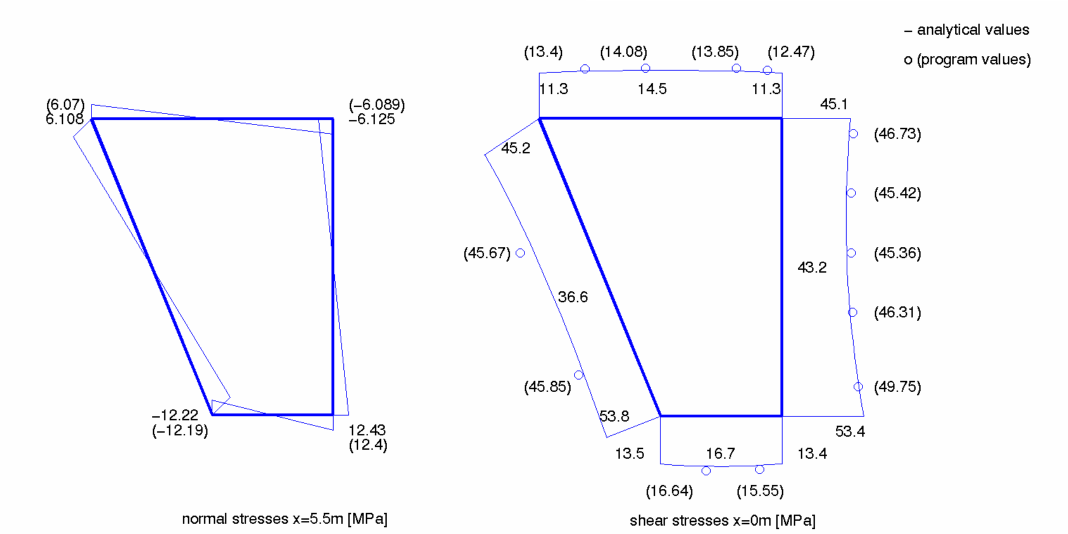

Figure 5.17 Normal and shear stresses in case of non uniform torsion for a closed cross section beam

Example 7: non uniform torsion of continuous beam with three spans
A continuous beam with three spans is analyzed in order to compare the proposed finite element solution with another finite element solution based on the theory of Vlassov [Batoz, 1990, page 211].

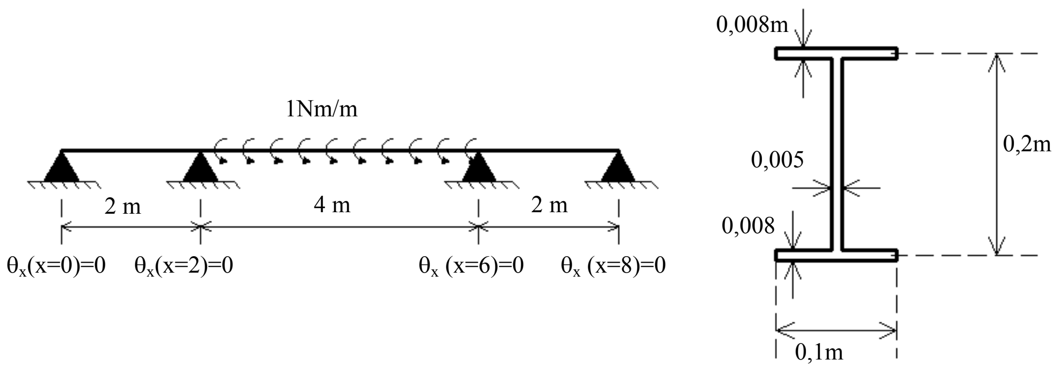

Figure 5.18: Continuous beam with three spans submitted to a uniform density of torque at central span

The beam geometry and loading are shown in figure 5.18. The beam is simply supported at its four supports (where the torsional angle is prevented, and the end sections are free to warp). The central span is submitted to a uniform density of torque. The beam has an open I cross section. G=77GPa; E=200GPa.

Figure 5.19 gives the distribution of rotating angle and bimoment along the left half of the beam. For the finite element solution with Prokić kinematic formulation, the bimoment is calculated from the forces f_i associated with the warping degrees of freedom which are the warping longitudinal displacements of the transversal nodes. Results obtained with FEM2 based on Prokić kinematic formulation and with the finite element based on Vlassov theory match precisely. It is again shown that the maximal rotating angle (θ_x=2,6 10^{-4} rad pour x=4m) would be very poorly estimated by de Saint Venant theory where θ_x = 6,12 10^{-4}rad (the difference is 136%).

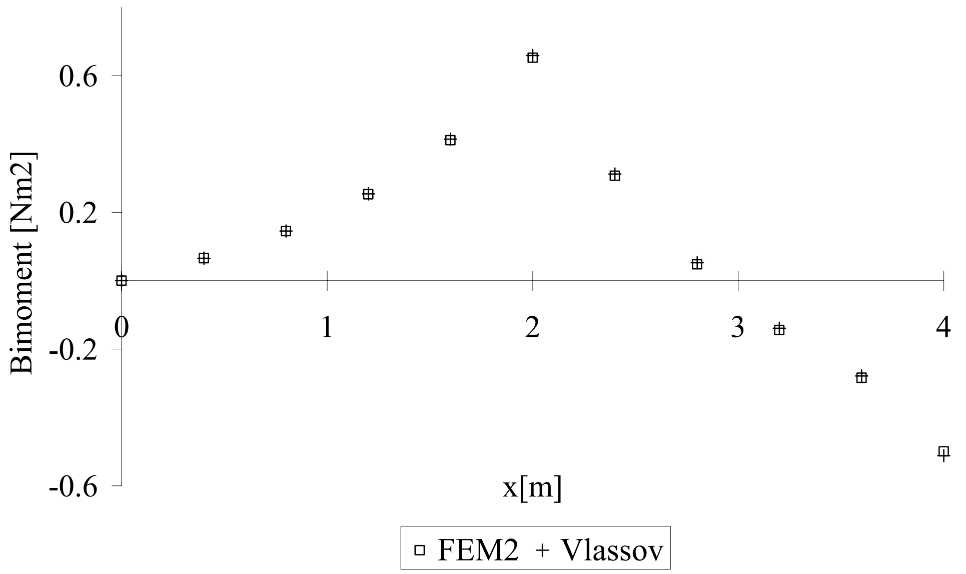

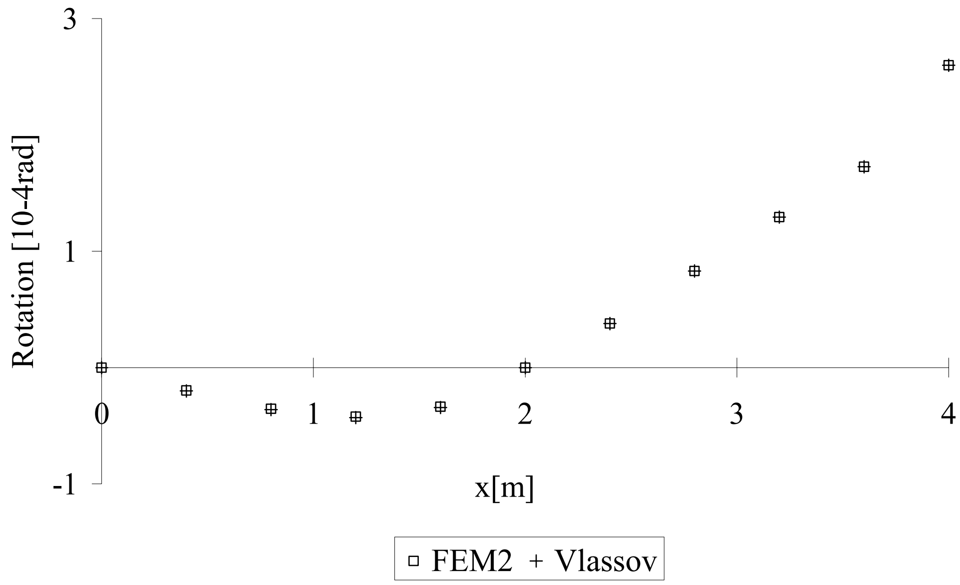

Figure 5.19: Distributions of rotating angle and bimoment along the beam in figure 5.18

Example 8: warping of an I beam due to a single axial load P

This example illustrates a particular case in which thin walled structures exhibit a torsional behavior in the absence of applied torsional torques. A load P = 100kN parallel to the longitudinal axis acts at one corner at the right end of the beam (L = 10m) in figure 5.20. At both ends, the torsional angle is prevented and the end sections are free to warp.

It is well known that three cases of loading (figure 5.21a,b,c) are induced in this case involving an axial force and two bending moments about the y and the z axes. These internal loads are easily deduced from the applied load by using simple equilibrium equations (longitudinal force equilibrium and moment equilibrium around the transversal axes). The moment equilibrium around the longitudinal axis gives zero torsional moment. This set of loads is in a general Strength of Materials type of analysis sufficient to describe the behavior of the part of the beam some distance away from the surface loading. However, in this loading case, thin walled structures have a complex behavior and additional stresses, resulting from other effects, do not attenuate as quickly along the length of the beam as in beams with solid cross sections. When the cross section is an assembly of different thin rectangles, the cross section does not remain plane but warps [Murray 1986, page 6].

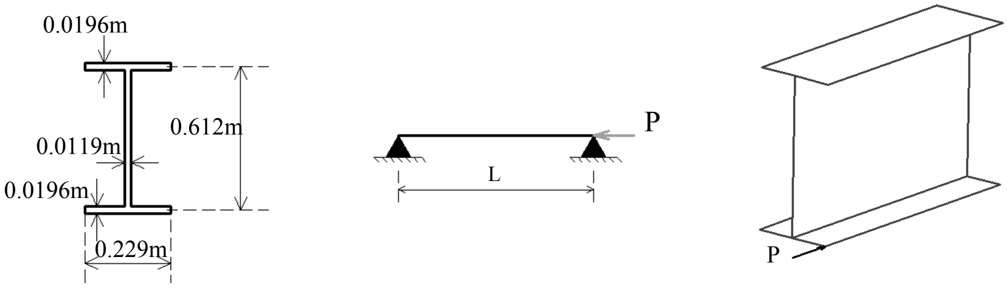

Figure 5.20 An I beam submitted to an eccentric single axial load

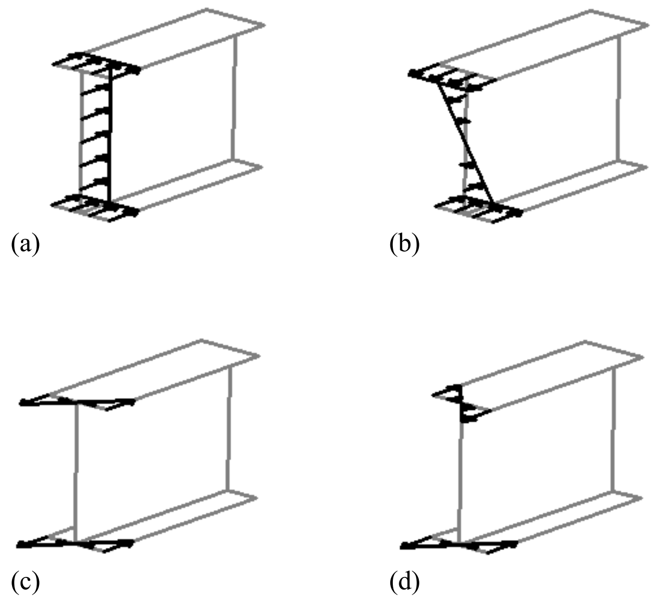

Figure 5.21 Longitudinal stresses corresponding to four sets of loading resulting from a single load applied in 5.20; a: compression, b &c: bending, d: torsional warping

A fourth set of stress distributions is hereby considered (figure 5.21d). The corresponding load is the torsional bimoment that is associated with the cross section warping. A twisting occurs along the longitudinal axis even in absence of applied torsional torques and a torsional moment appears when the bimoment varies along the length of the beam (equation 2.38 for Vlassov theory and equation 4.18 for the present analyses). The analogy between the flexure and the torsion presented in paragraph 2.2.3 can be used to clearly illustrate this phenomenon. If a simply supported beam is submitted to a flexural couple at one end, the bending moment distribution is linear and the shear force distribution is uniform

over the length inducing transversal stresses. Even if there are no applied forces, the couple induces a reaction force at each end of the simply supported beam in order to ensure equilibrium.
For the loading given in figure 5.20, analytical computations are developed by using Vlassov warping function in order to qualify the present finite element results. The different analytical and numerical values of rotating angle at mid length and of warping at the left support of the beam are compared in table 5.2. The value of the constant torsional moment along the beam has been found to be exact for all the calculations (M_x = 1401.48Nm). The distribution of the torsional rotation along the beam is given in figure 5.22.

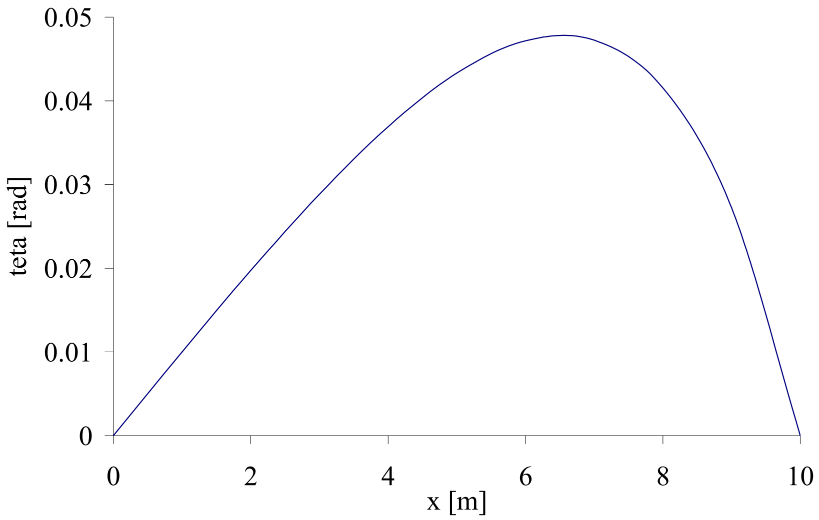

Figure 5.22 Diagram of torsional rotation [rad] along the longitudinal beam in figure 5.20

Table 5.2 Rotating angle [rad] and warping [m] along the longitudinal beam in Figure 5.20

	Analytical	FEM, 1elt	FEM, 2elts	FEM, 10elts	FEM, 20elts
twist at mid length	4.3282E-02	5.0588E-02	5.0588E-02	4.3487E-02	4.3333E-02
warping at left end	3.5198E-04	7.0951E-04	3.9734E-04	3.5398E-04	3.5248E-04

Axial stresses are maximal at the right end of the beam where the load is applied (on the right lower part of the cross section: -181.94MPa). They are induced by an axial load (N), bending moments (M_y and M_z) and a torsional bimoment (B) as follows: from N : 3.38%; from M_y : 18.33%; from M_z : 4.82% and from B : 73.47%. Warping normal stresses are shown to be larger than bending stresses and cannot be ignored.

Example 9: influence of warping boundary conditions

This example analyses the effect of warping restraint on the torsional behavior of a simple beam submitted to a torque (Figure 5.23). The supports are taken to be either free to warp or partially or completely prevented from warping. The beam is divided into sixteen identical finite elements. E = 200GPa and G = 80GPa. Seven types of warping conditions are considered:
- fully restrained warping at both ends; (Case I, figure 5.23b).
- partially restrained cross sections at both ends (➊➋ is restrained); (Case II),
- partially restrained cross sections at both ends (➋➌ is restrained); (Case III),
- free warping at left end and totally restrained warping at right end; (Case IV),
- partially restrained cross sections at both ends (➌➍ is restrained); (Case V),
- free at left end and partially restrained (➌➍ is restrained) at right end; (Case VI),

- free warping for both ends; (Case VII).

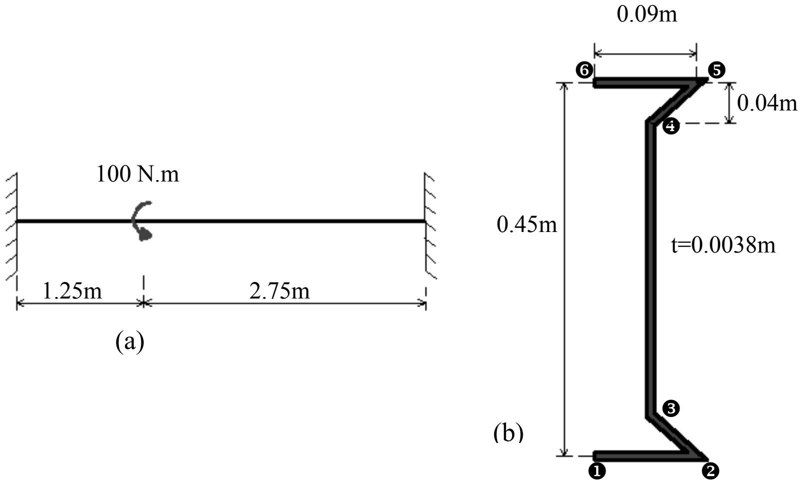

Figure 5.23 A Beam submitted to torsion

Table 5.3 Rotating angle [rad] at 1.75m from left end for different types of warping conditions

restrained	partial 12	partial 23	indep_restr.	partial 34	indep_partial	indep
0.00314482	0.00315434	0.00316903	0.00708769	0.01188824	0.01255013	0.01255013

Figure 5.24 gives the distribution of rotation angle along the beam and table 5.3 gives the value of the rotation angle at 1.75m from left end. For the first and last cases, the rotating angle and the bimoment distributions obtained from the present warping function are in excellent agreement with analytical values obtained with Vlassov warping function. It is expected to find that the torsional angle is maximal in case of free warping and minimal in case of totally restrained warping. The solutions for partially restrained warping are between these two extremes. The decreasing value of torsional angle depends on the amount of restrained warping. By taking the free warping case as a reference, the torsional angle decreases of 5.27%, 74.75% and 74.87% if respectively ❸❹, ❷❸ and ❶❷ are restrained. This is related to the fact that the warping is more important on segment ❶❷ than on ❸❹. It could be concluded that in such structures, warping resistance is important. The torsional stiffness is significantly increased when cross sections are fully or partially restrained against warping.

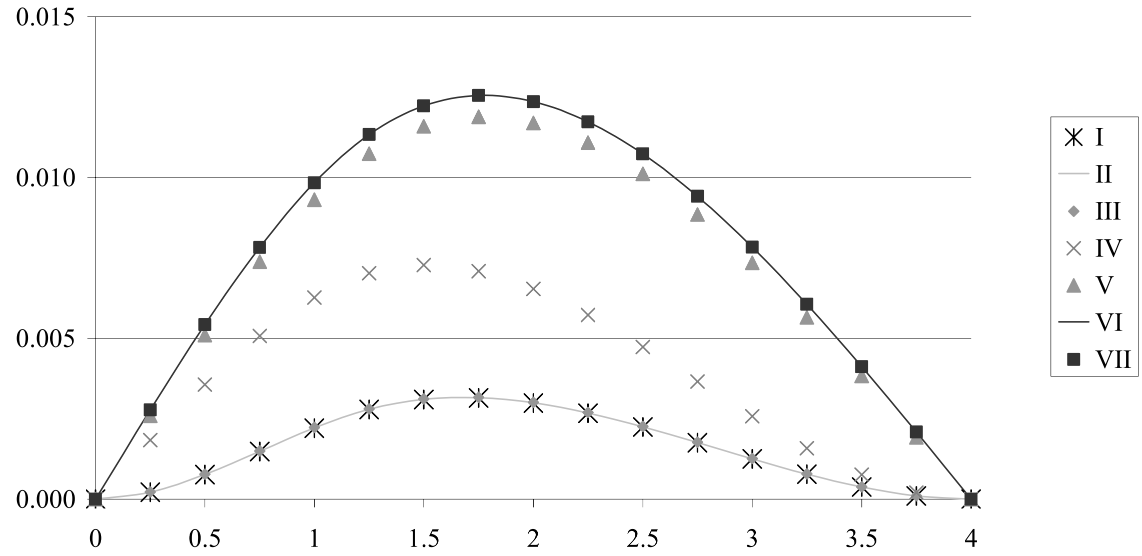

Figure 5.24 distribution of rotating angle [rad] along the beam for different types of warping conditions at supports

5.2.7 Applications involving connections

Two examples are presented in order to analyze the linear behavior of structures combining beams with different thin-walled cross-sections and to investigate the influence of the torsional warping transmission on the overall behavior. The numerical results are compared with other results obtained by using shell finite element analyses.

Example 1 Transmission of torsional warping through a connection in a frame
This example illustrates the influence of the joint description on the behavior of a frame.

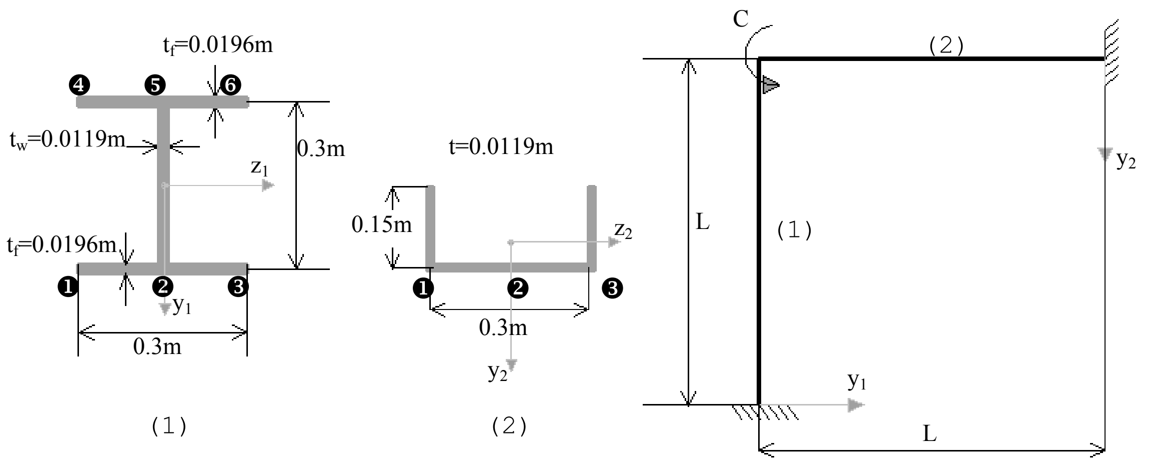

Figure 5.25 Portal frame geometry with H (1) and U (2) cross sections

The frame consists of a vertical column (1) with a H-section connected to a horizontal beam (2) with a U-section (Figure 5.25). A torque C acts along the longitudinal axis of the beam (2). The two supports are clamped but keep the warping free: 6 degrees of freedom (u, v, w, θ_x, θ_y, θ_z) are set equal to zero. The torsional rotation is calculated at the connection by assuming different warping transmission modes at the corner of the frame. E = 200GPa, G = 80GPa, L = 10m.

If the connection at the corner allows the complete transmission of forces and moments, the value of the maximal rotating angle obtained by a beam finite element using Vlassov warping function (Batoz, 1990, page 211) is 0.028024 rad for C = 100kNm. The difference between this result and the results of the beam element 'FEM2' by assuming that warping is continuous as shown in Figure 5.26.

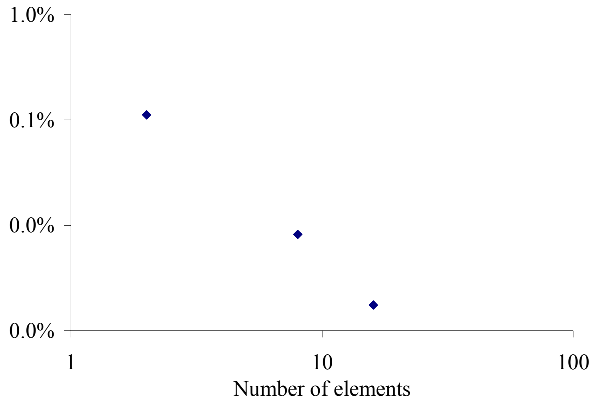

Figure 5.26 Difference with Vlassov finite element solution for the torsional rotation at the connection and FEM2

Table 5.4 gives the results of the analysis with 'FEM2' by assuming different transmission modes of warping:
-independent warping for both profiles,
-warping transmitted along one transversal node: ❶ for H profile (beam 1) section and ❶ for U profile (beam 2)
-warping transmitted at a common segment: ❶❷❸ for H profile (beam 1) section and ❶❷❸ for U profile (beam 2)
-restrained warping for both profiles.
The influence of the transmission of warping varies within a range of 0.37%.

Table 5.4 Rotating angle at the rigid joint

transmission of warping	[rad]
independant warping	0.0279448
partial (1common point)	0.0279243
partial (1common segment)	0.0279239
restrained warping	0.0279223

If the joint at the corner is a simple hinge allowing independent rotations for the connected members with independent warping, the horizontal U beam is then submitted to a uniform torsion. Finite element analyses with the present warping function 'FEM2' and with Vlassov warping function (Batoz, 1990, page 211) give the same results for the case of independent warping of the U beam and the H column (for C = 1kNm, θ_x = 0.078125rad) and the numerical solutions do not depend on the number of elements. When the transmission of warping changes, the rotating angle varies within a range of 9.9%; when warping is restrained, $\theta_x = 0.07108$rad.

Example 2: Assembly of beam elements

The second example, already solved in the literature (Gunnlaugsson & Pedersen 1982, Pedersen 1991), illustrates an application involving the assembly of beam elements with different cross sections within a simple beam structure. A simply supported beam (L = 2.4m) is divided in three prismatic thin walled beam elements. The two end elements have a tubular thin cross section and the connecting element has an open U shaped cross-section. The wall thickness is constant and equal to 0.003m. The beam is loaded by torques at its ends C = 1kNm (Figure 5.27). E=210 MPa, ν =0.3.

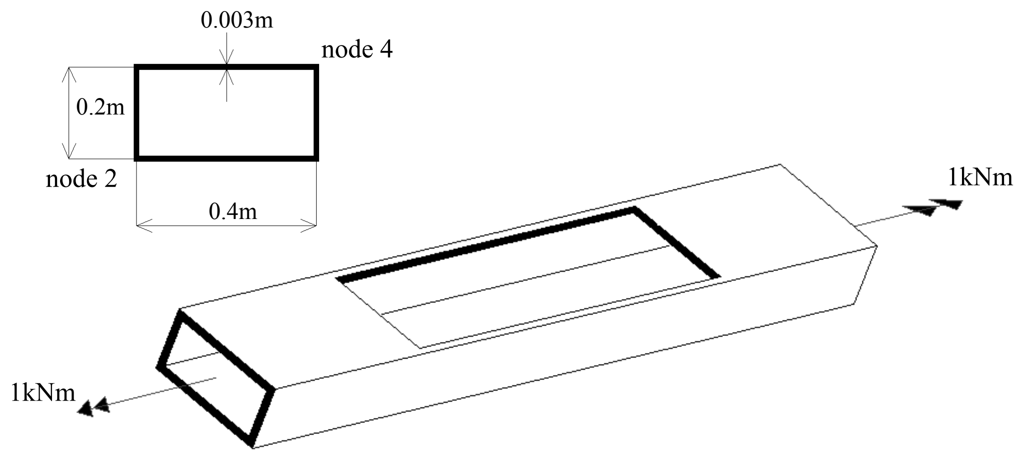

Figure 5.27 Box girder with large opening submitted to torsion

Gunnlaugsson (1982) and Pedersen (1991) have computed the variation of the rotating angle along the beam. The values of the rotating angle and the warping axial stresses of Gunnlaugsson beam element are shown by the continuous line (curves a) in Figure 5.28.

He compared his results with those of a plane stress finite element model (curves c). He also used a beam model assembled in such a way that the warping function is continuous (curves b) (Fig. 5.28).

The finite element 'FEM2' is used with sixteen beam elements. Two superposed finite element nodes are taken at each intersection where the cross section geometry changes abruptly in order to capture the discontinuity of the warping function. FEM2 results are not influenced significantly by the choice of the connection point at the contour (for the maximal rotation angle, the difference is 0.0001% if the cross sections are assembled by node 2 or node 4). For the results in figures 5.29 and 5.30, the connection point is taken at node 2. The torsional angle distribution is represented by the triangles in Figure 5.29 along the right half of the beam. FEM2 results are compared with the results given by Pedersen (1991). The variation of the rotating angle along the beam is much larger in the open part than in the closed part of the beam. The present finite element solution with transmission of warping matches the results of the analysis with the plane stress finite element model performed by Pedersen. The variations given by the elements of Gunnlaugsson (curve a, Figure 5.28) and Pedersen (Figure 5.29) are slightly lower. The torsional rotation calculated by a beam theory neglecting the discontinuity of the warping function is much larger (curve b, Figure 5.28). When warping is restrained at the connection, the torsional rotation is smaller: the solution is given by the diamond shaped points in Figure 5.29.

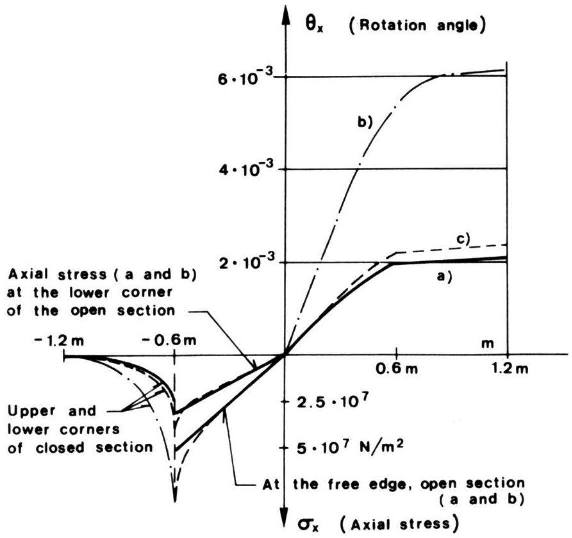

__ two beam elements (curve a)
-¨-¨- beams assembled in such a way that the warping function is continuous (curve b)
- - - plane stress finite element model (720 elts) (curve c)

Figure 5.28 Results from Gunnlaugsson (1982)

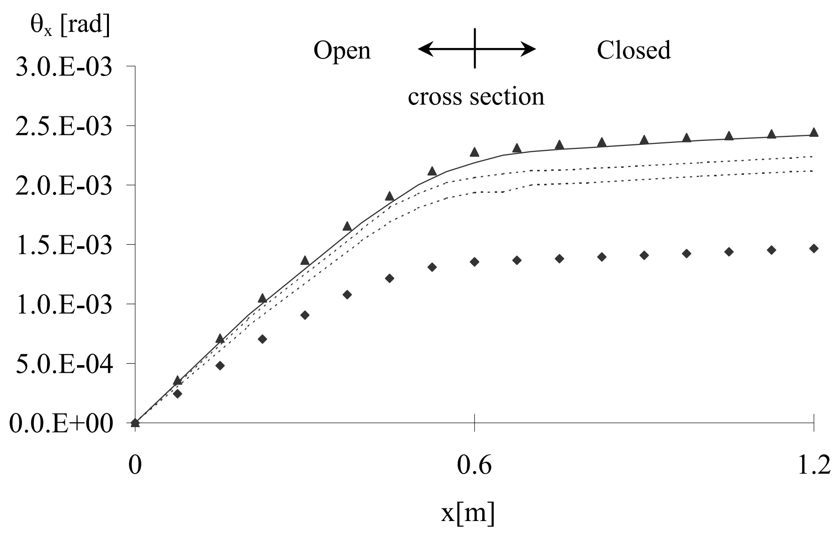

__ FEM2 solution with 16 beam elements, warping restrained at the connection
▲▲▲▲ FEM2 solution with 16 beam elements, warping transmitted
----- Pedersen 1991 two beam finite elements
___ Plane stress finite element (Pedersen 1991)

Figure 5.29 Comparison of the rotation angle along the girder by using 'FEM2' (16 beam elements) and the results of Pedersen (1991)

The normal stresses result from the resistance of the cross sections to the non uniform warping. The distribution found by the present finite element analysis (given in Figure 5.30) matches the distribution calculated by Gunnlaugsson (Figure 5.28, curve c). At the connection between the open and the closed cross sections (x = 0.6m), the plane stress finite element gives the local stress concentration. The beam theory gives a discontinuity in the distribution of the normal stresses since the hypothesis of Saint Venant is no longer verified. This inaccuracy that occurs at most junctions because of the overlap of the cross sectional areas has a small effect and can be disregarded. Anywhere else, the stresses given by 'FEM2' are closer to the plane stress finite element solution than to Gunnlaugsson beam solution whose model is stiffer. However, the response given by the beam finite element model that does not take into account the warping function discontinuity at the connection is that of a more flexible structure.

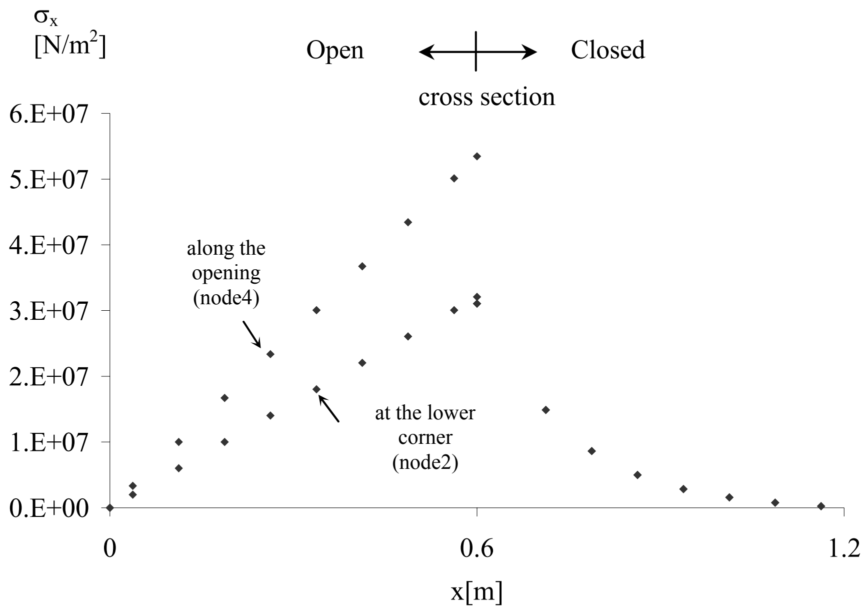

Figure 5.30 Values of axial stresses due to non uniform warping along the girder by using 'FEM2' with 16 beam elements

5.3 Finite element with shear bending warping

5.3.1 Displacement field

In order to develop numerical methods for accurate shear bending results within the objectives fixed in paragraphs 3.3 and 4.3, another beam element 'FEM3' is presented in this paragraph. The kinematics is adapted by relating $\sum\Omega^i u_i$ to the warping due to bending shear forces. Prokić warping function is represented by a contour (or first order) warping assumed to vary linearly along each polygonal segment of the contour. This new approach presents the advantage of automatic data generation and unified geometric characteristic computations regardless the type of the cross section (closed, open, asymmetric…). For simplicity, the developments in this paragraph deal with bending in (xz) axis. Similar analyses are done for (xy) axis but are not presented hereby. Tension/compression and torsion are not taken into account since they are analyzed in previous paragraphs. The efforts required to solve a general problem by taking into account not only torsional but also bending warping shear effects are not justified –in our opinion– because the accuracy gained in practical problems is not so high. However, for the finite element 'FEM2' in particular and for Timoshenko beam theory in general, the transverse shear strain is assumed to be constant through a beam cross section and a corrective modification has to be introduced in order to calculate the displacements and stresses resulting from a flexural loading. The present developments will be mainly used in this study in order to determine the shear correction factor for arbitrary profiles. As stated in §2.1.2, the shear correction factor is mostly evaluated in the literature by an energetical approach. It is a function of the distribution of the first moment over the area of the cross section. Evaluating the first moment is not always simple since it depends on the profile geometry and specifically different methods are required for open and closed thin-walled profiles.

The displacement field, introduced in (3.23) in order to accommodate the warping of the cross section without the need of a corrective factor, describes the displacement vector at any point q within the cross section (§3.3):

$$\begin{Bmatrix} u_q \\ v_q \\ w_q \end{Bmatrix} = \begin{Bmatrix} z\theta_y + \sum_{i=1}^{n} \Omega^i(y,z)u_i(x) \\ 0 \\ w \end{Bmatrix} \tag{5.66}$$

5.3.2 Finite element definition

As in paragraph (5.2.1), the interpolation functions are taken quadratic for the transversal displacement (w) and the rotation (θ_y) and linear for the warping longitudinal displacements (u_j).

$$\langle N \rangle^T = \begin{Bmatrix} 1-3\xi \ +2\xi^2 \\ 4\xi(1-\xi) \\ -\xi(1-2\xi) \end{Bmatrix} \ ; \ \langle N_u \rangle^T = \begin{Bmatrix} 1-\xi \\ \xi \end{Bmatrix} \ \text{with} \ \xi = \frac{x}{L} \tag{5.67}$$

The displacements ($w,\theta_y,u_i,\ldots$) can be related to the nodal displacements by using the interpolation functions as follows:

$w = \langle N \rangle \{q_w\}$

$\theta_y = \langle N \rangle \{q_{\theta y}\}$

$u_i = \langle N_u \rangle \{q_{ui}\}$; i=1,2,…n (5.68)

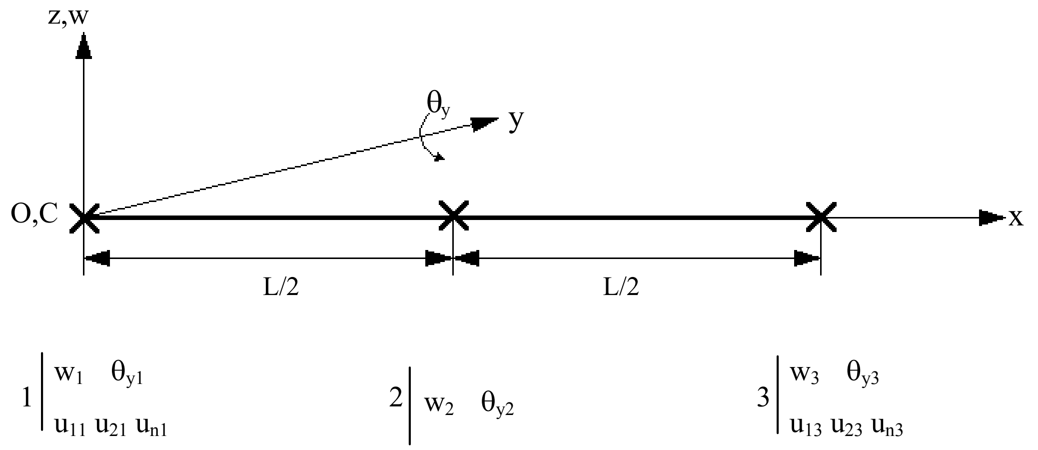

Figure 5.31 Finite element with (xz) bending shear warping effects

5.3.3 Stiffness matrix and additional equations

The finite element calculations are derived in the same usual manner as in the previous paragraphs (e.g. §5.2.2). It is important to note that the problem is not well defined without the orthogonality relationships (5.69) and the non zero shear boundary conditions (5.70). These additional equilibrium equations are given by equations (4.22):

$$\sum_{i=1}^{n} S_{\Omega^i} u_i = 0$$
$$\sum_{i=1}^{n} S_{\Omega^i,y} u_i = 0$$
$$\sum_{i=1}^{n} I_{y\Omega^i} u_i = 0 \qquad (5.69)$$

u_e-u_d=0, where e is an edge node and d is the adjacent one. (5.70)

Similarly to the torsional warping, if the additional constraints (5.69) are satisfied, the bending warping (xz)/tension-compression coupled terms and the bending warping (xz)/bending (xy) coupled terms vanish in the calculation of internal forces and stiffness matrix terms. The warping degrees of freedom associated with (xz) bending do not induce normal forces, shear forces (Ty) or bending moments (Mz). Inversely, the tension-compression and (xy) bending generalized forces should not derive from the terms u_i. This eliminates the symmetrical coupled terms in the stiffness matrix. The non zero terms of k^{el} obtained after this elimination are given in appendix A5.

Equations (5.69) have been again used in order to relate the degrees of freedom 'u_i' and to restrain these general parameters to the bending shear warping (xz). Depending on the profile geometry (more precisely the number of edges in an open profile), additional relations are written in the form of equation 5.41 and are added to the initial equilibrium system written in the form given in appendix A5. The resulting set of equilibrium equations is solved by using the Lagrange multipliers (equation 5.42).

The development of the present beam finite element is based on the displacement field for which the constant shear strain hypothesis is relaxed. Numerical examples (§5.3.4) are analyzed in order to show that:

- the shear locking phenomenon, induced by the inconsistency of the straightness hypothesis does not occur in this ‘FEM3’ finite element;
- ‘FEM3’ gives accurate results when analyzing shear warping bending effects on arbitrary profiles.

Since the modified Timoshenko model (including shear correction factor) gives accurate results when computing the deformation of a thin walled structure submitted to bending, it is then concluded that combining torsional warping (FEM3) and shear bending warping (FEM2) effects for a 3D thin-walled structural analysis is not justified. The number (6+2n) of degrees of freedom per node increases significantly the computational costs while Timoshenko modified model gives accurate transverse displacement results. The present developments are thus suitable for inclusion as a ‘black box’ in the finite element code ‘FEM2’ in order to accurately and automatically determinate the shear correction factor for arbitrary profiles. The analysis of a 3D structure containing multi-shaped open and closed profiles, achieved by using modified Timoshenko model ‘FEM2’ and torsional warping effects (paragraph 5.2.2), will begin by a separate routine that determines the shear correction factor:
A simply supported beam is submitted to a uniformly distributed force. The maximal deflection is computed by using ‘FEM3’. The analytical value of this maximal deflection is taken from the modified Timoshenko model (eq 2.13), where the shear correction factor k is the unknown. Equating these two solutions allows the determination of the shear correction factor.
Finally, it is important to note that the shear stresses computations resulting from ‘FEM3’ consist in a variable distribution of stresses over the profile contour (one value for each transversal segment) while ‘FEM2’ gives one approximate value (one for the entire profile).

5.3.4 Applications on bending shear warping

In this paragraph, applications aim mainly at validating the finite element ‘FEM3’ which includes shear bending warping effects. Comparisons are done with Euler Bernoulli beam theory and Timoshenko beam theory to demonstrate the ability of the theory to enhance available solutions provided by existing beam theories when the aspect ratio of the beam varies.
The different results are:
- analytical results with Bernoulli beam theory ‘BBT’ which is based on the normality assumption and neglects shear bending effects;
- analytical results based on Timoshenko beam theory ‘TBT’ which is based on the planar assumption and considers a constant shear strain state without the shear correction factor (or, more exactly, with the shear correction factor set to unity);
- analytical results based on the Modified Timoshenko beam theory ‘TBTM’ taking into account the shear correction factor [§2.1.2]; this model is considered to be the reference for all the other theories while computing differences in Figures 5.32, 5.33, 5.34 and 5.35 and table 5.6. The difference is calculated as follows:

$$\%\text{difference} = \frac{\text{Value}_{\text{TBTM}} - \text{Value}_{\text{theory}}}{\text{Value}_{\text{TBTM}}} \tag{5.71}$$

- finite element results ‘FEM1’ based on Bernoulli kinematic formula (BBT) and developed in paragraph 5.2.1. The stiffness matrix is given in Appendix 2.
- finite element results ‘FEM2’ based on Timoshenko beam kinematics shown in paragraph 5.2.2 with quadratic interpolations for the displacement w and the rotation θ_y and a selective reduced integration. The stiffness matrix is given in Appendix 3.

- finite element results 'FEM3' (paragraph 5.3) which takes into account the shear bending warping of the cross section by considering a linear interpolation of (nn) additional degrees of freedom (Appendix 5). Two discretizations are required for 'FEM3': the usual finite element discretization and in addition, a kinematic discretization. The kinematic formulation uses linear functions Ω_i associated to the nn degrees of freedom u_i which are related to the transversal nodes of the discretized cross section. The thin profile is divided into a finite number of transversal segments which represent polygonal parts connected by transversal nodes. An edge transversal node in an open cross section is connected to only one transversal segment (e.g. in a T section, there are three edge nodes while in Figure 5.36a, nodes 1 & 6 are the only edge nodes). The warping of the cross section is approximated by linear variations along the transversal segments. The inaccuracy induced by this approximation is maximal for the minimum discretization required to describe the geometry of the profile and is reduced for refined discretizations. With increasing transversal nodes and segments, the linear warping between adjacent transversal nodes approaches the exact distribution of warping in order to insure the convergence of the kinematic approach and to give accurate results. Higher order functions Ω_i may be used to formulate exactly the problem with minimum discretization. For the elastic isotropic cross sections studied in this work, this approach is not considered.

In addition, other displacement-based finite elements are considered in order to evaluate in some cases the locking phenomenon and to detect whether the behavior of FEM2 becomes poor (an overview of displacement finite element models of shear deformation beam theories is presented in [Reddy, 1997]):
- TLE is based on modified Timoshenko kinematic formula (TBTM) with linear interpolation and presents locking shear phenomenon (Appendix 6). The stiffness matrix and the force vector are given in (5.72) and (5.73) [Batoz, 1990, page 86].

$$[K] = \frac{GA}{L}\begin{bmatrix} 0 & 0 & 0 & 0 \\ & 1 & 0 & -1 \\ & & 0 & 0 \\ & & & 1 \end{bmatrix} + EI_y L \begin{bmatrix} \frac{1}{L^2} & -\frac{1}{2L} & -\frac{1}{L^2} & -\frac{1}{2L} \\ & \frac{1}{3} & \frac{1}{2L} & \frac{1}{6} \\ & & \frac{1}{L^2} & \frac{1}{2L} \\ & & & \frac{1}{3} \end{bmatrix} \tag{5.72}$$

$$\langle f \rangle = \left\langle q\frac{L}{2} \quad 0 \quad q\frac{L}{2} \quad 0 \right\rangle \tag{5.73}$$

- RIE is the reduced integration linear Timoshenko beam element and is based on a reduced integration for the stiffness coefficients associated with the transverse shear strain and a full integration for the other terms. The shear locking problem is avoided for identical (and especially linear) interpolations for w and θ_y by approximating the shear strain distribution by a constant shear strain. The shear correction factor is taken into account.
Among displacement-based finite elements, this approach is widely used to overcome the locking problem. The stiffness matrix and the force vector for RIE are given in (5.74) and (5.73).

$$[K] = \frac{EI}{4L^3\varphi}\begin{bmatrix} 4 & -2L & -4 & -2L \\ & (1+4\varphi)L^2 & 2L & (1-4\varphi)L^2 \\ & & 4 & 2L \\ & & & (1+4\varphi)L^2 \end{bmatrix} \tag{5.74}$$

where $\varphi = \dfrac{12EI_y}{L^2 k_y GA}$

- CIE is a consistent interpolation Timoshenko beam element with a quadratic interpolation for the displacement w and a linear interpolation for the rotation θ_y. The shear correction factor is taken into account. The element has end nodes having two degrees of freedom and the middle node has only a deflection as degree of freedom. The middle node degree of freedom can be condensed in order to reduce the matrix size. The stiffness matrix is then found to be equal to (5.74). However, the force vector for uniform loading is found to be equal to:

$$\langle f \rangle = \left\langle q\frac{L}{2} \quad -q\frac{L^2}{12} \quad q\frac{L}{2} \quad q\frac{L^2}{12} \right\rangle \tag{5.75}$$

Example 1

A simply supported beam with span L = 10m and thin rectangular cross section (bxh) is analyzed. The beam is submitted to a uniform load q. Three longitudinal nodes (two finite elements), required for the description of the problem, are taken for all the finite elements.

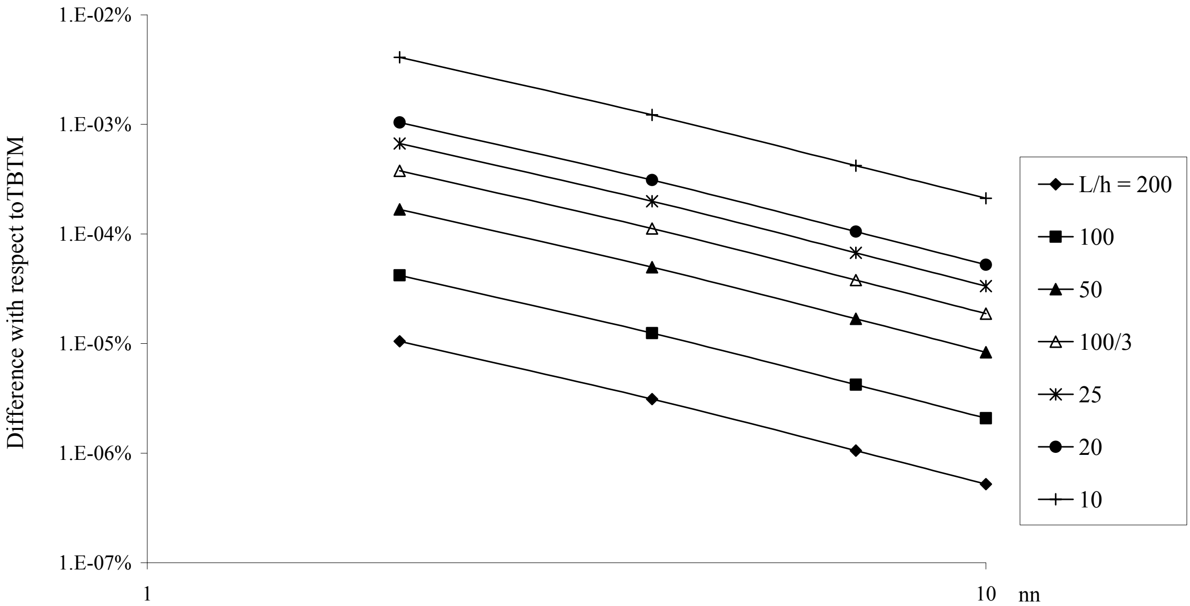

Figure 5.32 Difference between FEM3 and TBTM for a simply supported beam submitted to uniform load

Table 5.5 BBT, TBTM and PBT results [m] for maximal deflection of a simply supported rectangular beam submitted to uniform load 10N/m

b	h	L	BBT	TBTM	FEM3, nn=2	FEM3, nn=4	FEM3, nn=7	FEM3, nn=10	FEM3, nn=20
0.002	0.05	10	0.297619048	0.297637798	0.2976347	0.2976369	0.2976375	0.2976376	0.2976378
0.002	0.1	10	0.037202381	0.037211756	0.0372102	0.0372113	0.0372116	0.0372117	0.0372117
0.002	0.2	10	0.004650298	0.004654985	0.0046542	0.0046548	0.0046549	0.0046549	0.0046550
0.002	0.3	10	0.001377866	0.001380991	0.0013805	0.0013808	0.0013809	0.0013810	0.0013810
0.002	0.4	10	0.000581287	0.000583631	0.0005832	0.0005835	0.0005836	0.0005836	0.0005836
0.002	0.5	10	0.000297619	0.000299494	0.0002992	0.0002994	0.0002995	0.0002995	0.0002995
0.002	1	10	0.000037202	0.000038140	0.0000380	0.0000381	0.0000381	0.0000381	0.0000381

The values of the maximal displacement obtained by Bernoulli and Timoshenko beam theories and 'FEM3' with increasing kinematic discretization are compared in Table 5.5 for varying values of the aspect ratio (L/h). nn is the number of transversal nodes whose longitudinal displacements are taken as degrees of freedom to model the warping of the cross section. Figure 5.32 shows the difference between FEM3 and TBTM when the kinematic discretization is refined. The convergence is shown for different values of L/h.

Table 5.6 and figures 5.32 and 5.33 present additional results from which it can be concluded:
- By comparing FEM1 results in table 5.6 to BBT results in table 5.5, the Hermite cubic element FEM1 is found to give the exact solution of Bernoulli analytical results with minimum finite element discretization. However, it does not coincide with TBTM values (the difference is 2.5% for L/h=10).

Table 5.6 Finite element maximal deflection [m] for simply supported beam L=10m, and thin rectangular cross sections with b = 0.002m and varying values of height h

h	TBTM	FEM1	TLE	RIE	CIE	FEM3, nn=2	FEM3, nn=7	FEM3, nn=20
0.05	0.2976378	0.2976190	0.0000750	0.1785902	0.2381140	0.2976347	0.2976375	0.2976378
0.1	0.0372118	0.0372024	0.0000375	0.0223308	0.0297713	0.0372102	0.0372116	0.0372117
0.2	0.0046550	0.0046503	0.0000187	0.0027949	0.0037249	0.0046542	0.0046549	0.0046550
0.3	0.0013810	0.0013779	0.0000124	0.0008298	0.0011054	0.0013805	0.0013809	0.0013810
0.4	0.0005836	0.0005813	0.0000092	0.0003511	0.0004674	0.0005832	0.0005836	0.0005836
0.5	0.0002995	0.0002976	0.0000073	0.0001804	0.0002400	0.0002992	0.0002995	0.0002995
1	0.0000381	0.0000372	0.0000034	0.0000233	0.0000307	0.0000380	0.0000381	0.0000381

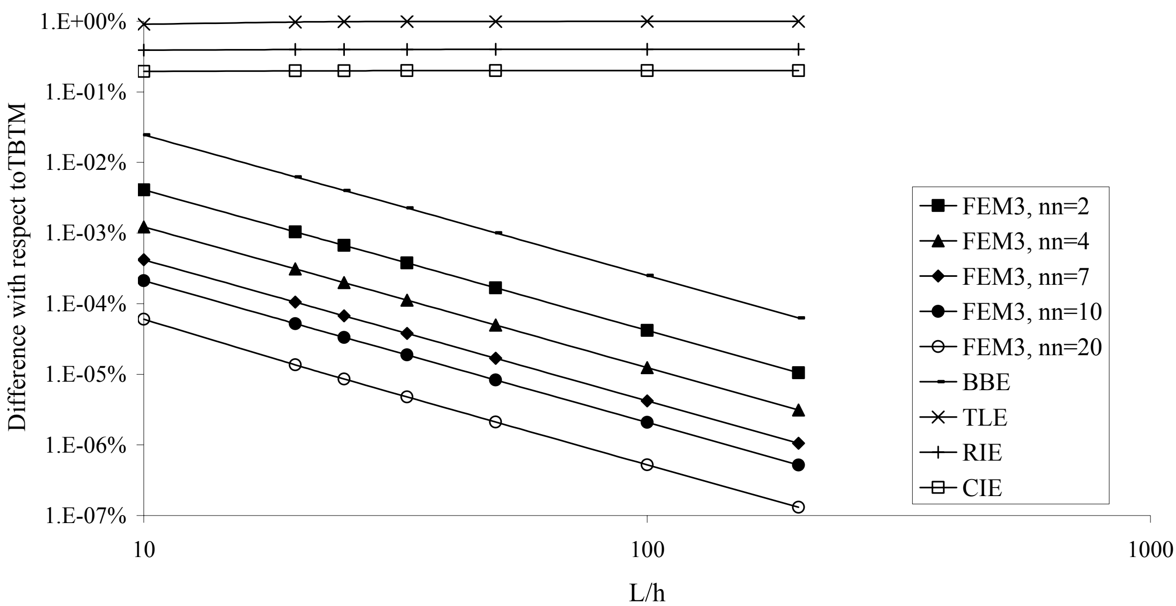

Figure 5.32 Finite element errors for maximal deflection of simply supported beam submitted to a uniformly applied load with varying aspect ratio (L/h); all finite element analyses performed with two elements

- In figure 5.32, it is shown that as for Bernoulli theory 'BBT', the difference between FEM3 and the analytical solution TBTM increases with increasing values of h. FEM3 is shown to be locking free and the solution approaches the modified Timoshenko solution with finer kinematic discretization.

- The TLE element (table 5.6 and figures 5.32 & 5.33) is excessively poor with two elements. The shear locking phenomenon appears clearly since the error increases with increasing aspect ratio (decreasing thickness beam), the error is 99.975% for L/h=200!
- In figure 5.33b, it is clear that the RIE and CIE are not completely free of locking. This remark coincides with the literature analyses, e.g. Reddy [1997], where it is noted that, in addition, refined meshing is necessary since it is shown that, for CIE and RIE, two elements give unacceptable solutions.

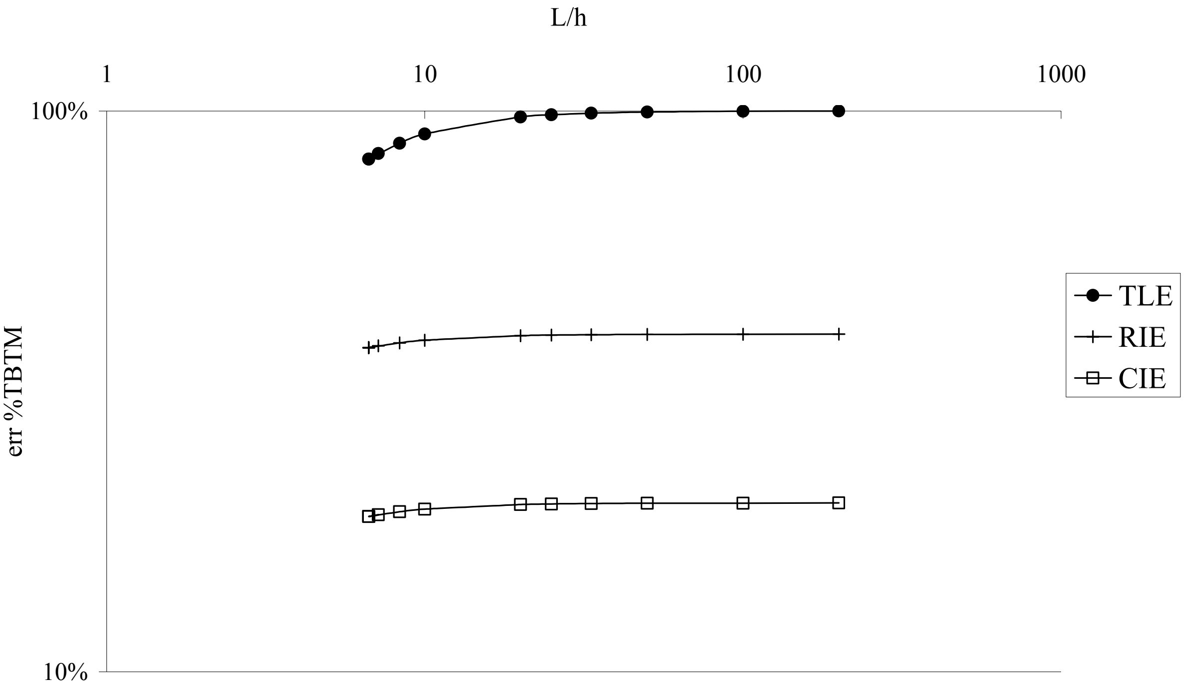

Figure 5.33b Illustration of shear locking shear phenomenon; two finite elements (enlargement of figure 5.32)

Example 2
The simply supported beam in the first example is now considered to be submitted to a pure bending. Two couples are applied at the extremeties of the beam (figure 5.34).

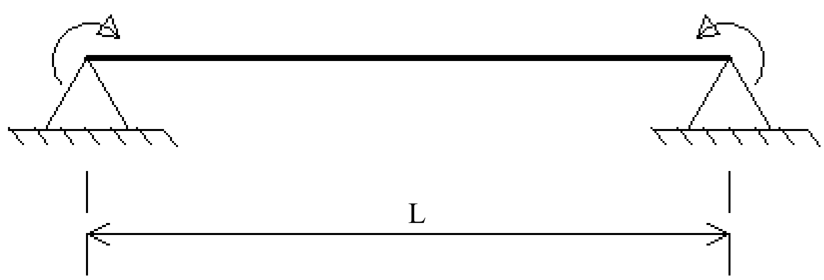

Figure 5.34 Simply supported beam submitted to a pure bending

In this theoretical case, Bernoulli solution ‘BBT’ is exact since shear forces vanish along the length of the beam. TLE, RIE and CIE are then compared with the finite element ‘FEM2’ with selective reduced integration. The results obtained here are given for two finite elements.

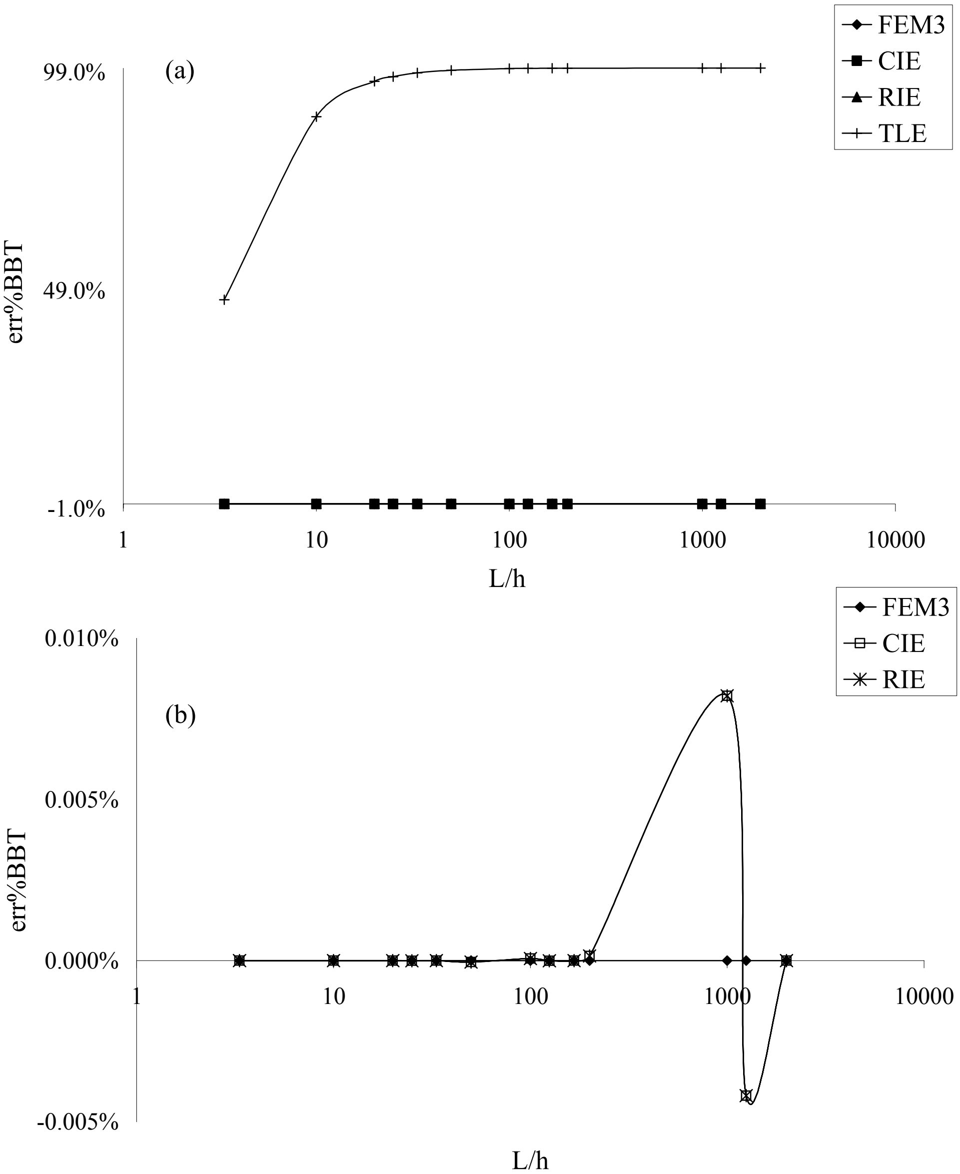

Figure 5.35 (a) Locking shear phenomenon for the maximal deflection of a simply supported beam submitted to a pure bending with varying aspect ratio (L/h); (b): enlargement of figure 5.35a with CIE, RIE and FEM3 values

In figure 5.35a, ‘TLE’ exhibits a locking shear phenomenon. For increasing values of L/h, the error between the exact solution ‘BBT’ and ‘TLE’ becomes higher. Besides, as stated by Reddy (1997), the linear equal interpolation reduced integration element (RIE) and the consistent interpolation element (CIE) are not completely locking free. The minimum discretization (e.g. one element per member) for both methods does not give the exact solution. Figure (5.35b) represents an enlargement of (5.35a) and shows the performance of CIE, RIE and FEM3. Between CIE, RIE and FEM3, FEM3 is the least free of locking element. In the case where L/h=1000, the differences between BBT and TLE, CIE, RIE and FEM3 respectively for the maximal deflection are 99.999%, 0.00821%, 0.00821%, 0.667E-9% respectively.

Example 3

A hollow flange beam (45090HFB38) [Avery, 2000] is studied by neglecting the bend radius at the corners (Figure 5.36b). As stated by Avery (2000), this cross section is developed by 'Palmer Tube Mills Pty Ltd'. It is used for its efficient structural behavior that results from torsionally rigid closed triangular flanges and its economical fabrication processes although it has complicated behavior characteristics. A second profile having the same overall dimensions than the two-celled profile is considered as an open (Figure 5.36a).

For both profiles, a simply supported beam with span L is submitted to a uniformly distributed load q acting through the centroid. E = 200GPa, G = 80 GPa.

The values of the maximal deflection, calculated by using Bernoulli and Timoshenko theories, are compared with the results obtained by the finite element FEM3 based on the kinematics developed above. The minimum transversal discretization that describes the profile geometry consists in dividing the thin profiles (Figure 5.36a & Figure 5.36b) into five and seven transversal segments (ns = 5 & 7 respectively) connected by six transversal nodes (nn = 6). This kinematic and transversal minimal discretization is required in order to describe the behavior of the profile. Refined discretizations are obtained by dividing the previously described transversal segments into equal parts and are characterized by the total number of transversal nodes (nn).

Figures 5.37 and 5.38 compare, for both profiles, the results of the above mentioned analytical and finite element methods for the maximal deflection of the simply supported beam for varying values of beam length L. In Figures 5.37a and 5.38a, the difference (eq. 5.71) between different models (BBT, TBT, FEM2 and TBTM) is plotted against the length L of the beam. In Figures 5.37b and 5.38b, the difference (eq. 5.71) between the finite element taking into account shear bending effects (FEM3) and 'TBTM' is plotted for different values of beam length against the total number of transversal nodes 'nn'.

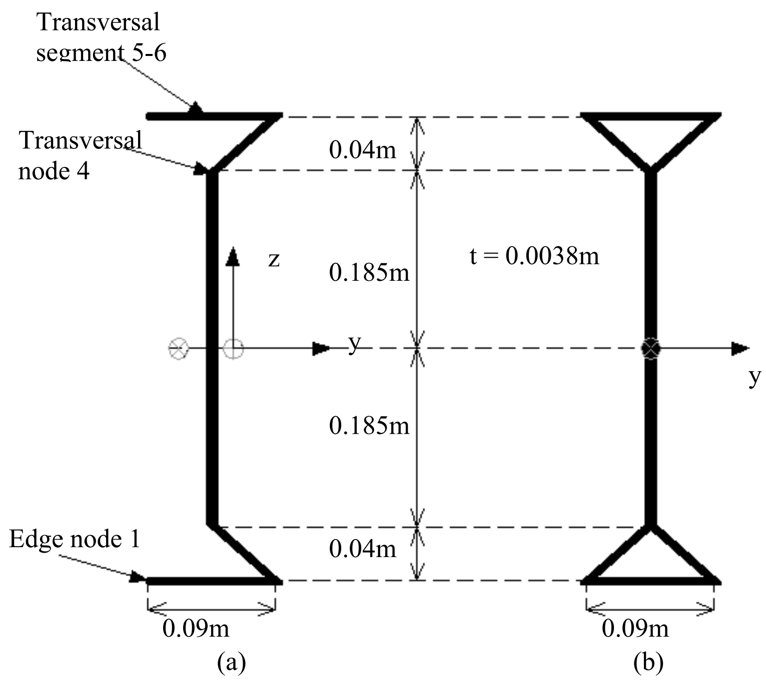

Figure 5.36 (a) open cross section, (b) two-celled cross sections

For different values of the span L and for the open profile, Figure 5.37a illustrates the difference between the analytical results of Bernoulli 'BBT' (and similarly Timoshenko 'TBT') and the modified

Timoshenko 'TBTM' theories; 'TBTM' being taken as reference. The finite element 'FEM2' based on Timoshenko kinematics *without* the correction factor gives exactly the same results as TBT for both profiles (In figure 5.37a, curves TBT & FEM2 match exactly).
The effects of shear deformation on the beam deflection depend on the length L of the beam (Figure 5.37a, curve BBT). Neglecting shear deformation effects in short beams leads to an error (measured by the difference between BBT and TBTM) of 32.67% for h/L = 0.3. For a long beam (e.g. h/L = 0.0225), this error is equal to 0.272%. The shear correction factor in Timoshenko theory is also important for short beams for the same reason (Figure 5.37a, curve TBT). By increasing the beam length (where h/L varies from 0.3 to 0.0225), the difference between TBT and TBTM decreases from 12.95% to 0.108%. Figure 5.38a illustrates the same results for the closed cross section. The error that results from neglecting shear deformation effects (measured by the difference between BBT and TBTM) is very important for short beams and varies from 36.28% to 0.319% for h/L decreasing from 0.3 to 0.0255. The difference between TBT and TBTM that measures the importance of the shear correction factor in Timoshenko theory varies from 16.1% to 0.142% for the same variation of h/L.

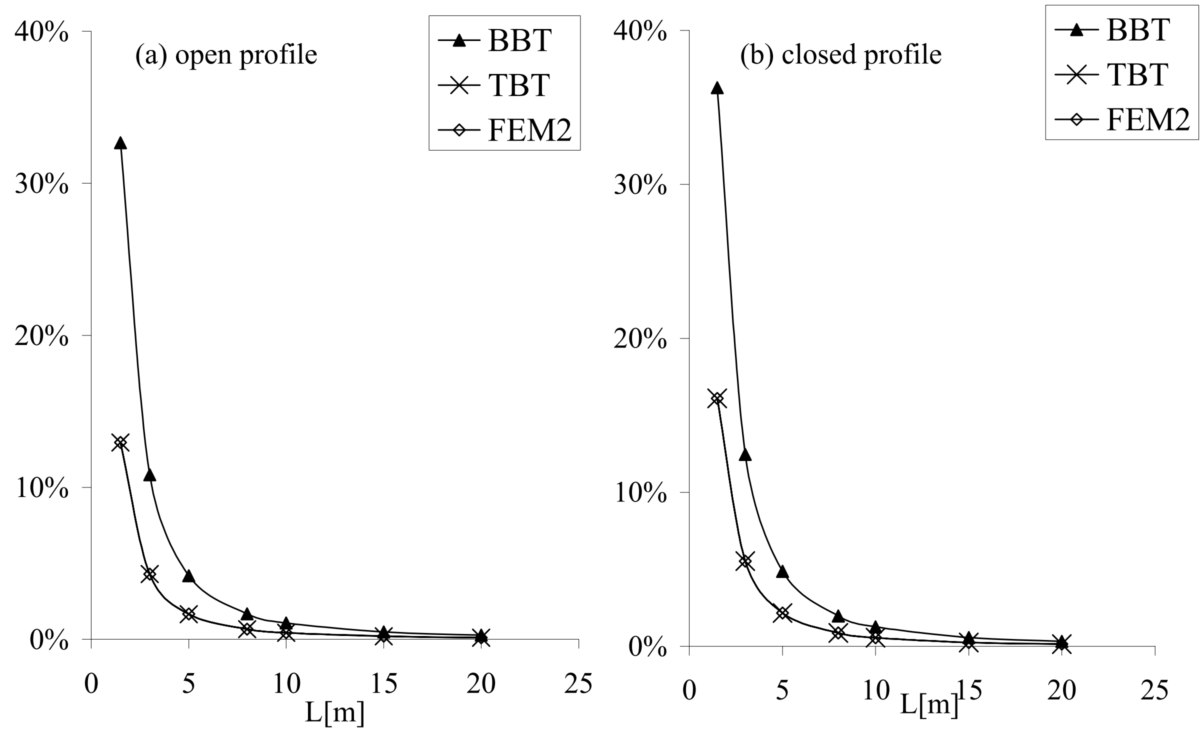

Figure 5.37 Differences between TBTM and BBT, TBT & FEM2 for maximal deflection of simply supported beam with the open profile (a) and the closed profile (b)

Figures 5.37b and 5.38b show the application of the model when shear bending effects are taken into account by modeling the warping due to shear forces. It is interesting to note that no shear correction factor is needed here since this model respects the no shear boundary condition (equation 5.70). This solution, which is automatically deduced from the geometry of arbitrary cross sections, is shown to converge to the modified Timonshenko beam theory (TBTM): the difference between the 'FEM3' finite element analysis and the 'TBTM' results decreases when refining the discretization. The minimum discretization (nn = 6 for the profile represented in Figure 5.36a) does not give the exact solution and refined meshing is required to approximate the non linear distribution by small linear variations between adjacent transversal nodes in order to give more accurate results. This is due to the kinematics where the warping, representing the longitudinal displacement of the deformed profile, is modeled as varying linearly along the contour (Ω^i are linear functions).

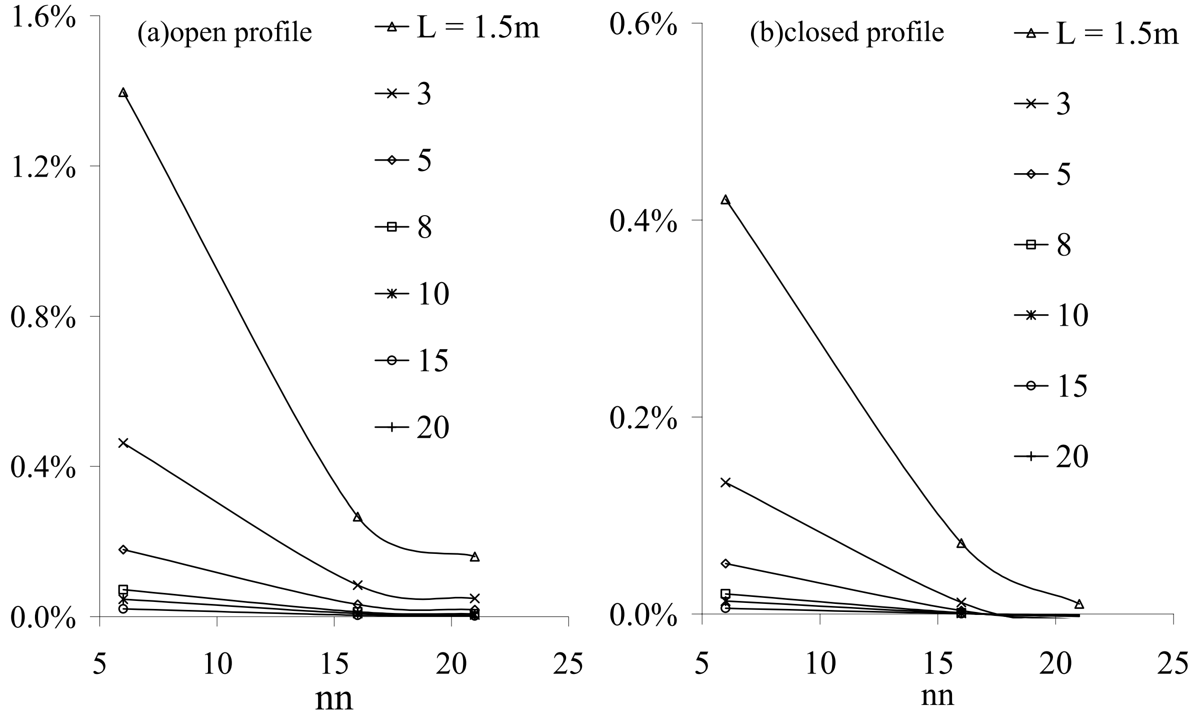

Figure 5.38 Comparing beam shear theories for maximal deflection of simply supported beam with the closed profile.

5.4 Finite element with distortional warping

5.4.1 Displacement field

In this section, a numerical method is developed in order to study profile distortions within the objectives fixed in paragraphs 2.3, 3.4 and 4.4. A beam finite element 'FEM4' is developed by adapting Prokić warping function, a contour (or first order) warping assumed to vary linearly along each profile polygonal segment, in order to take into account the distortional warping. The axial, bending and torsional behavior, are not taken hereby into account. The displacement field has been introduced (3.31) at any point q within the cross section for one distortional mode I:

$$\begin{Bmatrix} u_q \\ v_q \\ w_q \end{Bmatrix} = \begin{Bmatrix} -\omega_I \bar{\mu}_I \theta_{xI,x} + \sum_{i=1}^{n} \Omega^i u_i \\ -(z-\bar{z}_{CI})\bar{\mu}_I \theta_{xI} \\ (y-\bar{y}_{CI})\bar{\mu}_I \theta_{xI} \end{Bmatrix} \tag{5.89}$$

Each distortional mode is associated with a joint I selected from the transversal nodes in order to separate the profile into rigid parts. $\bar{y}_{CI}$, $\bar{z}_{CI}$ and $\bar{\mu}_I$ are functions of the profile coordinate s. For each distortional mode I and for each associated contour part, $\bar{y}_{CI}$ and $\bar{z}_{CI}$ are the coordinates of the distortional centers, $\bar{\mu}_I$ is the specific rotation ratio with respect to a reference part. $\bar{\mu}_I \theta_{xI}$ measures the distortional rotation. For instance, if an open profile without ramifications is considered, and if the right part is considered to be the reference part, θ_{xI} measures the rotation of all the material points located at the right of the joint I, while $\mu_I\theta_{xI}$ measures the rotation of all the material points located at the left part.

5.4.2 Finite element definition

The interpolation functions (5.90) are taken quadratic for the rotations (θ_{xI}) and linear for the warping longitudinal displacements (u_j).

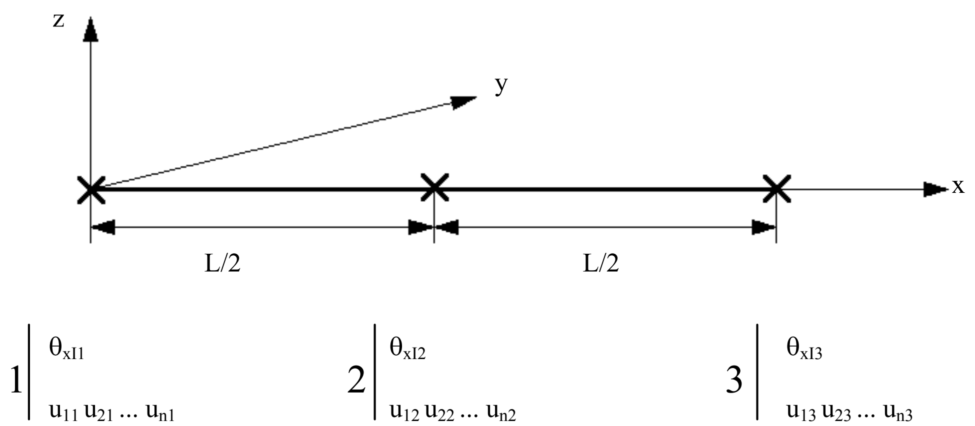

Figure 5.39 The finite element with distortional effects

$$\langle N\rangle^T = \begin{Bmatrix} 1-3\xi \ +2\xi^2 \\ 4\xi(1-\xi) \\ -\xi(1-2\xi) \end{Bmatrix} \ ; \ \langle N_u\rangle^T = \begin{Bmatrix} 1-\xi \\ \xi \end{Bmatrix} \ \text{with} \ \xi = \frac{x}{L} \tag{5.90}$$

The displacements (θ_{xI}, u_i,…) can be related to the nodal displacements by using the interpolation functions as follows:

$$\theta_{xI} = \langle N\rangle\{q_{\theta xI}\} \ ; \ I=1,2,\dots m$$
$$u_i = \langle N_u\rangle\{q_{ui}\}; \ i=1,2,\dots n \tag{5.91}$$

5.4.3 Stiffness matrix and additional equations

The finite element calculations are derived in the same usual manner as in previous paragraphs (e.g. §5.2.2). The equilibrium equations must be written in their uncoupled form. The three kinematical equations (equations 3.32, 3.33 and 3.34) have to be satisfied for each longitudinal node. (5.92 – 5.94), expressing the finite formulation of the previous equations and including the interpolation functions N and N_u, have to be satisfied for arbitrary values of x.

$$(3.32) \quad \Rightarrow \quad \sum_{i=1}^{n} S_{\Omega^i}\langle N_u\rangle\{q_{u_i}\} = 0 \tag{5.92}$$

$$(3.33) \quad \Rightarrow \quad -I_{z\bar{\mu}_I\omega_I}\langle N'\rangle\{q_{\theta_{xI}}\} + \sum_{i=1}^{n} I_{z\Omega^i}\langle N_u\rangle\{q_{u_i}\} = 0 \tag{5.93}$$

$$(3.34) \quad \Rightarrow \quad -I_{y\bar{\mu}_I\omega_I}\langle N'\rangle\{q_{\theta_{xI}}\} + \sum_{i=1}^{n} I_{y\Omega^i}\langle N_u\rangle\{q_{u_i}\} = 0 \tag{5.94}$$

It could be easily seen that, if the kinematic equations (5.92, 5.93 and 5.94) vanish for any value of x, the axial force and bending moments (N, M_y and M_z) are reduced to their uncoupled usual form. Equations (5.95-5.97) are derived from the elimination of the coupled terms when computing the bending shear forces and the torsional moment by using the finite element discretization:

$$(T_y) \quad \Rightarrow \quad -(S_{\bar{\mu}_I\omega_{I,y}} + S_{\bar{\mu}_I z} - S_{\bar{z}_{CI}\bar{\mu}_I})\langle N'\rangle\{q_{\theta_{xI,x}}\} + \sum_{i=1}^{n} S_{\Omega^i_{,y}}\langle N_u\rangle\{q_{u_i}\} = 0 \tag{5.95}$$

$$(T_z) \quad \Rightarrow \quad (-S_{\bar{\mu}_I\omega_{I,z}} + S_{\bar{\mu}_I y} - S_{\bar{y}_{CI}\bar{\mu}_I})\langle N'\rangle\{q_{\theta_{xI,x}}\} + \sum_{i=1}^{n} S_{\Omega^i_{,y}}\langle N_u\rangle\{q_{u_i}\} = 0 \tag{5.96}$$

$$\begin{aligned}
(M_{xI}{}^1) \quad \Rightarrow \quad & (I_{z\bar{\mu}_I\bar{\mu}_J\omega_{I,y}} - I_{y\bar{\mu}_I\bar{\mu}_J\omega_{I,z}} - S_{\bar{z}_{CJ}\bar{\mu}_I\bar{\mu}_J\omega_{I,y}} + S_{\bar{y}_{CJ}\bar{\mu}_I\bar{\mu}_J\omega_{I,z}} + I_{\bar{\mu}_I\bar{\mu}_J\omega_{I,y}\omega_{J,y}} + I_{\bar{\mu}_I\bar{\mu}_J\omega_{I,z}\omega_{J,z}} \\
& + I_{\bar{\mu}_I\bar{\mu}_J zz} + I_{\bar{\mu}_I\bar{\mu}_J yy} - S_{\bar{\mu}_I\bar{\mu}_J\bar{z}_{CJ}z} - S_{\bar{\mu}_I\bar{\mu}_J\bar{y}_{CJ}y} + I_{z\bar{\mu}_I\bar{\mu}_J\omega_{J,y}} - I_{y\bar{\mu}_I\bar{\mu}_J\omega_{J,z}} \\
& - S_{\bar{\mu}_I\bar{\mu}_J\bar{z}_{CI}z} - S_{\bar{\mu}_I\bar{\mu}_J\bar{y}_{CI}y} + A_{\bar{\mu}_I\bar{\mu}_J\bar{z}_{CI}\bar{z}_{CJ}} + A_{\bar{\mu}_I\bar{\mu}_J\bar{y}_{CI}\bar{y}_{CJ}} - S_{\bar{\mu}_I\bar{\mu}_J\bar{z}_{CI}\omega_{J,y}} + S_{\bar{\mu}_I\bar{\mu}_J\bar{y}_{CJ}\omega_{J,z}})\langle N'\rangle\{q_{\theta_{xI}}\} \\
& + \sum_{i=1}^{n}(-I_{z\bar{\mu}_I\Omega^i_{,y}} + S_{\bar{\mu}_I\bar{z}_{CI}\Omega^i_{,y}} + I_{y\bar{\mu}_I\Omega^i_{,z}} - S_{\bar{\mu}_I\bar{y}_{CJ}\Omega^i_{,z}})\langle N_u\rangle\{q_{u_i}\}
\end{aligned} \tag{5.97}$$

The distortion/tension-compression, the distortion/bending and the distortion/torsion uncoupling have been thus ensured in the calculation of internal forces and stiffness matrix terms. The distortional warping degrees of freedom do not induce normal forces, shear forces (T_y and T_z), bending moment (M_y and M_z) or torsional resultants (M_x^1 and M_ω). The tension-compression, bending and torsional generalized forces do not derive from the terms u_i describing the distortion.

Expressions 5.92 to 5.97 must be satisfied for any value of x, which implies that:

(5.92) => $$\sum_{i=1}^{n} S_{\Omega^i}(u_i) = 0 \tag{5.98}$$

(5.93) => $$I_{z\bar{\mu}_I\omega_I}\frac{1}{L}\{3\theta_{xI1} - 4\theta_{xI2} + \theta_{xI3}\} + \sum_{i=1}^{n} I_{z\Omega^i}\{u_{i1}\} = 0 \tag{5.99}$$

(5.93) => $$I_{z\bar{\mu}_I\omega_I}\frac{1}{L}\{-\theta_{xI1} + 4\theta_{xI2} - 3\theta_{xI3}\} + \sum_{i=1}^{n} I_{z\Omega^i}\{u_{i3}\} = 0 \tag{5.100}$$

(5.94) => $$I_{y\bar{\mu}_I\omega_I}\frac{1}{L}\{3\theta_{xI1} - 4\theta_{xI2} + \theta_{xI3}\} + \sum_{i=1}^{n} I_{y\Omega^i}\{u_{i1}\} = 0 \tag{5.101}$$

(5.94) => $$I_{y\bar{\mu}_I\omega_I}\frac{1}{L}\{-\theta_{xI1} + 4\theta_{xI2} - 3\theta_{xI3}\} + \sum_{i=1}^{n} I_{y\Omega^i}\{u_{i3}\} = 0 \tag{5.102}$$

(5.95) => $$(S_{\bar{\mu}_I\omega_{I,y}} + S_{\bar{\mu}_I z} - S_{\bar{z}_{CI}\bar{\mu}_I})\frac{1}{L}\{3\theta_{xI1} - 4\theta_{xI2} + \theta_{xI3}\} + \sum_{i=1}^{n} S_{\Omega^i_{,y}}\{u_{i1}\} = 0 \tag{5.103}$$

(5.95) => $$(S_{\bar{\mu}_I\omega_{I,y}} + S_{\bar{\mu}_I z} - S_{\bar{z}_{CI}\bar{\mu}_I})\frac{1}{L}\{-\theta_{xI1} + 4\theta_{xI2} - 3\theta_{xI3}\} + \sum_{i=1}^{n} S_{\Omega^i_{,y}}\{u_{i3}\} = 0 \tag{5.104}$$

(5.96) => $$(S_{\bar{\mu}_I\omega_{I,z}} - S_{\bar{\mu}_I y} + S_{\bar{y}_{CI}\bar{\mu}_I})\frac{1}{L}\{3\theta_{xI1} - 4\theta_{xI2} + \theta_{xI3}\} + \sum_{i=1}^{n} S_{\Omega^i_{,z}}\{u_{i1}\} = 0 \tag{5.105}$$

(5.96) => $$(S_{\bar{\mu}_I\omega_{I,z}} - S_{\bar{\mu}_I y} + S_{\bar{y}_{CI}\bar{\mu}_I})\frac{1}{L}\{-\theta_{xI1} + 4\theta_{xI2} - 3\theta_{xI3}\} + \sum_{i=1}^{n} S_{\Omega^i_{,z}}\{u_{i3}\} = 0 \tag{5.106}$$

Similar developments are done for equation (5.97).
By neglecting second order distortional warping (calculations similar to those in equation 5.30), (5.99, 5.100, 5.101 and 5.102) are reduced to (5.107 and 5.108).

$$\sum_{i=1}^{n} I_{y\Omega^i} u_i = 0 \tag{5.107}$$

$$\sum_{i=1}^{n} I_{z\Omega^i} u_i = 0 \tag{5.108}$$

The stiffness matrix results from developing general equations (5.10). By combining the above described orthogonality relationships (equations 5.95-5.108), the coupled terms in the stiffness matrix are eliminated. The non zero terms of k^{el} obtained after this elimination are given in Appendix 7.
Kinematical equations (3.32, 3.33, 3.34 and 3.35) are added to the initial equilibrium system in order to relate the degrees of freedom ‘u_i’ and to restrain the warping parameters to distortional warping. Similarly to the case of torsional warping developments (§5.2.3), two methods can be used (the

condensation technique and the method involving lagrange multipliers). The additional relations (5.95, 5.96 and 5.97) together with the relations resulting from the joint/distortional_centers dependency (2.76 and 2.77) are used in order to determine the values of μ_I, y_{CI}, z_{CI}… The approach used in this study for unbranched profiles consists in considering 5m unknowns (y_{CI}, z_{CI}, $\mu_I y_{CI}$, $\mu_I z_{CI}$, μ_I; I=1,…m) to be calculated or condensed from five equations (5.95, 5.96, 5.97, 2.76 and 2.77). These five equations are linear with respect to the five unknowns.

5.4.4 Applications on distortional warping

The performance and the convergence of the elastic beam finite element 'FEM4' including distortional warping are shown by comparing the results with analytical computations using Takahashi model [1978, 1980…] and numerical shell calculations. The Poisson coefficient is taken equal to zero in the numerical shell computations that aim at validating the finite element 'FEM4' based on the assumption HYPT4 (paragraph 2.3.3). In the first example, the distribution of rotations, normal stresses and shear stresses associated with distortion are compared and discussed for a monosymmetrical profile. The second example compares the flexural, torsional and distortional behaviors exhibited by a beam submitted to a single transversal load applied at one corner of its asymmetrical profile.

Example 1: Distortion of an open monosymmetrical profile

The distortional rotation and warping of a clamped-free beam with an open thin walled profile (four polygonal segments [Ls = 0.08m] x [t = 0.001m]; Figure 5.40b) is prevented at the clamped end. At the free end, the beam is submitted to two opposite horizontal loads of 100N (Figure 5.40a). G=84GPa; E=210GPa.

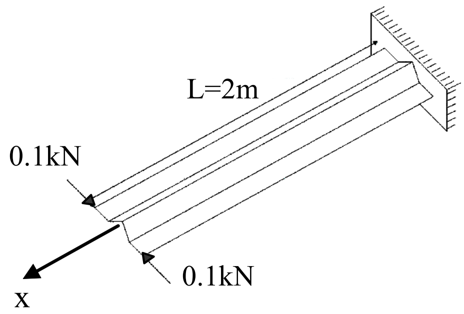

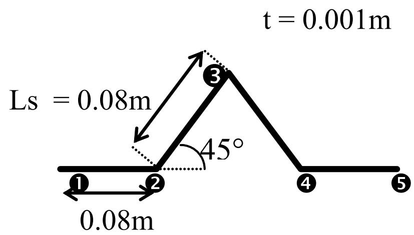

Figure 5.40 Clamped-free beam submitted to distortional loading

<u>Problem definition</u>

This profile, already analyzed by Takahashi (1978), presents a simple case of a monosymmetrical profile with one distortional mode (associated with the joint 3). The distortional deformation of the profile consists in the rotation of two rigid parts (left: 1-2-3 and right: 3-4-5) separated by the joint 3. Since the two rigid parts are symmetrical with respect to the vertical axis passing through the joint 3, the rotational angles are expected to have equal magnitude but opposite sign (μ = -1). Due to symmetry and to the alignment of the joint and the associated distortional centers (equation 2.77), the distortional centers are expected to be situated on the horizontal axis passing through the joint 3. The coordinates of the distortional centers are computed within the present finite element analyses by applying equations (5.95-5.97). For uniform distortion without additional local plate bending (uniform distribution of distortional moment along the beam length; distortional rotation prevented at one end

with free warping), the computed location (figure 5.41b) coincides exactly with that found by Takahashi (1978). Similarly to Vlassov computations, Takahashi warping function is assumed to be the same for arbitrary loading and boundary conditions since it assumes zero warping shear stresses at the contour (HYPT2 in §2.3.3). The position of the distortional centers, computed by Takahashi theory (equations 3.36-3.39), depends only on the geometrical shape and dimensions of the profile. However, in the present finite element analyses, the location of the distortional centers depends on the solution in arbitrary loading cases and boundary conditions but is always found to be positioned on the horizontal axis passing through node 3 for this monosymmetrical profile.
The distribution of M^s_{xI} along the profile contour resulting from plate additional bending and defined in §2.3.4 is given in figure 5.41a. The loading in figure 5.40a induces a distortional torque M_{xI} = -11.32N.m associated with the joint 3 and computed from equation 4.45.

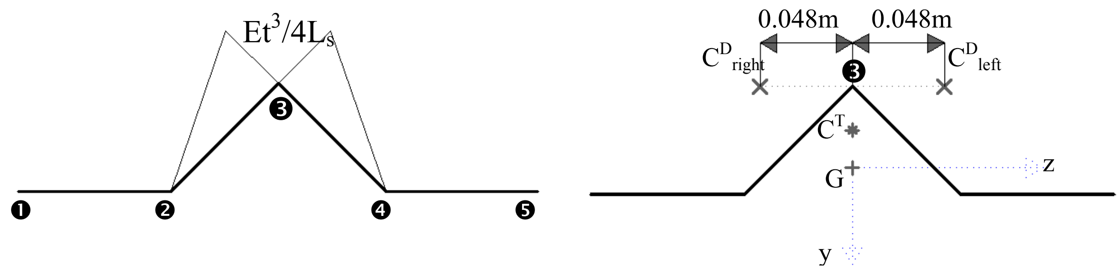

Figure 5.41 (a): Stiffening effects (distribution of M^s_{xI} along the profile contour). (b): Position of distortional centers

<u>Finite element calculations</u>
Results with the finite element 'FEM4' developed in §5.5 are compared with analytical computations (see also Mahieux 2003) with Takahashi theory and numerical results with shell elements (400 elements; figure 5.42) by using the software Samcef (Samtech s.a. 2002).

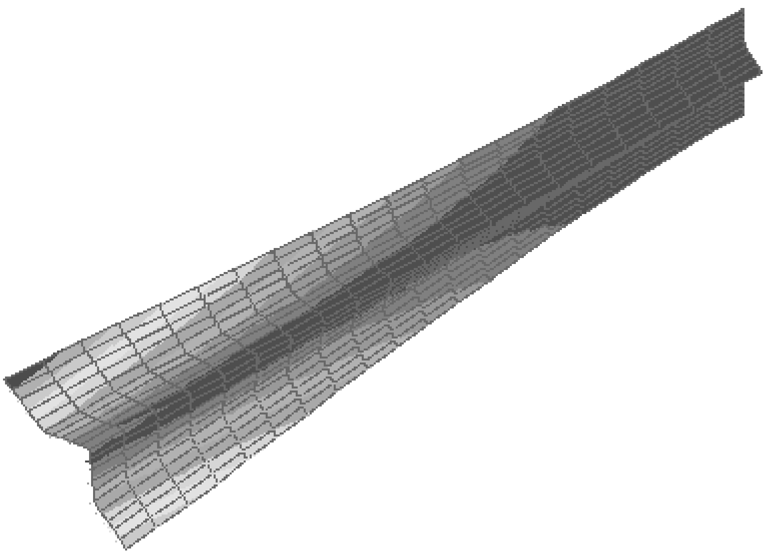

Figure 5.42 Meshing with Samcef shell finite elements

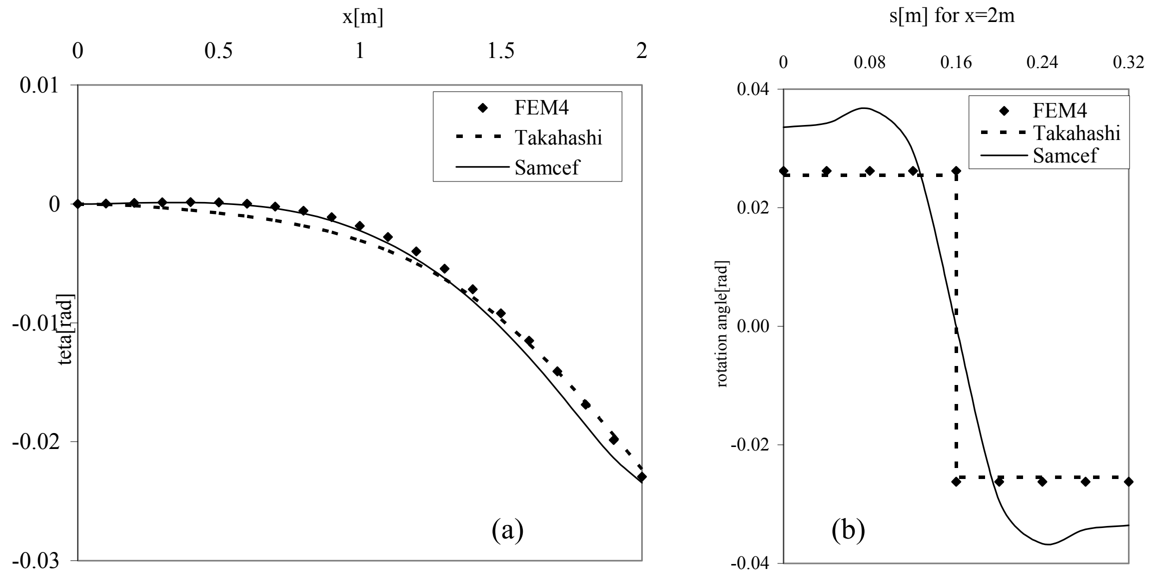

Figure 5.43 (a): Distortional rotating angle distribution along the longitudinal axis (x); (b): Rotating angle distribution along the contour coordinate (s) for x=2m

The diagram of the distortional angle along the longitudinal axis of the beam is first investigated. The distortional rotation of the right part of the profile is plotted in figure 5.43a. For shell elements, a rotation angle is calculated as the average of rotations of all the nodes that belong to the right part (s = 0.16-0.32m). The differences between shell results and the finite element analysis 'FEM4' (with 20 elements) and Takahashi analytical solution for the maximal distortional rotation angle are 2.13% and 4.88% respectively. It is important to note that the assumption of rigid part rotations in beam theories (Takahashi and FEM4) is relaxed in shell element analyzes.

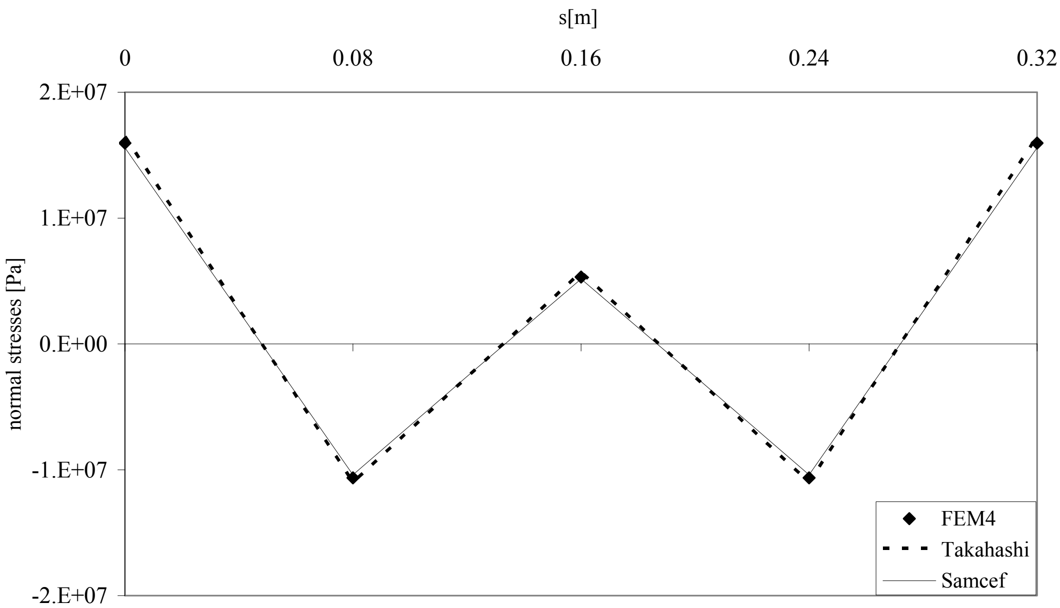

Figure 5.44 Normal stresses σ_x due to distortion of a monosymmetrical open profile for x = 1.5m

Figure (5.43b) shows that, for beam theories, the distortional angle is uniform in each part (left: s = 0-0.16m; right : s = 0.16-0.32m) while, for shell results (continuous line), it varies slowly along each part and drops sharply around the joint (s = 0.16m). In both cases, it is opposite in the left and right parts due to the profile monosymmetry.
Figures 5.44 and 5.45 show the distributions of normal stresses (σ_x, σ_s) at x = 1.5m. The beam finite element results 'FEM4' are compared with analytical computations based on Takahashi theory and with numerical results from Samcef shell analyzes. An excellent agreement was found.

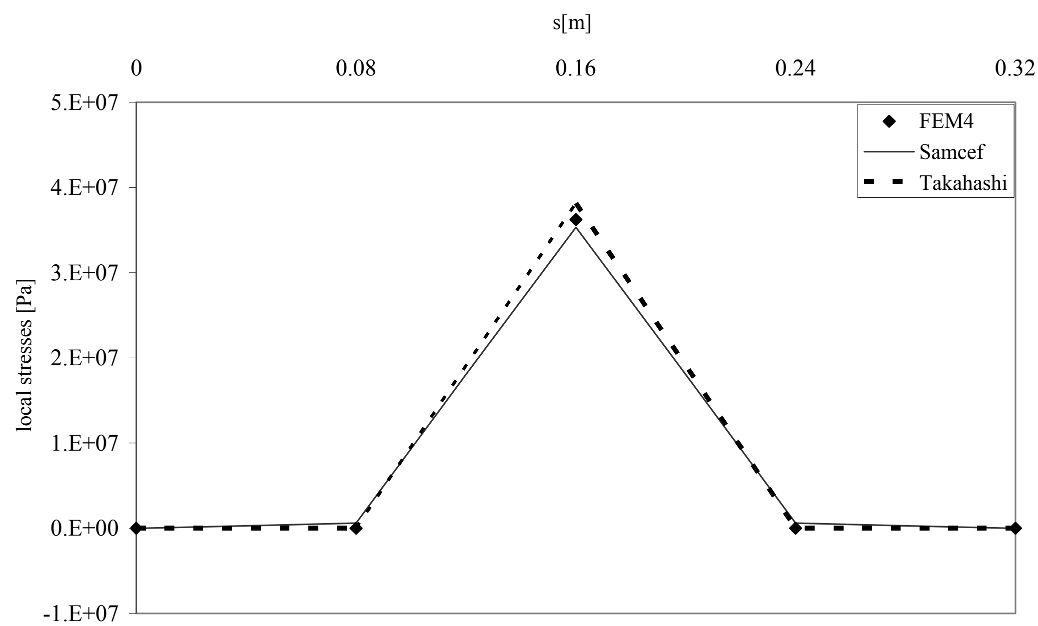

Figure 5.45 Local stresses σ_s at the upper skin for x = 1.5m

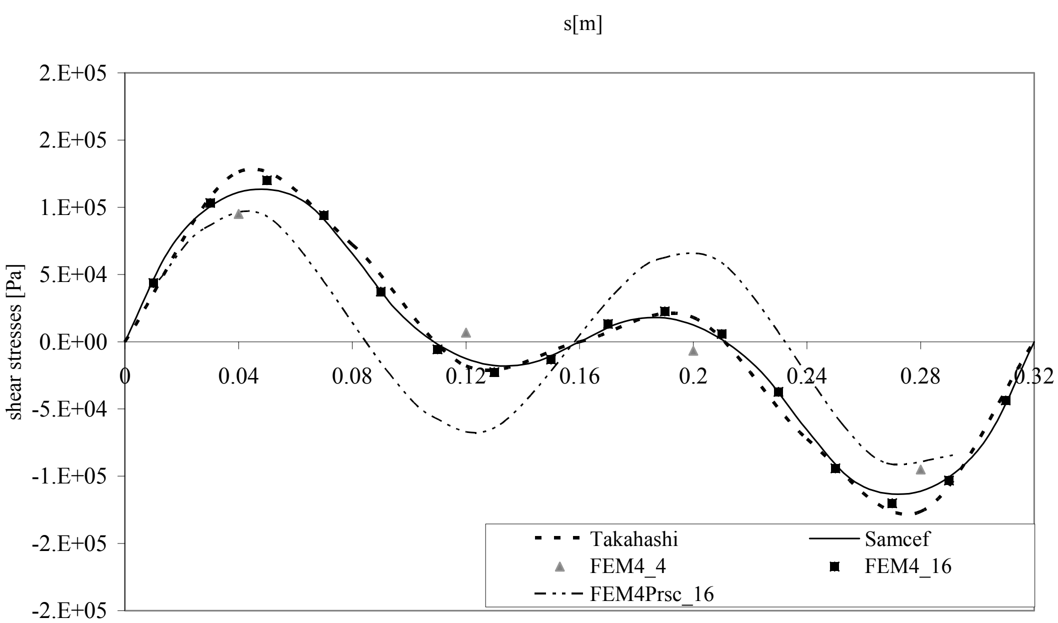

Figure 5.46 Shear τ_{xs} stresses due to distortion of a monosymmetrical open profile for x = 1.5m

It is important to highlight that the distortional centers are prescribed as being those of a uniform distorsional case –except for the results concerning warping shear stresses–. In Takahashi beam theory, the shear stresses are computed from normal stresses by using longitudinal equilibrium equation. Similarly to Vlassov theory, they cannot be computed from kinematics by using Hooke law since they would be equal to zero. However, in 'FEM4' analyzes, the zero midwall shear assumption is relaxed and shear stresses are calculated from Hooke law for each transversal segment of the profile. Figure 5.46 shows the distribution of contour warping shear stresses τ_{xs} at x = 1.5m by condensing the location of the distortional centers. Since warping shear stresses τ_{xs}^{ω} have a parabolic shaped distribution (Takakashi or Samcef results in figure 5.46), 'FEM4' results need refined discretization of the contour by a finite number of nodes and segments (16 transversal segments are used for results FEM4_16 in figure 5.46; 4 transversal segments are used for results FEM4_4). The curve FEM4Prsc_16 (16 transversal segments) presents the erroneous warping shear stresses that would appear if the distortional centers are prescribed as those of Takahashi. It is interesting to note that the difference between prescribing (as being that of uniform distortion) and condensing the location of the distorstional centers is found to be very small for the values of the distorsional angle and the normal stresses.

Example 2: Distortion of an open asymmetrical profile

A clamped-free beam is considered with an asymmetrical open profile (Figure 5.47b; all the degrees of freedom are constrained at the clamped end). The thickness is t = 0.001m. The dimension of the contour is given by the lengths of transversal segments: Ls_{12} = 0.06m; Ls_{23} = 0.15m; Ls_{34} = 0.06m; Ls_{45} = 0.075m]. A horizontal load P = 100N acts at the free end (Figure 5.47a). G=84GPa; E=210GPa.

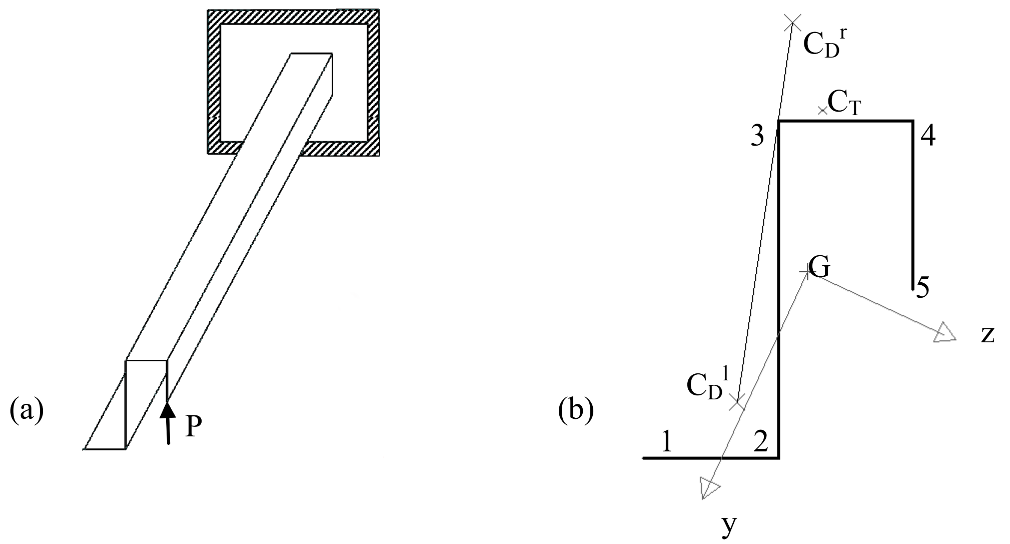

Figure 5.47 (a) Clamped-free beam submitted to bending, torsion and distortion; (b) Position of torsional and distortional centers

<u>Problem definition</u>

According to the approach proposed in this work, the behavior of the thin walled beam is evaluated as being originated by four different cases (a + b + c + d) induced by the applied load P (figure 5.49).

case a- A force Fy (-100N x cos24.11 = -91.279N), resulting from the projection of the load P on the principal axis (y), captures the (xy) bending behavior. A uniform shear force Ty and a linear bending moment Mz are distributed along the beam length.

case b- A force Fz (-100N x sin24.11 = -40.844N), resulting from the projection of the load P on the other principal axis (z), captures the (xz) bending behavior. A shear force Tz and a bending moment My are uniformly and linearly distributed along the beam length respectively.

case c- A torsional torque Cx^T (100N x 0.04002m = 4.002Nm), resulting from the product of the intensity of the force vector and the radius distance from the center of rotation C_T to the point of application of the load, captures the torsional behavior. A torsional moment (Mx) is uniformly distributed along the beam while the restrained warping at the clambed end of the beam induces a non uniform distribution of a torsional bimoment with respect to the longitudinal direction.

case d- A distortional 'torque' Cx^D (100N x 0.05360m = 5.36Nm) resulting from the product of the intensity of the load P and the radius distance from the center of right rotation C_D^r to the point of application of the load. Similarly to the case (c) related to torsion, a distortional moment and a distortional bimoment are uniformly and non uniformly distributed along the beam length.

The distortional mode considered hereby is associated with the joint 3. The distortional deformation of the profile involves the rotation of two rigid parts (θ_D^l for the left rigid part: 1-2-3 and θ_D^r for the right rigid part: 3-4-5) around the respective distortional centers C_D^l and C_D^r). Since the profile is not symmetrical, the rotating angles are not the same ($\theta_D^l = \mu\theta_D^r$; $\mu \neq -1$). The distribution of M^s_{xI} (resulting from plate stiffening effects) along the profile contour is given in figure 5.48.

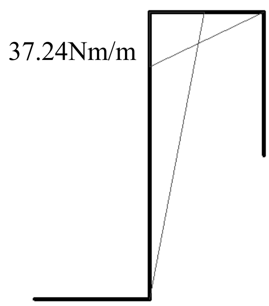

Figure 5.48 Distribution of M^s_{xI} along the profile contour

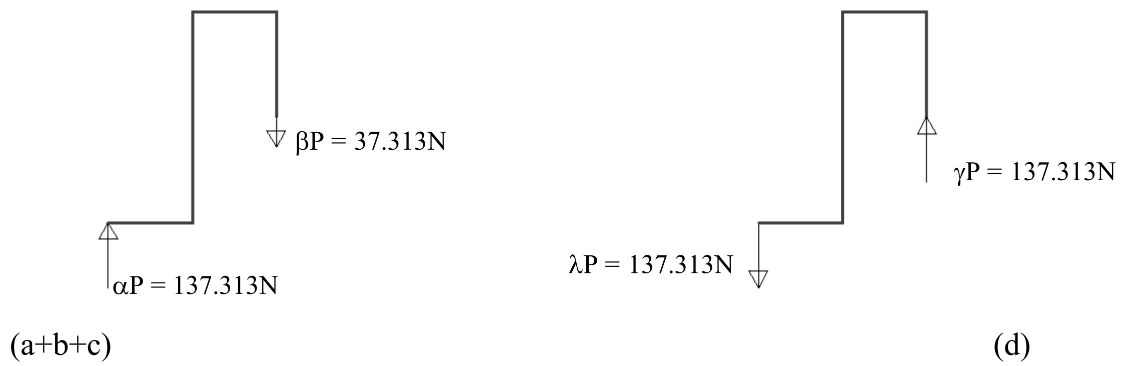

Figure 5.49 Separating distortional loading cases (d) from the bending/torsional loading case (a+b+c) for the case of loading in figure 5.47a

Figure 5.49 presents the distortional case (d) when uncoupled from the well known bending/torsional cases (a+b+c). For the distortional configuration d, the applied load P is divided into two forces (γP) and (λP) acting respectively on the left and right parts of the cross section. The coefficients γ and λ are computed by setting that the flexural and torsional resultants are equal to zero ($\gamma P + \lambda P = 0$) while the distortional moment is equivalent to that of the initial configuration resulting from the applied load

$P(\mu\, d_D^l\, \gamma P + d_D^r\, \lambda P = d_D^r\, P)$. d_D^l and d_D^r are the radius distances from the center of left rotation C_D^l and the center of right rotation C_D^r to the point of application of loads acting on the right part and the left part respectively. The flexural torsional configuration (a+b+c) is determined by setting that the flexural and torsional resultants are those of the applied load P ($\alpha P + \beta P = P$) and that the distortional moment $\mu\, d_D^l\, \alpha P + d_D^r\, \beta P = 0$) is equal to zero. This way of decomposing the forces in not single and is presented hereby for the purpose of enhancing the understanding of the problem definition.
The coordinates of the torsional and distortional centers and the value of the distortional ratio are computed within the present finite element analyses by using equations (5.34-5.35) & (5.95-5.97). They are found to coincide exactly with those of Vlassov and Takahashi theories in the cases of uniform torsion and uniform distortion without including the additional local plate bending (uniform distribution of torsional and distortional moment along the beam length; torsional and distortional rotation prevented at one end with free warping). As previously discussed, this is due to the fact that Vlassov and Takahashi warping functions assume zero warping shear stresses at the contour (HYPV2 in § 2.2.3.1 for torsion & HYPT2 in §2.3.3 for distortion).

Finite element calculations involving distortion
Results with the finite element 'FEM4' are compared with analytical computations with Takahashi theory and simulations with shell elements (7000 elts; figure 5.50) by using the software Samcef (Samtech s.a. 2002).

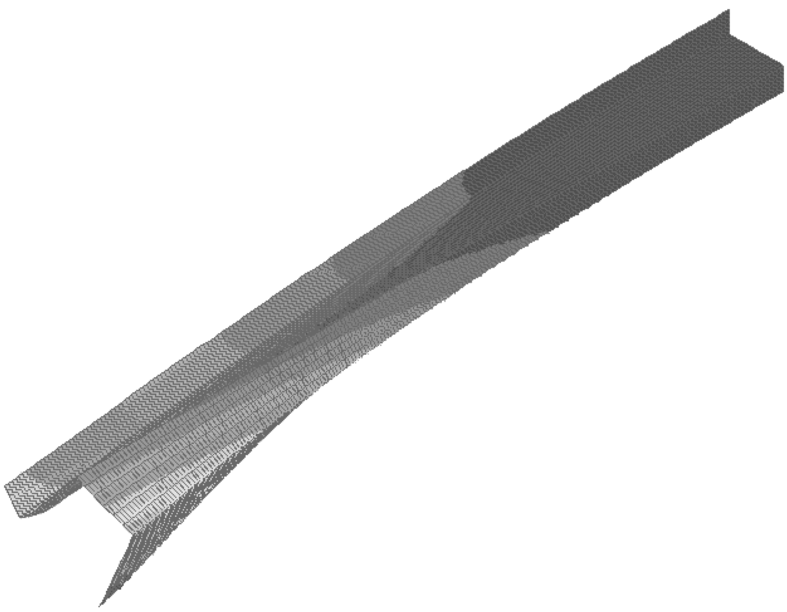

Figure 5.50 Meshing with Samcef shell finite elements

The distribution of the distortional angle θ_D^r along the longitudinal axis of the beam is plotted in figure 5.51. The differences between shell results and the finite element analysis 'FEM4' (with 20 elements) and analytical solutions with Takahashi formulation for the maximal distortional rotation angle are respectively 0.75% and 2.245% for the right part rotation.
Figure 5.52 compares the distribution of the rotating angle along the contour coordinate (s) at the end of the beam. The local effects captured in shell simulations and not considered in Takahashi and FEM4 calculations are shown to be more important in the left part (the differences between shell results and FEM4 and Takahashi solutions are 14.69% and 13.3% respectively).

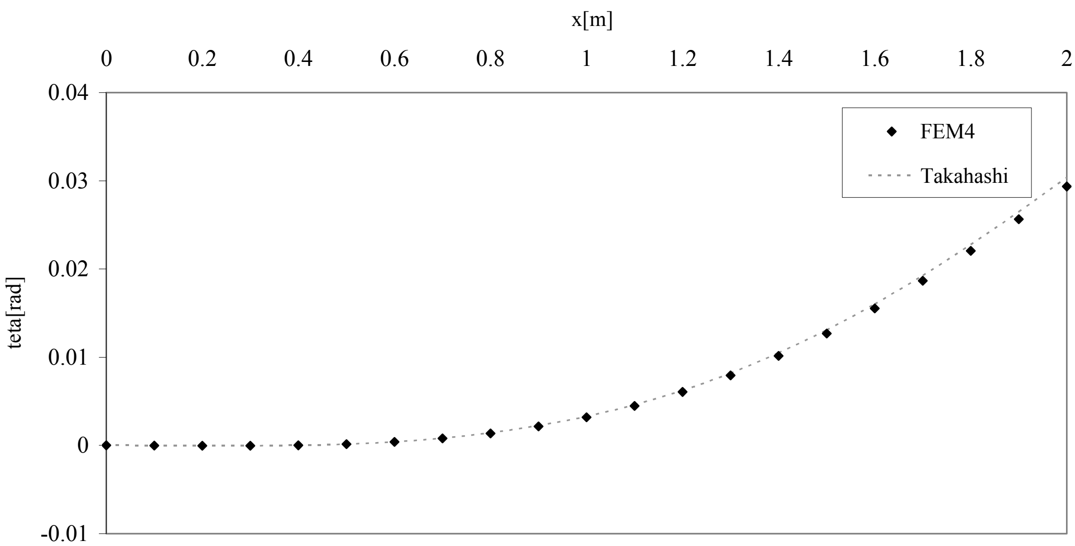

Figure 5.51 Distribution of the distortional rotating angle along the beam length (x)

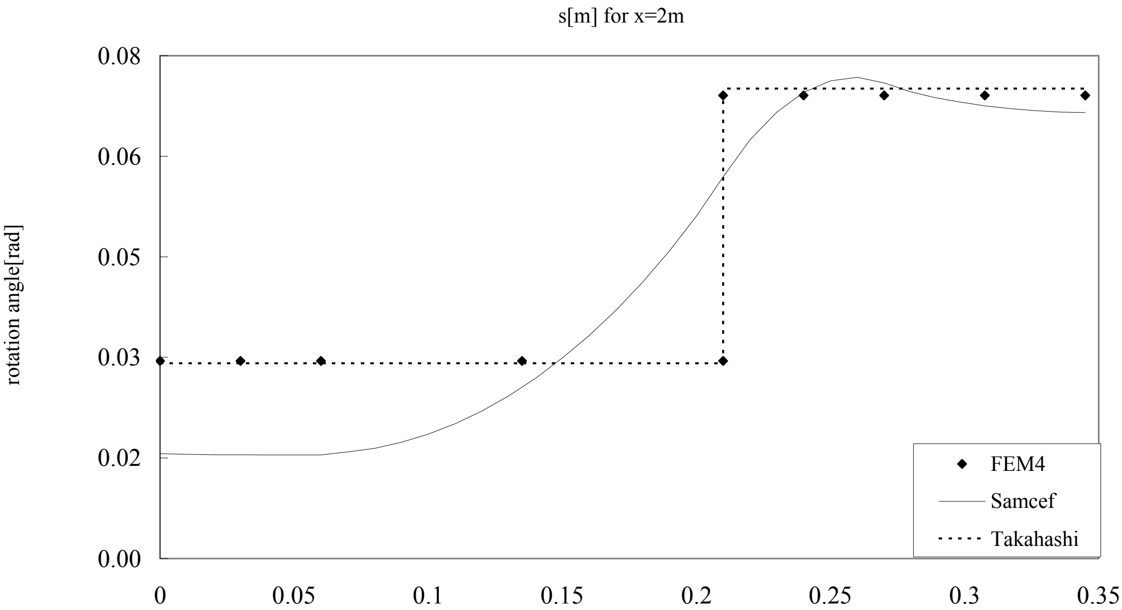

Figure 5.52 Rotating angle (torsion+distortion) distribution along the contour coordinate (s) for x=2m

In this example, a very good agreement is found between the results of the proposed theory and those resulting from a complete shell analysis. The distortional behavior is shown to be important since, in this simple example, the distortional rotation (0.029rad) is not negligible if compared with the torsional rotation (0.040rad).

Figure 5.53a shows the distributions of normal stresses (σ_x) resulting from the distortional mode at x = 1.5m. The beam finite element results (FEM with 20elements) are compared (figure 5.53b) with numerical results from Samcef shell analyzes and with analytical computations based on Takahashi theory for distorsion. The contribution of each loading cases (a, b, c & d) in the total value of normal stresses for this example is shown in table 5.7. The distortional behavior in this example is very important and neglecting it leads to erroneous results. For the transversal node 5 (s = 0.345m), the distortional contribution in normal stresses is equal to 2.9 times that of bending and 3.3 times that of torsion.

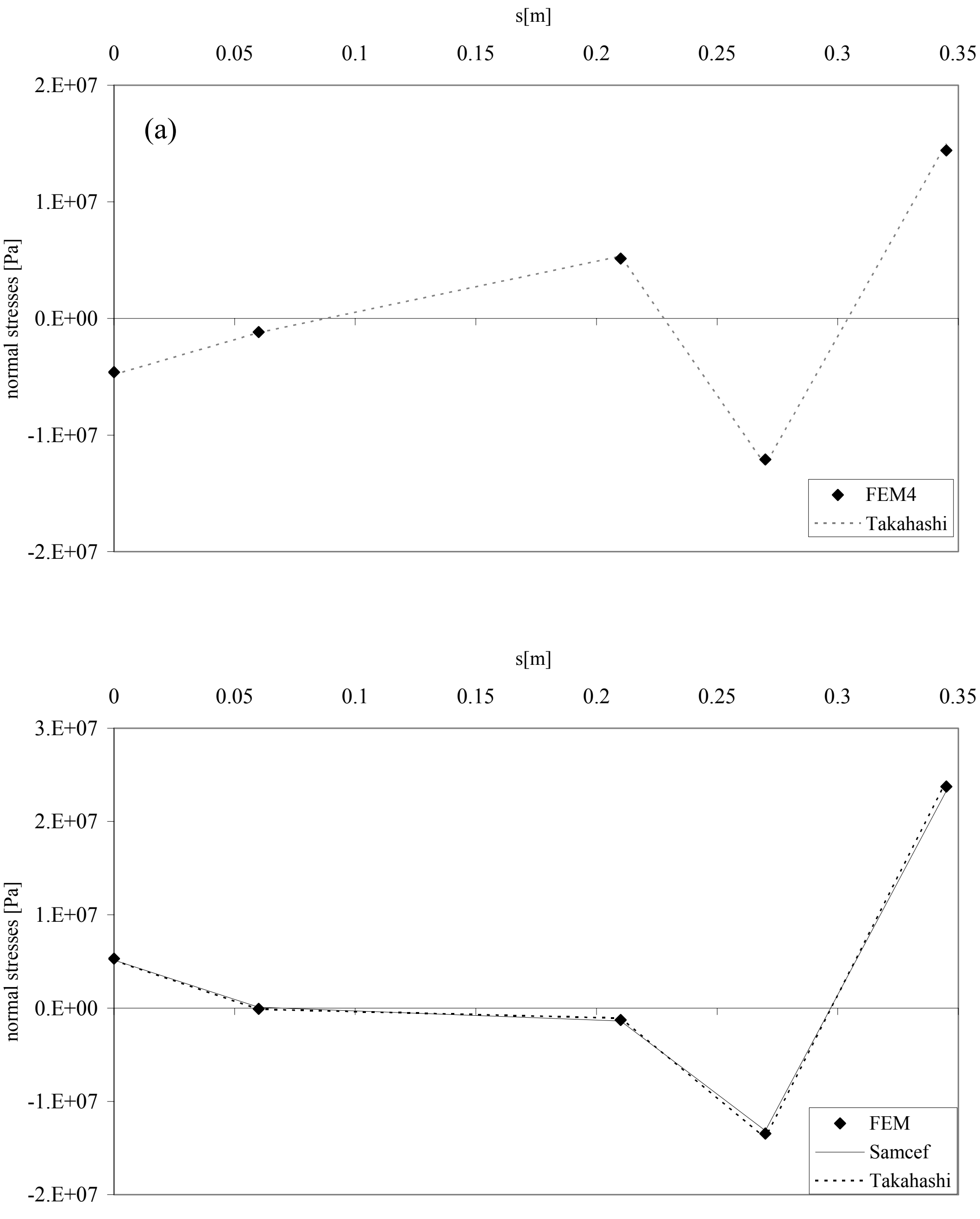

Figure 5.53 Normal stresses for x = 1.5m resulting from (a) distortion only; (b) bending, torsion and distortion

Table 5.7 Normal stresses [Pa] of different loading cases

s\loading case	a	b	c	d
	(xy) bending	(xz) bending	torsion	distortion
0	3,847,393.64	-3,808,521.25	9,877,579.22	-4,615,217.35
0.6	2,956,705.64	2,568,510.51	-4,432,300.53	-1,177,381.73
0.21	-2,027,070.50	-4,565,335.31	191,409.80	5,127,592.35
0.27	-2,919,214.48	1,811,696.44	-234,833.07	-12,096,150.68
0.345	-427,326.41	5,378,037.19	4,395,130.21	14,404,655.36

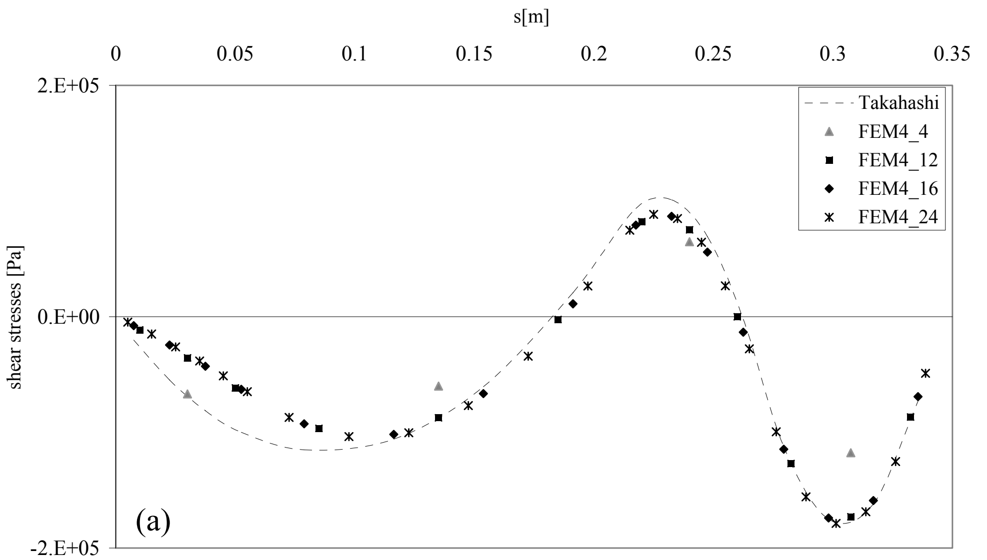

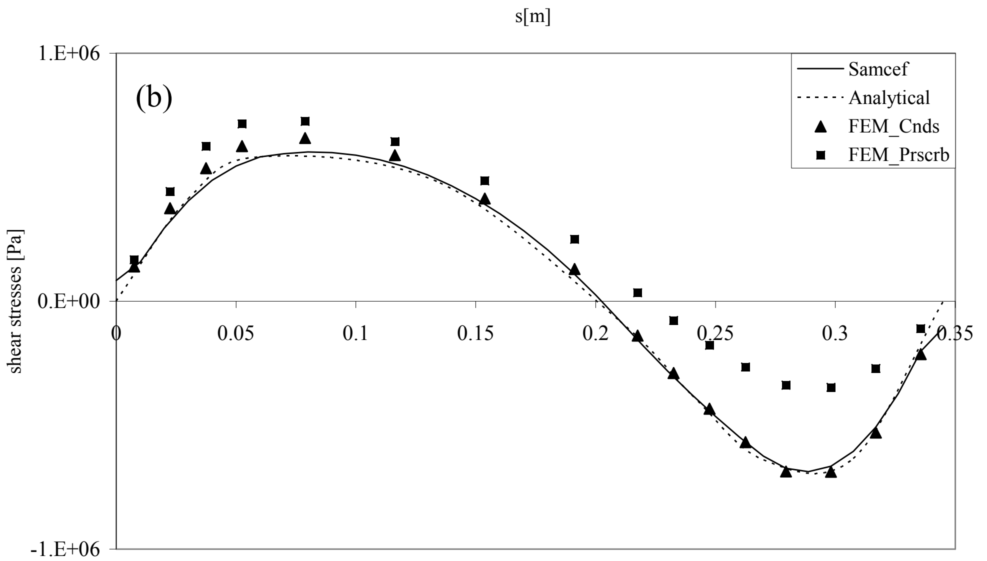

Figure 5.54 shear stresses for x = 1.5m resulting from (a) distortion only; (b) bending, torsion and distortion

Similarly to the previous example, the results –except those concerning warping shear stresses– are done by prescribing the torsional center, the distortional centers and the distortional ratio as being those of a uniform torsional and distorsional case.

Figure 5.54a shows the distribution of distortional warping shear stresses τ_{xs} at x = 1.5m by condensing the location of the distortional centers and the value of the distortional ratio. Since warping shear stresses τ_{xs}^{ω} have a parabolic shaped distribution, 'FEM4' results need refined discretization of the contour by a finite number of nodes and segments (12 transversal segments are used for results FEM4_12 in figure 5.54a…). For Vlassov and Takahashi theories, the shear stresses are computed from normal stresses by using the longitudinal equilibrium equation. The curve FEMPrsc_16 (with 16 transversal segments) presents the erroneous warping shear stresses that would result if the location of the distortional centers is prescribed as being that of a uniform distorsional case. Once again, the difference between prescribing and condensing the location of the distortional centers is found to be very small for the values of the distorsional angle and the normal stresses.

The distance GC_T (in figure 5.47b) between the torsional center C_T and the centroid G and the distance GC_D^1 (in figure 5.47b) between the left distorsional center C_D^1 and the centroid G are found to vary along the longitudinal axis of the beam. The values associated with the uniform torsional (GC_T = 0.0718m) and uniform distortional cases (GC_D^1 = 0.066m) are taken as the reference value in order to compute the differences computed for GC_T and GC_D^1 along the beam length. These differences are maximal at the clamped end for which non uniform torsional and distortional effects are dominant when compared to the uniform torsional and distortional effects. These differences are plotted in figure 5.55.

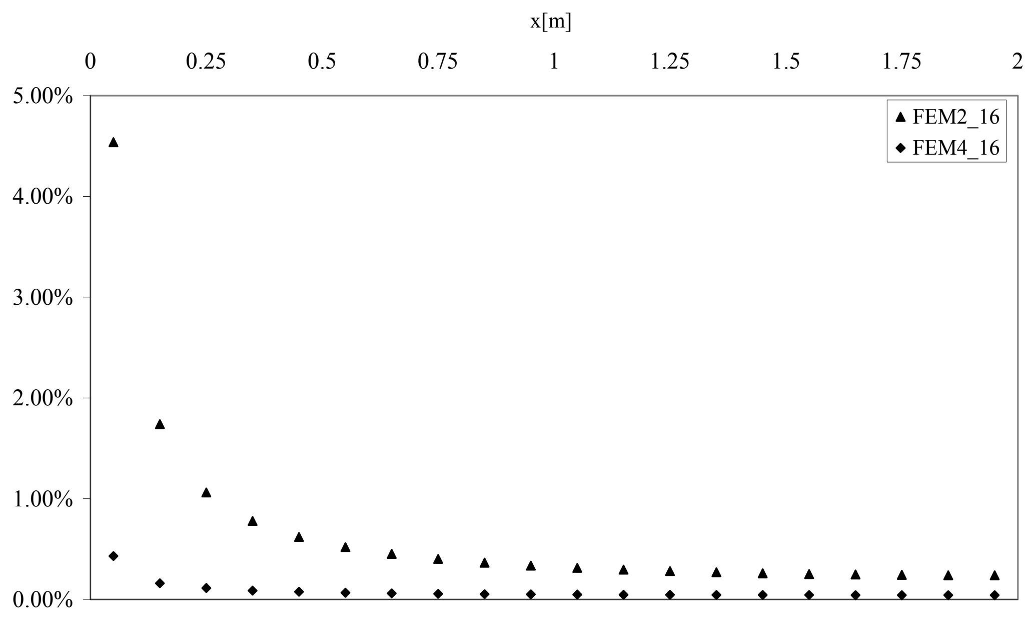

Figure 5.55 Curve FEM2_16: difference for the distance between the centroid and the torsional center; curve FEM4_16: difference for the distance between the centroid and the left distortional center

5.5 Non linear element for buckling analyses

5.5.1 Step by step solution

When the relation between the displacement field and the applied forces is non linear, the solution requires a linearization process and robust numerical algorithms. The non linear problem is transformed into a set of linear problems that follow the evolution of a configuration. The solution follows the equilibrium path in a step by step procedure. The aim is to evaluate equilibrium positions at successive discrete states.

At each step, the equilibrium of the structure must be satisfied and the values of the kinematic and static variables must be determined. This is repeated until the complete solution path has been obtained.

The equilibrium of any deformed configuration is expressed by the virtual work principle. Two forms are given in Appendix 2. The updated lagrangian description is used hereby so that the reference configuration is the last known equilibrium configuration C^i of the structure. The virtual work principle expressed in the current configuration as reference is given by (5.109). Similar developments can be done for any other description.

$$\{R\} = \int_v \overset{*}{\varepsilon}_{ij}\sigma_{ij}dv - \int_v f_{vi}\overset{*}{u}_i dv - \int_a f_{ai}\overset{*}{u}_i da = 0 \tag{5.109}$$

If the current configuration is out of equilibrium, {R} does not vanish and is called the vector of residuals or vector of out-of-balances forces.

All the variables, coordinates, displacements and stresses are known in C^i and are supposed to satisfy (5.109). In order to determine the solution process for the next step (next configuration C^{i+1}), an approximation must be taken for the coordinates of points in C^{i+1}. The computed stresses depend on the path chosen between the two configurations as well as on the integration scheme along this path. Since approximations are done during this process, the stresses will not be in equilibrium with the applied forces and the out of balance forces will not be equal to zero. It is then necessary to search for another configuration that will be closer to equilibrium. An iterative procedure is needed to correct the coordinates and to reach an acceptable configuration closer to equilibrium.

5.5.2 Updated lagrangian formulation

Let {dx} be the vector of nodal coordinate increments. The corresponding increment of the out of balance forces {dR} is related to {dx} by:

$$\{dR\} = [K_T]\,\{dx\} \tag{5.110}$$

where $[K_T]$ is the tangent stiffness matrix defined as the derivative of {R} (5.109) with respect to x. Its expression can be obtained by differentiating (5.109). The differential is in general not simple since the configuration is changing.

To simplify the developments, body forces are only considered in order to shorten the notations. Similar developments can be done for the surface forces. The change in virtual work is expressed between two very close configurations C^i and C^{i+1}. u_i are the unknown increments in the displacements occurring between situation i and situation i+1 at which the two configurations C^i and C^{i+1} are in equilibrium. V is the volume in C^i. F is the incremental applied force assumed to be a deformation independent loading: the load is not affected by a perturbation of the coordinates of C^i. The value of df

which represents the perturbation of the applied loads induced by dx vanishes since the loading is conservative.
In the unknown configuration C^{i+1}, the applied forces, stresses and strains are not known and thus the virtual work is written by taking the known configuration C^i as reference (see Appendix 8, equation A8.24):

$$\{R\} = \int_V \overset{*}{E}_{ij} S_{ij} dV - \int_V \overset{*}{u}_i F_{Vi} dV = 0$$

$$\int_V \overset{*}{E}_{ij} S_{ij} dV = \int_V \overset{*}{u}_i F_{Vi} dV \tag{5.111}$$

The linear part of the E_{ij} Green strain tensor is found to be the infinitesimal strain:

$$\varepsilon_{ij} = \frac{1}{2}\left(\frac{\partial u_i}{\partial x_j} + \frac{\partial u_j}{\partial x_i}\right) \tag{5.112}$$

The incremental strain, stress and applied force decompositions are:

$$E_{ij} = \frac{1}{2}\left(\frac{\partial u_i}{\partial x_j} + \frac{\partial u_j}{\partial x_i} + \frac{\partial u_k}{\partial x_i}\frac{\partial u_k}{\partial x_j}\right) = \varepsilon_{ij} + e_{ij} \tag{5.113}$$

$$S_{ij} = \sigma_{ij} + \Delta s_{ij} \tag{5.114}$$

$$e_{ij} = \frac{1}{2}\left(\frac{\partial u_k}{\partial x_i}\frac{\partial u_k}{\partial x_j}\right) \tag{5.115}$$

In (5.114) the unknown PK2 stress tensor components S_{ij} are decomposed into two parts: one part known at the situation C^i (σ_{ij}) and an unknown increment (Δs_{ij}). F_i are the body forces of the situation C^{i+1} measured in C^i.
For a hyperelastic material (Appendix 0), in case of large displacements but small strain, the second Piola Kirchhoff stress tensor is computed from:

$$dS_{ij} = d_{ijkl} dE_{kl} \tag{5.116}$$

where d_{ijkl} is the stress-strain tensor at the configuration C^i. In practice, d_{ijkl} are constant components of elastic tensor defined in a manner similar to the small deformation ones.

Since C^{i+1} and C^i are very close configurations, the application of (5.116) can be approximated by [see also De Ville 1990 page 5.36…]:

$$\Delta s_{ij} = d_{ijkl} E_{kl} \tag{5.117}$$

By using (5.117), (5.113) and (5.114), equation (5.111) can be written as:

$$\int_V \overset{*}{E}_{ij} d_{ijkl} E_{kl} dV + \int_V \overset{*}{e}_{ij} \sigma_{ij} dV + \int_V \overset{*}{\varepsilon}_{ij} \sigma_{ij} dV = \int_V \overset{*}{u}_i F_{Vi} dV \tag{5.118}$$

This represents a non linear equation for the incremental displacements u_i and thus cannot be directly solved. In order to linearize the equilibrium equations, approximate solutions will be obtained by assuming that:

$$E_{ij} = \varepsilon_{ij} \tag{5.119}$$

By using the approximation (5.119), the non linear term $\overset{*}{e}_{ij}\Delta s_{ij}$ which is a higher order term in u_i will be dropped and the following incremental constitutive equation will be used:

$$\Delta s_{ij} = d_{ijkl}\varepsilon_{kl} \tag{5.120}$$

Thus, the approximate equilibrium equation to be solved is:

$$\int_V \overset{*}{\varepsilon}_{ij} d_{ijkl}\varepsilon_{kl} dV + \int_V \overset{*}{e}_{ij}\sigma_{ij} dV = \int_V \overset{*}{u}_i F_{vi} dV - \int_V \overset{*}{\varepsilon}_{ij}\sigma_{ij} dV \tag{5.121}$$

Due to the non-linearities of the system, linearization will not give an exact solution and iterations may be required within each loading step to approach the exact solution of (5.111).

5.5.3 Discretized equilibrium equations

Since no analytical solution exists for any arbitrary geometry, loading and boundary conditions, numerical buckling calculations are developed with the finite element method. The finite element 'FEM2' based on Timoshenko model for bending and including torsional warping effects is developed for buckling analyses.
As introduced in paragraph 5.2.2, the displacement field is interpolated by:

$$\begin{pmatrix} u_q \\ v_q \\ w_q \end{pmatrix} = [\eta]\{q\} \tag{5.122}$$

where $\{q\}$ is the nodal displacement vector with respect to a cartesian reference base, and $[\eta]$ is given by (5.15).
As it was already noted, the virtual work principle is discretized by using the actualized lagrangian description with C^t as reference. Similar developments can be done with any other description.
Under matrix form, the first term of equation (5.121) can be written as in linear elastic calculations (5.10) as follows:

$$\{q\}^T \left\{ \int_V ([B_L]^T [H][B_L]) dV \right\} \{\delta q\} \tag{5.123}$$

$$K_L = \int_V [B_L]^T [H][B_L] dV \tag{5.124}$$

For the second term of (5.121), identically, a matrix form can be established (see also Prokić1996). The second term can then be expressed as follows:

$$\{q\}^T \left\{ \int_V (\left[B_{NL} \right]^T [\sigma] \left[B_{NL} \right]) dV \right\} \{\delta q\} \tag{5.125}$$

$$K_{NL} = \int_V \left[B_{NL} \right]^T [\sigma] \left[B_{NL} \right] dV \tag{5.126}$$

where [σ] is the Cauchy matrix.

$$[\sigma] = \begin{bmatrix} \sigma_x & 0 & 0 & \tau_{xy} & 0 & \tau_{xz} & 0 \\ 0 & \sigma_x & 0 & 0 & \tau_{xy} & 0 & \tau_{xz} \\ 0 & 0 & \sigma_x & 0 & 0 & 0 & 0 \\ \tau_{xy} & 0 & 0 & 0 & 0 & 0 & 0 \\ 0 & 0 & \tau_{xy} & 0 & 0 & 0 & 0 \\ \tau_{xz} & 0 & 0 & 0 & 0 & 0 & 0 \\ 0 & \tau_{xz} & 0 & 0 & 0 & 0 & 0 \end{bmatrix} \tag{5.127}$$

$$[B_{NL}] = \begin{bmatrix} \frac{\partial}{\partial x} & 0 & 0 \\ 0 & \frac{\partial}{\partial x} & 0 \\ 0 & 0 & \frac{\partial}{\partial x} \\ \frac{\partial}{\partial y} & 0 & 0 \\ 0 & 0 & \frac{\partial}{\partial y} \\ \frac{\partial}{\partial z} & 0 & 0 \\ 0 & \frac{\partial}{\partial z} & 0 \end{bmatrix} \{\eta\} \tag{5.128}$$

B_{NL} is a matrix relating the deformations to the nodal displacements.

By denoting the tangent matrix K_T with $K_L + K_{NL} = K_T$, the equilibrium equations can be written with a weak form by using the actualized lagrangian configuration as follows:

$$[\ K_T]\ \{q\} = \{R\} - \{F\} \tag{5.129}$$

{F} includes the finite element evaluation of internal forces:

$$\{F\} = \int_v \left[B_L \right]^T [\sigma] dv \tag{5.130}$$

{R} is the finite element evaluation of applied loads as in paragraph 5.2.4.

5.5.4 Tangent Stiffness matrix calculation

The displacement at any point is deduced from the 6+n degrees of freedom as follows:

$$\begin{Bmatrix} u_q \\ v_q \\ w_q \end{Bmatrix} = \begin{Bmatrix} u_0 \\ 0 \\ 0 \end{Bmatrix} + \begin{Bmatrix} z\theta_y \\ 0 \\ w \end{Bmatrix} + \begin{Bmatrix} -y\theta_z \\ v \\ 0 \end{Bmatrix} + \begin{Bmatrix} -\omega\theta_{x,x} + \sum_{i=1}^{n}\Omega^i(y,z)u_i(x) \\ -(z-z_C)\theta_x \\ (y-y_C)\theta_x \end{Bmatrix} \tag{5.131}$$

The interpolation functions are used and the calculation of B_{NL} is based on the following calculations:

$$\begin{Bmatrix} u_{,x} \\ v_{,x} \\ w_{,x} \\ u_{,y} \\ w_{,y} \\ u_{,z} \\ v_{,z} \end{Bmatrix} = \begin{Bmatrix} \langle N'_u\rangle\{q_{u_0}\} \\ 0 \\ 0 \\ 0 \\ 0 \\ 0 \\ 0 \end{Bmatrix} + \begin{Bmatrix} z\langle N'\rangle\{q_{\theta_y}\} \\ 0 \\ \langle N'\rangle\{q_w\} \\ 0 \\ 0 \\ \langle N'\rangle\{q_{\theta_y}\} \\ 0 \end{Bmatrix} + \begin{Bmatrix} -y\langle N'\rangle\{q_{\theta_z}\} \\ \langle N'\rangle\{q_v\} \\ 0 \\ -\langle N'\rangle\{q_{\theta_z}\} \\ 0 \\ 0 \\ 0 \end{Bmatrix} + \begin{Bmatrix} -\omega\langle N''\rangle\{q_{\theta_x}\} + \sum\Omega^i(y,z)\langle N'_u\rangle\{q_{u_i}\} \\ -(z-z_C)\langle N'\rangle\{q_{\theta_x}\} \\ (y-y_C)\langle N'\rangle\{q_{\theta_x}\} \\ -\omega_{,y}\langle N'\rangle\{q_{\theta_x}\} + \sum\Omega_{,y}{}^i(y,z)\langle N_u\rangle\{q_{u_i}\} \\ \langle N\rangle\{q_{\theta_x}\} \\ -\omega_{,z}\langle N'\rangle\{q_{\theta_x}\} + \sum\Omega_{,z}{}^i(y,z)\langle N_u\rangle\{q_{u_i}\} \\ -\langle N\rangle\{q_{\theta_x}\} \end{Bmatrix} \tag{5.132}$$

$$B_{NL}=\begin{bmatrix} \langle N'_u\rangle & & & -\omega\langle N''\rangle & z\langle N'\rangle & -y\langle N'\rangle & \Omega^i\langle N'_u\rangle \\ & \langle N'\rangle & & -(z-z_c)\langle N'\rangle & & & \\ & & \langle N'\rangle & (y-y_c)\langle N'\rangle & & & \\ & & & -\omega_{,y}\langle N'\rangle & & -N & \Omega^i{}_{,y}\langle N_u\rangle \\ & & & \langle N\rangle & & & \\ & & & -\omega_{,z}\langle N'\rangle & \langle N\rangle & & \Omega^i{}_{,z}\langle N_u\rangle \\ & & & -\langle N\rangle & & & \end{bmatrix} \tag{5.133}$$

$$B_{NL}{}^T=\begin{bmatrix} \{N'_u\} & & & & & & \\ & \{N'\} & & & & & \\ & & \{N'\} & & & & \\ -\omega\{N''\} & -(z-z_c)\{N'\} & (y-y_c)\{N'\} & -\omega_{,y}\{N'\} & \{N\} & -\omega_{,z}\{N'\} & -\{N\} \\ z\{N'\} & & & & & \{N\} & \\ -y\{N'\} & & & -\{N\} & & & \\ \Omega^i\{N'_u\} & & & \Omega^i{}_{,y}\{N_u\} & & \Omega^i{}_{,z}\{N_u\} & \end{bmatrix} \tag{5.134}$$

5.5.5 Solution procedures

The incremental iterative technique, implemented for solving the nonlinear system of equations (5.129), combines the Newton Raphson method with the constant arc length of incremental displacements. It assumes that the solution is known at an initial discrete step (t), and iterations are performed to calculate the (t+1) equilibrium configuration by considering the equilibrium between the exterior load forces and the nodal interior forces (equivalent to stresses in the element). Critical loads are calculated by taking into consideration that the structure, already in equilibrium, reaches instability if there is more than one equilibrium position for the same loading level. The criterion to determine this buckling state is the singularity of the tangent stiffness matrix $[K_T]$ of the structure. This solution procedure is fully described in Appendix A9.

5.5.6 Applications to buckling problems of thin walled structures

The influence of non uniform torsional warping on the flexural torsional buckling of elastic thin walled structures is analyzed and discussed by comparing different kinematical formulations. The proposed warping function offers the advantage of automatic data generation and geometrical characteristic computations of arbitrary asymmetric cross sections. The 3D nonlinear finite element beam model, based on developments in paragraphs 5.5.3 & 5.5.4, is validated for various profile geometries and loading cases by comparison with existing analytical solutions. The following numerical examples involve the minimal discretisation required for the geometrical description of the contour profile: 4 transversal nodes and 4 transversal segments are required for a rectangular tubular profile, 6 nodes and 5 segments are required for an I profile... Besides, the shear center is prescribed to be that of uniform torsion (as in Vlassov or Benscoter computations).

Example 1: Plane frame flexural buckling

The first example illustrates the plane flexural buckling of a portal frame (Figure 5.56a). The columns and the beam of the frame are identical and the closed cross section is given in figure 5.56b. E = 210GPa, G = 80GPa.

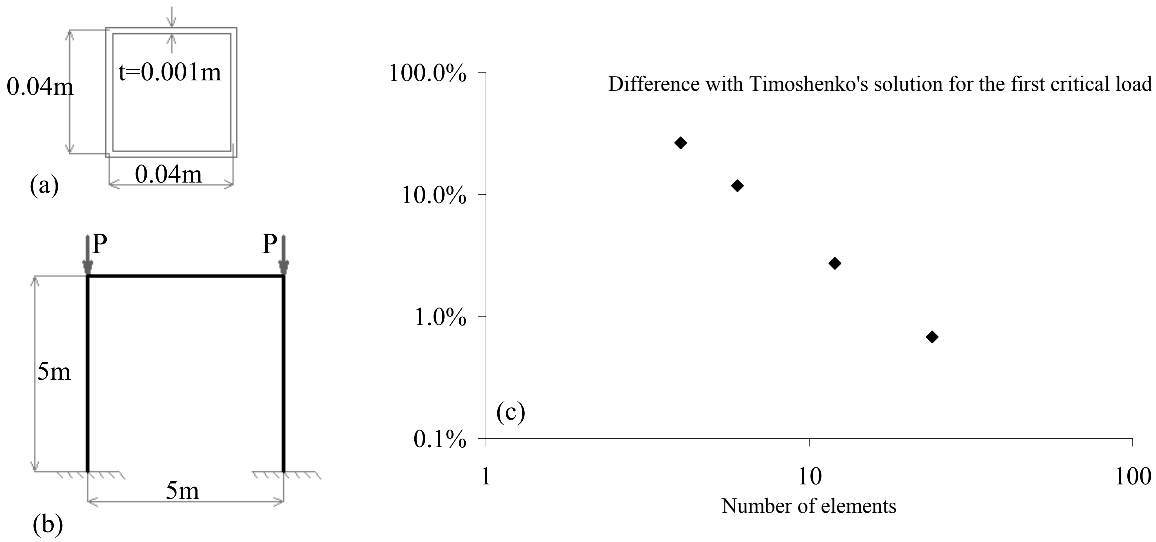

Figure 5.56 Buckling of a frame consisting of members with closed cross section

The frame buckles first in a sway mode in bending. The difference between the finite element results and the solution given by Timoshenko (1961) is shown in Figure 5.56c. The numerical value of the first critical load converges to the value given by the analytical solution of Timoshenko (P_{cr} = 652N) when the total number of elements increases.

Example 2: Pure torsional buckling of a column

A column with a cruciform section submitted to an axial load is considered (Figure 5.57). The thickness of the walls is t = 4mm. L = 1m, G = 80.8GPa, E = 210GPa.

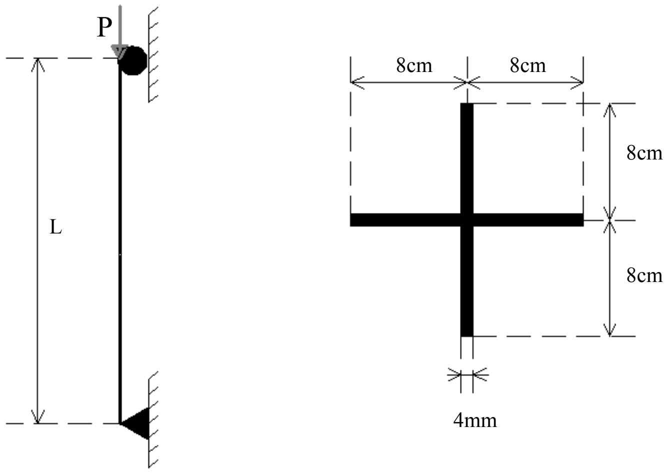

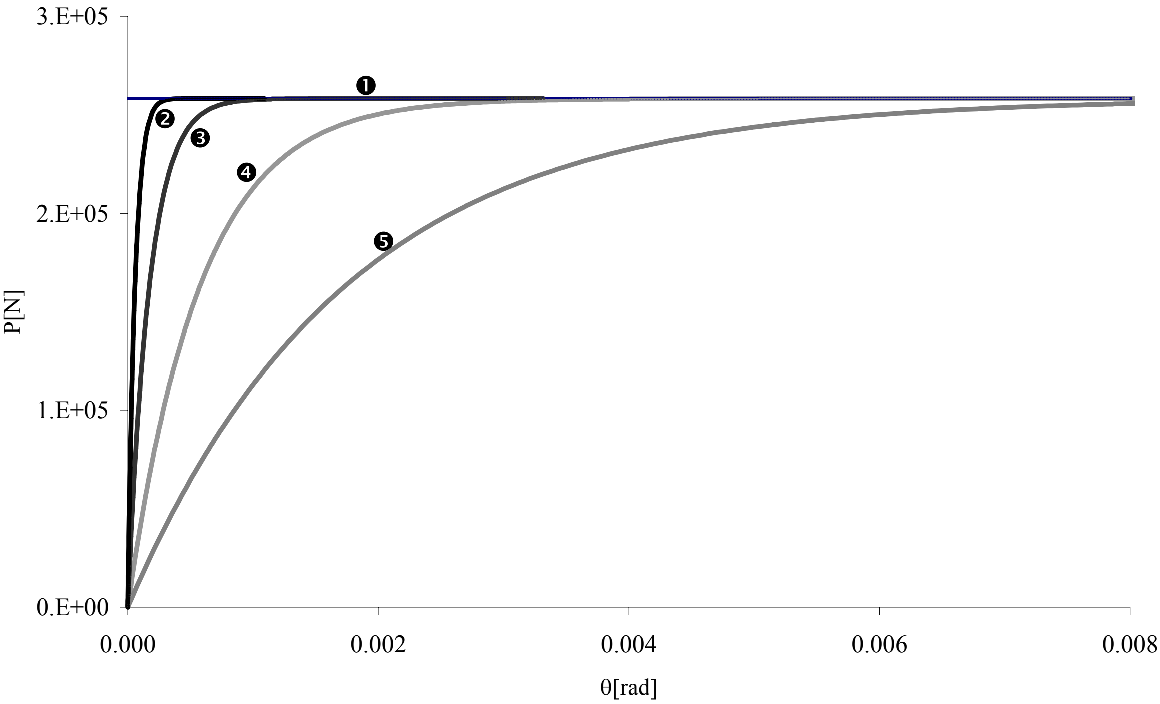

Figure 5.57 Torsional buckling of a column with cruciform cross section

According to Vlassov theory, this kind of cross section does not warp. The theoretical torsional Eulerian buckling load is 258398N. To initiate the torsional buckling of the column, a small perturbation is needed in the finite element analysis; this is introduced by applying a small torsional moment M_x at mid height of the column. Figure 5.57 gives the relationship between the axial load and the angle of twist at mid height for increasing values of P and M_x. The horizontal line ❶ is the critical load 258398N. The curves represent the geometrical non-linear variation of the angle of twist at mid height for different values of the ratio M_x/P: $M_x/P = 5.10^{-7}$ m for the curve❷, 15.10^{-7}m for❸, 5.10^{-6} m for❹ and 15.10^{-6} m for❺. The relationship between the load and the angle of twist is obviously influenced by the magnitude of the applied torsional perturbation, but all curves reach asymptotically the level of the elastic buckling load corresponding to pure torsional buckling.

Example 3: Flexural torsional buckling of a column

A column with an open monosymmetric cross section is submitted to an axial load passing through the centroid (Figure 5.58): L = 20m, E = 210GPa, G = 80GPa.

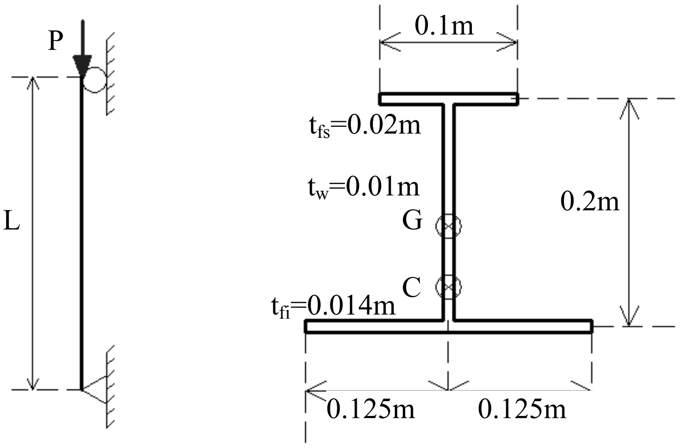

Figure 5.58 A column with open monosymmetric cross section

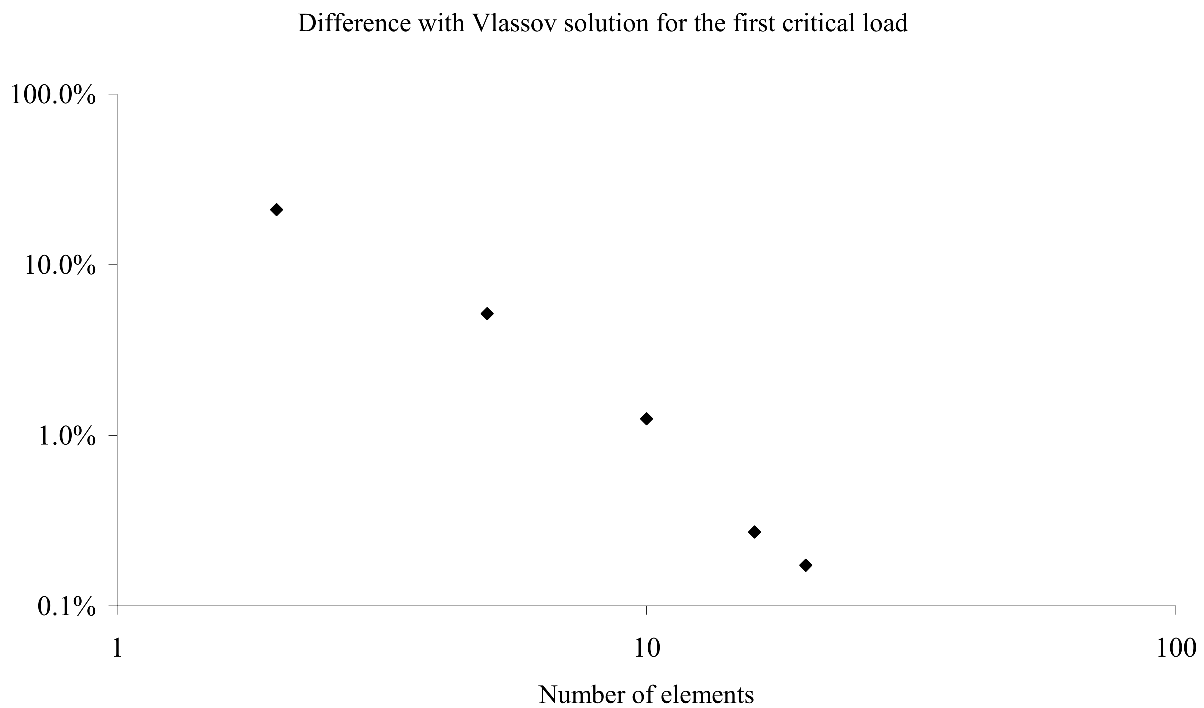

Figure 5.59 Buckling analysis of a column with open monosymmetric cross section

Numerical results are compared with two analytical solutions. The first one is based on Vlassov theory for columns with open cross sections and the second is based on the proposed warping function. The

non linear buckling equations are developed from a state of combined torsion, bending and axial compression. They are obtained from general equilibrium equations written for the deformed beam or column. The solution is given by taking into consideration the boundary conditions.
The first critical load is computed by using Vlassov theory. The analytical result (P_{cr} = 102223N) is then compared with the one based on Prokić warping function. The two analytical calculations give similar results with a difference of 0.0001%. The difference between the finite element solution and the reference value based on Vlassov theory is illustrated in Figure 5.59.

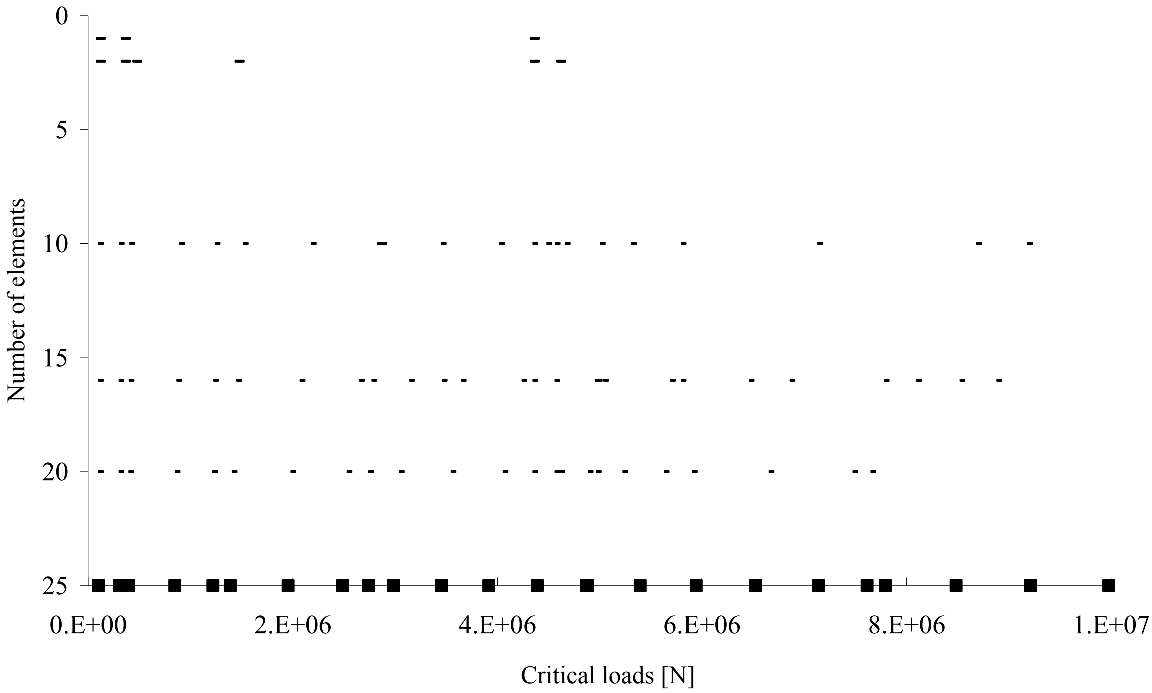

Figure 5.60 Critical loads for the centrally loaded column (figure 5.58)

In a general flexural torsional buckling of a beam-column, the (xy) bending modes, the (xz) bending modes and the twisting modes are coupled. The first-order theory gives three homogeneous equations and represents an eigenvalue problem. When, the shear center (C) and the centroid (G) coincide, the equations are uncoupled and the solution gives a discrete set of buckling modes. The lowest critical load is, in general, of practical significance. When C and G do not coincide (examples 1 and 2), buckling involves simultaneously torsion and bending, and the critical load is lower than if torsional effects are ignored.

Numerically, when the number of finite elements increases, the number of detected critical loads increases. Figure 5.60 shows the critical values obtained for the same example (figure 5.58) up to 10MN. The squares along the horizontal axis of figure 5.60 represent the reference values of the buckling loads (based on Vlassov theory). The other sets of values correspond to buckling loads detected by finite element analyses with increasing number of elements (1, 2, 10, 16 and 20 elements). For one element, there are only three critical values when the applied load P increases from zero to 10MN. For two elements, the numerical values of buckling loads are improved and other critical loads appear and so on... Each critical value converges to the reference solution when the number of elements increases.

Example 4: Lateral torsional beam buckling

An I beam (Figure 5.61) is loaded by two couples at its ends and is therefore submitted to uniform bending. L = 20m, E = 300GPa, G = 99.5GPa. The critical value of the bending moment corresponding to the lateral torsional buckling is computed analytically by using Vlassov warping function (M_{cr} = 6262.26Nm). Figure 5.61b shows how the numerical solution converges to the reference solution based on Vlassov theory.

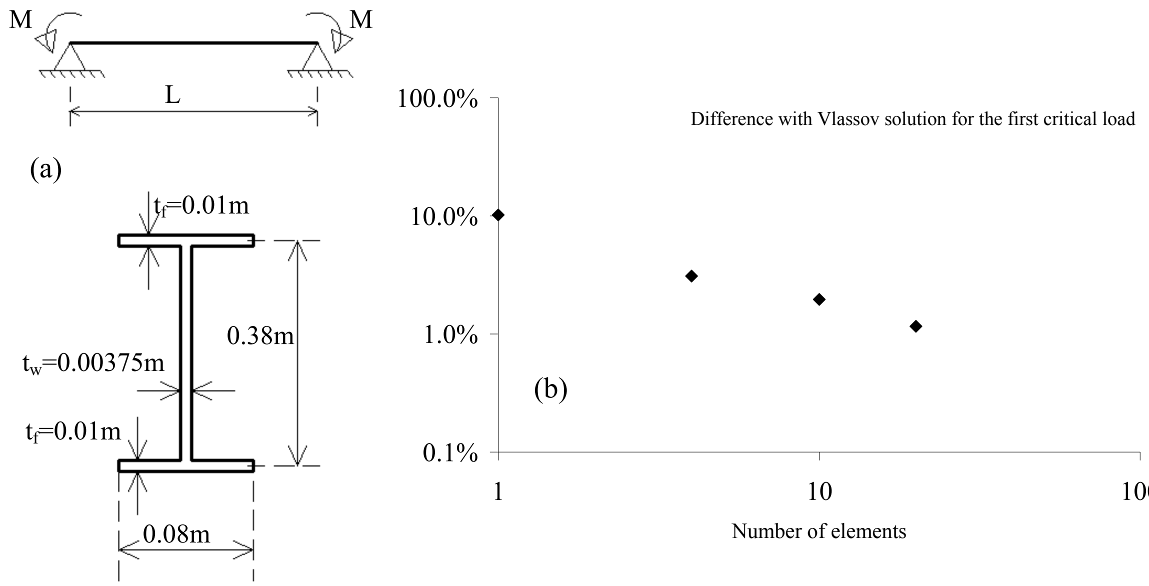

Figure 5.61 Lateral torsional buckling of an I beam

Example 5: Buckling of a one-celled monosymmetrical cross section

A column (Figure 5.62a) submitted to an axial load and a beam (Figure 5.62b) submitted to uniform bending are considered. The cross section (Figure 5.62c) consists of one cell and two walls. L = 20m, E = 206GPa, G = 82.4GPa. The analytical solution of this problem was already presented in paragraph 4.4.7.

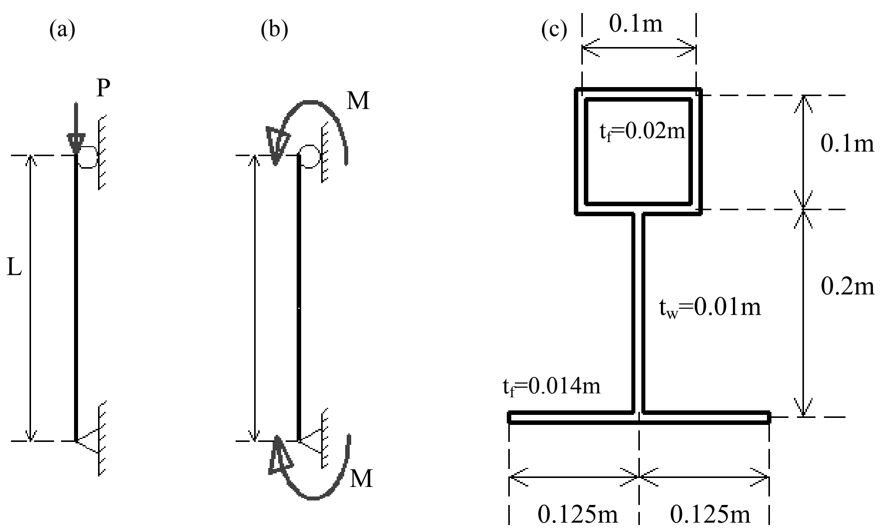

Figure 5.62 Flexural torsional and lateral torsional bukcling of an I beam with one cell

For the first case (figure 5.62a), the lowest critical load is a coupling of flexural and torsional buckling. The difference between the analytical value (161kN; see table 4.2) and the present finite element solution is 21.53% for a two finite element discretization and 0.79% for a ten finite element discretisation.

In the second case, the beam (Figure 5.62b) is subjected to a uniform plane bending that induces compression in the thin walled cell and traction in the bottom flange. In this case of lateral torsional buckling, the differences between the present finite element and the analytical calculations (528Nm; see table 4.2) is 8.82% for a two finite element discretization and 1.01% for a ten finite element discretisation.

Example 6: Buckling of columns with different cross sections

A column with two different cross sections (1) and (2) is submitted to an axial load P (Figure 5.63b). The thickness is constant and equal to 20mm, E = 200 GPa, G = 80 GPa, L_1 = 6m, and L_2 = 14m.

Two cases are considered:

- two thin rectangular profiles as in figure 5.63a,
- I and U profiles as in figure 5.63c.

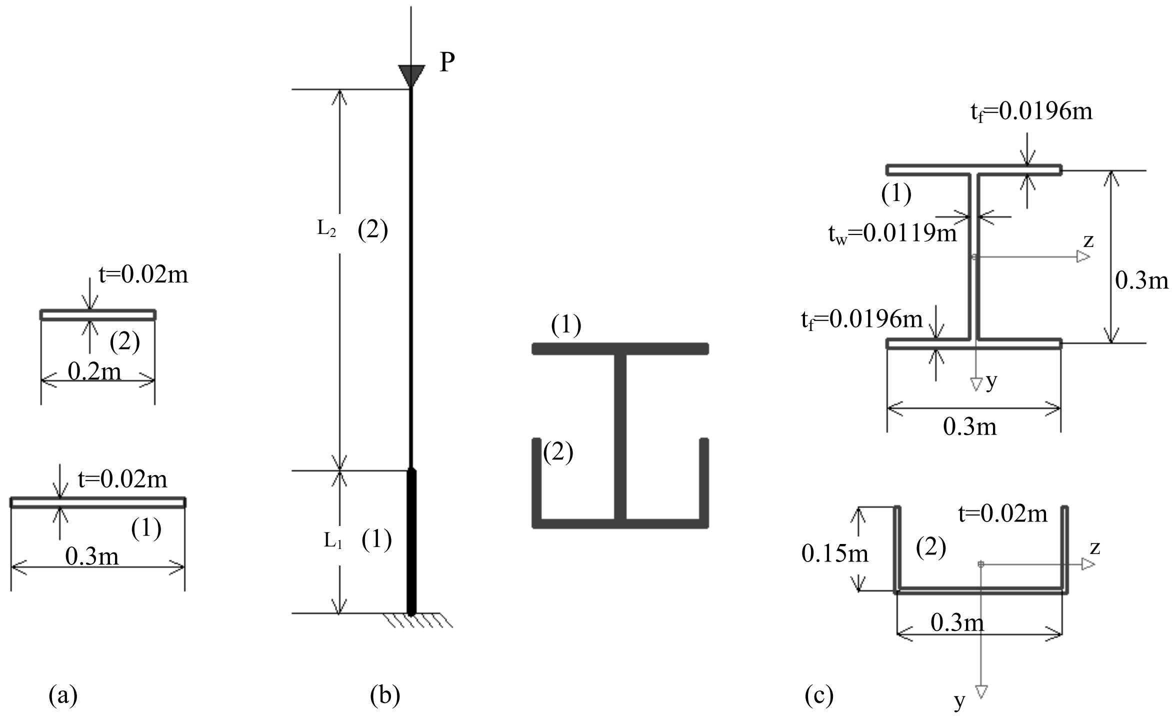

Figure 5.63 A column (b) with two cases of a change in the cross sectional geometry: case (a) and case (c)

For the first case, a method for estimating theoretically the Eulerian flexural buckling load of such a column with different cross sections can be found in (Timoshenko 1961); the value obtained for the critical load is 200.3N. Other solutions (table 5.8) give higher values since they derive from energy methods. By performing an Eulerian stability analysis with shell elements (Samcef; Samtech s.a. 2002), P_{cr} is equal to 201.2N. The Eulerian stability analysis with Samcef beam elements (that include Saint Venant torsional theory) gives also an acceptable solution since the contour warping vanishes for the thin rectangular profiles. The buckling load obtained by a buckling analysis with 20 present beam elements is P_{cr} = 201.4N.

Table 5.8 Flexural buckling loads

	Pcr [N]
Timoshenko, exact method	200.3
Timoshenko, approximated method	202.0
Samcef beam, 50 elts	201.9
Samcef shell, 1840 elts	201.2
Present beam finite element, 20 elts	201.4

For the second case (with the cross sections I and U given in Figure 5.63c), the difference between the values of the first critical load found by an analysis with shell elements (880 elements, P_{cr} = 65.64kN) and the present finite element analysis (20 beam elements) is 0.4%.

CHAPTER 6. CONCLUSIONS AND RECOMMENDATIONS

In this chapter, the previously stated objectives are shown to be met within the presented work. A summary of the principal key points of the thesis is followed by a general discussion of the results. The main achievements and conclusions of the work are provided. Several areas of further research that could complete the work presented in this dissertation are suggested.

6.1 Objectives

This thesis has investigated the behavior of thin walled 3D beam structures with arbitrary profiles. The main objectives have been:

- a detailed understanding of mechanical behaviors such as non uniform torsion, shear bending and distortion,
- the elaboration of an efficient theoretical formulation and the implementation of the associate finite element model in order to analyze:
    - uniform and non uniform torsion
    - bending shear effects
    - distortion

  of thin walled beams by using a single warping function for:
    - a broad variety of cross sectional shapes comprising multiple branches and cells
    - asymmetrical profiles where the shear center does not coincide with the centroid
    - partial transmissions of warping in beam assemblies...

6.2 Complexity

Thin walled beams are usually cold formed from flat strips or welded from thin plates, resulting in a wide variety of cross sectional shapes and forms. Their behavior is poorly described by elementary formulations for which the mechanical components are reduced to stretching, bending and uniform torsion. In practical applications, large shear strains and stresses are exhibited. A significant non uniform warping arises from restrained supports and from general non uniform distributions of shear forces, torsional moments, torsional bimoments or other resultants associated with the in-plane deformation of the entire cross section, and called within this dissertation distortional moments and bimoments.

The representation of these important effects in structural applications was a big challenge: approaching the intricate problem by a simplified and ‘computationally manageable’ formulation. Several complex mechanical aspects had to be taken into consideration in order to obtain an accurate representation of the real structural behavior.

6.3 Research topics

The reviewed research that describes the main topics concerned with the present work was presented in the first part of the dissertation ‘Overview’.
In chapter 1, some basic assumptions and computations were surveyed for thin walled beam analyses. The complexity of the relevant computational schemes was highlighted and the present work was positioned by comparison with published literature. Even at the early stage of bibliographical work, difficulties arose from abundant and diversified literature concerning the subject, lack of early publications or translations, unclear correlations between approximations and conclusions, missing links or justifications…
The objective of improving the understanding of the mechanical components of existing thin walled beam theories was met in Chapter 2. The concept and history of main theories have been discussed in order to improve the understanding of the mechanical behavior and to prepare the theoretical and numerical developments presented in parts II and III.
The performance of any beam method for the calculation of shear bending effects was shown to depend closely on adequate correction factors. The shear correction factor in Timoshenko formulation was found to depend on the geometrical aspect of the cross section, and particularly whether the profile does comprise or does not closed cells. In the kinematical description of the displacement field in high order bending shear theories, some coefficients were found to depend on the geometrical shape of the cross section.
Some remarks and results have been correlated with the undertaken assumptions: torsional shear stresses found to be zero when computed from Vlassov kinematics, Vlassov warping function inadmissible for closed profiles, erroneous torsional moments when computed as internal resultants of stresses resulting from Benscoter kinematics, influence of the thickness warping function, deducing the thickness warping from the normality assumption of thin plates, limitations of Prokić analyses concerning the torsional behavior of monosymmetrical and asymmetrical profiles… The mechanical interpretation of some assumptions, approximations and relations has been improved: identifying the distortional behavior as located somewhere between local and global classifications, selecting ‘global’ distortional modes, computing local plate bending due to the membrane stiffening, describing the bi-rotation of ‘hinged’ profile frame, calculating the coordinates of the distortional centers, evaluating the distortional centers and joints dependency…
A brief presentation of elastic buckling of beams and columns was followed by analytical developments using Benscoter warping function for the calculations of flexural-torsional and lateral-torsional buckling in the case of a multi-branched profile comprising a closed cell.

6.4 Methodologies

Based on the knowledge and the in depth assessments of Chapter 2, a unified approach with a single warping function has been formulated in this work in order to compute the response of thin walled beams with arbitrary profiles. Starting from Prokić work, the contour warping was represented by a linear combination of longitudinal displacements at cross sectional nodes. The expression ($\sum\Omega^i u_i$), involving a sum of variables with constant ‘coefficients’ placed in front of each, allows a separation between:

- *the variables* ‘u_i’ which are longitudinal displacements varying with the longitudinal beam coordinate (x);

and

- *the functions* 'Ω^i' which are constant with respect to x and linear with respect to the cross sectional contour coordinate (s).

This warping function, presented in Chapter 3, is very general since –unlike Vlassov, Benscoter, Takahashi warping functions or high-order bending theories– its qualitative distribution over a cross section is not predetermined or associated with a specific problem (e.g. torsional, distortional, shear bending…). One of the main achievements of this thesis was to develop adequate enhancements of this general warping function in order to qualitatively and quantitatively reflect and capture the nature of mechanical behaviors. Specific constraints linked to different mechanical effects had to be introduced at both kinematical and equilibrium levels.

At the kinematical level, constraints have been prescribed in order to dedicate the general expression ($\sum\Omega^i u_i$) to a specific mechanical warping (torsional, distortional or bending shear). These constraints, developed in Chapter 3, concern the expression of the displacement field. They are found by linking the warping degrees of freedom to one specific physical sub-problem and by decoupling this problem from the other stretching, bending, torsional and/or distortional terms. The satisfaction of these kinematical relations resulted in a twofold uncoupling at the level of the virtual work principle and the resulting equilibrium equations:

(i) the dependency of normal forces and bending moments on torsional and distortional warping degrees of freedom was relaxed;

(ii) the contribution of stretching and bending rotational degrees of freedom –when not involved in warping– in the computation of bimoments and warping resultants disappeared.

At the equilibrium level, additional relations were formulated in order to eliminate similar twofold dependencies:

(i) bending shear forces from torsional and distortional degrees of freedom; torsional moment from distortional warping degrees of freedom…;

(ii) torsional and distortional moments and bimoments from bending degrees of freedom and so on…

Other requirements –such as the no shear boundary condition in bending, the dependency between distortional joint and centers…– contributed to the definition of the mechanical problem. In order to capture the physical problem, all the previously described constraints –most were already used in the uncoupling process– have been re-introduced in the proposed formulation according to the following classification:

– those involving undetermined torsional and distortional characteristics have been used in order to condense and evaluate these unknowns (coordinates of the torsional center, coordinates of the distortional centers, distortional rotation ratio);
– those driven at the stage of the displacement field description have been added to the equilibrium equations in order to identify the nature of warping represented by the additional degrees of freedom u_i.

6.5 Result summary and discussion

The building of a robust method that efficiently captures many complex physical behaviors has been a cautious and tedious task. Simple techniques of identifying, superposing and decoupling the different mechanical components constituted a crucial key of success for the developing process. The ability of the proposed model to capture the response of thin-walled beam structures was assessed under various loading cases by developing analytical formulations for simple problems (chapter 4) and finite element models for complete 3D beam structures (chapter 5). The results may be discussed in five different categories: (i) torsional behavior, (ii) flexural behavior, (iii) distortional behavior, (iv) buckling and (v) discussion on the general concept and suitability of warping functions and location of torsional and distorsional centers.

6.5.1 The torsional behavior

The first developments handled the torsional behavior of thin walled beams. A 2-node beam element (FEM1) included the normality assumption (Bernoulli theory) for bending and related n warping degrees of freedom –where n is the number of transversal nodes of the beam element profile– to the torsional behavior. This finite element model is based on a linear polynomial interpolation of torsional rotations and warping degrees of freedom. Exact solutions were found with minimum finite element discretization for the following cases of uniform torsion, i.e.:

- the case of a uniform variation of warping and of torsional moment distribution along the beam length;
- the case of arbitrary loading and boundary conditions for particular thin profiles with zero warping (e.g. those presenting radial symmetry…).

However, for the remaining cases, the influence of non uniform torsional effects was not captured accurately since the exact solution consists in an exponential-varying torsional rotation and warping along the longitudinal beam. Numerical examples in Chapter 5 showed that 'FEM1' gave acceptable results in the case of minor non uniform torsional effects and behaved rather poorly in the case of strong non uniform torsional effects. This motivated the implementation of a 3-node beam element (FEM2) by applying linear interpolation functions for longitudinal displacements and quadratic shape functions for the other degrees of freedom. The resulting finite element is based kinematically on Timoshenko model for shear bending and on relating the warping degrees of freedom to non uniform torsional effects.

A wide variety of beam structures with different profile geometries was analyzed for various loading cases. The torsional rotation, the amount of warping as well as normal and shear stresses were computed. The numerical examples of Chapter 5 showed an excellent agreement with analytical computations including Vlassov theory for open profiles and Benscoter theory for closed profiles, with shell finite element simulations in Samcef (Sametch s.a.) and with some published results from the literature. The accuracy of 'FEM2' was shown to depend on the finite element discretization that aims at approaching the exponential –with respect to the longitudinal axis x– nature of the response by polynomial functions. It could be concluded that, for a standard beam member, a discretization with ten elements gives reasonable accuracy while a twenty element discretization gives an excellent agreement. Similarly to other contributions, warping restraints were found to have a strong impact on the beam response. Partial or full warping restraints were shown to stiffen significantly the torsional behavior of beam structures, particularly for open profiles exhibiting an important non uniform torsional behavior. The accuracy was also assessed in the case of beam assemblies with different shaped profiles where the connection type determines the nature of the warping transmission. The discontinuity of warping at the assembly point was found to influence strongly the beam response.

6.5.2 The flexural behavior

The 2-node finite element 'FEM1' with Hermitian cubic shape functions gave –as expected and well known in the literature– the exact solution of Bernoulli. The assumption of Bernoulli theory was shown to be unacceptable in some cases, especially for short beams with high and thin profiles. The 3-node finite element, based on Timoshenko, has been modified by a reduced integration scheme for the stiffness terms associated with shear bending effects in order to avoid the shear locking problem. Exact solutions were found in the cases of linear and quadratic distributions of bending moment. The shear correction factor was also introduced. The resulting modified ‘FEM2’ gave an excellent agreement with the modified Timoshenko analytical solution under uniformly distributed applied loads.

The necessity of an automatic and unified computational method of the shear correction factor constituted an additional motivation for adapting the present warping function to bending shear warping effects. Full developments (FEM3) aimed therefore at capturing the influence of warping due to shear bending. The effects of shear deformation on the beam deflection were evaluated for different profile forms and dimensions: rectangular cross sections with different height/width ratios, an open asymmetrical profile with many branches, a high thin profile comprising closed cells. It was concluded that the benefit of including shear bending warping in order to predict the displacements of a structure is marginal when compared to the benefit of including torsional warping. The accuracy gained in computing torsional warping, when compared to the Saint Venant solution, was found to be much more important than the accuracy gained in computing bending shear warping, when compared to the modified Timoshenko solution. As a result, it was suggested to keep the modified 3-node element ‘FEM2’ for the general analysis of 3D beam structures and to apply the developments including bending shear warping effects for the calculation of the shear correction factor only. Since the proposed warping function allows automatic and accurate computations for arbitrary profiles, ‘FEM3’ was included as a ‘black box’ in ‘FEM2’ in order to compute the shear correction factor before analyzing the flexural behavior of a 3D beam structure with the modified Timoshenko model.

6.5.3 The distortional behavior

Additional developments involved the distortional behavior of thin walled profiles. The kinematics of this work (and particularly the general warping function $\sum\Omega^i u_i$) was adapted and introduced in a finite element model (FEM4) in order to capture the response of a structure exhibiting one mode of distortional behavior. The mechanical nature of profile distortions was defined and described in an approach similar to that currently used by Takahashi. Important similarities have been identified between the distortional theory and the torsional theory with uniform and non uniform effects. The torsional mode was found to be a particular mode of the distortional modes. The cross sectional distortion was identified as being induced by particular external loads which are statically equivalent to zero. The resulting stresses attenuate very slowly along the length of the beam. The location of distortional centers and the distortional rotational ratio were determined. An excellent agreement was found between ‘FEM4’ results and other results involving Takahashi analytical beam theory and numerical shell computations using the commercial code Samcef for the distortional rotation, normal and shear stresses distributions. The influence of the distortion on the stresses, usually ignored in thin-walled beam designs, was shown to be important when compared to bending and torsion even in simple loading cases (e.g. second example in paragraph 5.4.4).

6.5.4 Buckling

A non linear finite element based on the updated lagrangian formulation was developed by including Timoshenko kinematics and torsional warping degrees of freedom for 3D thin walled beam structures. An incremental iterative method using the arc length and the Newton-Raphson methods were used to solve the non linear problem. The resulting non linear finite element model was validated for beams, columns and frames submitted to various loading cases. Numerical computations of critical loads were compared with analytical solutions using Vlassov or Benscoter warping functions, and to numerical simulations with shell finite elements. The proposed finite element was found to converge to reference solutions when mesh is refined. It was shown again that, for a single beam, an acceptable agreement is found for a discretization with ten elements and an excellent agreement is found for a twenty elements discretization. The present non linear element was able to capture the pure flexural, pure torsional, flexural torsional and lateral torsional buckling of beam structures with different forms of profile (monosymmetrical, asymmetrical, open, comprising cells…).

6.5.5 Discussion on warping functions and locations of torsional and distortional centers

The simplest solution of a torsional problem corresponds to the case of a uniform distribution of cross sectional warping along the beam axis. The corresponding theory, commonly known as the de Saint Venant method, restricts its applications to a few exceptional cases. The non uniform torsional behavior is extremely complex and an exact theory involves unfortunately laborious mathematical complications for general cases of profile geometries, torsional loading and boundary conditions. Approximate theories have been developed for thin walled beams. Open profiles are commonly analyzed by Vlassov theory which assumes an inflexible cross sectional contour. Warping shear strains are assumed to vanish in the middle surface of the thin walled structure and the out of plane displacement (or warping) of the profile is obtained as a function of the rotating angle. Starting from the kinematics of this approximate theory, the longitudinal warping stresses are also expressed as a function of the rotating angle while shear warping stresses are found to be equal to zero.

Closed thin walled profiles have been analyzed by approximate theories based on the assumption that the distribution of warping is the same as in the case of uniform torsion. A new parameter is introduced and is found to depend on the angle of rotation of the profile. Longitudinal warping stresses are found to be function of this new parameter while shear stresses cannot be derived directly from the kinematics but have to be found by other methods.

Within the previously overviewed methods, and as a result of the undertaken approximations, the warping function and the location of the torsional centers were found to depend only on the geometry of the cross section.

Within this thesis work, it was shown how these approximations were relaxed. The warping function and the torsional center do not represent a pure characteristic of the profile geometry. They depend on the solution of the problem, and thus, on the applied loading and on the boundary conditions. These more general computations give accurate analyses in the cases where shear warping stresses at the midwall are large (e.g. short beams with thin profiles).

The location of the shear center, as computed by Vlassov for open asymmetrical profiles or by Benscoter for closed asymmetrical profiles, is found with the present analyses in the case of uniform torsion; i.e. the case of uniform distribution of torsional moment and free warping. For this particular loading case and boundary conditions, the present finite element calculations give exactly the location of torsional center as computed by Vlassov and Benscoter. This coincidence could be expected since Vlassov and Benscoter theories do not take into account warping shear stresses in their kinematical formulations. In the case of a uniform torsional case, warping shear stresses vanish and the present finite element results coincide with those of Vlassov and Benscoter. However, in general loading cases and boundary conditions, Vlassov and Benscoter computations use the same warping function and torsional center –as in the case of absence of warping shear stresses– while the present computations do not. If the location of the torsional center is prescribed in the finite element computations as being that of uniform torsion, the torsional rotation and longitudinal stress distributions are found to be those of Vlassov and Benscoter. However, erroneous shear stresses are obtained if calculated from the kinematics by using Hooke's law. This error vanishes for bisymmetrical profiles and gets larger with increasing distance between the torsional center and the centroid.

Similar observations were found for the distortional behavior. The locations of the distortional centers were found to be exactly those of Takahashi in the case of uniform distortion (uniform distribution of distortional moment and free warping along the length of the beam) without taking into account the local plate bending. Similarly to the torsional behavior, the location of the distortional center and the amount of warping were found to vary along the beam in general loading cases and boundary conditions.

6.6 Suggestions for further works

The introduction of this thesis stated that the main aim of this work was to investigate 3D thin walled beam structures for arbitrary geometry, loading cases and boundary conditions and to enable an accurate representation of the widest range possible of behaviors. The target was reached; all the designed and developed models gave satisfactory results and were conclusive. The work has provided important information that enhances the understanding of structural problems and the fundamental physical principles that underlie them.

The developed model proved to be applicable to the examined behaviors. However more situations could fall within the scope of the formulation. For example, the distortional model, developed for arbitrary cases of profile geometry, could be validated for other profiles. The finite element with bending shear effects could be validated for the calculation of shear stresses. The variation of the position of the shear center could be investigated for a structure exhibiting buckling…

A wide range of practical problems (central cores of towers, bridge decks, naval structures…), that initially motivated this research, could be deeply explored and fully analyzed by the 3D developed model. Such a complete application might reveal additional questions to be answered, would explore the advantageous effects of the presented advanced beam model and would certainly give a better understanding of its limitations.

Finally, the present work provides the opportunity to explore new horizons:

- applying the presented analyses in order to optimize the geometry of a profile or the bracing of a structure,
- developing additional non linear computations with the presented warping function in order to study the distortional buckling and its interaction with the other effects,
- studying the plastic and the full non linear post buckling behaviors within the present formulation.

References

Avery P., Mahendran M. & Nasir A. 2000. Flexural capacity of hollow flange beams. *Journal of Constructional Steel Research,* 53(3): 201-223.

Akoussah E., Beaulieu D. & Dhatt G. 1987. *Analyse non linéaire des structures à parois minces par éléments finis et son application aux bâtiments industriels*. Report GCT-87-07. University Laval, Canada.

Back S. & Will K. 1998. A shear-flexible element with warping for thin walled open beams. *International Journal for Numerical Methods in Engineering*, 43: 1173-1191.

Bakker M.C.M. & Peköz T. 2001. The finite element method for thin walled members- basic principles, *Proceedings of the Third International Conference on Thin-Walled Structures (ICTWS 2001)*, Krakow, Poland. Elsevier: 417-425.

Bathe K.J., Ramm E. & Wilson E.L. 1975. Finite element formulations for large deformation dynamics, *International Journal of Numerical Methods Engineering,* 9: 353-386.

Batoz J.L. & Dhatt G. 1990. *Modélisation des structures par éléments finis. Volume 2, poutres et plaques*. Hermès edition, Paris.

Batoz J.L., Dhatt G. & Fafard M. 1999. Algorithmes et strategies de resolution pour l'analyse non linéaire. *Modélisation des structures minces par éléments finis.* 1(4): 1-53. Institut pour la promotion des sciences de l'ingénieur, Paris.

Bažant Z.P. & Cedolin L. 1991. *Stability of structures : elastic, inelastic, fracture and damage theories*. Oxford University Press, Oxford.

Bažant Z.P. 2000. Stuctural stability. *International Journal of Solids and Structures,* 37: 55-67.

Belytschko T., Kam L.W. & Moran B. 2000. *Non-linear Finite Elements for Continua and Structures*. Wiley, Chichester, England.

Benscoter SU. 1954. A theory of torsion bending for multicell beams. *Journal of Applied mechanics*, 21(1), March: 25-34.

Bleich F. 1952. *Buckling strength of metal structures*. McGraw-Hill, New York, USA.

Binkevich E.V., Mamuzich I., Shynkarenko V.B. & Vodopivec F. 1988. Locking-suppression techniques and their application to the FEM-analysis of processes of deformation of thin-walled objects. *Journal of Materials Processing Technology,*75: 27-32.

Bradford M.A. & Cuk P. 1988. Lateral buckling of tapered monosymmetric I-beams. *Journal of Structural Engineering ASCE,* 120(8): 1607-1629.

Bradford M.A. 1992. Lateral distortional buckling of steel I-section members. *Journal of Construction Steel Research,* 23: 97-116.

Bradford M.A. & Ge. X.P. 1997. Elastic distortional buckling of continuous I-beams. *Journal of Construction Steel Research,* 41(2-3): 249-266.

Bradford M.A. 1997. Lateral distortional buckling of continuously restrained columns. *Journal of Construction Steel Research,* 42(2):121-139.

Bradford M.A. 1998. Distortional buckling of elastically restrained cantilevers. *Journal of Construction Steel Research,* 47: 3-18.

Bradford M.A. 1999. Elastic distortional buckling of tee-section cantilevers. *Thin-walled Structures,* 33: 3-17.

Braham M. 2001. Le déversement élastique des poutres en I à section monosymétrique soumises à un gradient de moment de flexion. *Revue Construction Métallique*, 1 : 17-28.

Calgaro J.-A. 1988. *Projet et construction des ponts*. Presses de l'Ecole Nationale des Ponts et Chaussées, Paris.

Chan S. 1990. Buckling analysis of structures composed of tapered members. *Journal of Structural Engineering ASCE,* 116(7): 1893-1906.

Chan S.L. 1995. Stability analysis of semirigid steel scaffolding. *Engineering Structures,* 17(8): 568-574.

Chan S.L. 2001. Non linear behavior and design of steel structures. *Journal of Constructional Steel Research*, 57: 1217-1231.

Chen H. & Blanford G. 1989. A C0 finite element formulation for thin walled beams. *International Journal of Numerical Methods in Engineering*, 28: 2239-2255.

Chen H. & Blandford G.E. 1991. Thin-Walled space frames: I-Large deformation analysis theory. *Journal of Structural Engineering ASCE,* 117(8):2499-2539

Cheung M.S., Li W. & Chidiac S.E. 1996. Finite strip analysis of bridges. E&FN Spon, London.

Cheung Y.K. & Than L.G. 1998. Finite strip method. CRC Press, Boca Raton.

Conci A. 1992. Large displacement analysis of thin-walled beams with generic open section. *International Journal of Numerical Methods in Engineering,* 33: 2109-2127.

Cowper, G. R. 1966. The shear coefficient in Timoshenko's beam theory. *Journal of Applied Mechanics,:*335-340.

Criesfield M. A. 1997. *Non-linear Finite Element Analysis of Solids and Structures*. Wiley, Chichester, England.

Davis J.M. 1998. Generalized beam theory (GBT) for coupled instability problem. *Coupled instabilities in metal structures, CISM courses and lectures, International Center for Mechanical Sciences NO. 379*: 151-224. Springer Wien New York.

Davis J.M. 2000. Recent research advances in cold-formed steel structures. *Journal of Constructional Steel research*, 55(1-3): 267-288.

Degée H. 2000. *Contribution à la prise en compte de la déformabilité de la section droite dans un élément fini de type poutre*. Ph.D. thesis, University of Liège, Belgium.

De Ville De Goyet V. 1989. *L'analyse statique non linéaire par la méthode des éléments finis des poutres à section non symétrique*. Ph.D. thesis, University of Liège, Belgium.

Djalaly H. 1974. Calcul de la résistance ultime au déversement. *Revue Construction Métallique* 1: 58-77.

Dube G.P. & Dumir P.C. 1996. Tapered thin open section beams on elastic foundation –I-Buckling analysis. *Computers and Structures*, 61(5): 845-857.

Dvorkin E. N., Celentano D., Cuitino A. & Gioia G. 1989. A Vlassov beam element. *Computers and Structures*, 33(1): 187-196.

Eisenberger M. 2003. An exact high order beam element. *Computers and Structures*, 81: 147-152.

ENV 1993-1-1 (1992). *Eurocode 3: Design of steel structures, Part 1-1: General rules and rules for buildings*. CEN, Brussels (in French).

Frey F. 1977. *L'analyse statique non linéaire des structures par la méthode des éléments finis et son application à la construction métallique*. Ph.D. thesis, University of Liège, Belgium.

Frey F. 2000. Analyse des structures et milieux continus. *Traité de Génie Civil de l'Ecole polytechnique fédérale de Lausanne. Volume 2.* Presses Polytechinques et Universitaires Romandes, CH-1015 Lausanne.

Galéa Y. 2002. Déversement élastique d'une poutre à section bi-symétrique soumise à des moments d'extrémité et une charge répartie ou concentrée. *Revue Construction Métallique* 2: 59-83.

Gjelsvik A. 1981. *The theory of thin walled bars*. Wiley.

Gonçalves R. & Camotin D. 2003. Buckling behavior of thin-walled aluminium and stainless steel columns using Generalised Beam Theory. *Proceedings of the international conference on Advances in Structures* (ASSCCA'03), Sydney, Australia, June 22-25. Balkema, ISBN 90-5809-588-6, 1: 405-411.

Gonçalves R. & Camotin D. 2004. GBT local and global buckling analysis of aluminium and stainless steel columns . *Computers & Structures*, 82(17-19): 1473-1484.

Gunnlaugsson G. A. & Pedersen P. T. 1982. A finite element formulation for beams with thin walled cross-sections. *Computers and Structures*, 15(6): 691-699.

Hancock G.J. 1978. Local distortional and lateral buckling of I-beams, *Journal of the Structural Engineering ASCE*, 104(11): 1787-1798.

Hancock G.J. 1985. Distortional buckling of steel storage rack columns, *Journal of the Structural Engineering ASCE*, 111(12): 2770-2783.

Hancock G.J. 1997. Design for distortional buckling of flexural members. *Thin-walled Structures,* 27: 3-12.

Hancock G.J. 1998. Finite strip buckling and non linear analyses and distortional buckling analysis of thin-walled structural members. *Coupled instabilities in metal structures, CISM courses and lectures, International Center for Mechanical Sciences NO. 379*: 225-289. Springer Wien New York.

Hancock G.J. 2003. Cold-formed steel structures. *Journal of Constructional Steel Research*, 59: 473-487.

Hsiao K.M. & Wen Y.L. 2000. A co-rotational formulation for thin-walled beams with monosymmetric open section. *Computer Methods for Applied Mechanical Engineering*, 190: 1163-1185.

Jirousek J. 1984. On the capacity of the isoparametric quadratic beam element to solve accurately a uniformly loaded beam segment. *Computers & Structures*, 19: 693-695.

Kesti J. & Davies J.M. 1999. Local and distortional buckling of thin-walled short columns. *Thin-walled Structures,* 34: 115-134.

Kim S.B. & Kim M.Y. 2000. Improved formulation for spatial stability and free vibration of thin-walled tapered beams and space frames. *Engineering Structures,* 22(5): 446-458.

Kim M.Y., Chang S.P. & Park H.G. 2000. Spatial postbuckling analysis of nonsymmetric thin-walled frames. *Journal of Engineering Mechanics ASCE,* 127(8): 769-778.

Kitipornchai S., Wang C.M. & Trahair N.S. 1986. Buckling of monosymmetric I-beams under moment gradient. *Journal of Structural Engineering ASCE,* 112(4):781-799.

Kitipornchai S. & Trahair NS. 1975. Elastic behavior of tapered monosymmetric I-beams. *Journal of the Structural Division ASCE*, 101(ST8): 1661-1678.

Kollbrunner C.F. & Basler K. 1970. *Torsion application à l'étude des structures*. SPES editor, Lausanne.

Kollbrunner C.F. & Hajdin N. 1972. *Dünnwandige Stäbe. Band 1 Stäbe mit undeformierbaren Querschnitten*. Springer–Verlag Berlin.

Krajcinovic D. 1970. Matrix force analysis of thin-walled structures. *Journal of the Structural Division ASCE*, 96(ST1) : 107-121.

Kwak H.G., Kim D.Y. & Lee H.W. 2001. Effect of warping in geometric nonlinear analysis of spatial beams. *Journal of Constructional Steel Research*, 57: 729-751.

Kwon Y.B. & Hancock G.J. 1992. Strength tests of cold-formed channel sections undergoing local and distortional buckling, *Journal of the Structural Engineering ASCE*, 117(2) : 1786-1803.

Mahieux A. 2003. *Méthode de calculs des structures à parois minces avec prise en compte des instabilités*. Final-year engineering project. Université Libre de Bruxelles, Belgium.

Massonnet C.E. 1983. A new approach (including shear lag) to elementary mechanics of materials. *International Journal of Solids and Structures*, 19(1):33-54.

Meek J.L. & Ho P.T.S. 1983. A simple finite element model for the warping torsion problem. *Computer methods in applied mechanics and engineering*, 37: 25-36.

Meek J.L. & Loganathan S. 1989. Large displacement analysis of space-frame structures, *Computer Methods in Applied Mechanics and Engineering*, 72(1):57-75.

Meek J.L. & Qiang X. 1998. A study on the instability problem for 3D frames. *Computer Methods in Applied Mechanics and Engineering*, 158: 235-254.

Mennink J., Soetens F., Snijder H.H. & van Hove B.W.E.M. 2003. Buckling experiments and FE simulations on complex aluminium extrusions. *Proceedings of the international conference on Advances in Structures* (ASSCCA'03), Sydney, Australia, June 22-25. Balkema, ISBN 90-5809-588-6, 1: 421-426.

Mohri F., Brouki A. & Roth J.-C. 2000. Déversement des poutres en I sous chargements asymétriques. *Revue Construction Métallique* 2, 41-52.

Mohri F., Brouki A. & Roth J.-C. 2003. Theoretical and numerical stability analyses of unrestrained monosymmetric thin-walled beams. *Journal of Constructional Steel Research*, 59: 63-90.

Mottershead J. 1988. Warping torsion in thin walled open section beams using the semiloof beam element. *International Journal for Numerical Methods in Engineering,* 26: 231-243.

Mukherjee S., Reddy J.N. & Krishnamoorthy C.S. 2001. Convergence properties and derivative extraction of the superconvergent Timoshenko beam finite element*. Computer Methods in Applied Mechanics and Engineering*, 190 : 3475-3500.

Musat S.D. & Epureaunu B.I. 1996. Study of warping torsion of thin-walled beams with closed cross-section using macro-elements. *International Journal for Numerical Methods in Engineering,* 12: 873-884.

Musat S.D. & Epureaunu B.I. 1999. Study of warping torsion of thin-walled beams with open cross-section using macro-elements. *International Journal for Numerical Methods in Engineering,* 44: 853-868.

Murray N. 1986. *Introduction to the theory of thin-walled structures*. Oxford University Press, New York, USA.

Nowinski J. 1959. Theory of thin-walled bars. *Applied Mechanics Reviews*, 12(4): 219-227.

Pedersen P. T. 1991. Beam theories for torsional-bending response of ship hulls. *Journal of Ship Research*, 35(3): 254-265.

Peng J.L., Pan A.D.E. & Chan S.L. 1998. Simplified models for analysis and design of modular falsework. *Journal of Constructional Steel Research*, 48: 189-209.

Prokić A. 1990. *Thin walled beams with open and closed cross section*. Ph.D. thesis, Univ. of Belgrade, Yugoslavia (in Serbian).

Prokić A. 1993. Thin walled beams with open and closed cross section. *Computers & Structures*, 47(6): 1065-1070.

Prokić A. 1994. Material nonlinear analysis of thin-walled beams. *ASCE Journal of Structural Engineering*, 120(10): 2841-2852.

Prokić A. 1996. New warping function for thin-walled beams I: theory. *Journal of Structural Engineering ASCE*, 122(12): 1437-1442.

Prokić A. 1996. New warping function for thin-walled beams II: finite element method and applications. *Journal of Structural Engineering ASCE*,122(12): 1443-1452.

Prokić A. 2002. New finite element for analysis of shear lag. *Computers and Structures,* 80(11): 1011-1024.

Pilkey W. 1994. *Formulas for stress, strain, and structural matrices*. New York. Wiley.

Rajasekaran S. 1994. Equations for tapered thin-walled beams of generic open cross-section. *Journal of Engineering Mechanics, ASCE*, 120(8): 1607-1629

Ram E. & Osterrieder P. 1983. *Ultimate load analysis of three dimensional beam structures with thin-walled cross sections using finite elements*. Preliminary report on Stability of Metal Structures, Paris.

Razaqpur A.G. Hangang L. 1991. Thin-walled multicell box-girder finite element. *Journal of Structural Engineering ASCE*, 117(10): 2953-2971.

Reddy J.N. 1997. On locking shear deformable beam finite elements. *Computer methods in applied mechanics and engineering*, 149: 113-132.

Reddy J.N., Wang C.M. & Lee K.H. 1997. Relationships between bending solutions of classical and shear deformation beam theories. *International Journal of Solids and Structures*, 34(26): 3373-3384.

Reilly J. 1972. Stiffness analysis of grids including warping. *Journal of the Structural Division ASCE*, 98(ST7): 9022-1523.

Ronagh H.R. & Bradford M.A. 1996. A rational model for the distortional buckling of tapered members. *Computer methods in applied mechanics and engineering*, 130: 263-277.

Ronagh H.R. & Bradford M.A. 1999. Non-linear analysis of thin-walled members of open cross-section. *International Journal for Numerical Methods in Engineering*, 46: 535-552.

Ronagh H.R. & Bradford M.A. 2000. Nonlinear analysis of thin-walled members of variable cross-section. *Computers and Structures*, 77: 285-313.

Saadé K., Espion B. & Warzée G. 2004. Non-uniform torsional behavior and stability of thin-walled elastic beams with arbitrary cross sections. *Thin-Walled Structures*, 42 (6): 857-881.

Saadé K., Espion B. & Warzée G. 2004. Discussion of 'exact finite element for nonuniform torsion of open sections' by Magdi Mohareb and Farhood Nowzartash, *Journal of Structural Engineering ASCE*, 130(9): 1420-1420.

Samtech S.A. 2002. *Samcef software v9.1* (file:///opt/Samcef91/doc/index.html) Samtech S.A. 8, rue des Chasseurs ardennais; 4031 Angleur, Belgium.

Serrette R. & Peköz T. 1997. Bending strength of standing seam roof panels. *Thin-Walled Structures*, 27(1): 55-64.

Shakourzadeh H., Guo YQ & Batoz J.L. 1995. A torsion bending element for thin-walled beams with open and closed cross sections. *Computers & Structures*, 55(6): 1045-1054.

Shakourzadeh H., Guo YQ & Batoz J.L. 1996. On the large displacement and instability of 3D elasto-plastic thin walled beam structure. *Proceedings of the Second ECCOMAS Conference on Numerical Methods in Engineering,* Paris, France, September 9-13. Désidéri J.A., Le Tallec P., Oñate E., Périaux J. & Stein E. editors. Wiley: 197-203.

Shakourzadeh, H., Guo Y.Ch. & Batoz J.L. 1999. Modeling of connections in the analyses of thin-walled space frames. *Computers and Structures,* 71: 423-433.

Sharman P.W. 1985. Analysis of structures with thin walled open sections. *International Journal of Mechanical Science*, 27(10): 665-677.

Silvestre N. & Camotim D. 2002. First-order generalised beam theory for arbitrary orthotropic materials. *Thin-Walled Structures*, 40(9): 755-789.

Silvestre N. & Camotim D. 2002. Second-order generalised beam theory for arbitrary orthotropic materials. *Thin-Walled Structures*, 40(9): 791-820.

Silvestre N. & Camotim D. 2004. Distortional buckling formulae for cold-formed steel C and Z-section members: Part I-derivation. *Thin-Walled Structures*, 42(11): 1567-1597.

Silvestre N. & Camotim D. 2004. Distortional buckling formulae for cold-formed steel C and Z-section members: Part II-validation and application. *Thin-Walled Structures*, 42(11): 1599-1629.

Silvestre N. & Camotim D. 2003. GBT buckling analysis of pultruded FRP lipped channel members, *Computers & Structures*, 81(18-19): 1889-1904.

Takahashi K. & Mizuno M. 1978. Distortion of thin-walled open cross section members (one degree of freedom and singly symmetrical cross-section). *JSME*, 21(160): 1448-1454.

Takahashi K. & Mizuno M. 1980. Distortion of thin-walled open cross section members (for the case of distortion of multi-degree-of-freedom). *JSME*, 23(182): 1290-1296.

Takahashi K. Yonago A. & Mizuno M. 1982. Analysis of thin-walled open cross section curved members considering cross sectional distortion. *JSCE*, 320: 47-55.

Takahashi K. & Mizuno M. 1987. A new buckling mode of thin-walled open cross section members. *Applied solid mechanics-2,* 1(620): 553-573.

Takahashi K., Hitoshi N. & Imamura K. 2001. Pure distortional buckling of closed cross section columns. *Proceedings of the Third International Conference on Thin-walled Structures (ICTWS 2001)*, Krakow, Poland. Elsevier: 623-630.

Takahashi K. 2003. Analytical and numerical solutions for distortional instabilities of thin-walled beams under bending moment. *Coupled instabilities in metal structures,* Lisbon. Imperial College Press: 73-81.

Timoshenko S. 1913. Sur la stabilité des systèmes élastiques. *Annales des Ponts et Chaussées,* 9th series, 16 (4): 73-132.

Timoshenko S. & Gere J. 1961. *Theory of Elastic Stability*. McGraw-Hill, New York.

Trahair N.S. 1993. *Flexural torsional buckling of structures.* E&FN Spon, London.

Trahair N.S. & Bradford M.A. 1995. *The behavior and design of steel structures.* E&FN Spon, London.

Van Impe R. 2001. Torsional buckling of steel members: the flexural buckling analogy. *Advances in Structural Engineering*, 4(3):181-185.

Villette M. (2002). Propositions pour de nouvelles courbes de déversement. *Revue Construction Métallique*, 2 : 17-39.

Vlassov VZ. 1961. *Thin walled elastic beams*. Israel Program for Scientific Translations, Jerusalem.

Volokh K.Yu. & Vilnay O. 2001. On the prediction of geometrical non-linearity of slender structures, *International Journal of Numerical Methods Engineering,* 9: 353-386.

Von Karman TH. 1944. Methods of analysis for torsion with variable twist, *Journal of the Aeronautical Sciences,* 11: 110-124.

Von Karman TH. 1946. Torsion with variable twist, *Journal of the Aeronautical Sciences,* 13: 503-510.

Wang C.M., Reddy J.N. & Lee K.H. 2000. *Shear deformable beams and plates*. Elsevier, NewYork.

Waszczyszyn Z., Cichoń C. & Radwaskań M. 1994. *Stability of Structures by Finite Element Methods.* Elsevier, Amsterdam.

Yang D. & Hancock J. G. 2003. Compression tests of cold-reduced high strength steel chanel columns failing in the distortional mode, *Proceedings of the international conference on Advances in Structures (ASSCCA'03)*, Sydney, Australia, June 22-25. Balkema, ISBN 90-5809-588-6, 1: 303-308.

Yunhua L. 1998. Explanation and elimination of shear locking and membrane locking with field consistence approach. *Computer methods in applied mechanics and engineering*, 162: 249-269.

Zienkiewicz O.C. & Taylor R.L. 2000. *The finite element method volume 1 The basis.* Butterworth-Heinemann, Oxford.

Appendix 0. Constitutive relations

The calculation of the constitutive relations that describe the stress-strain relation is important for the analysis of the behavior of structures. In order to complete any finite element development and to ensure sufficient equilibrium equations for the unknowns to be found, it is necessary to describe how the material behaves when submitted to deformation histories. Constitutive laws depend on the physical constitution of the material and are introduced to describe the macroscopic behavior under loading. They link the kinematic and static variables of a deformed body in order to fit accurately the observed physical behavior. Clearly, this task is not easy and is a subject of lots of research [De Ville 1989 §5.6…]. The simplest law for solids is the elastic linear Hooke law. The behavior of elastic materials depends only on the current level of the strain. This implies that the loading and unloading stress-strain relations are identical and that the original shape is recovered upon unloading. The solids are considered to return to their initial undeformed configuration upon stress removal. The constitutive law implies that the stresses in a given configuration only depend on the strains in this configuration and not on a strain history.

For a general behavior of a non linear material, the constitutive equations are given by a relation between the rate of stresses and the rate of strains. This work is restricted to the elastic behavior of thin walled structures. The purely mechanical behavior of metallic structures generates large displacements and small deformations. When thermodynamic effects such as heat conduction are not considered, the response of the material may then be modeled by a simple extension of linear elastic laws by replacing the stress by the PK2 stress and the linear strain by the Green strain [De Ville 1989 §5.6.2]. This is called a Saint Venant-Kirchhoff material:

$$S_{ij}=d_{ijkl}E_{kl} \tag{A0.1}$$

d_{ijkl} are the components of the fourth-order tensor of elastic moduli which are constants for the Kirchhoff materials. The corresponding rate relationship is:

$$dS_{ij} = d_{ijkl}dE_{kl} \tag{A0.2}$$

d_{ijkl} are called the tangent moduli.

Appendix 1. Calculation of geometrical properties

$$A = \int_A dA \qquad A = \sum_{k=1}^{ns} l_k ep_k$$

$$I_y = \int_A z^2 dA \qquad I_y = \sum_{k=1}^{ns} \frac{1}{4}(y_1 + z_1)^2 ep_k l_k + \frac{1}{12} l_k ep^3{}_k \sin\alpha_k{}^2 + \frac{1}{12} l^3{}_k ep_k \cos\alpha_k{}^2$$

$$I_z = \int_A y^2 dA \qquad I_z = \sum_{k=1}^{ns} \frac{1}{4}(y_1 + y_2)^2 ep_k l_k + \frac{1}{12} l_k ep^3{}_k \cos\alpha_k{}^2 + \frac{1}{12} l_k^3 ep_k \sin\alpha_k{}^2$$

$$S_{\omega,y} = \int_A \omega_{,y} dA \qquad S_{\omega,y} = \sum_k^{ns} (y_1 - y_C) l_k ep_k \cos\alpha_k \sin\alpha_k - \frac{l_k^2}{2} ep_k \cos\alpha_k - (z_1 - z_C) l_k ep_k \cos\alpha_k{}^2$$

$$S_{\omega,z} = \int_A \omega_{,z} dA \qquad S_{\omega_{,z}} = \sum_{k=1}^{ns} -(z_1 - z_C) l_k ep_k \cos\alpha_k \sin\alpha_k - \frac{l_k^2}{2} ep_k \sin\alpha_k + (y_1 - y_C) l_k ep_k \sin\alpha_k{}^2;$$

$$I_{y\omega} = \int_A y\omega dA \qquad I_{y\omega} = \sum_{k=1}^{ns} \frac{ep_k^3}{12} \cos\alpha_k (y_1 l_k \sin\alpha_k - z_1 l_k \cos\alpha_k - \frac{l^2}{2})$$

$$I_{z\omega} = \int_A z\omega dA \qquad I_{z\omega} = \sum_{k=1}^{ns} \frac{ep_k^3}{12} \sin\alpha_k (y_1 l_k \sin\alpha_k - z_1 l_k \cos\alpha_k - \frac{l^2}{2})$$

$$I_{\omega_{,y}\omega_{,y}} = \int_A \omega_{,y}\omega_{,y} dA$$

$$I_{\omega,y\omega,y} = \sum_k^{ns} (z_1 - z_C)^2 l_k ep_k \cos\alpha_k{}^4 + (z_1 - z_C) l_k^2 ep_k \cos\alpha_k{}^3 - 2(z_1 - z_C)(y_1 - y_C) l_k ep_k \cos\alpha_k{}^3 \sin\alpha_k$$
$$+ (y_1 - y_C)^2 l_k ep_k \cos\alpha_k{}^2 \sin\alpha_k{}^2 + (y_1 - y_C) l_k^2 ep_k \cos\alpha_k{}^2 \sin\alpha_k + \frac{1}{3} l_k^3 ep_k \cos\alpha_k{}^2 + \frac{1}{12} l_k ep_k^3 \sin\alpha_k{}^2$$

$$I_{\omega_{,z}\omega_{,z}} = \int_A \omega_{,z}\omega_{,z} dA$$

$$I_{\omega_{,z}\omega_{,z}} = \sum_k^{ns} (y_1 - y_C)^2 l_k ep_k \sin\alpha_k{}^4 - (y_1 - y_C) l_k^2 ep_k \sin\alpha_k{}^3 - 2(z_1 - z_C)(y_1 - y_C) l_k ep_k \cos\alpha_k in\alpha_k{}^3$$
$$+ (z_1 - z_C)^2 l_k ep_k \cos\alpha_k{}^2 \sin\alpha_k{}^2 + (z_1 - z_C) l_k^2 ep_k \cos\alpha_k \sin\alpha_k{}^2 + \frac{1}{3} l_k^3 ep_k \sin\alpha_k{}^2 + \frac{1}{12} l_k ep_k^3 \cos\alpha_k{}^2$$

$$I_\omega = \int_A (z\omega_{,y} - y\omega_{,z}) dA$$

$$I_\omega = \sum_{k=1}^{ns} (l_k \frac{ep_k^3}{12} - ep_k \frac{l_k^3}{3} + (y_1 \sin\alpha_k - z_1 \cos\alpha_k) ep_k l_k^2 - (y_1 \sin\alpha_k - z_1 \cos\alpha_k)^2 ep_k l_k)$$

$$S_{\Omega^i} = \int_A \Omega^i dA$$

$$S_{\Omega^i_{,y}} = \int_A \Omega^i{}_{,y} dA \qquad S_{\Omega^i,y}(i) = \sum_{k=1}^{nd} ep_k \sin\alpha_k + \sum_{k=1}^{na} -ep(k)\sin\alpha(k);$$

$$S_{\Omega^i_{,z}} = \int_A \Omega^i{}_{,z} dA \qquad S_{\Omega_{i,z}} = \sum_{k=1}^{nd} -ep_k \cos\alpha_k + \sum_{k=1}^{na} ep_k \cos\alpha_k$$

$$I_{y\Omega^i} = \int_A y\Omega^i dA \qquad I_{y\Omega^i} = \sum_{l=1}^{nd} \frac{1}{2} y_1 l_k ep_k - \frac{\sin\alpha_k}{6} l_k^2 ep_k + \sum_{k=1}^{na} \frac{1}{2} y_1 l_k ep_k + \frac{\sin\alpha_k}{6} l_k^2 ep_k$$

$$I_{z\Omega^i} = \int_A z\Omega^i dA \qquad I_{z\Omega^i} = \sum_{k=1}^{nd} \frac{1}{2} z_1 l_k ep_k + \frac{\cos\alpha_k}{6} l_k^2 ep_k + \sum_{k=1}^{na} \frac{1}{2} z_1 l_k ep_k - \frac{\cos\alpha_k}{6} l_k^2 ep_k$$

$$I_{y\Omega^i_{,z}} = \int_A y\Omega^i_{,z} dA$$

$$I_{y\Omega^i{}_{,z}} = \sum_{1}^{nd} - y_1 ep_k \cos\alpha_k + \cos\alpha_k \sin\alpha_k \frac{l_k}{2} ep_k + \sum_{k=1}^{na} y_1 ep_k \cos\alpha_k + \cos\alpha_k \sin\alpha_k \frac{l_k}{2} ep_k$$

$$I_{z\Omega^i_{,y}} = \int_A z\Omega^i_{,y} dA$$

$$I_{z\Omega^i{}_{,y}} = \sum_{k}^{nd} + z_1 ep_k \sin\alpha_k + \cos\alpha_k \sin\alpha_k \frac{l_k}{2} ep_k + \sum_{k=1}^{na} - z_1 ep_k \sin\alpha_k + \frac{\cos\alpha_k \sin\alpha_k l_k ep_k}{2}$$

$$I_{\Omega^i_{,z}\Omega^j_{,z}} = \int_A \Omega^i_{,z}\Omega^j_{,z} dA \qquad I_{\Omega^i{}_{,z}\Omega^i{}_{,z}} = \sum_{k=1}^{nd+na} \frac{ep_k}{l_k)} \cos\alpha_k{}^2 \qquad I_{\Omega^i{}_{,z}\Omega^k{}_{,z}} = -\frac{ep_m}{l_m} \cos^2\alpha_m$$

$$I_{\Omega^i_{,y}\Omega^j_{,y}} = \int_A \Omega^i_{,y}\Omega^j_{,y} dA \qquad I_{\Omega^i{}_{,y}\Omega^i{}_{,y}} = \sum_{k=1}^{nd+na} \frac{ep_k}{l_k} \sin\alpha_k{}^2 \qquad I_{\Omega^i{}_{,y}\Omega^k{}_{,y}} = -\frac{ep_m}{l_m} \sin\alpha_m{}^2$$

$$I_{\Omega^i} = \int_A (-y\Omega^i_{,z} + z\Omega^i_{,y}) dA$$

$$I_{\Omega^i\Omega^j} = \int \Omega^i\Omega^j dA \qquad I_{\Omega^i\Omega^i} = \sum_{k=1}^{nd+na} \frac{1}{3} l_k ep_k$$

$I_{\Omega^i\Omega^j} = \frac{1}{6} ep_m l_m$ m is the segment whose end nodes are i et k.

$$I_{\omega\omega} = \int \omega\omega dA$$

$$I_{y\omega_{,z}} = \int y\omega_{,z} dA$$

$$I_{z\omega_{,y}} = \int z\omega_{,y} dA$$

$$I_{\omega_{,y}\Omega^j_{,y}} = \int \omega_{,y}\Omega^j_{,y} dA$$

$$I_{\omega_{,z}\Omega^j_{,z}} = \int \omega_{,z}\Omega^j_{,z} dA$$

$$I_h = \int_A ([z+\omega_{,y}]^2 + [y-\omega_{,z}]^2) dA \qquad I_h = \sum_{k=1}^{ns} (h_k{}^2 ep_k l_k + \frac{1}{3} l_k ep_k^3)$$

where $h_k^2 = z_1^2 \sin^2\alpha_k + y_1^2 \cos^2\alpha_k$

$$I_h^* = \int_A ([z-z_C+\omega_{,y}]^2 + [y-y_C-\omega_{,z}]^2) dA \quad I_h^* = I_h + (y_C^2 + z_C^2)A - 2z_C S_{\omega,y} + 2y_C S_{\omega,z}$$

$$I_h^{*D_I} = \int_A (\bar{\mu}_I^2 [z - \bar{z}_{CI} + \omega_{I,y}]^2 + \bar{\mu}_I^2 [y - \bar{y}_{CI} - \omega_{I,z}]^2) dA$$

$$D_{ISM} = \int_A \frac{12}{e^3} M_I^2 dA$$

$$I_{y\Omega^i_{,z}}^{D_I} = \int_A \bar{\mu}_I y \Omega^i_{,z} dA$$

$$I_{z\Omega^i_{,y}}^{D_I} = \int_A \bar{\mu}_I z \Omega^i_{,y} dA$$

$$S_{z_{CI}\Omega^i_{,y}}^{D_I} = \int_A \bar{\mu}_I \bar{z}_{CI} \Omega^i_{,y} dA$$

$$S_{y_{CI}\Omega^i_{,z}}^{D_I} = \int_A \bar{\mu}_I \bar{y}_{CI} \Omega^i_{,z} dA$$

Appendix 2. Elementary stiffness matrix (without shear effects)

$$k^{el} < q_{u0}, q_{u0} > = EA[K_4]$$

$$k^{el} < q_v, q_v > \ = \ E\mathbf{I_z}\left[K_1^{\ *}\right]$$

$$k^{el} < q_w, q_w > \ = EI_y\left[K_2^{\ *}\right]$$

$$k^{el} < q_{\theta_x}, q_{\theta_x} > = GI_h^*[K_4]$$

$$k^{el} < q_{\theta_x}, q_{u_i} > \ = G[I_{y\Omega^i_{,z}} - I_{z\Omega^i_{,y}} + z_c S_{\Omega^i_{,y}} - y_c S_{\Omega^i_{,z}}]\left[K_7^{\ *}\right]$$

$$k^{el} < q_{u_i}, q_{u_j} > \ = EI_{\Omega^i\Omega^j}\left[K_4\right]^T + G[I_{\Omega^i_{,y}\Omega^j_{,y}} + I_{\Omega^i_{,z}\Omega^j_{,z}}]\left[K_3^{\ *}\right]$$

where

$$\left[K_1^{\ *}\right] = \frac{1}{L^3}\begin{bmatrix} 12 & 6L & -12 & 6L \\ 6L & -4L^2 & -6L & 2L^2 \\ -12 & -6L & 12 & -6L \\ 6L & 2L^2 & -6l & 4L^2 \end{bmatrix}$$

$$\left[K_2^{\ *}\right] = \frac{1}{L^3}\begin{bmatrix} 12 & -6L & -12 & -6L \\ -6L & 4L^2 & 6L & 2L^2 \\ -12 & 6L & 12 & 6L \\ -6l & 2L^2 & 6l & 4L^2 \end{bmatrix}$$

$$\left[K_3^{\ *}\right] = \frac{L}{6}\begin{bmatrix} 2 & 1 \\ 1 & 2 \end{bmatrix}$$

$$[K_4] = \frac{1}{L}\begin{bmatrix} 1 & -1 \\ -1 & 1 \end{bmatrix}$$

$$\left[K_7^{\ *}\right] = \begin{bmatrix} -0.5 & -0.5 \\ 0.5 & 0.5 \end{bmatrix}$$

Appendix 3. Elementary stiffness matrix with Timoshenko shear effects

$\{q_{u0}\}^T = <u_{01}, u_{03}>$

$\{q_v\}^T = <v_{01}, v_{02}, v_{03}>$

$\{q_w\}^T = <w_{01}, w_{02}, w_{03}>$

$\{q_{\theta x}\}^T = <\theta_{x1}, \theta_{x2}, \theta_{x3}>$

$\{q_{\theta y}\}^T = <\theta_{y1}, \theta_{y2}, \theta_{y3}>$

$\{q_{\theta z}\}^T = <\theta_{z1}, \theta_{z2}, \theta_{z3}>$

$\{q_{ui}\}^T = <u_{i1}, u_{i3}>$; $i=1,2,\ldots n$

$$k^{el} < q_{u0}, q_{u0} > = EA[K_4]$$

$$k^{el} < q_v, q_v > = GA[K_2]$$

$$k^{el} < q_v, q_{\theta_z} > = -GA[K_5]$$

$$k^{el} < q_{\theta_z}, q_{\theta_z} > = EI_z[K_2] + GA[K_1]$$

$$k^{el} < q_w, q_w > = GA[K_2]$$

$$k^{el} < q_w, q_{\theta_y} > = GA[K_5]$$

$$k^{el} < q_{\theta_y}, q_{\theta_y} > = EI_y[K_2] + GA[K_1]$$

$$k^{el} < q_{\theta_x}, q_{\theta_x} > = GI_h^*[K_2]$$

$$k^{el} < q_{\theta_x}, q_{u_i} > = G[I_{y\Omega^i_{,z}} - I_{z\Omega^i_{,y}} + z_c S_{\Omega^i_{,y}} - y_c S_{\Omega^i_{,z}}][K_7]$$

$$k^{el} < q_{u_i}, q_{u_j} > = EI_{\Omega^i\Omega^j}[K_4] + G[I_{\Omega^i_{,y}\Omega^j_{,y}} + I_{\Omega^i_{,z}\Omega^j_{,z}}][K_3]$$

where

$$[K_1] = \frac{L}{15}\begin{bmatrix} 2 & 1 & -0.5 \\ 1 & 8 & 1 \\ -0.5 & 1 & 2 \end{bmatrix}$$

If the selective reduced integration method is used (§5.2.2), K_1 is evaluated by using a two point Gauss integration rule (equation 5.28):

$$\left[K_1^s\right]=\frac{L}{9}\begin{bmatrix}1 & 1 & -0.5\\ 1 & 4 & 1\\ -0.5 & 1 & 1\end{bmatrix}$$

$$\left[K_2\right]=\frac{1}{3L}\begin{bmatrix}7 & -8 & 1\\ -8 & 16 & -8\\ 1 & -8 & 7\end{bmatrix}$$

$$\left[K_3\right]=\frac{L}{6}\begin{bmatrix}2 & 1\\ 1 & 2\end{bmatrix}$$

$$\left[K_4\right]=\frac{1}{L}\begin{bmatrix}1 & -1\\ -1 & 1\end{bmatrix}$$

$$\left[K_5\right]=\frac{1}{6}\begin{bmatrix}-3 & -4 & 1\\ 4 & 0 & -4\\ -1 & 4 & 3\end{bmatrix}$$

$$\left[K_6\right]=\frac{1}{3}\begin{bmatrix}0.5 & 0\\ 1 & 1\\ 0 & 0.5\end{bmatrix}$$

$$\left[K_7\right]=\frac{1}{6}\begin{bmatrix}-5 & -1\\ 4 & -4\\ 1 & 5\end{bmatrix}$$

$$\left[K_8\right]=\frac{1}{1}\begin{bmatrix}1 & -1\\ 0 & 0\\ -1 & 1\end{bmatrix}$$

Appendix 4. Transition to global axes

The equilibrium equations and the finite element calculations have been developed in this dissertation in principal axes related to the orientation of each beam element of the structure. To analyze a complete structure, the assembly process of different elements needs to refer to a common axis system. Since detailed information can be found in the literature on the finite element method, only basic formulae and equations are given hereafter.

Transition from principal axes to given local axes
If the longitudinal axis x of an element remains the same, the matrix [t] allows the transformation of nodal forces or displacements from the local principal axis to an arbitrary local axis system. [t] is an identity matrix modified to insert a rotation matrix R_β (A4.1) of principal axes y and z. β is the angle between principal axes and the local axes where the cross section geometry is described.

$$[R_\beta] = \begin{bmatrix} 1 & 0 & 0 \\ 0 & \cos\beta & -\sin\beta \\ 0 & \sin\beta & \cos\beta \end{bmatrix} \qquad \text{(A4.1)}$$

$$\{q_n\}_{loc} = [t]^T \{q_n\}_{prnc}$$

$$[k]_{loc} = [t]^T [k]_{prnc} [t]$$

$$\{f_n\}_{loc} = [t]^T \{f_n\}_{prnc}$$

$$[t]^T = [t]^{-1} \qquad \text{(A4.2)}$$

Transition from local axes to global axes
Equations (A4.2) are used with a rotation matrix Q[3x3] that allows the transformation from local axes (x,y,z) to global axes (X,Y,Z). Batoz and Datt [Batoz 1990, page 183] gave the following transformation matrix.

$$[Q] = [Q_A][R_\alpha] \qquad \text{(A4.3)}$$
where:

$$[Q_A] = \begin{bmatrix} a & \dfrac{-ab}{\sqrt{a^2+c^2}} & \dfrac{-c}{\sqrt{a^2+c^2}} \\ b & \sqrt{a^2+c^2} & 0 \\ c & \dfrac{-bc}{\sqrt{a^2+c^2}} & \dfrac{a}{\sqrt{a^2+c^2}} \end{bmatrix}$$

with

$$< a \;\; b \;\; c > = \frac{1}{L} < X_{21} \;\; Y_{21} \;\; Z_{21} >$$

X_{21}, Y_{21} and Z_{21} are the differences of co-ordinates of extreme nodes of the element. The length of the element L is thus:

$$L^2 = X_{21}^2 + Y_{21}^2 + Z_{21}^2$$

The position of the local axes y and z of the cross section is characterized by the angle α between the local axis y and the intersection between the planes (x,Y) and the cross section plane (yz).
This angle of orientation (α) can be given as a data [Batoz 1990, page 183], or computed from the coordinates of an arbitrary point D (X_D, Y_D, Z_D) at the positive part of the local axis y is taken at the second node of the element. The distance between the extreme node 2 and the arbitrary point D is L_{2D}.

α is the angle between the local axis y whose direction is defined by the unit vector coordinates d_i (A4.4) and the intersection vector between the planes (x,Y) and the cross section plane (yz) that is defined by its unit vector coordinates o_i (A4.5).

$$\langle d \rangle = \left\langle \frac{X_D - X_2}{L_{2D}}, \frac{Y_D - Y_2}{L_{2D}}, \frac{Z_D - Z_2}{L_{2D}} \right\rangle \tag{A4.4}$$

$$\langle o \rangle = \left\langle \frac{-ab}{\sqrt{a^2 + c^2}}, \sqrt{a^2 + c^2}, \frac{-bc}{\sqrt{a^2 + c^2}} \right\rangle \tag{A4.5}$$

$[R_\alpha]$ can be directly calculated by inserting the expressions (A4.6) and (A4.7) of $\cos\beta$ and $\sin\beta$ in (A4.1).

$$\mathbf{cos}\alpha = \sum_3 o_i d_i \tag{A4.6}$$

$$\mathbf{sin}\alpha = \sqrt{(o_2 d_3 - o_3 d_2)^2 + (o_1 d_3 - o_3 d_1)^2 + (o_1 d_2 - o_2 d_1)^2} \tag{A4.7}$$

If the local axis x is parallel to the global axis Y (a = 0 et c = 0), the angle ψ between the global X and the local z characterizes the rotation.

If x and Y have the same direction

$$[Q] = \begin{bmatrix} 0 & \sin\psi & \cos\psi \\ -1 & 0 & 0 \\ 0 & \cos\psi & -\sin\psi \end{bmatrix} \tag{A4.8}$$

with

$$\mathbf{cos}\psi = \frac{Z_D - Z_2}{L_{2D}} \tag{A4.9}$$

$$\mathbf{sin}\psi = \frac{X_D - X_2}{L_{2D}} \tag{A4.10}$$

If x and Y have the opposite direction,

$$[Q] = \begin{bmatrix} 0 & \sin\psi & \cos\psi \\ -1 & 0 & 0 \\ 0 & -\cos\psi & \sin\psi \end{bmatrix} \tag{A4.11}$$

with

$$\mathbf{cos}\psi = \frac{Z_2 - Z_D}{L_{2D}} \tag{A4.12}$$

$$\mathbf{sin}\psi = \frac{X_2 - X_D}{L_{2D}} \tag{A4.13}$$

Appendix 5. Elementary linear stiffness matrix with (xz) bending warping effects

$\{q_v\}^T = <v_{01}, v_{02}, v_{03}>$

$\{q_w\}^T = <w_{01}, w_{02}, w_{03}>$

$\{q_{\theta y}\}^T = <\theta_{y1}, \theta_{y2}, \theta_{y3}>$

$\{q_{\theta z}\}^T = <\theta_{z1}, \theta_{z2}, \theta_{z3}>$

$\{q_{ui}\}^T = <u_{i1}, u_{i3}>$; i=1,2,…n

$$k^{el} < q_v, q_v > = GA[K_2]$$

$$k^{el} < q_v, q_{\theta_z} > = -GA[K_5]$$

$$k^{el} < q_{\theta_z}, q_{\theta_z} > = EI_z[K_2] + GA[K_1]$$

$$k^{el} < q_w, q_w > = GA[K_2]$$

$$k^{el} < q_w, q_{\theta_y} > = GA[K_5]$$

$$k^{el} < q_{\theta_y}, q_{\theta_y} > = EI_y[K_2] + GA[K_1]$$

$$k^{el} < q_w, q_{u_i} > = G[S_{\Omega^i_{,z}}][K_7]$$

$$k^{el} < q_{\theta_y}, q_{u_i} > = EI_{z\Omega^i}[K_8] + GS_{\Omega^i_{,z}}[K_6]$$

$$k^{el} < q_{u_i}, q_{u_j} > = EI_{\Omega^i\Omega^j}[K_4]^T + G[I_{\Omega^i_{,y}\Omega^j_{,y}} + I_{\Omega^i_{,z}\Omega^j_{,z}}][K_3]$$

$[K_1]$, $[K_2]$…$[K_8]$ are given in Appendix 3.

Appendix 6. Shear locking problem presentation

Timoshenko model deals with bending behaviors by including shear bending effects as it has been seen in §2.1.2. The simplest beam finite element with linear interpolations for both transversal displacement and section rotation displays strong over-stiffening and significant errors in some cases. In this appendix, a brief presentation of this problem, the so-called *locking phenomenon*, is introduced and developments are done, for simplicity, for a two dimensional (xz) beam lying along the x-axis.
In Timoshenko model, the generalized strains are the shear strain (A6.1) and the curvature χ (A6.2):

$$\gamma_{xz}^{F} = w_{0,x} + \theta_y \tag{A6.1}$$

$$\chi = \theta_{y,x} \tag{A6.2}$$

For a two-node beam Timoshenko element, (A6.1) and (A6.2) can be developed as follows:

$$\gamma_{xz}^{F} = \left\{ -\frac{1}{L} w_1 + \frac{1}{L} w_2 \right\} + \frac{1}{2}(1-\frac{x}{L})\theta_{y1} + \frac{1}{2}(1+\frac{x}{L})\theta_{y2} \tag{A6.3}$$

$$\chi = -\frac{1}{2L}\theta_{y1} + \frac{1}{2L}\theta_{y2} \tag{A6.4}$$

For this simple linear Timoshenko element, the absence of shear strain (A6.5) along the entire length of the beam induces two equations (A6.6). The second equation of (A6.6) leads to zero curvature (A6.7):

$$\gamma_{xz}^{F} = 0 \tag{A6.5}$$

$$\begin{aligned} & -\frac{1}{L} w_1 + \frac{1}{L} w_2 + \frac{1}{2}\theta_{y1} + \frac{1}{2}\theta_{y2} = 0 \\ & -\frac{1}{2L}\theta_{y1} + \frac{1}{2L}\theta_{y2} \end{aligned} \tag{A6.6}$$

$$\chi = \theta_{y,x} = 0 \tag{A6.7}$$

This shows that for linear Timoshenko element, the shear locking represents the inability of the element to represent exact pure bending.
In particular, if a pure state of bending (A6.8) is considered, (A6.3) gives the corresponding shear strain (A6.9).

$$w_1 = w_2 = 0\,, \qquad \theta_{y1} = -\theta_{y2} = \alpha \tag{A6.8}$$

$$\gamma_{xz}^{F} = -\frac{x}{l}\alpha \tag{A6.9}$$

From (A6.9), it could be seen that the strain is found to be nonzero along the element except at x = 0. This is incompatible with the equilibrium equation of the state of pure bending where the shear and hence the strain should vanish when the moment is constant. The transverse shear which appears in this state of pure bending is often called parasitic shear and has large effects on the behavior of the element.

$$\frac{1}{2}\int_{\Omega}\sigma_x\varepsilon_x d\Omega = E\frac{bh^3}{24}\int_0^L \theta_{y,x}{}^2 dx = E\frac{bh^3\alpha^2}{24L} \qquad \text{(A6.10)}$$

$$\frac{1}{2}\int_{\Omega}\tau_{xz}\gamma_{xz}^F d\Omega = \frac{1}{2}Gbh\int_0^L \gamma_{xz}^{F\,2} dx = G\frac{bhL\alpha^2}{6} \qquad \text{(A6.11)}$$

Consequently, the ratio between the shear energy and the bending energy (A6.10 and A6.11) for the case of pure bending of a rectangular (bxh) beam is proportional to $(L/h)^2$. The shear energy should be equal to zero in case of pure bending but for this element, the parasitic shear energy absorbs a large part of the available energy. The displacement solution is influenced by shear effects where it should be only associated to bending effects.

Appendix 7. Elementary stiffness matrix with distortional effects

$\{q_{\theta xI}\}^T = <\theta_{xI1}, \theta_{xI2}, \theta_{xI3}>$; I=1,2,…m

$\{q_{ui}\}^T = <u_{i1}, u_{i3}>$; i=1,2,…n

$$k^{el} < q_{\theta_{xI}}, q_{\theta_{xI}} > \; = GI_h^{*D_I}\left[K_2\right] + ED_{ISM}\left[K_1\right]$$

$$k^{el} < q_{\theta_{xI}}, q_{u_i} > \; = G[I^{D_I}_{y\Omega^i_{,z}} - I^{D_I}_{z\Omega^i_{,y}} + S^{D_I}_{z_{CI}\Omega^i_{,y}} - S^{D_I}_{y_{CI}\Omega^i_{,z}}]\left[K_7\right]$$

$$k^{el} < q_{u_i}, q_{u_j} > = EI_{\Omega^i\Omega^j}\left[K_4\right] + G[I_{\Omega^i_{,y}\Omega^j_{,y}} + I_{\Omega^i_{,z}\Omega^j_{,z}}]\left[K_3\right]$$

$[K_1]$, $[K_2]$…$[K_7]$ are given in Appendix 3.

Appendix 8. Basic concepts of non-linear analyses

The analysis of slender thin-walled structures which offer a high resistance for a relatively light weight takes into account economy and stability. As thin walled structures have a very high loading capacity, their design is usually determined by structural instabilities. Due to their small thickness, they are subject during the loading process to large deflections and to significant changes in stiffness so that the load-deflection curve becomes non linear. The hypothesis of linearity and the principle of superposition cannot be adopted and the reference configuration cannot be kept as the undeformed structure. The non linear displacement response is thus determined by applying gradually the load and solving linear sets of equations. The load is divided into a series of increments and the stiffness of the structure is adjusted at the end of each increment. The purpose of this paragraph is to introduce the nonlinear analysis in order to study the elastic stability. The kinematic equations describing the geometric movement of a structure and the basic mechanics relations introducing the stress concepts are given. As the instability often occurs after a small deformation of most thin walled structures, the hypotheses of moderate rotations and small stress-strain relations are kept forwardly.

The finite deformation solid mechanics is detailed in standard references (Criesfield 1997; Belytschko 2000; Zienkiewicz 2000;…). This appendix, based mainly on the work of Akoussah (1987) and De Ville (1989), presents a brief outline of the basic equations. A deformable three dimensional body is considered. Different successive positions in the space and during the deformation history are analyzed. A configuration denotes a set of positions of the structure for a given load level. If C^1 et C^2 are two configurations and if the coordinates of C^1 are taken as independent variables to describe C^2, the configuration C^1 is called reference configuration and the description of the movement is called lagrangian. The deformed structure is referred by the position vector position of material points in a chosen reference configuration in a three dimensional space.

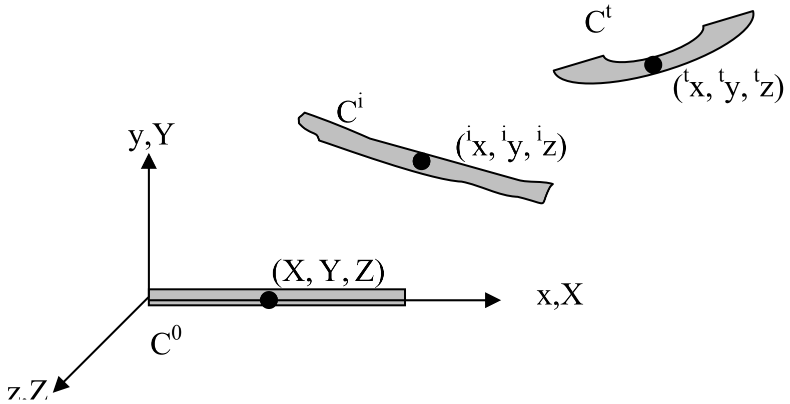

Figure A8.1: Undeformed, intermediate and deformed configurations for finite deformation problems.

Three successive configurations are considered:

-the initial configuration C^0 refers to the unloaded and undeformed state of the structure,

-the deformed or current C^t represents the deformed state or the position at a load level t of the structure,

-an intermediate configuration C^i refers to an intermediate state between the first two configurations.

A Cartesian system is used and the description is called actualized since the reference configuration is taken as C^t.

Deformation

The position vector has three coordinates that can be treated as components of one column matrix:

$$\langle x(X,t)\rangle = \langle X\rangle + \langle u(X)\rangle \qquad (A8.1)$$

The displacement vector <u> = <u,v,w> is introduced as the change of arbitrary point p between two frames (C^0 ,C^t) in a Cartesian system.
<X> = <X,Y,Z> is the initial position vector.

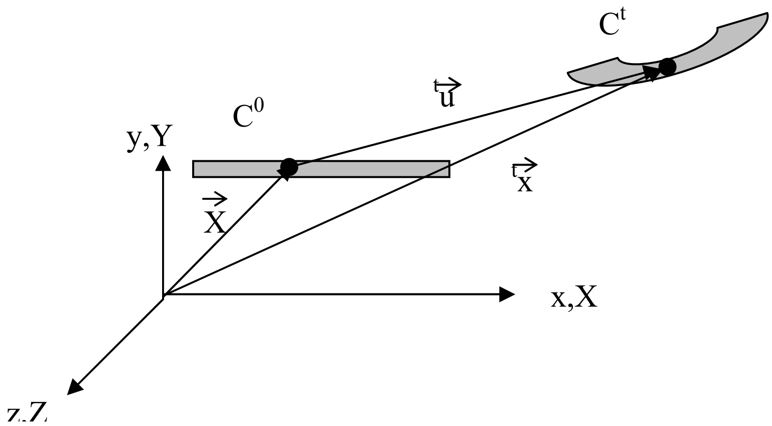

Figure A8.2 Common reference for all the configurations

The displacement components (U_k or u_k), with respect to either a reference configuration C^0 (U_k) or a current configuration C^t (u_k) respectively, are related through:
$U_i = u_i$ (A8.2)

Both components may be used equally for finite element developments.
A fundamental measure of deformation is described by the deformation gradient [J] which is a direct measure that maps a differential line element dx in the reference configuration C^0 into one in the current configuration as:

$$\langle dx\rangle = \langle dX\rangle + \langle du\rangle \qquad \{dx\} = \left[I + \frac{\partial u}{\partial X}\right]\{dX\} = [J]\{dX\}$$

$$[J] = \left[\frac{\partial x}{\partial X}\right] = \begin{bmatrix} 1+\frac{\partial u}{\partial X} & \frac{\partial u}{\partial Y} & \frac{\partial u}{\partial Z} \\ \frac{\partial v}{\partial X} & 1+\frac{\partial v}{\partial Y} & \frac{\partial v}{\partial Z} \\ \frac{\partial w}{\partial X} & \frac{\partial w}{\partial Y} & 1+\frac{\partial w}{\partial Z} \end{bmatrix} \qquad (A8.3)$$

where [I] is the identity matrix.

$J = \det[J] > 0$ (A8.4)
[J] is subject to the constraint (A8.4) to ensure that material volume elements remain positive. F may be used to determine the change in length and direction of a differential line element and the determinant J maps a volume element in the reference configuration into one in the current configuration:

$$\langle dx\rangle = \langle dX\rangle [J]^T$$
$$dV = (dX * dY).dZ \text{ becomes } dv = (dx * dy).dz = JdV \qquad (A8.5)$$

The following relations are also given:

$$\overrightarrow{dA}^{0} = (\overrightarrow{dX} * \overrightarrow{dY}) = \vec{n}^{0} dA^{0} \qquad \overrightarrow{dA} = (d\vec{x} * d\vec{y}) = \vec{n} dA$$

$$\{n\} dA = J[J]^{-T}\{n^{0}\} dA^{0} \qquad \{dA\} = J[J]^{-T}\{dA^{0}\} \qquad \text{(A8.6)}$$

If dl^0 and dl are the lengths of differential elements dX and dx respectively, the following relations are obtained:

$$\left(dl^{0}\right)^{2} = \langle dX\rangle\{dX\} \qquad (dl)^{2} = \langle dx\rangle\{dx\}$$

$$(dl)^{2} = \langle dX\rangle[J]^{T}[J]\{dX\} \qquad \text{(A8.7)}$$

It is common to introduce the Green strain [E] for deformation measurements:

$$(dl)^{2} - \left(dl^{0}\right)^{2} = \langle dX\rangle([J]^{T}[J]-[I])\{dX\} = 2\langle dX\rangle[E]\{dX\}$$

where $[E] = \frac{1}{2}\left([J]^{T}[J]-[I]\right)$ or $E_{ij} = \frac{1}{2}\left(J_{ki}J_{kj} - \delta_{ij}\right)$

In terms of the reference displacements,

$$E_{ij} = \frac{1}{2}\left(\frac{\partial U_i}{\partial X_j} + \frac{\partial U_j}{\partial X_i} + \frac{\partial U_k}{\partial X_i}\frac{\partial U_k}{\partial X_j}\right) \qquad \text{(A8.8)}$$

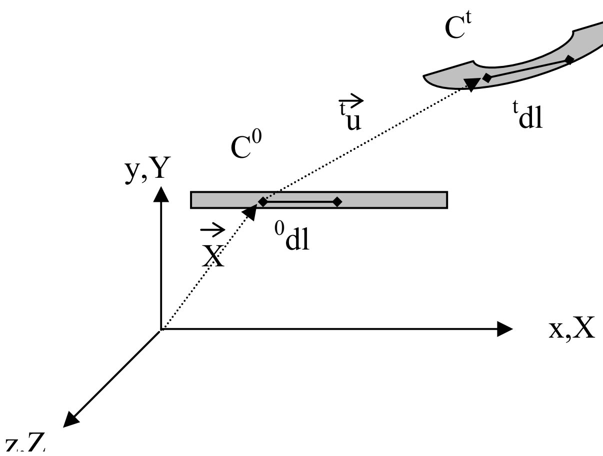

Figure A8.3 Movement of a differential element

The right hand side of equation (A8.8) can be split into linear and nonlinear strains. The linear strain is noted ε_{ij}.

Stress measures

In the following developments, capital and small letters are used to design respectively the variables in a reference configuration C^i and in the current configuration C^t.

Stresses measure the amount of force per unit of area. p is a material point of the deformed configuration C^t and Δa is an elementary surface which orientation is defined by a normal $\vec{n}$. Let Δf be the force vector acting at this area element. The definition of the stress vector $\vec{t}$ (n) at p is given by the limit:

$$\vec{t}(\vec{n}) = \lim_{\Delta a \to 0} \frac{\overrightarrow{\Delta f}}{\Delta a} \qquad \text{(A8.9)}$$

This vector is defined by unit of deformed area in the configuration C^t and can be expressed in different manners.

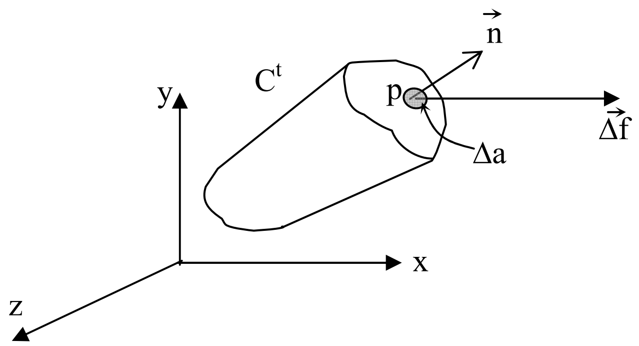

Figure A8.4 Stress measures

<u>Cauchy stress</u>
In finite deformation problems, the stress is defined with respect to the chosen configuration. If the current configuration is selected, the Cauchy (true) stress is a symmetric measure defined as follows:

$$t_j da = \sigma_{ij} n_i da = \sigma_{ij} da_i$$
$$\vec{t}(\vec{n}) = [\sigma]^T \{n\} \qquad \text{(A8.10)}$$

with

$$[\sigma] = \begin{bmatrix} \sigma_{xx} & \tau_{xy} & \tau_{xz} \\ \tau_{yx} & \sigma_{yy} & \tau_{yz} \\ \tau_{zx} & \tau_{zy} & \sigma_{zz} \end{bmatrix} \qquad \text{(A8.11)}$$

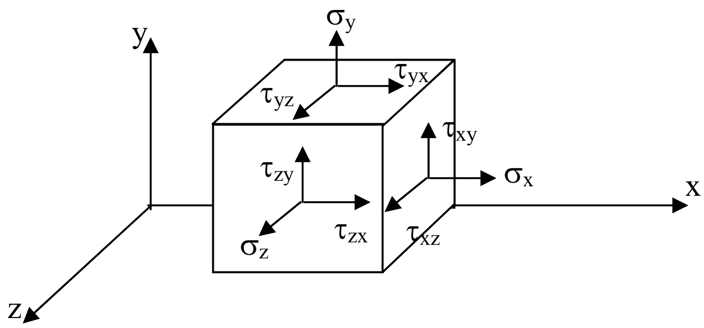

Figure A8.5 Components of $[\sigma]$

They are usually used to define general constitutive equations for materials.
If $\vec{df}$ is the load acting on the differential area da which normal is $\vec{n}$ in the configuration C^t, then:

$$\{df\} = \{t\}da = [\sigma]\langle da\rangle \qquad (A8.11)$$

Second Piola Kirchhoff stress

The second Piola Kirchhoff stress S is a symmetric stress measure with respect to the reference configuration and is related to the true or Cauchy stress through the deformation gradient as:

$$\sigma_{ij} = \frac{1}{J} J_{ik} S_{kl} J_{jl} \qquad (A8.13)$$

The force vector {F} and the stress vector {T}, associated with the Piola Kirchhoff stress definition, are related as follows:

$$\{dF\} = \{T\}dA = [S]\langle dA\rangle \qquad (A8.14)$$

{T} is a surface traction defined by:

$\{t\}\ da = \{T\}\ dA$ (A8.15)

The elementary area da in C^t results from the deformation of an elementary area dA in C^i.

Identically, a volume force $f_v = \rho_t.f$ in C^t can be related (A8.17) to F_V in any known configuration C^i by using (A8.16):

$$\rho_t dv = \rho_i dV \qquad (A8.16)$$

$$f_v\, dv = F_V\, dV \qquad (A8.17)$$

ρ_t is the mass density in the current configuration and f is body force per unit mass. The relation with the reference configuration mass density ρ_i results from the principle of mass conservation.

It should be noted that the values of Piola-Kirchhoff stresses (expressed by unit undeformed area) can be very different from those of Cauchy (expressed by unit of deformed area) if the solid is subjected to large deformations.

Equilibrium equations

By keeping quantities relating to the current deformation, the equilibrium equations for a solid subjected to finite deformation are deduced from the principle of conservation of movement quantity. They describe the macroscopic behavior of materials under loading effects.

Let v be a volume in the configuration C^t having a as contour and submitted to external forces f_v per unit of deformed volume and f_s par unit of deformed surface. The equilibrium in the current configuration is:

$$\frac{\partial \sigma^{ij}}{\partial x_j} + f_{vi} = 0 \qquad i,j=1,3 \qquad (A8.19)$$

The equilibrium equations are nearly identical to those of small deformation.

The boundary conditions consist of two types :

-mechanical or traction boundary conditions $[\sigma]\{n\} = \{f\}_s$ on a_f

-geometrical or displacement boundary conditions on a_u

where
$a = a_u \cup a_f$ and $a_u \cap a_f = 0$ (A8.20)

By using a matrix formulation :

$$[b]^T\{\sigma\} + \{f\} = 0 \tag{A8.21}$$

where $\langle\sigma\rangle = \langle \sigma_x \quad \sigma_y \quad \sigma_z \quad \tau_{xy} \quad \tau_{yz} \quad \tau_{xz} \rangle$

$$\text{et } [b]^T = \begin{bmatrix} \frac{\partial}{\partial x} & 0 & 0 & \frac{\partial}{\partial y} & 0 & \frac{\partial}{\partial z} \\ 0 & \frac{\partial}{\partial y} & 0 & \frac{\partial}{\partial x} & \frac{\partial}{\partial z} & 0 \\ 0 & 0 & \frac{\partial}{\partial z} & 0 & \frac{\partial}{\partial y} & \frac{\partial}{\partial x} \end{bmatrix} \tag{A8.22}$$

Virtual work principle
In order to construct finite element approximations, it is necessary to write a formulation in a weak or variational form. In this work, analyses are developed for materials behaving elastically when subjected to deformation histories. To simplify the numerical developments, capital and small letters are used to design respectively the variables in a reference configuration C^i and in the current configuration C^t.

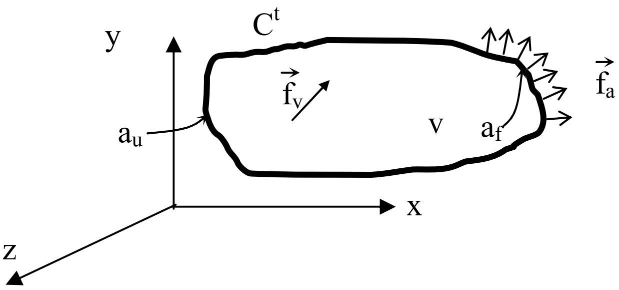

Figure A8.6 Boundary conditions in the equilibrated configuration

The principle of virtual work for real forces and virtual displacements implies that, at equilibrium, the virtual work done by internal forces is equal to the work done by external forces for any virtual displacement field. v and V denote the volume in C^t and C^i; a and A represent the part of the surface of C^t and C^i on which specified tractions f_a and F_A are applied; f_v and F_V are body forces in C^t and C^i, σ represents the Cauchy stresses and is associated with the virtual infinitesimal strain tensor ε.
The equivalence between two reference configuration formulations (A8.23) in C^t and (A8.24) in C^i is developed hereby.

$$\text{In } C^t\text{: } W^* = \int_v \varepsilon^*_{ij}\sigma_{ij}dv - \int_v u^*_i f_{vi}dv - \int_a u^*_i f_{ai}da = 0 \tag{A8.23}$$

$$\text{In } C^i\text{: } W^* = \int_V E^*_{ij}S_{ij}dV - \int_V U^*_i F_{Vi}dV - \int_A U^*_i F_{Ai}dA = 0 \tag{A8.24}$$

u* and U* are assumed to be kinematically homogenous virtual displacements (assumed to vanish on geometric boundary conditions so that reactions do not appear in virtual work formulation). These virtual displacements can be chosen as infinitesimal and taken as arbitrary variations of displacement δu or δU (equation A8.2).

The choice of the selected stress tensor (and hence the expression of the virtual work) depends on the adopted reference configuration (C^t or C^i). By using a reference configuration (A8.24), the second Piola-Kirchhoff stress tensor S is found to be conjugated to the Green strain E.
The equivalence between the internal work in (A8.23) and (A8.24) (see also De Ville 1989 §5.5.2.2) is shown below in (A8.29) by using equations (A8.25…28) which are deduced from (A8.2), (A8.5), (A8.8) and (A8.13).

$$\int_v dv = \int_V JdV \tag{A8.25}$$

$$U_i = \delta_{ij}\, u_j \tag{A8.26}$$

$$\sigma_{ij} = \frac{1}{J}\frac{\partial x_i}{\partial X_k} S_{kl} \frac{\partial x_j}{\partial X_l}{}_{jl} \tag{A8.27}$$

The Green strain tensor is expressed in terms of reference displacements as

$$E_{ij} = \frac{1}{2}\left(\frac{\partial U_i}{\partial X_j} + \frac{\partial U_j}{\partial X_i} + \frac{\partial U_k}{\partial X_i}\frac{\partial U_k}{\partial X_j}\right) \tag{A8.28}$$

The first term of (A8.23) is developed as follows:

$$\int_v \sigma_{ij}\delta\varepsilon_{ij} dv = \int_V \frac{1}{2}\frac{\partial x_i}{\partial X_k} S_{kl}\frac{\partial x_j}{\partial X_l}\left(\frac{\partial X_m}{\partial x_j}\frac{\partial \delta u_i}{\partial X_m} + \frac{\partial X_m}{\partial x_i}\frac{\partial \delta u_j}{\partial X_m}\right) dV$$

$$\int_v \sigma_{ij}\delta\varepsilon_{ij} dv = \int_V \frac{1}{2} S_{kl}\left(\frac{\partial x_i}{\partial X_k}\frac{\partial X_m}{\partial X_l}\frac{\partial \delta u_i}{\partial X_m} + \frac{\partial x_j}{\partial X_l}\frac{\partial X_m}{\partial X_k}\frac{\partial \delta u_j}{\partial X_m}\right) dV$$

$$\int_v \sigma_{ij}\delta\varepsilon_{ij} dv = \int_V \frac{1}{2} S_{kl}\left(\frac{\partial (X_i + U_i)}{\partial X_k}\delta_{ml}\frac{\partial \delta u_i}{\partial X_m} + \frac{\partial (X_j + U_j)}{\partial X_l}\delta_{mk}\frac{\partial \delta u_j}{\partial X_m}\right) dV$$

$$\int_v \sigma_{ij}\delta\varepsilon_{ij} dv = \int_V \frac{1}{2} S_{kl}\left((\delta_{ik} + \frac{\partial (U_i)}{\partial X_k})\frac{\partial \delta u_i}{\partial X_l} + (\delta_{jl} + \frac{\partial (U_j)}{\partial X_l})\frac{\partial \delta u_j}{\partial X_k}\right) dV$$

$$\int_v \sigma_{ij}\delta\varepsilon_{ij} dv = \int_V \frac{1}{2} S_{kl}\left(\frac{\partial \delta u_k}{\partial X_l} + \frac{\partial \delta u_l}{\partial X_k} + \frac{\partial U_i}{\partial X_k}\frac{\partial \delta u_i}{\partial X_l} + \frac{\partial U_j}{\partial X_l}\frac{\partial \delta u_j}{\partial X_k}\right) dV$$

$$\int_v \sigma_{ij}\delta\varepsilon_{ij} dv = \int_V S_{kl}\delta E_{kl} dV \tag{A8.29}$$

The equivalence between the external work in (A8.23) and (A8.24) is directly found by using (A8.25), (A8.15) and (A8.17).

Appendix 9. Solution methods for the non linear problem

Significant changes of shape can take place suddenly without warning for structural members with elastic behaviour. Such phenomenon of loss of equilibrium stability constitutes a typical failure mode for some structures. The theory of stability is a basis for design and examination of the safety of new and existing structures. It deals with critical loads and deformations associated with sudden changes of the states of a structure.
In a general loading process, a structure becomes more flexible and is subject to large geometric changes when the loading reaches critical values. The configuration must be actualized since the associated governing equations are nonlinear. This appendix shows how the loss of stability is detected for the elastic structures under conservative loading that are analyzed in paragraph 5.5. The following developments are based on the work of Criesfield (1997, chapter 9) and on that of Fafard (Batoz 1999, course 4).

The energy functional in paragraph 5.5.2 is reformulated in general terms as:

$$\pi(u,\lambda) = \Pi(u) - \lambda u^T F \qquad \text{(A9.1)}$$

where π is the total potential energy, Π is the strain energy which is function of a finite set of displacement variables u, F is a fixed external load vector and the applied loads vary in magnitude by a single scalar multiplier λ.
With λ fixed, a small change in potential energy, $\delta\pi$, is approximated by truncated Taylor series:

$$\delta\pi = \frac{\partial\pi}{\partial u}\delta u + \frac{1}{2}\delta u^T \frac{\partial^2\pi}{\partial u^2}\delta u + ... \qquad \text{(A9.2)}$$

$$\frac{\partial\pi}{\partial u} = R \qquad \text{(A9.3)}$$

$$\frac{\partial^2\pi}{\partial u^2} = K_T \qquad \text{(A9.4)}$$

By using the notations in paragraph 5.5, (A9.3) can be identified as the out of balance forces or gradient R and (A9.4) can be identified as the tangent stiffness matrix K_T.

$$\delta\pi = R\delta u + \frac{1}{2}\delta u^T K_T \delta u + ... \qquad \text{(A9.5)}$$

Higher order terms in (A9.5) are omitted. In order to ensure equilibrium, the energy change in (A9.5) should be stationary with respect to δu. The theorem of equilibrium state sets that the conservative system is in equilibrium if the first variation of potential energy equals zero:

$$\frac{\partial\pi}{\partial u} = R(u,\lambda) = 0 \qquad \text{(A9.6)}$$

The set of non linear equilibrium equations (A9.6) for n degrees of freedom of the discrete model determines the configuration that an elastic structure assumes under a given set of loads. Stable configurations of equilibrium are determined according to the Lagrange-Dirichlet theorem. For stable equilibrium, a small change of energy must be positive for any small perturbation δu about the equilibrium point. The potential energy is positive definite and a minimum of potential energy occurs in the stable equilibrium configuration.

$$\delta u^T K_T \delta u > 0 \qquad \text{(A9.7)}$$

(A9.7) must be satisfied for all δu.

In case of conservative system, an equilibrium state is unstable if the change in energy is negative for a small perturbation δu. K_T is no more positive definite and will have at least one negative eigenvalue.

A neutral state is defined by the fact that the second variation of potential energy is equal to zero. K_T has a zero eigenvalue.

$$\det(K_T) = 0 \qquad \text{(A9.8)}$$

Given a solution at a level A involving u_A et λ_A, a Taylor expansion of (A9.6) for λ varying gives by neglecting higher order terms:

$$\frac{\partial R}{\partial u}\Big|_A \Delta u + \frac{\partial R}{\partial \lambda}\Big|_A \Delta\lambda = K_T \Delta u - \Delta\lambda F = 0 \qquad \text{(A9.9)}$$

In order to find the equilibrium path for the structure, (A9.10) must be solved:

$$\Delta u = \Delta\lambda K_T^{-1} F \qquad \text{(A9.10)}$$

When equation (A9.8) is satisfied, (A9.10) does not have a solution and the associated state is called critical. The potential system reaches a critical state of equilibrium if the first and second variations of potential energy equal zero. This critical or singular point can be either a limit point (figure A9.1a) or a bifurcation point (figure A9.1b) and corresponds either to a snapping or to a buckling phenomenon respectively.

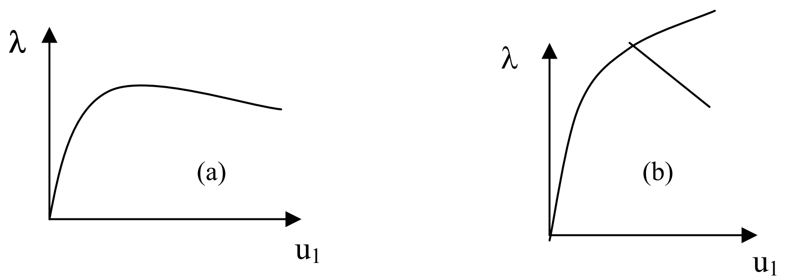

Figure A9.1 Singular points: Limit point (a) and bifurcation point (b)

In the (n+1) dimensional space, a curve (figure A9.1) is constituted by plotting a set of points with coordinates λ and u_1 which are solutions of (A9.6). The curves in the (n+1) dimensional space constitute the equilibrium path. The primary branch passes through the origin of the coordinate system and the secondary branch does not.

Parameterization of load displacement curve

The concept of scalar load multiplier λ is thus introduced as a factor multiplying a load vector up to the desired level.

A parameterization of the load-displacement curve is necessary to introduce functional aspects of the resolution. n+1 is the total number of unknowns where n is the number of degrees of freedom and the n+1 unknown is the scalar load multiplier λ.

$$\{R\} = \lambda\{F\} - \{R_{int}\} = \{0\} \tag{A9.11}$$

F corresponds to equivalent nodal forces. It depends strictly on the external loading given for a problem. R_{int} is the internal force vector that depends on the displacements u. λ is the load level parameter.

It is crucial to choose the most suitable parameter that dictates the path tracing of the load-displacement curve. If the parameter is chosen to be λ or any displacement u_i, the algorithm fails at limit points or at 'snap-throughs'. To overcome this, the arc length method is used and a curvilinear axis coordinate s that follows the load displacement curve is taken hereby as a parameter (A9.12).

$$\begin{aligned} \lambda &= \lambda(s) \\ \{u\} &= \{u(s)\} \end{aligned} \tag{A9.12}$$

The load level parameter λ is therefore the variable to be determined as a function of s.

The tangent unit vector at the point s of the curve is:

$$\{t\} = \begin{Bmatrix} \{\dot{u}\} \\ \dot{\lambda} \end{Bmatrix} \tag{A9.13}$$

where $\{\dot{u}\} = \frac{1}{m}\left\{\frac{du}{ds}\right\}$, $\dot{\lambda} = \frac{1}{m}\frac{d\lambda}{ds}$, with $m = \sqrt{\left\langle\frac{du}{ds}\right\rangle\left\{\frac{du}{ds}\right\} + \left(\frac{d\lambda}{ds}\right)^2}$

As t is a unit vector,

$$\langle t\rangle\{t\} = \langle\dot{u}\rangle\{\dot{u}\} + (\dot{\lambda})^2 = 1 \tag{A9.14}$$

In order to approximate the equilibrium path by a broken line of chords whose end points correspond to successive discrete values, the incremental form is used instead of the differential one. (A9.14) is discretized as follows:

$$\{\dot{u}\} = \left\{\frac{\Delta u}{\Delta s}\right\} \tag{A9.15}$$

$$\dot{\lambda} = \frac{\Delta\lambda}{\Delta s} \tag{A9.16}$$

$$\langle\Delta u\rangle.\{\Delta u\} + (\Delta\lambda)^2 = (\Delta s)^2 \tag{A9.17}$$

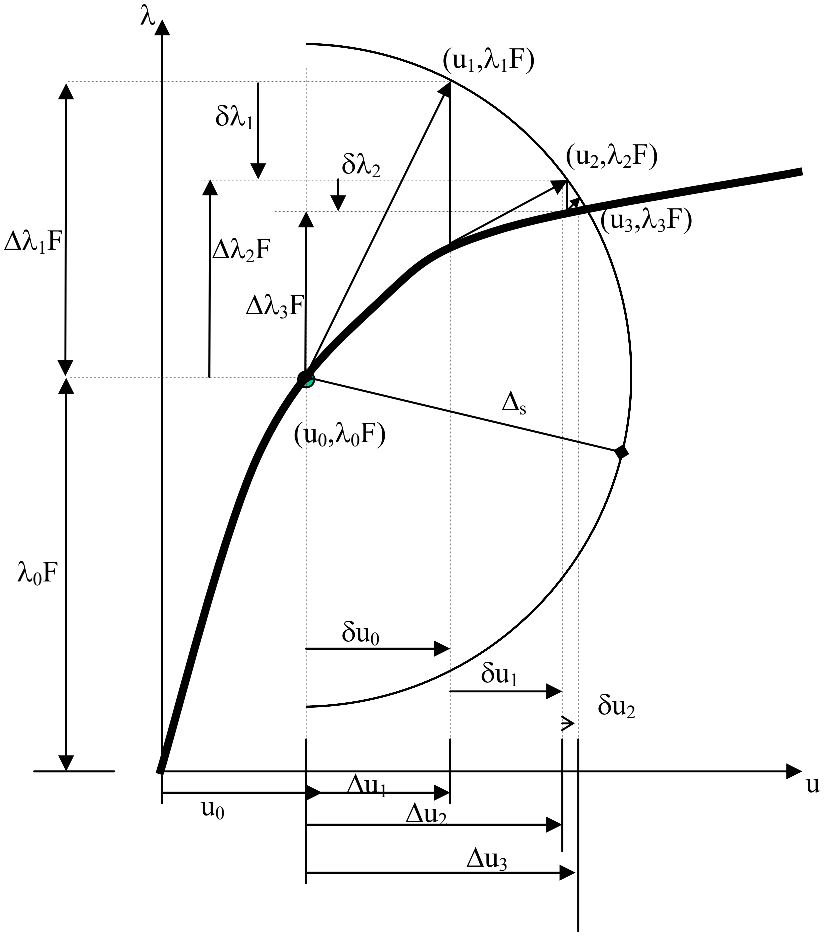

Figure A9.2 Spherical arc length procedure for one degree of freedom (after Criesfield 1997)

In (A9.17), a scaling parameter ψ is required because the load contribution depends on the adopted scaling between the load and displacement terms.

$$\langle \Delta u \rangle . \{\Delta u\} + \psi^2 (\Delta\lambda)^2 = (\Delta s)^2 \qquad \text{(A9.18)}$$

If the loading term involving ψ is set to zero (A9.19), the method is known as cylindrical rather than spherical [Criesfield 1997 page 274, …]. (A9.18) is thus reduced to (A9.20).

$$\psi = 0 \qquad \text{(A9.19)}$$
$$\langle \Delta u \rangle . \{\Delta u\} = (\Delta s)^2 \qquad \text{(A9.20)}$$

Equation A9.17 describes the evolution from step to step by using the arc length method. Δs, the discrete arc length value of the curve $(\{u\}, \lambda)$, represents at each step the fixed radius of the desired intersection (see figure A9.2 & A9.3). $\Delta\lambda$ and Δu are incremental and relate back to the last converged equilibrium state.

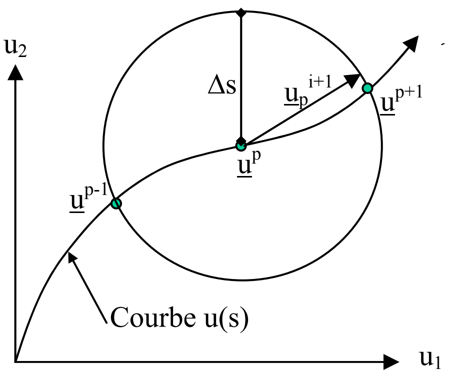

Figure A9.3 Cylindrical arc length method for 2 degrees of freedom (after Batoz 1999)

Cylindrical arc length method calculations

Solving equation (A9.11)

Let Δu_i be the increment in the displacement u from the beginning of a step till the current iteration i. δu_i is the increment in the displacement between two consecutive iterations i-1 and i. Identically, let $\Delta\lambda_i$ be the increment in the load parameter from the beginning of a step till the current iteration and $\delta\lambda_i$ is the increment between two consecutive iterations i-1 and i.

At a new unknown level, the change in displacement δu_i must be calculated from (A9.11) to ensure the equilibrium.

$$\{\delta u_i\} = [K_t]^{-1}\left(\{R_i\} + \delta\lambda_i\{F_{ext}\}\right) \quad \text{(A9.21)}$$

The iterative displacement δu_i can be split into two parts involving internal and external forces:

$$\{\delta u_i\} = [K_t]^{-1}\{R_i\} + \delta\lambda_i [K_t]^{-1}\{F_{ext}\} \quad \text{(A9.22)}$$

$$\{\delta u_i\} = \{\delta u_{iR}\} + \delta\lambda_i\{\delta u_{iF}\} \quad \text{(A9.23)}$$

$\delta\lambda_i$ is still unknown and the new incremental displacement can be written as:

$$\{\Delta u_{i+1}\} = \{\Delta u_i\} + \{\delta u_{iR}\} + \delta\lambda_i\{\delta u_{iF}\} \quad \text{(A9.24)}$$

$$\Delta\lambda_{i+1} = \Delta\lambda_i + \delta\lambda_i \quad \text{(A9.25)}$$

Then, (A9.24) is inserted into (A9.20) and a scalar quadratic equation is solved in order to determine $\delta\lambda_i$.

$$a(\delta\lambda)^2 + b(\delta\lambda) + c = 0 \quad \text{(A9.26)}$$

where

$$a = \langle\delta u_{iF}\rangle\{\delta u_{iF}\} \quad \text{(A9.27)}$$

$$b = 2\{\delta u_{iF}\}(\{\Delta u_i\} + \{\delta u_{iR}\}) \quad \text{(A9.28)}$$

$$c = (\{\Delta u_i\} + \{\delta u_{iR}\})(\{\Delta u_i\} + \{\delta u_{iR}\}) - (\Delta s)^2 \quad \text{(A9.29)}$$

This is applied for each iteration in order to let the Euclidean norm of the vector Δu equal to Δs.

Finding the appropriate root to (A9.26)

For a regular curve, there are two intersection points between the circle and the load displacement curve (figure A9.4). Equation (A9.26) has then two roots and the appropriate one must be chosen. Both solutions ($\delta\lambda_{i1}$ and $\delta\lambda_{i2}$) are computed and the closest to the previous incremental direction is kept in order to prevent

the solution from diverging or 'doubling back on it tracks' [Criesfield 1997 page 277]. This criterion is based on the fact that during the iteration process, two consecutive iterated vectors point roughly in the same direction.
The solution with minimum angle between Δu_i and Δu_{i+1} is kept (with maximum cosine of the angle):

$$\cos(\theta_i) = \frac{\{\Delta u_i\}\{\Delta u_{i+1}\}}{(\Delta s)^2} \tag{A9.30}$$

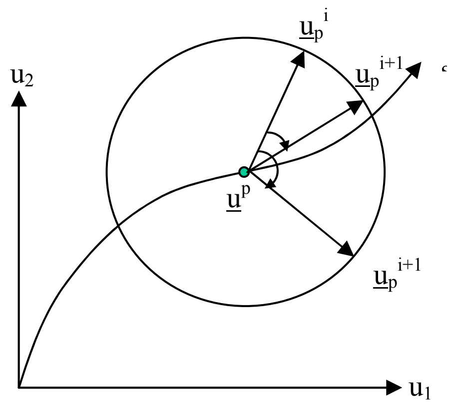

Figure A9.4 Selection of solution for the cylindrical arc length method (after Batoz 1999)

<u>Predictor solution</u>
The set of linear problems is solved starting from a first estimate. At the first step (s = 0) of calculation, the value of Δs can be determined from a given value $\Delta\lambda$ of the load increment:

$$\Delta\lambda_1 = \overline{\Delta\lambda}$$

$$\overline{\Delta s} = \overline{\Delta\lambda}\sqrt{\langle \Delta u^1_F \rangle \{\Delta u^1_F\}} \tag{A9.31}$$

In this particular case for s = 0, the problem is linear and $[K_T] = [K]$.

In the beginning of any other step p (arbitrary values of s), the value of $\Delta\lambda$ is calculated from (A9.32):

$$\Delta\lambda_1 = \pm \frac{\overline{\Delta s}}{\sqrt{\langle \Delta u^1_F \rangle \{\Delta u^1_F\}}} \tag{A9.32}$$

Real values of (A9.32) are found if :

$$\left\| \{\Delta u_i\} + \{\delta u_{iR}\} \right\| \leq (\Delta s)$$

Two predictors are possible and the sign of $\langle \Delta u \rangle_p^{p-1} \{\Delta u^1_F\}$ is prevalent. If the tangent matrix is positive definite, the positive sign is kept. However, if it is not the case, a negative pivot implies one negative eigenvalue for the tangent matrix. Discussion about the nature of this singular point is found in [Criesfield 1997 page 286].

List of figures

List of tables